UNIVERSITÉ DU QUÉBEC À MONTRÉAL

COSTIMULATORY PROTEINS QUANTIFICATION METHODS: THE SIGNIFICANT ROLE IN DIAGNOSIS AND APTAMER-BASED THERAPEUTICS IN RHEUMATOID ARTHRITIS

THESIS

PRESENTED

AS A PARTIAL REQUIREMENT OF

THE DOCTORATE CHEMISTRY

BY
ABEER MALKAWI

JUIN 2024

UNIVERSITÉ DU QUÉBEC À MONTRÉAL

LES MÉTHODES DE QUANTIFICATION DES PROTÉINES COSTIMULATRICES: LE RÔLE SIGNIFICATIF DANS LE DIAGNOSTIC ET LES THÉRAPIES BASÉES SUR LES APTAMÈRES DANS LA POLYARTHRITE RHUMATOÏDE

THÈSE

PRÉSENTÉE

COMME EXIGENCE PARTIELLE

DU DOCTORAT EN CHIMIE

PAR

ABEER MALKAWI

JUIN 2024

ACKNOWLEDGEMENTS

Words cannot express my gratitude to everyone who supported me during my Ph. D journey. I would like to express my deepest gratitude to my supervisor, professor Mohamed Siaj, for his unwavering support, invaluable guidance, and insightful feedback throughout the entire process of completing this thesis. His expertise and encouragement have been instrumental in shaping the direction of my research and enhancing the quality of this work.

I am also indebted to the members of my thesis examining committee, professor Steve Bourgault, Professor Marc Lussier from UQAM, and Elodie Boisselier from Université Laval for their constructive criticism, thoughtful insights, and dedication to the academic rigor of this project. Their collective expertise has greatly enriched the depth and breadth of my research.

A special note of appreciation goes to my collaborators and coauthors, Dr. Anas Abdel Rahman from KFSH&RC, Riyadh, Saudi Arabia, Professor Lekha Sleno and Leanne Olund from CERMO (UQAM), Dr. Refat Nimer from JUST (Jordan), Dr. Afshan Masood (UQAM), Maziar Jafari (UQAM), Maha Almogren from KFSH&RC, Riyadh, Saudi Arabia, Dr. Hicham Benabdelkamel and Dr. Abdulrahman S. Alarfaj from king Saud university, Riyadh, Saudi Arabia whose collaboration and contributions have significantly strengthened the findings presented in this thesis. Working with such talented individuals has been a privilege, and I am grateful for the collaborative spirit that defined our research endeavors. Additionally, this endeavor would not have been possible without the generous support from FRNQ.

I extend heartfelt thanks to my family for their unwavering support, patience, and understanding. To my husband, Anas Abdel-Rahman, his belief in me has kept my spirits and motivation high during this process, and his encouragement has been a constant source of motivation and confidence. To my daughters, Naya and Tia, I am grateful for the sacrifices they made to allow me the time and space to pursue this academic journey, their love patient guiding me through the challenges during this thesis. To my parents, their prayers and unwavering support have been a

constant source of strength and serving as a profound motivation that propels me forward on this ongoing journey. I am also grateful to my sisters, brothers, and the other member of family for their appreciative support.

Finally, I would like to thank all those friends and colleagues who have played a role, big or small, in shaping my academic and personal growth. Your encouragement and camaraderie have been invaluable.

This thesis is a testament to the collective effort of a supportive community, and I am deeply grateful for the guidance and encouragement I have received.

TABLE OF CONTENTS

LIST OF TABLES

LIST OF FIGURES

LIST OF SCHEMES

LIST OF ABBREVIATIONS

Apt: Aptamer

MS: Mass spectrometry

MRM: Multiple reaction monitoring

SELEX: Systematic Evolution of Ligands by Exponential Enrichment

NGS: Next generation sequencing

ESI: Electron spray ionization

APCI: Atmospheric pressure chemical ionization

EI: Electron impact

CI: Chemical ionization

MALDI: Matrix-assisted laser desorption ionization

DESI: Desorption electrospray ionization

Q: Quadrupole

IT: Ion trap

FTICR: Fourier-transform ion cyclotron resonance

TOF: Time-of-Flight

QQQ: triple quadrupoles

QTOF: quadrupoles with the time of flight

QFTICR: quadrupoles with Fourier-transform ion cyclotron resonance.

IM: Ion mobility

DDA: Data-Dependent Acquisition

DIA: Data-Independent Acquisition

ssDNA: single-strand DNA

PTMs: Post-translational modification

SRM: Selected Reaction Monitoring

LC: liquid chromatography

AptA: Aptamer affinity

GFP-Apt: Green fluorescent protein aptamer

SAMDI-MS: Self-assembled monolayer desorption ionization-MS

ITO: Indium Tin oxide

Au: Gold

PESI: Probe electrospray ionization technology

REIMS: Rapid evaporative ionization MS

SPR: surface plasmon resonance

SAW: Surface acoustic wave

LOD: limit od detection.

IDMS: Isotope dilution MS

KCE-MS: kinetic capillary electrophoresis-MS

PEG: Polyethylene glycol

RA: Rheumatoid arthritis

CD: Cluster of differentiation

TNF: tumor necrosis factor

RF: Rheumatoid factor

ACPA: anti-citrullinated protein antibodies

DAS28: 28-joint disease activity score

SDAI: simple disease activity index

CDAI: clinical disease activity index

TCR: T-cell receptor

APC: antigen-presenting cell

CP: costimulatory pathway

Ig-V: Immunoglobulin-like domain variant

Ig-C: Immunoglobulin-like domain constant

QQQ: triple quadrupole

CAN: acetonitrile

FA: formic acid

DTT: dithiothreitol

IAA: iodoacetamide

ABC: ammonium bicarbonate

ESR: erythrocyte sedimentation rate

CRP: (Puscasu et al., 2021)-reactive protein

SIL: stable isotope labeled.

IS: internal standards

ESI: electrospray ionization

UPLC: ultra-high-pressure liquid chromatography

SPE: Solid-phase extraction

QC: quality control

LOQ: lower limits of quantification

LQC: low-QC

MQC: Medium-QC

HQC: High QC

SD: standard deviation

RT: retention time

Q1: precursor ion

Q2: product ion

SP: signature peptide

AUC: area under the curve

CI: confidence interval

S/N: Signal/Noise ratio

$R^{2;}$ correlation coefficients

CV: coefficient of variation

AA: Amino acid

SELEX: Systematic evolution of ligands by exponential enrichment

NTA-Ni: Nitriloacetic acid-Nickle beads

PCR: polymerase chain reaction

AuSPE: A screen-printed gold electrode

MCH: 6-mercapto-1-hexanol

PBS: phosphate buffer saline

AFM: Atomic force microscopy

PiFM: photo-induced force microscopy

NS: Negative selection

CS: Counter-selection

HRMS: High-resolution mass spectrometry

CV: Cyclic voltammetry

EIS: Electrochemical impedance spectroscopy

SAM: Self-assembled monolayer

R_{ct}: Charge transfer resistance

PiF-IR: Photo induce force- infra-red.

RSD: Relative standard deviation

FDA: Food and Drug Administration

MHC: major histocompatibility complex

TCR: T-cell receptor

CTLA4-Ig: Cytotoxic T-lymphocyte–associated antigen 4 – Immunoglobulin (Abatacept)

ABC: Ammonium bicarbonate

IAM: iodoacetamide

HLP-SPE: Hydrophilic-lipophilic balance solid phase extraction

ACS: Acetonitrile

FA: formic acid

DDA: Data-dependent acquisition

ICH: International Conference on Harmonisation

PTM: post-translational modification

Q1: Precursor ion

Q2: product ion

XIC: Extracted ion chromatograms.

TIC: Total ion chromatogram

IC_{50}: Half maximum inhibitory effect

RÉSUMÉ

L'importance de la voie co-stimulatrice CD28-B7 et des molécules associées dans les maladies auto-immunes est soulignée par leur rôle crucial dans la régulation du système immunitaire. Cette voie joue un rôle clé dans le maintien de la réponse auto-immune, ce qui en fait un accent central pour comprendre les mécanismes sous-jacents de maladies telles que l'arthrite rhumatoïde (RA) et pour développer des stratégies diagnostiques et thérapeutiques spécifiques. L'investigation de ces molécules comme biomarqueurs potentiels et cibles thérapeutiques montre un potentiel pour améliorer la gestion et les résultats de santé de plusieurs maladies auto-immunes.

Cette thèse présente un travail analytique unique pour développer un diagnostic et un traitement basé sur les aptamères pour les maladies auto-immunes, en se concentrant principalement sur CD28, CD80, CD86 et CTLA-4 dans l'arthrite rhumatoïde (RA), comme a été développé dans le Chapitre 1. Initialement, dans le Chapitre 2, nous avons développé des méthodes analytiques novatrices en utilisant la chromatographie liquide couplée à la spectrométrie de masse en tandem (LC-MS/MS) de grade clinique pour quantifier la forme soluble de ces quatre molécules dans des échantillons de plasma humain (patients RA et contrôle sain). Par la suite, dans le Chapitre 3, l'un des biomarqueurs significatifs de la RA, CD80, a été choisi pour développer un aptasenseur pour un diagnostic sensible et reproductible qui pourra être utilisé durant les soins cliniques. Cet aptamère a été développé en utilisant la méthode *Systematic evolution of ligands by exponential enrichment* (SELEX) pour la fabrication d'électrode fonctionnalisée pour une détection électrochimique. Comme les aptamères sélectionnés pourraient avoir une valeur thérapeutique potentielle une fois liée à la cible, type CD80, un outil analytique pour cette évaluation a été développé dans le Chapitre 4 en utilisant l'aptamère développé comme modèle pour la thérapie biologique (*Abatacept*) pour l'arthrite rhumatoïde.

Suivant cette approche unique, la méthode LC-MS/MS de surveillance des réactions multiples (MRM) a été développée et validée en utilisant des peptides signature pour chaque protéine, et en suivant respectivement les directives de l'Agence fédérale américaine des produits alimentaires et médicamenteux (FDA). Contrairement à sCD28, cette étude rapporte des niveaux élevés de sCD80, sCD86 et sCTLA-4 dans le plasma des patients ayant la RA par rapport aux individus sains, suggérant leur potentiel en tant que biomarqueurs de diagnostiques. La haute sensibilité et la précision de la méthode la positionnent comme un outil prometteur pour les diagnostics de routine et la quantification des biomarqueurs dans les paramètres cliniques. Des biosenseurs, spécifiquement des aptasenseurs, ont été développés pour sCD80 en utilisant l'approche SELEX et un outil de détection électrochimique dans des matrices biologiques. Cette plateforme analytique a montré une sensibilité et une spécificité comparables aux kits ELISA disponibles dans le commerce.

Cibler la voie co-stimulatrice CD28-B7 est une stratégie prometteuse pour la thérapie des maladies auto-immunes, illustrée par l'*Abatacept* (CTLA4-Ig), un médicament approuvé par la FDA pour la RA. Une méthode LC-MS/MS a été développée en utilisant des peptides signature similaires dans différentes plateformes MRM pour évaluer l'effet inhibiteur in vitro sur la voie CD28-B7. Cela a ouvert des voies pour étudier des inhibiteurs potentiels, tels que l'aptamère sélectionné pour chaque molécule. La sensibilité et la précision du test permettent d'évaluer les effets inhibiteurs des aptamères sur sCD80 et sCD86, avec des étapes futures incluant des études sur des lignées cellulaires et in vivo.

Cette thèse a introduit pour la première fois une double approche d'étude d'une voie ciblée de maladie sous les angles diagnostique et thérapeutique. Le modèle de l'arthrite rhumatoïde a été utilisé pour exploiter ce concept en suivant la même démarche pour d'autres molécules clés. Le développement futur d'aptasenseurs pour sCD86 et CTLA-4 est en cours, avec un potentiel prometteur pour transformer la mesure des biomarqueurs liés à l'immunité, ce qui se reflétera sur les résultats de santé des patients.

ABSTRACT

The importance of the CD28-B7 costimulatory pathway and related molecules in autoimmune diseases is underscored by their pivotal role in regulating the immune system. This pathway plays a key role in maintaining autoimmune response. This makes it a central focus for comprehending the mechanisms underlying diseases such as Rheumatoid arthritis (RA) and devising specific diagnostics and therapeutic strategies. Investigating these molecules as potential biomarkers and therapeutic targets shows potential for enhancing the management and health outcomes for several autoimmune diseases.

This thesis introduces unique analytical workflow for developing aptamer-based diagnostic and therapeutic for autoimmune diseases, with a focus mainly on CD28, CD80, CD86, and CTLA-4 in rheumatoid arthritis (RA) as reviewed in Chapter 1. Initially, in chapter 2, we developed novel analytical methods using clinical grade liquid chromatography-tandem mass spectrometry (LC-MS/MS) for quantifying the soluble form of these four molecules in human plasma samples (RA patients and healthy control). Afterward, one of the RA significant biomarkers, CD80, in Chapter 3, was selected to develop a sensitive and reproducible diagnostic-grade aptasensor for clinical care using SELEX and electrochemical detection. As selected aptamers might have potential therapeutic value once bound to the target, CD80, an analytical tool for this evaluation has been developed in Chapter 4 using Abtacept as a therapeutic model for this health condition.

Following this unique approach, the multiple reaction monitoring (MRM) LC-MS/MS method was developed and validated using signature peptides for each protein, and following the FDA guideline, respectively. This study, unlike sCD28, reports elevated levels of sCD80, sCD86, and sCTLA-4 in the plasma of RA patients compared to healthy individuals, suggesting their potential as diagnostic biomarkers. The method's high sensitivity and precision position it as a promising tool for routine diagnostics and biomarker quantification in clinical settings. Biosensors,

specifically aptasensors, were developed for sCD80 using the SELEX approach and electrochemical detection tool in biological matrices. This analytical platform showed comparable sensitivity and specificity to commercially available ELISA kits.

Targeting the CD28-B7 costimulatory pathway is a promising strategy for autoimmune disease therapy, exemplified by Abatacept (CTLA4-Ig), an FDA-approved drug for RA. An LC-MS/MS method was developed using similar signature peptides in different MRM platforms to assess the in-vitro inhibitory effect on the CD28-B7 pathway. This opened avenues for studying potential inhibitors, such as the aptamer selected for each molecule. The assay's sensitivity and accuracy allow for evaluating aptamers' inhibitory effects on sCD80 and sCD86, with future steps including cell line and in vivo studies.

This thesis introduced, for the first time, a dual approach to studying diseases targeted pathway from a diagnostic and therapeutic perspectives. After following the same approach in the other key molecules, the RA model will harness the concept. The future development of aptasensors for sCD86 and CTLA-4 is underway, with promising potential for reshaping immune-related biomarker measurement, which will be reflected in the patient’s health outcome.

IN-CONTEXT

1. Background

Rheumatoid Arthritis (RA) is a chronic inflammatory disease that causes local inflammation in synovial joints (synovitis), resulting in the erosion of bones and the destruction of joints. (Chimenti et al., 2015) As shown in Figure 1, T-cells enter the synovial joints during inflammation and become activated to secrete various cytokines such as interleukins and tumor necrotic factor-α (TNF-α). The differential expression of cytokines provokes bone resorption and cartridge erosion and promotes the secretion of pro-inflammatory markers, which derives the disease's chronic characteristics. (Yamada et al., 2002) T-cell activation stimulates B-cell differentiation and produces autoantibodies, such as rheumatoid factor (RF) and anti-citrullinated protein antibodies (ACPA). (Chimenti et al., 2015) The RF and ACPA auto-antibodies are biomarkers for determining the diagnosis and the prognosis and monitoring the RA treatment. (Chimenti et al., 2015)

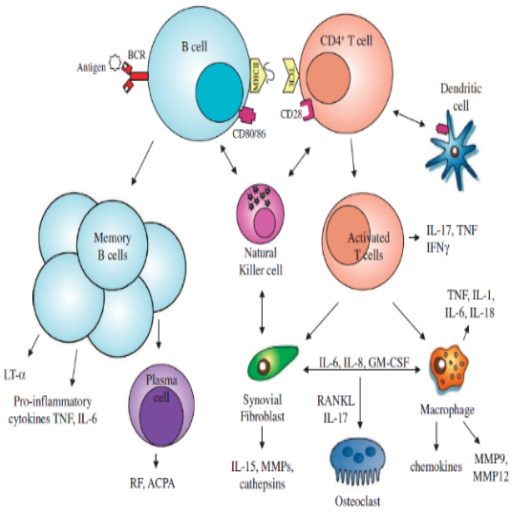

Figure 1: Immune pathways in rheumatoid arthritis. BCR, B cell receptor; TCR, T cell receptor; MHC, major histocompatibility complex. (Chimenti *et al.*, 2015)

Typically, full T-cell activation requires two signals. The first signal comes from the binding of the T-cell receptor (TCR) to the Major Histocompatibility Complex (MHC) molecule on the surface of the antigen-presenting cell (APC). In contrast, the second signal comes from the costimulatory pathway (CP), where the T-cell Surface Receptor (TCR) binds to a specific antigen (APC). (Yamada *et al.*, 2002)

The conventional CP for T-cell activation is the CD28-B7 pathway, where both Cluster of Differentiation (CD) costimulatory proteins, CD80 (B7-1) and CD86 (B7-2), interact with the CD28 receptor expressed on the T-cell surface. Cytotoxic T-lymphocyte-associated protein 4 (CTLA-4) is another receptor on T-cells that binds to the same antigens, resulting in an adverse immune response and controlling the T-cell activity. (Uehara et McGrath, 2019; Walunas *et al.*, 1996) Figure 2 illustrates the CP response under different conditions.

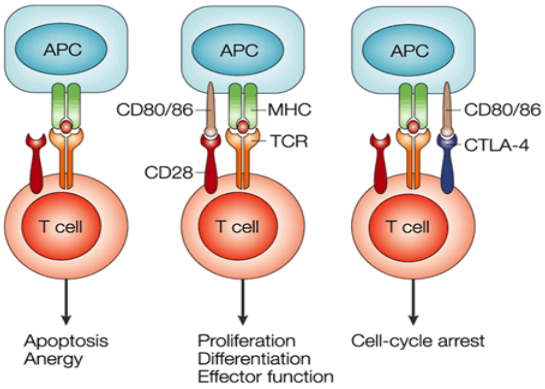

Figure 2: The response of T-cells under different conditions. APC, antigen-presenting cell, MHC, major histocompatibility complex, TCR, T-cell receptor. (Uehara et McGrath, 2019)

1.1. RA diagnosis and treatment

RA diagnosis and treatment monitoring rely heavily on the presence of rheumatoid factor (RF) and anti-citrullinated protein antibodies (ACPA), recognized as primary biomarkers. However, their utility as standalone diagnostic tools is limited due to the lack of specificity. RF can be present in other autoimmune conditions like systemic lupus erythematosus, while some RA patients test negative for ACPA. To address these challenges, various disease activity scoring systems like the American College of Rheumatology/European League Against Rheumatism (ACR/EULAR) score, the 28-joint disease activity score (DAS28), simple disease activity index (SDAI), and clinical disease activity index (CDAI) have been devised. (Atzeni *et al.*, 2017) C-reactive protein (CRP) and Erythrocyte sedimentation rate (ESR) as markers of inflammation, which are also included as components of the ACR/EULAR and the DAS28 scores. Although these conventional markers have been used routinely, their utility is questionable. Previous studies have shown that patients with active disease do not display elevations in their levels (Kay *et al.*, 2014).

Despite their use, these scoring systems have drawbacks due to their reliance on selective criteria. To overcome these limitations, a multi-biomarker disease activity test has emerged as a promising approach for disease monitoring. This approach involves leveraging large-scale genomic, transcriptomic, proteomic, and other 'omic' technologies to identify novel biomarkers for RA. Such advancements can potentially revolutionize early diagnosis and treatment strategies for RA.

Because co-stimulatory proteins are directly involved in RA development, their levels can correlate better with disease activity than conventional biomarkers. Moreover, since they are involved in early immune responses and T-cell activation, which occur even before the onset of clinical symptoms, they have the potential to serve as early diagnostic biomarkers. (Kotulska *et al*., 2015)

The treatment of rheumatoid arthritis (RA) follows guidelines that prioritize early diagnosis and aggressive management to control inflammation, prevent joint damage, and improve quality of life. Initial therapy typically involves disease-modifying antirheumatic drugs (DMARDs) like methotrexate, to achieve low disease activity or remission. For those with moderate to severe RA or inadequate response to conventional DMARDs, biologic DMARDs or targeted synthetic DMARDs are recommended. Nonsteroidal anti-inflammatory drugs (NSAIDs), corticosteroids, and analgesics are used for symptom relief and as adjuncts to DMARD therapy. Lifestyle modifications like exercise, weight management, and joint protection strategies complement pharmacological treatments. Regular monitoring, including disease activity assessments and medication adjustments, optimizes RA management and long-term outcomes.

1.2. CD80, CD86, CD28 and CTLA-4 costimulatory proteins

CD80, CD86, CD28 and CTLA-4 are crucial costimulatory molecules in autoimmune disease development. (Cao *et al.*, 2012) These costimulatory molecules belong to the immunoglobulin superfamily, sharing in common immunoglobulin (Ig))-like domains. (Buck, 1992) These Ig-like domains, either variant (IgV)- or constant (IgC))-like domains, are represented in the extracellular domains of the costimulatory molecules essential for the binding and biological activity. (Kakoulidou *et al.*, 2007) Several isoforms of these molecules have been identified for these costimulatory molecules. The soluble forms of these molecules have been found in the circulation of healthy individuals, and elevated levels have been detected in the serum of hematological malignancies, asthma, and RA. (Hock *et al.*, 2004; Ip *et al.*, 2006; Tector *et al.*, 2009; Wong *et al.*, 2005)

The discovery of the soluble costimulatory proteins in human circulation and the correlation between their level and the development of different autoimmune diseases, such as RA, increase the attention to studying these molecules for more understanding of the pathology of these diseases and utilizing them as surrogate biomarkers. The significant correlation and association between the circulating level of these molecules and RA activity, the inter-correlation between serum sCTLA4 and sCD28, sCD28 and sCD80, or sCTLA4 and sCD80 in RA patients, and the ability for non-invasive measurement of all are advantages for using these molecules as disease biomarkers for early diagnosis and more personalized treatment.

1.3. Measurement of CD80, CD86, CD28 and CTLA-4 levels in human serum using conventional techniques

The measurement of these molecules in biological fluids is commonly carried out using an immunoassay-based technique such as (ELISA). (Cao *et al.*, 2012; Ip *et al.*, 2006; Kakoulidou *et al.*, 2007) Although ELISA is considered a sensitive method, it has potential cross-reactivity regarding the usage of specific antibodies. The cost associated with the antibody production, the analysis time, and the animals' use are the main drawbacks of using ELISA. An alternative, fast, sensitive, and relatively inexpensive technique for biologically active proteins such as the costimulatory molecules is a consistent demand.

1.4. Biological-based inhibitor of CD28-B7 CP

Inhibiting T-cell activation is one of the main therapeutic strategies in autoimmune diseases. For instance, in RA, interrupting the CD28-B7 pathway by an infusion protein CTLA4-Ig (Abatacept) is considered an efficient biological therapy, as shown in Figure 3. (Weisman *et al.*, 2006) Abatacept competitively binds to CD80/CD86 and inhibits its binding to the CD28 receptor, reducing T-cells' activation. (Xu *et al.*, 2012) Unlike Abatacept, aptamer-based medicines can be synthesized chemically in a reproducible approach that reduces the cost and the structural variations. (Kaur *et al.*, 2018) Several aptamers have been developed and shown to modulate the immune response by blocking or activating immune receptors, such as in cancer therapy. (Soldevilla *et al.*, 2016) CD80/CD86 selected aptamers are potentially therapeutic advancement for RA since they inhibit CP by interrupting the binding of CD28-B7, as in

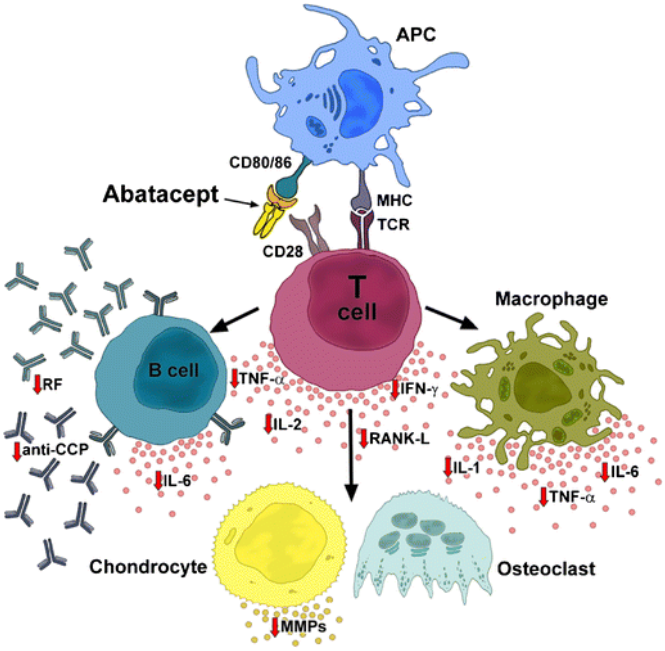

Figure 3: The inhibition of CD28-CD80/CD86 using CTLA4-Ig (Abatacept)(von Kempis et al., 2012)

Abatacept. This potential treatment will have several advantages over Abatacept, including production consistency.

2. Thesis hypothesis and Objectives:

The significance of the CD28-B7 costimulatory pathway and its related molecules in autoimmune diseases stems from their crucial role in immune system regulation. This pathway is essential for maintaining autoimmune responses, making it a central focus for understanding diseases like Rheumatoid arthritis (RA) and devising targeted diagnostics and treatments. Exploring these molecules as potential biomarkers and therapeutic targets holds promise for improving the management and outcomes of various autoimmune conditions. This thesis introduces a novel analytical workflow for developing aptamer-based diagnostics and therapeutics for autoimmune diseases, particularly focusing on CD28, CD80, CD86, and CTLA-4 in RA.

The main objectives of this thesis are *(i)* Investigating the potential of costimulatory proteins as biomarkers for Rheumatoid Arthritis (RA). This was accomplished by developing and utilizing LC-MS/MS in MRM mode and thoroughly analyzing RA patient samples.. ***(ii)*** Developing a sensitive and reproducible diagnostic-grade electrochemical aptasensor for one of the significant RA biomarkers, sCD80. ***(iii)*** Using the LC-MS/MS method, we are creating an analytical tool to explore the inhibition of selected aptamers of the CD28-B7 pathway, establishing a viable strategy for autoimmune disease therapy

3. In context

This thesis presents an innovative strategy for targeting the core pathway of Rheumatoid Arthritis (RA) from both diagnostic and therapeutic standpoints. This approach focuses on the CP molecule within this pathway, targeted by selecting a specific aptamer. These aptamers hold promise for the development of diagnostic sensors and therapeutic interventions. Mass

spectrometry plays a crucial role in both these aspects, discovering disease biomarkers and validating therapeutic molecules and diagnostic sensors.

Chapter 1 provides a comprehensive literature review on the role of mass spectrometry in aptasensor and aptamer-based therapeutic development. This chapter outlines the pipeline involved in developing aptasensors and aptamer-based therapeutics, highlighting the significance of mass spectrometry at various stages, such as biomarker discovery, bead-target confirmation, and validation.

Contrary to existing literature, which does not support the study of co-stimulatory molecules as confirmed diagnostic markers for RA, this project delves into a clinical study involving RA patients and healthy controls. The study focuses on measuring the concentrations of sCD80, sCD86, sCTLA-4, and sCD28 using a novel Multiple Reaction Monitoring (MRM)-tandem mass spectrometry method detailed in **Chapter 2** and published in Clinica Chemica Acta.

Chapter 3 centers on sCD80 as a potential biomarker and discusses the development of an aptasensor for quantifying this protein using electrochemical detection in human plasma. An MRM tandem mass (a high-resolution mass spectrometry method) was used to measure protein levels on a bead setup similar to the one used in the SELEX experiment, facilitating the evaluation of sCD80-selected aptamers.

Chapter 4 introduces a novel approach for assessing the inhibition activity of a drug (abatacept) and potentially other aptamers. Chapter 5 concludes the thesis by summarizing the entire work undertaken in this study and outlining avenues for future research.

References

Atzeni, F., Talotta, R., Masala, I. F., Bongiovanni, S., Boccassini, L. et Sarzi-Puttini, P. (2017, Aug). Biomarkers in Rheumatoid Arthritis. *Isr Med Assoc J*, *19*(8), 512-516. https://www.ncbi.nlm.nih.gov/pubmed/28825772

Buck, C. A. (1992, Jun). Immunoglobulin superfamily: structure, function and relationship to other receptor molecules [Research Support, U.S. Gov't, P.H.S. Review]. *Semin Cell Biol*, *3*(3), 179-188. https://doi.org/10.1016/s1043-4682(10)80014-5

Cao, J., Zou, L., Luo, P., Chen, P. et Zhang, L. (2012, Dec). Increased production of circulating soluble co-stimulatory molecules CTLA-4, CD28 and CD80 in patients with rheumatoid arthritis. *Int Immunopharmacol*, *14*(4), 585-592. https://doi.org/10.1016/j.intimp.2012.08.004

Chimenti, M. S., Triggianese, P., Conigliaro, P., Candi, E., Melino, G. et Perricone, R. (2015, Sep 17). The interplay between inflammation and metabolism in rheumatoid arthritis [Review]. *Cell Death Dis*, *6*, e1887. https://doi.org/10.1038/cddis.2015.246

Hock, B. D., Starling, G. C., Patton, W. N., Salm, N., Bond, K., McArthur, L. T. et McKenzie, J. L. (2004, Oct). Identification of a circulating soluble form of CD80: levels in patients with hematological malignancies. *Leuk Lymphoma*, *45*(10), 2111-2118. https://doi.org/10.1080/10428190410001712199

Ip, W. K., Wong, C. K., Leung, T. F. et Lam, C. W. (2006, Jul). Plasma concentrations of soluble CTLA-4, CD28, CD80 and CD86 costimulatory molecules reflect disease severity of acute asthma in children. *Pediatr Pulmonol*, *41*(7), 674-682. https://doi.org/10.1002/ppul.20432

Kakoulidou, M., Giscombe, R., Zhao, X., Lefvert, A. K. et Wang, X. (2007, Nov). Human Soluble CD80 is generated by alternative splicing, and recombinant soluble CD80 binds to CD28 and CD152 influencing T-cell activation [Research Support, Non-U.S. Gov't]. *Scand J Immunol*, *66*(5), 529-537. https://doi.org/10.1111/j.1365-3083.2007.02009.x

Kotulska, A., Kopeć-Mędrek, M., Grosicka, A., Kubicka, M., & Kucharz, E. J. (2015). Correlation between erythrocyte sedimentation rate and C-reactive protein level in patients with rheumatic diseases. *Reumatologia, 53*(5), 243-246. doi:10.5114/reum.2015.55825

Kaur, H., Bruno, J. G., Kumar, A. et Sharma, T. K. (2018). Aptamers in the Therapeutics and Diagnostics Pipelines [Review]. *Theranostics*, *8*(15), 4016-4032. https://doi.org/10.7150/thno.25958

Kay, J., Morgacheva, O., Messing, S. P., Kremer, J. M., Greenberg, J. D., Reed, G. W., Gravallese, E. M. et Furst, D. E. (2014, 2014/02/03). Clinical disease activity and acute phase reactant levels are discordant among patients with active rheumatoid arthritis: acute phase reactant levels contribute separately to predicting outcome at one year. *Arthritis Research & Therapy*, *16*(1), R40. https://doi.org/10.1186/ar4469

Soldevilla, M. M., Villanueva, H. et Pastor, F. (2016). Aptamers: A Feasible Technology in Cancer Immunotherapy [Review]. *J Immunol Res*, *2016*, 1083738. https://doi.org/10.1155/2016/1083738

Tector, M., Khatri, B. O., Kozinski, K., Dennert, K. et Oaks, M. K. (2009, Sep 22). Biochemical analysis of CTLA-4 immunoreactive material from human blood. *BMC Immunol*, *10*, 51. https://doi.org/10.1186/1471-2172-10-51

Uehara, M. et McGrath, M. M. (2019, Mar). The Role of Costimulatory Pathways in Transplant Tolerance [Research Support, Non-U.S. Gov't Review]. *Clin Lab Med*, *39*(1), 87-106. https://doi.org/10.1016/j.cll.2018.10.009

Walunas, T. L., Bakker, C. Y. et Bluestone, J. A. (1996, Jun 1). CTLA-4 ligation blocks CD28-dependent T cell activation [Research Support, Non-U.S. Gov't Research Support, U.S. Gov't, Non-P.H.S. Research Support, U.S. Gov't, P.H.S.]. *J Exp Med*, *183*(6), 2541-2550. https://doi.org/10.1084/jem.183.6.2541

Weisman, M. H., Durez, P., Hallegua, D., Aranda, R., Becker, J. C., Nuamah, I., Vratsanos, G., Zhou, Y. et Moreland, L. W. (2006, Nov). Reduction of inflammatory biomarker response by abatacept in treatment of rheumatoid arthritis [Clinical Trial, Phase II Multicenter StudyRandomized Controlled Trial Research Support, Non-U.S. Gov't]. *J Rheumatol*, *33*(11), 2162-2166. https://www.ncbi.nlm.nih.gov/pubmed/17014006

Wong, C. K., Lit, L. C., Tam, L. S., Li, E. K. et Lam, C. W. (2005, Aug). Aberrant production of soluble costimulatory molecules CTLA-4, CD28, CD80 and CD86 in patients with systemic lupus erythematosus. *Rheumatology (Oxford)*, *44*(8), 989-994. https://doi.org/10.1093/rheumatology/keh663

Xu, Z., Juan, V., Ivanov, A., Ma, Z., Polakoff, D., Powers, D. B., Dubridge, R. B., Wilson, K. et Akamatsu, Y. (2012, Nov 1). Affinity and cross-reactivity engineering of

CTLA4-Ig to modulate T cell costimulation. *J Immunol*, *189*(9), 4470-4477. https://doi.org/10.4049/jimmunol.1201813

Yamada, A., Salama, A. D. et Sayegh, M. H. (2002, Feb). The role of novel T cell costimulatory pathways in autoimmunity and transplantation [Review]. *J Am Soc Nephrol*, *13*(2), 559-575. https://www.ncbi.nlm.nih.gov/pubmed/11805188

CHAPTER 1

INTRODUCTION (REVIEW ARTICLE)
APTAMERS AND MASS SPECTROMETRY: PIONEERING INSIGHTS INTO BIOSENSOR TECHNOLOGY AND THERAPEUTIC ADVANCEMENTS

Abeer Malkawi[1], Mohamed Siaj[1*]

[1] Department of Chemistry, Université du Québec à Montréal, Montréal, H3C 3P8, Quebec, Canada

This chapter has been submitted to Critical Review in Analytical Chemistry,

* Email: siaj.mohamed@uqam.ca

CONTRIBUTION OF THE MAIN AUTHOR AND CO-AUTHORS

Abeer Malkawi and Prof. Mohamed Siaj conceived the idea of this review. Abeer Malkawi reviewed the literature and drafted the manuscript, and Prof. Siaj has critically reviewed the manuscript. The authors approved the current version of the manuscript for publication.

Abstract

Aptamers, single-stranded DNA, and RNA molecules have emerged as powerful agents capable of selectively binding to diverse biomolecules, including proteins, lipids, and metabolites. Their versatile nature allows them to engage in intricate interactions, forming complexes that yield analytical signals in vitro and evoke precise biological responses in vivo. This review underscores the multifaceted utility of aptamers, particularly in biosensor technology and biologics development. Notably, aptamers possess the unique ability to discern and interact with diverse biomolecular perturbations often associated with distinct disease phenotypes, distinguishing them from conventional biosensors.

Moreover, aptamers offer a distinct advantage by selectively binding to therapeutic targets associated with diseases, potentially enhancing clinical outcomes with heightened specificity and reduced side effects, setting them apart from antibodies. This comprehensive review casts a spotlight on the instrumental role of mass spectrometry (MS) in advancing biosensors and aptamer-based therapies across multiple developmental stages. From the initial selection of aptamers to their final applications and clinical validation, MS contributes significantly, especially in confirming ssDNA aptamer binding to target molecules.

Furthermore, this review delves into the intricate challenges encountered during this developmental journey, spanning the elucidation of aptamer-protein interactions and the comprehension of aptamer structural reassembly in vivo. Additionally, we highlight the significance of chemical refinements to aptamers, aimed at optimizing therapeutic outcomes while mitigating undesired effects. This in-depth exploration aims to foster a profound understanding of aptamer binding mechanisms, their pivotal role in addressing pressing analytical challenges, and their transformative potential in revolutionizing point-of-care diagnostics and personalized medicine.

Keywords:

Aptamer; Biosensor; SELEX; aptatherapy; Mass Spectrometry (MS)

1.1 Introduction

Laboratory medicine is the core of modern healthcare, underpinning diagnostic precision and therapeutic efficacy through bioanalytical methodologies. These methodologies are essential to laboratory practices, facilitating the quantitative elucidation of an array of biomolecular entities in biological specimens. This key role is paramount in affording diagnostic insights, monitoring treatment regimens, and pursuing scholarly inquiries across various disciplines, including clinical chemistry, pharmacology, toxicology, and molecular biology. The following explains important aspects of how different methods are used in laboratory medicine and highlights their various uses and ways they are used.

Bioanalytical methodologies demonstrate a versatile capacity to determine a broad spectrum of biomolecular entities, such as Proteins (e.g., enzymes, antibodies, cytokines, and hormones), Nucleic Acids (e.g., DNA and RNA moieties), Small Molecules (metabolites, pharmaceutical agents, toxicants), and Lipids (e.g., cholesterol, lipoproteins, and fatty acids). Several methodological paradigms are connected for bioanalysis, encompassing chromatography (e.g., high-performance liquid chromatography HPLC, gas chromatography GC), mass spectrometry (MS), Nuclear magnetic resonance (NMR), Immunoassays (e.g., immunoblotting, enzyme-linked immunosorbent assay ELISA), Polymerase Chain Reaction (PCR), Spectroscopy (e.g., UV-visible, infrared, fluorescence), Electrophoresis (e.g., gel-electrophoresis, and capillary electrophoresis(CE)), and biosensors (Aptasensor and immunosensor).

Identifying the ideal biomarker for disease diagnosis, prognosis, and therapeutics monitoring is the key feature for the success of personalized medicine and the enhancement of clinical outcomes, as most of the health conditions' phenotypes are associated with biomolecular disturbances. Although the genome, in some diseases, is the main cause of the condition, the small molecules (metabolomics) are the closest to the ongoing phenotypes' processes. The diagnostic methodology selection is based on the structure and size of the biomolecule. In the last couple of decades,

biosensor technology has played a significant role in laboratory medicine by introducing bedside tools for faster diagnosis or screening for crucial diseases, mainly those that require immediate interventions, such as infectious diseases, metabolic disorders such as diabetes Meletus, pregnancy test, and many others. (Barrera-Avalos et al., 2021; Gnoth & Johnson, 2014; Yoo & Lee, 2010)

Biosensors combine biology and technology to target molecules, such as proteins and small molecules, through their recognition parts. The specific binding of these recognition parts of the target molecules sends a measurable signal for quantitative or qualitative diagnostics. Biosensors are categorized based on the type of recognition materials (Enzyme, tissue, DNA) and the aptamer or antibodies. Oxidoreductases, polyphenol oxidases, peroxidases, and amino oxidases enzymes are common for biosensing. (Akyilmaz, Yorganci, & Asav, 2010; Venugopal, 2002; J. Wang, 2008)

The first tissue-based sensor was developed to detect the amino acid glutamine. (Rechnitz, 1978) Immunosensors depend on specific antibodies for the target molecules, such as rapid antigen testing for SARS-CoV-2 diagnosis. (Barrera-Avalos et al., 2021) Recently, aptamer-based biosensors have gained more attention in studying biomarkers and bioanalytical technology, such as aptamer-based biosensors for bacterial detection in sepsis. (H. Shen et al., 2016)

Another categorization of biosensors depends on the sensor platform and nanomaterials: Nanostructure metals; nanoparticles (NPs) (gold, silver, nickel, etc.), semiconductors (e.g., TiO_2, ZiO, SnO_2, CeO_2, etc.), and carbon material have been widely used in biosensors. For example, an indium (Conte et al.) oxide (In_2O_3) nanowire was used in label-free electrical detection of virus N-protein in acute respiratory syndrome. (Ishikawa et al., 2009) NPs were used in several studies to improve the sensitivity of glucose sensors. (Q. Yang et al., 2020) Graphene and its derivatives are used in biosensing due to their excellent sensing performance. (Bai, Xu, & Zhang, 2020) The main transducers and detection methods are electrochemical, optical, and gravimetric biosensors, mass-based sensing, and thermal biosensors. (Naresh & Lee, 2021)

The advantages of biosensors, from the speed of analysis, the lower cost, and the ease of use, help healthcare providers with instant diagnosis and intervention and improve health outcomes. These biosensors are utilized in one-time tests and real-time monitoring, such as glucose continuous monitoring that measures the glucose level 24 hours a day. (Jackson, Ahmann, & Shah, 2021) The real-time monitoring of bacterial growth using aptasensors can continuously and timely monitor internal infection and the effectiveness of antibiotics. (Song et al., 2019)

Antibodies and aptamers are the main recognition elements in the biosensors, where both could bind to the target molecule in vivo and might regulate its function therapeutically. Several antibodies and aptamers-based therapeutic molecules have been developed and are commercially available for treating many diseases, such as cancer, autoimmune disease, and organ transplant rejection. For instance, Muromonab-CD3 anti-CD3 antibody is an FDA-approved drug used in kidney transplant rejection, and the anti-epithelial growth factor receptor (anti-EGFR) Cetuximab is an available drug for colorectal cancer. (Lu et al., 2020) Macugen, RNA aptamer, is the first FDA-approved drug for treating wet AMD (age-related molecular degeneration). (Kourlas & Schiller, 2006) The development of these biologics for treatment and diagnosis must go through a rigorous process with multiple levels of control to ensure the specificity of the target molecules with minimal side effects on the patients.

MS has been utilized for over half a century in molecular characterization based on the mass-to-charge ratio (m/z). In bioanalysis, MS played a significant role in studying biological systems through structural analysis of single molecules (e.g., protein, lipid, and small molecules) and in global fashion (e.g., proteomics, glycomics, metabolomics, and lipidomics). In this review, we will focus on the role of mass spectrometry in advancing aptamer-based biosensor technology and therapeutic efficiency. In addition, we are highlighting the integration of aptamer recognition in the inlet methods of MS.

1.2 Aptamer-based biosensor

Biosensors have emerged as cutting-edge technology that has transformed the field of diagnostics and analysis. Among the various types of biosensors, aptamer-based biosensors have attracted significant attention due to their impressive versatility and specificity. Aptamers can bind specifically to target molecules accurately. The aptamer is a single-strand oligonucleotide folded in a three-dimensional structure upon binding with the target. (Ellington & Szostak, 1990) These distinctive characteristic forms the foundation of aptamer-based biosensors, enabling them to selectively detect a wide range of substances, from small molecules to complex biomolecules. Small molecules play an important role in biological processes and cell-signaling pathways. Many therapeutics drugs, toxins, metabolites, and sugar were targets for aptamer selection and aptasenosr development. In 1990 and 1992, the first RNA and DNA aptamers for small molecules were selected by Ellington and Szostak against organic dyes. (Ellington & Szostak, 1990, 1992)

Although RNA aptamers were most of the selected aptamers for small molecules until 2007, the high stability and the lower synthetic cost increased the produced DNA aptamers since then. (McKeague & Derosa, 2012) The label-free fluorescence DNA aptasensor for Ochratoxin monitoring was developed as a tool for food safety. (McKeague et al., 2014) For highly selective, sensitive, and rapid screening of antibiotics, a multiplex aptasensing platform was elaborated using the fluorescence resonance energy transfer technique (FRET). (Youn et al., 2019) Several aptasensors for the narrow therapeutic index drugs, such as theophylline, were developed for serum drug monitoring. (Ferapontova, Olsen, & Gothelf, 2008) Aptasensors for small molecules were extensively reviewed by Franziska Pfeiffer and Günter Mayerin (2016). (Pfeiffer & Mayer, 2016) Different examples of aptasensors for small molecules are summarized in Table 1.1.

Although proteins are the biggest group of target molecules, a few are detected using aptasensors. Aptamer binds to more complex molecules through hydrogen bonding, electrostatic interaction, shape complementary, and stacking interaction. This enables the selection of high-affinity aptamer

and more than one aptamer for the same target, allowing a sandwich-assay-based biosensor. (Strehlitz, Nikolaus, & Stoltenburg, 2008) Abdollah Salimi et al. (2014) developed a highly sensitive electrochemical aptasensor for immunoglobulin E (Bilik et al.) based on a sandwich assay using an enzyme-linked aptamer. (Salimi, Khezrian, Hallaj, & Vaziry, 2014) Some examples of protein aptasensors are available in Table 1.1.

Incorporating aptamers into biosensor platforms has opened new avenues across multiple domains, including medical diagnostics, (Hong, Li, & Li, 2012) environmental monitoring, (S. H. Kim, Thoa, & Gu, 2019), and pharmaceutical research. (Mo et al., 2022) These biosensors offer several advantages over conventional methods, including their rapid response time, portability, and capability to operate within intricate sample environments. By combining the binding affinity of aptamers with the signal transduction capabilities of biosensor platforms, these systems deliver robust and highly sensitive detection mechanisms. Scheme 1.1 shows the steps of aptasensor development.

Herein, we embark on a comprehensive exploration of aptamer-based biosensors. We focus on shedding light on their underlying design principles, diverse applications, and profound impact on analytical sciences. Through this exploration, we aim to unveil the role of aptamer-based biosensors in addressing prevailing analytical challenges, their potential to reshape point-of-care diagnostics, and their pivotal role in advancing the frontiers of personalized medicine. By unraveling the intricacies of aptamer-based biosensors, we anticipate a deeper understanding of their binding mechanisms and the broader integration of these biosensors into a wide array of analytical platforms.

1.2.1 Aptamer selection

Selecting aptamers is critical in harnessing their binding competence for various applications, especially in developing aptamer-based biosensors. Diverse selection approaches are employed for aptamers that are significant in expanding biosensor technology's scope.

The systematic Evolution of Ligands by Exponential Enrichment (SELEX) is the cornerstone of aptamer selection. It involves iterative binding, separation, and amplification cycles to enrich aptamers with high affinity for the target. It begins with a random library of oligonucleotides (single-strand DNA or RNA (ssDNA and ssRNA)) subjected to binding with the target. A typical oligonucleotide library consists of 10^{13}-10^{15} random sequences with 15-80 random bases. (de-los-Santos-Álvarez, Lobo-Castañón, Miranda-Ordieres, & Tuñón-Blanco, 2008) Unbound sequences are eliminated, while bound sequences are amplified and used as the input for subsequent rounds. In RNA aptamer, reverse transcription is needed before amplification, and the transcription step should be performed before the next cycle. SELEX can be tailored for specific target molecules, making it highly versatile. In-vitro SELEX has been reviewed extensively in different reviews. (Chai, Xie, & Grotewold, 2011; Fitzwater & Polisky, 1996; Kenan & Keene, 1999) Several modified SELEX Approaches enhance selection efficiency. These include Cell-SELEX, which employs live cells as targets, and Capture-SELEX, which incorporates solid-phase capture steps. These variations enable aptamer selection against complex targets like whole cells or tissues. (Zhao, Pei, Parekh, Salazar, & Zu, 2014) In Cell-SELEX, entire cells are targeted, mimicking physiological conditions. This approach yields aptamers targeting specific cell-surface markers, crucial for applications like targeted drug delivery. (Zhao et al., 2014)

Counter-SELEX is employed as subtractive steps to enhance aptamer specificity to eliminate sequences that bind non-specifically to undesired targets. This strategy refines the aptamer pool, enhancing selectivity for the intended target. For instance, using several proteins or cells negatively expressed proteins when selecting aptamer to a specific protein in vitro or Cell-SELEX in vivo. (Haghighi, Khanahmad, & Palizban, 2018)

Advancements in high-throughput technologies have revolutionized aptamer selection. Microfluidic-based methods reduce the number of selection rounds and obtain the desired aptamer

within a few days. Different technology is involved in the microfluidic-based selection, such as the microarray-chip method, which simultaneously screen sequences against thousands of target molecules, expediting the process and increasing the chances of identifying high-affinity aptamers. In 2017, Liu et al. developed a protein microarray microfluidic (PMM-SELEX) chip for aptamer selection of lactoferrin. (Xiaohui Liu, Li, Jia, Chen, & Xu, 2017)The same group developed a novel SELEX microarray platform with a smart scanner to simplify the fabrication and experimental procedure. (Yu, Li, Sun, Xu, & He, 2019) Next-generation sequencing (NGS) has revolutionized the landscape of aptamer selection. It enables the parallel sequencing of millions of aptamer candidates after each selection round, providing comprehensive insights into the enrichment process. The first application of NGS in SELEX was in 2002 by Emmanuelle Roulet et al. (Roulet et al., 2002) Since then, this approach has offered a high-throughput method and facilitates a deeper understanding of aptamer populations during selection. In addition, NGS combined different techniques, such as CE, as a quantification method of enrichment and enhancing enrichment with fewer rounds. (Riley et al., 2015) CE-SELEX leverages the separation capabilities of CE to screen large aptamer libraries rapidly. It involves labeling aptamer candidates and monitoring their migration in response to binding. Martínez-Roque et al. (2022) employed CE-SELEX combined with NGS to select a specific ssDNA aptamer for SARS-CoV-2 Spike glycoprotein. (Martinez-Roque et al., 2022) This technique streamlined the process and yielded aptamers with promising affinity and specificity. Surface Plasmon Resonance (SPR)-Based SELEX, known for real-time binding analysis, has been integrated into aptamer selection. It allows the direct monitoring of aptamer-target interactions. In a study by Eric Dausse et al. (2016), an RNA aptamer for structured RNA was selected using SPR-SELEX, showcasing the potential of this high-throughput technique to speed up the selection process as the selection and evaluation performed simultaneously. (Dausse et al., 2016) Computational Approaches in High-Throughput Selection methods are also gaining traction for aptamer selection. In-silico libraries generated through algorithms are virtually screened against target structures.

Yaroslav Chushak et al. (2009) developed an In silico selection method for RNA aptamers for small molecule targets. (Chushak & Stone, 2009) Methods and applications of In silico aptamer design and modeling Reviewed extensively by Buglak et al. (2020). (Buglak, Samokhvalov, Zherdev, & Dzantiev, 2020) High-throughput techniques offer unparalleled efficiency. Still, challenges remain in data analysis, bioinformatics, and the need for refined selection strategies. As technology advances, machine learning and artificial intelligence (AI) integration hold promise for accelerating data processing and enhancing aptamer selection. High-throughput techniques have catalyzed a paradigm shift in aptamer selection, expediting the discovery of aptamers with remarkable affinity and specificity. Real-world examples from microarray-based screening, NGS, CE-SELEX, SPR-based SELEX, and computational approaches underscore the transformative impact of these techniques. As researchers continue to explore and refine these methods, aptamer-based biosensors are poised to revolutionize diverse fields, from diagnostics to therapeutics. SomLogic™ Scan (https://somalogic.com/somascan-platform/) is a novel technology for screening about 7000 proteins in 10 µL of human plasma based on a specific aptamer for each protein is now made available for proteomics research. (Candia, Daya, Tanaka, Ferrucci, & Walker, 2022)

Aptamer selection is challenging, including ensuring aptamer stability and minimizing non-specific interactions. The continued exploration of novel selection approaches promises to unlock even greater potential in this exciting field.

1.2.2 Aptamer characterization

Selected aptamer characterization maximizes utility across various applications, including biosensing and therapy. This section underscores the profound significance of aptamer characterization, delineating its fundamental components and implications. A paramount facet of aptamer characterization involves unraveling their structural intricacies. Circular dichroism (CD), NMR, and X-ray crystallography illuminate aptamers' folding patterns and interactions and are

used for aptamer structural analyses. Takumi Ishizuka et al. (2017) employed NMR spectroscopy to illuminate the unique structure of a G-quadruplex DNA aptamer targeting thrombin. (Ishizuka, Yamashita, Asada, & Xu, 2017) The Chrystal structure of aptamers for small molecules obtained by x-ray or NMR and deposited in the protein data bank (PDB) was revised by Franziska Pfeiffer and Günter Mayer (2016). (Pfeiffer & Mayer, 2016) Studying the aptamer's physicochemical characteristics and target binding is critical for biosensing and therapeutics/diagnosis application, as reviewed by Plach et al. (2019). (Plach & Schubert, 2020)

Aptamer functionality hinges on their binding strength with targets. SPR, isothermal titration calorimetry (ITC), and fluorescence spectroscopy offer quantitative insights into binding affinity and kinetics. The thermodynamic-based technique, ITC, is useful for studying the aptamer-target binding affinity, such as determining the binding affinity between a DNA aptamer and 5-Hydroxymethylfurfural in food processing and storage applications. (X. Liu et al., 2023) In another study, the Kd value for aptamer selected against Kanamycin B was determined by SPR depending on the change in refractive index upon binding. (Kwon, Chun, Jeong, & Yu, 2001)

The specificity of aptamers towards their intended targets is essential, where several techniques encompassing competitive binding assays and selectivity profiling against similar molecules provide a nuanced understanding of aptamer specificity. The specific selection of the aptamer against enantiomer is another advancement in aptamer application, as in biosensing and target specific selector. Stereospecific DNA aptamer for the D-enantiomer of oligopeptide arginine-vasopressin was used as a target-specific chiral selector for HPLC to study the binding mechanism and the optimal elution conditions for the specific binding. (Michaud et al., 2003)

Aptamer stability under physiological conditions is instrumental for their functionality. Evaluating thermal stability and denaturation characteristics offers insights into aptamer robustness. Additionally, tracking aptamer (un)folding transitions is essential for the rational design of structure-switching aptasensors. In 2005, Nitiu et al. developed a novel In vitro selection method

to isolate the structure switching aptamers and modify it with fluorophore for sensing application. (Nutiu & Li, 2005)

Analogously, Ponikova et al. (2011) coupled CD spectroscopy, temperature-gradient gel electrophoresis (TGGE), and differential scanning calorimetry (DSC) to delineate the stability of a DNA aptamer dimer binding to the anticoagulant thrombin. (Ponikova, Tluckova, Antalik, Viglasky, & Hianik, 2011) In the study by Lin et al. (2011), the two-thrombin binding aptamers (15-mer and 29-mer) were characterized through CD, ITC, and SPR to ascertain the conformational change and specificity. (Lin et al., 2011)

Noteworthy challenges encompass pursuing accurate and reproducible data, especially for intricate interactions and atypical aptamer structures. Innovations in single-molecule techniques and computational simulations hold the potential to refine and augment aptamer characterization strategies. In summary, the characterization of aptamers occupies a pivotal niche in comprehending their behavior, enhancing their utility, and customizing them for specific applications. Employing various techniques to assess structural attributes, binding kinetics, specificity, and stability augments our grasp of aptamers. It stimulates their deployment in diverse spheres, spanning diagnostics to targeted therapeutics.

1.2.3 Aptasensor material platform

After selecting the most selective and high-affinity aptamer with good structural and functional characterization, establishing aptasensor hinges on the judicious selection of appropriate material platforms as foundational matrices for anchoring aptamers with high surface area and sensitive transducers. The manifold material platforms employed for immobilizing aptamers unravel their role in developing biosensors based on the application. In certain circumstances, the aptasensor signal depends on the type of the selected nanomaterial.

Gold nanoparticles (AuNPs), owing to their unique properties, have extensive utilization in aptasensors. (Malkawi *et al*,2023) Their high surface area facilitates aptamer loading and rapid target binding. AuNPs are amenable to colorimetric, optical, and electrochemical detection methods. Taking advantage of the change in the dispersion-aggregation state of AuNPs when interacting with the target, aptamer-AuNPs conjugate can be used as a rapid colorimetric detection method for different biomolecules. Giorgi-Coll et al. (2020) developed a colorimetric aptasensor for IL-6 as a biomarker in meningitis.(Giorgi-Coll, Marin, Sule, Hutchinson, & Carpenter, 2019) A thiol-modified aptamer conjugated with AuNPs was used to develop a colorimetric aptasensor for detecting thrombin. (Yi Peng, 2013) Different techniques have been incorporated with AuNPs-based aptasensors, such as SPR and Surface-enhanced Raman spectroscopy (SERS), to improve the sensitivity and enhance the colorimetric signal. (N. H. Kim, Lee, & Moskovits, 2010) Besides colorimetric-based aptasensors, AuNPs are widely used in electrochemical-based aptasensors. Different examples are shown in Table 1.1

Quantum dots (QDs) are semiconductor materials with exceptional FRET donor–acceptor properties. Jon et al. (2007) developed a novel QDs-aptamer as a carrier for doxorubicin for prostate cancer sensing and imaging. (Bagalkot et al., 2007) Graphene and Graphene Oxide (GO) materials offer immense surface areas and excellent conductivity, fitting for various detection methods. The strong interaction between aptamers and graphene surfaces enhances sensor sensitivity and leads to high-density platforms for detecting a wide range of targets. J JI et al. (2020) adeptly utilized single-layer graphene in label-free shear horizontal surface acoustic wave (SH-SAW) aptasensor for In vitro endotoxin detection. (Ji et al., 2020) RNA aptamer-GO conjugation was used for theophylline detection in serum using the questioning property of GO. (Ling et al., 2016)

The versatility of carbon nanotubes (CNTs) has been harnessed to bolster aptasensor sensitivity. Capitalizing on their expansive surface area and electronic properties, Abnous K et al. (2017) devised a remarkably sensitive amperometric aptasensor for Ochratoxin detection using carbon

nanotubes as the foundational scaffold. (Abnous, Danesh, Alibolandi, Ramezani, & Taghdisi, 2017)

Polymer matrices offer a versatile scaffold for aptamer immobilization, promoting aptamer stability. Their 3D environment can be coupled with optical and electrochemical detection. Peiyan Shen et al. (2022) adeptly employed a smart photonic polymer hydrogel to anchor aptamers targeting human serum thrombin, culminating in an effective electrochemical aptasensor by measuring the Debye diffraction ring. (P. Shen et al., 2022) Nonporous structures, including mesoporous silica nanoparticles (MSNs), enhance sensor performance by facilitating aptamer loading and target accessibility—nanoporous materials aligned well with optical and electrochemical detection methods. A noteworthy case is the utilization of MSNs by Hongxia Tan et al. (2019) to immobilize aptamers for aflatoxin B1 detection. (Tan et al., 2019) Also, Metal-Organic Frameworks (MOFs), characterized by tunable crystalline structures, emerge as platforms for tailored interactions with aptamers. Their adaptability suits both optical and electrochemical detection methods. Xiaoxue Fu (2019) work showcased the creation of a MOF-based electrochemical aptasensor for Thrombospondin-1 (TSP-1) detection as a biomarker for high-risk cardiovascular disease (CVD). (Fu et al., 2019) The recent advance in nanomaterial application in aptasensors for medical diagnosis has been reviewed by Olubunmi et al. (2021). (Ayodele, Adesina, Pourianejad, Averitt, & Ignatova, 2021)

The selection of a material platform must consider the target nature, aptamer stability, and desired detection method. Overcoming challenges like optimal surface coverage and non-specific interactions warrants innovative solutions. Advances in nanomaterial synthesis and functionalization techniques hold promise for refining aptasensor performance. In summary, material platforms for aptamer immobilization decisively shape the landscape of aptasensor technology. Real-world instances underscore their versatility and impact. The adaptability of platforms like gold nanoparticles, graphene-based materials, carbon nanotubes, polymer matrices,

nanoporous structures, and metal-organic frameworks to various detection methods paves the way for innovative applications in medical diagnostics, environmental monitoring and beyond.

1.2.4 Aptasensor detection techniques

In modern biosensing, aptasensors stand out for their exceptional specificity and affinity, underpinned by diverse detection mechanisms. Among the frequently employed methods, optical, electrochemical, and piezoelectric approaches emerge as stalwarts, each grounded in distinct principles, offering unique advantages and enriching the expansive landscape of aptasensor applications. Using label strategies in aptasensors requires a good knowledge of the aptamer structure and the binding site. The label-free aptasensor technique is suitable for real-time monitoring and developing analytical assays.

Optical aptasensors operate on the principle of exploiting alterations in light properties upon aptamer-target interaction. This interaction induces resonance, color, or fluorescence changes that are then transduced into quantifiable signals. SPR is a powerful optical technique where aptamer-target binding shifts the resonance angle. Different technologies were incorporated with SPR for more sensitive and robust optical aptasensors, such as developing plastic optical fiber POF-SPR for thrombin detection. This effectively translates molecular interactions into detectable shifts in light properties. (Cennamo et al., 2019) Colorimetric aptasensors exhibit visible color changes due to binding events, allowing facile visual detection. AuNPs-aptamer conjugate was used as a simple colorimetric method for protein detection, taking advantage of color change due to gold aggregation. (Y. Wang et al., 2008) Fluorescence-based aptasensors, on the other hand, harness the change in fluorescence intensity, providing a platform for highly sensitive and quantitative measurements. Fluorescence aptasensors are widely employed due to the ease of aptamer modification with fluorophores and quencher molecules and the advantage of real-time detection. Molecularly engineered light-switching excimer aptamer probes were developed for fluorescence

detection of platelet-derived growth factor (PDGF). (C. J. Yang, Jockusch, Vicens, Turro, & Tan, 2005)

Electrochemical aptasensors function by exploiting changes in electrical properties due to aptamer-target interactions by probing the electron transfer feature of the redox moieties. These interactions result in current, potential, or impedance shifts, which are then transduced into quantifiable signals. Techniques like cyclic voltammetry (CV) measure changes in current at varying potentials, while amperometry records changes in current at a constant potential. Electrochemical impedance spectroscopy (EIS) gauges changes in the impedance of the electrode-solution interface. In an electrochemical thrombin aptasensor, forming a G-quadruplex structure upon aptamer binding with the target shielded the redox moiety (Methylene blue MB) from the electrode surface. (Xiao, Lubin, Heeger, & Plaxco, 2005) The method's real-time monitoring, exceptional sensitivity, and adaptability to miniaturization make it an invaluable asset in point-of-care diagnostics and food safety.

Piezoelectric aptasensors rely on the principle of monitoring shifts in mass due to aptamer-target binding facilitated by piezoelectric materials like quartz crystal microbalances (QCMs) or SAW devices. As binding occurs, the oscillation frequency of the piezoelectric device changes due to the added mass of the bound target. This change is then translated into quantifiable signals. This label-free method has garnered attention for its real-time detection and compatibility with continuous measurement. Tombelli et al.'s (2005) work with QCM-based aptasensors for detecting HIV-1 Tat protein is a notable example of this technique's application in medical diagnosis. (Tombelli, Minunni, Luzi, & Mascini, 2005)

In summation, aptasensor detection methods - optical, electrochemical, and piezoelectric - each founded on distinct principles, empower biosensing with their capacity to translate molecular interactions into quantifiable signals. The intricate dance between aptamer and target within each

detection mechanism transforms minute interactions into tangible and meaningful data, thus spotlighting the versatility and transformative potential inherent in aptasensors.

1.2.5 Biosensor analytical and clinical validation

The validation of biosensors through analytical and clinical dimensions is a cornerstone in affirming their credibility, precision, and applicability across diverse contexts. Commencing the journey of analytical validation entails a rigorous evaluation of biosensor performance parameters, ensuring accuracy, sensitivity, specificity, and reproducibility. Crucial parameters, including the limit of detection (LOD), the limit of quantification (LOQ), linearity, repeatability, and specificity, undergo meticulous scrutiny. Different validation criteria and guidelines are found to increase the specificity and improve the precision of analytical methods, such as the Food and Drug Administration (FDA), the International Council on Harmonization (ICH) guidelines, and the European Medicines Agency (EMA). Most validation studies on biosensors rely on experimental way (by performing validation experiments using standard materials), while few studies focus on computational modeling (In silico). Using the experimental validation method, Zheng et al. presented a specific and selective aptasensor for sulfadiazine detection in food and environment. (Zheng, Yang, Sun, Zhang, & Le, 2023) In 2014, Aseris et al. developed a computational model for glucose biosensor validation using competitive substrate conversion. (13) Some of the existing research contributions in biosensor validation have been reviewed by Meti et al. (2017). (Sangam, 2017)

Beyond the confines of the analytical performance in the laboratory, clinical validation ventures into authentic scenarios, assessing biosensor performance amidst real-world complexities. This phase focuses on the ability of the developed and validated biosensor to be utilized for diagnostics purposes with high clinical accuracy and specificity. In clinical validation, sample matrices, interferences, and potential variabilities assume central roles in using this device in clinical practice. An illustration unfolds in validating an aptamer-based biosensor for prostate-specific

antigen (PSA) detection, meticulously undertaken by Cao et al. (2018), wherein clinical immunoassays were invoked for comparative analysis. (Cao et al., 2018) In Ramezani's work in 2017, two types of aptasensors for streptomycin detection were developed and validated in milk and serum as a tool for antibiotics monitoring. (Ramezani, Abnous, & Taghdisi, 2017)

Navigating through analytical and clinical validation comes with challenges, ranging from sample heterogeneity to inter-laboratory deviations and latent biases. Methodical validation proactively averts misleading outcomes, instills user reliance, and steers the biosensor endeavor toward regulatory compliance. Successful validation is not merely an exercise in demonstrating sensor proficiency; it is a gateway to anchoring biosensors in practical medical paradigms, catalyzing advancements in patient care. As we peer into the future, the synergistic influence of microfabrication, nanotechnology, and machine learning (ML) is poised to amplify validation methodologies, augmenting sensor precision and accuracy. Furthermore, integrating biosensors into point-of-care and remote monitoring scenarios guides a demand for robust validation paradigms, resonating with the urgency of prompt and dependable decision-making.

Table 1.1. Examples of aptamer-based biosensors in literature for different applications.

Target molecule	**Type of aptamer**	**Aptamer Selection method**	**Aptamer/aptasensor Characterization**	**Biosensor platform**	**Biosensor Detection method**	**Biosensor application**	**Reference**
Ochratoxin	DNA	In vitro-SELEX	QGRS Mapper and RNA secondary structure analysis software for G-quadruplex and secondary structure analysis. Kd determination Magnetic Beads-Based Isocratic Elution Assay	Syper green-based biosensor platform	Label-free Fluorescence detection method	Food safety monitoring	(McKeague et al., 2014)
Multiplexed antibiotics (sulfadimethoxi	DNA	Sulfadimethoxine and Ampicillin: Magnetic beads-SELEX	Kd determination by fluorescence assay	DNase I-assisted cyclic enzymatic signal amplification (CESA) method combined with	Fluorescence resonance energy transfer (FRET) strategy	Rapid screening of multiple	(Youn et al., 2019)

Target molecule	Type of aptamer	Aptamer Selection method	Aptamer/aptasensor Characterization	Biosensor platform	Biosensor Detection method	Biosensor application	Reference
ne, kanamycin, and ampicillin)		Kanamycin: Affinity chromatography - Invitro selection		aptamer/graphene oxide complex		antibiotics (Milk)	
Progesterone	DNA	In Vitro-SELEX	Kd determination using fluorescence assay and EIS Target binding conformation using CD	Disulphide-modified aptamer on gold electrode	Label-free impedometry (EIS)	Monitoring Endocrine-disrupting chemicals in drinking water and food	(Contreras Jimenez et al., 2015)
IgE	RNA	In vitro-SELEX	SEM and electrochemical (CV, EIS)	Enzyme-linked aptamer sandwich assay using glassy carbon electrode modified with carbon	DPVs	Increase the sensitivity and selectivity of	(Salimi et al., 2014)

Target molecule	Type of aptamer	Aptamer Selection method	Aptamer/aptasensor Characterization	Biosensor platform	Biosensor Detection method	Biosensor application	Reference
				nanotubes/ionic liquid/chitosan nanocomposite		protein detection	
IgE	RNA	In vitro-SELEX	Cell-based ELISA for IgE-receptor binding assay Kd determination by nitrocellulose filter binding experiment	QCM	piezoelectric	Measuring IgE in serum	(Wiegand et al., 1996), (Yao et al., 2009)
postoperative lung cancer tissue,	DNA	Cell-SELEX	Validation of aptamer binding cancer cells using confocal microscopy experiment	MB-labeled aptamer on Screen-printed gold electrode	LSWV	Detection of cancer-derived protein in	(Zamay et al., 2016)

Target molecule	**Type of aptamer**	**Aptamer Selection method**	**Aptamer/aptasensor Characterization**	**Biosensor platform**	**Biosensor Detection method**	**Biosensor application**	**Reference**
biomarkers proteins						crude blood plasma	
Thrombin	RNA	Toggle SELEX	nitrocellulose-filter binding for Kd determination	Gold Nanogab-sensors	EIS	Detection of thrombin using specific aptamer and antibody simultaneously	(Schlecht, Malave, Gronewold, Tewes, & Lohndorf, 2006), (White et al., 2001)

Target molecule	**Type of aptamer**	**Aptamer Selection method**	**Aptamer/aptasensor Characterization**	**Biosensor platform**	**Biosensor Detection method**	**Biosensor application**	**Reference**
SARS-COV-2 S1 protein	DNA	In vitro-SELEX	Binding affinity, functional binding, and cross-reactivity were assessed by biolayer interferometry	Thin film gold electrode	EIS	Diagnosis of SARS-CoV-2	(Lasserre et al., 2022)
Irinotecan (Anti-neoplastic drug)	DNA	Displacement selection technique		Streptavidin-coated chip functionalized with biotinylated aptamer hybridized with complementary DNA	SPR	Therapeutic Drug monitoring	(Puscasu, 2021)

Target molecule	**Type of aptamer**	**Aptamer Selection method**	**Aptamer/aptasensor Characterization**	**Biosensor platform**	**Biosensor Detection method**	**Biosensor application**	**Reference**
epithelial ovarian cancer marker CA125	DNA	One-pot SELEX	Affinity determination by affinity prop capillary electrophoresis	A gold nanoparticle (AuNPs)/gallium nitride (GaN) Schottky junction	PEC (photoelectrochemical)	Cancer Diagnosis	(D. Hu et al., 2020)

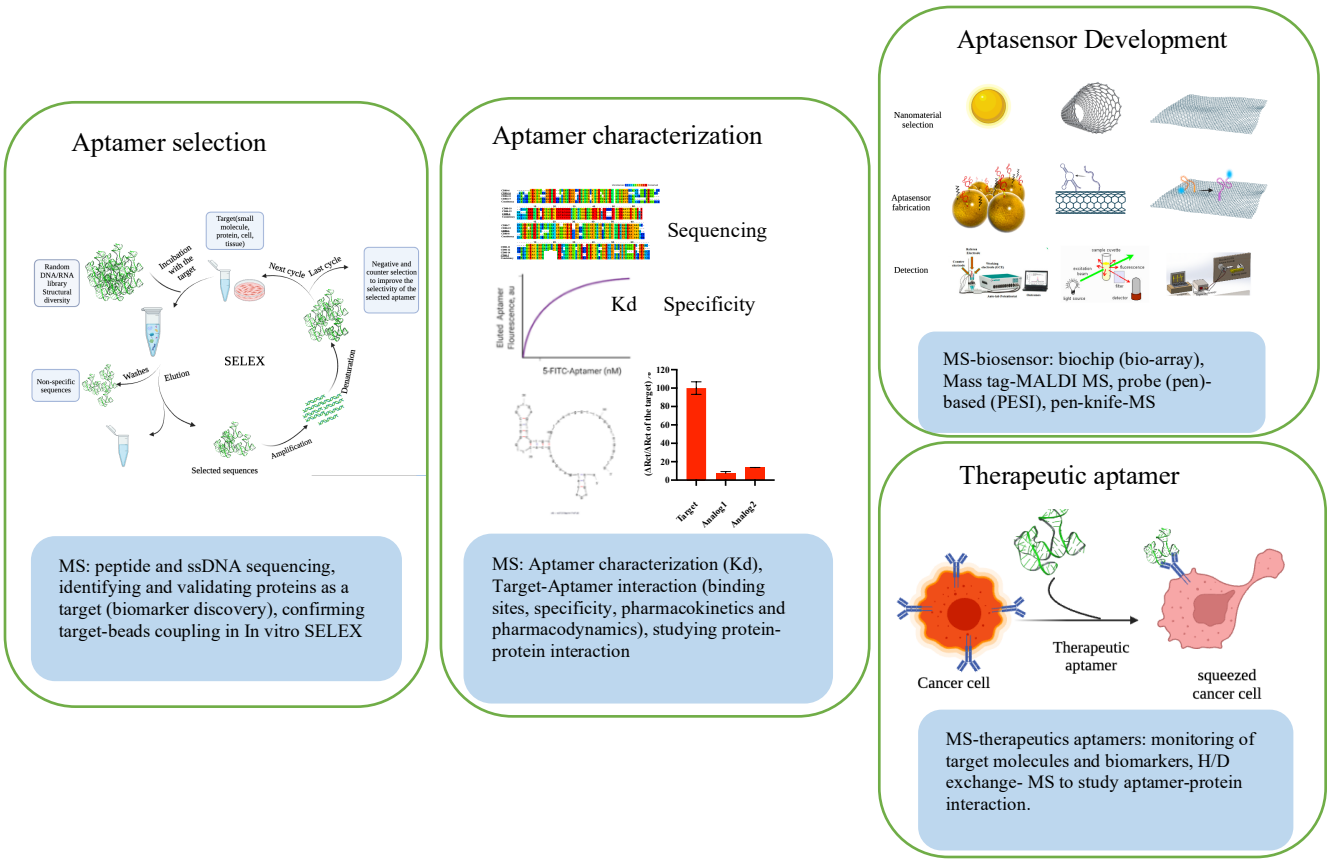

Scheme 1.1. Schematic illustration of the steps of aptasensor and therapeutic aptamer development and the role of MS in each step.

1.3 Aptamer-based therapy

Aptamer-based therapy is an emerging realm within biopharmaceutical research, capitalizing on the distinctive characteristics of aptamers to pave novel paths in precision medicine. Herein, A comprehensive exploration of aptamer-based therapy, unraveling its foundational theories, its application across diverse medical domains, case studies, the challenges encountered, and the intricate developmental process.

Aptamer-based therapy rests upon the elegant principle of molecular recognition. Aptamers, short strands of nucleic acids, possess an innate ability to precisely bind to specific targets such as proteins, cells, or even infectious agents. This capability forms the basis for creating therapeutic strategies that selectively interact with disease-related targets while avoiding non-disease-associated entities. The discovery of the small RNA molecules encoded by the human deficiency virus (HIV) that can bind to endogenous proteins and modulate their activity suggested using nucleic acid (RNA and DNA) as a therapeutic drug agent. Sullenger et al. 1990 developed the first RNA aptamer that binds to a viral protein and prevents viral replication. (Marciniak, Garcia-Blanco, & Sharp, 1990)

The high specificity, selectivity, stability, and low immunogenicity of aptamers increase the attention toward using these nucleic acids as alternatives to antibodies in therapy. Despite the increasing number of developed aptamers for therapeutic application, Macugen (anti- vascular endothelial growth factor (VEGF) aptamer) is the first FDA-approved therapeutic aptamer for treating AMD. (Ng et al., 2006) Recently, in 2023, Avacincaptad pegol, or Zimura, received full FDA approval as another treatment for AMD. (Drolet, Green, Gold, & Janjic, 2016) Other anti-angiogenic aptamers, Fovista and Pegnivacogen, are in advanced clinical trials for AMD treatment. (Prante, Segal, Scheper, Bahnemann, & Walter, 2020) More aptamers, such as anti-thrombin, are now being developed for systemic administration (Tasset, Kubik, & Steiner, 1997) and factor IXa (Sullenger, Woodruff, & Monroe, 2012), which are targets in the bloodstream. As well as the anti-

cell-surface targets, such as the anti-epithelial growth factor receptor (anti-EGFR). (Y. Liu et al., 2009)

The application of aptamer-based therapy encompasses a wide array of medical domains. In cancer therapy, aptamers are ingeniously employed as molecular guides to steer chemotherapy agents directly to cancer cells, sparing healthy cells from damage. Cardiac disorders benefit from aptamers tailored to hinder proteins contributing to the progression of diseases. Infectious diseases, too, experience the positive impact of aptamer-based antiviral agents that impede the replication of viruses. Different examples of therapeutic aptamers are summarized in Table 1.2.

Therapeutic aptamers act as agonists or antagonists by activating or inhibiting a protein-protein interaction. A 30 aptamer was developed against the oligomeric state of the extracellular domain of Human epidermal growth factor receptor-3 (HER3), which promotes protein oligomerization. OBJ The first antagonist aptamer was developed in 1992 against human thrombin, which acts as an antithrombosis agent. (Ellington & Szostak, 1992)

The efficiency of these therapies is determined in a dual-phase evaluation process. In vivo evaluation involves studying the aptamer's effects on living organisms. Animal models observe how the treatment influences disease progression and potential side effects. On the other hand, In vitro studies involve conducting experiments in controlled laboratory environments, often utilizing cell cultures. These studies help researchers understand how aptamers interact with target molecules and cells. Importantly, both evaluation phases ensure the therapy's safety and efficacy, paving the way for potential human applications.

While aptamer-based therapy shows remarkable promise, challenges like aptamer stability within the complex human body and efficient delivery to the right places persist. Nevertheless, progress is underway as scientists refine aptamer development methodologies and explore innovative delivery systems.

Aptamer-based therapy stands at the vanguard of precision medicine. By orchestrating interactions at the molecular level, aptamers offer potential breakthroughs in treatment strategies. The journey encompasses theoretical foundations, applications, real-world applications, and meticulous evaluations to ascertain efficacy. This manuscript strives to illuminate the path of aptamer-based therapy charts with the aspiration of advancing medical science and ultimately improving patient outcomes.

Table 1.2. Examples of aptamers selected for therapeutic application.

Aptamer	Kd (nM)	Selection Approach	Target	Type of nucleotide	Therapeutic application	Reference
Tog25	1-4	Toggle-SELEX	Thrombin	RNA	Anti-coagulant	(White et al., 2001)
RNA pseudoknots	1	In vitro-SELEX	HIV-1 reverse transcriptase	RNA	Prevent virus replication	(Tuerk, MacDougal, & Gold, 1992)
RNA aptamer	0.35	In vitro-SELEX	Fibroblast growth factor (FGF	RNA	Angiogenesis	(Jellinek, Lynott, Rifkin, & Janjic, 1993)
D17.4	10	In vitro-SELEX	IgE	ssDNA	Allergic diseases	(Wiegand et al., 1996)
Ligand 14.12	3	In vitro-SELEX	L-selectin	RNA	Modulate inflammation	(O'Connell et al., 1996)
Interferon-γ	68	In vitro-SELEX	Interferon-γ	RNA	Inhibit the interaction of IFN-γ with its receptor in lung carcinoma and inflammatory disease	(Kubik, Bell, Fitzwater, Watson, & Tasset, 1997)
aptCTLA-4	11.84	Cell-SELEX	CTLA-4	DNA	Suppress tumor cell growth	(Huang et al., 2017)
B4	5	In vitro-SELEX	HIV gp120	RNA	Inhibit viral infectivity	(Khati et al., 2003)
A30	45	In vitro-SELEX	HER3	RNA	Inhibit tumor development	(Chen et al., 2003)
14F	0.0003	In vitro-SELEX	Keratinocyte growth factor	RNA	Inhibit epithelial hyperproliferation	(Pagratis et al., 1997)
AP-9R	54.29	Cell-SELEX	CSC	DNA	For lung cancer	(Wu et al., 2022)

1.3.1 Developing Aptamer-based therapy

The development of aptamer-based therapies involves a methodical and intricate journey where scientific insights merge with systematic processes to yield targeted and effective treatments. This journey's initiation hinges on identifying a specific disease-associated molecule, such as a protein, cell, or virus, as the target. This meticulous selection is pivotal, laying the foundation for subsequent stages. Following target identification, the process of aptamer discovery commences. As detailed earlier, this involves aptamer selection (e.g., SELEX), wherein diverse DNA or RNA sequences are methodically synthesized, tested, and refined to unveil aptamers exhibiting optimal binding affinity to the selected target. Once the aptamer with the most robust binding characteristics is identified, it undergoes a comprehensive characterization phase. This step elucidates its binding kinetics, specificity, and affinity, providing a thorough understanding of its functional attributes. Steps of therapeutic aptamer development are shown in Scheme 1.1.

After characterization, as detailed earlier in this manuscript, aptamers often undergo optimization. Chemical modifications may be introduced to enhance their stability, pharmacokinetics, and target affinity, thereby bolstering their performance in complex biological systems. The most common modification involves 2′-amino pyrimidines, 2′-fluoro pyrimidines, 2′-O-methyl ribose purines and pyrimidines, and the modification of the antinucleotide linkage such as the phosphonothioate linkage. These modifications impart enhanced stability to the aptamer, prolonging its lifespan within complex biological environments and enhancing the target affinity. For instance, in a study by Burmeister et al. (2005), researchers introduced 2'-O-methyl modifications to a DNA aptamer targeting VEGF. This resulted in improved resistance to nuclease degradation and prolonged circulation half-life. (Burmeister et al., 2005) Aptamers can be coupled with functional moieties like polyethylene glycol (PEG) or NPs to facilitate targeted delivery and enhance pharmacokinetics. Baek et al. (2014) modified an aptamer targeting prostate-specific membrane antigen (PSMA) by conjugating it with PEGylated liposomes (Aptamosome), efficiently delivering therapeutic agents to PSMA-overexpressing cancer cells. (Baek et al., 2014)

Site-specific modifications offer precise control over aptamer properties. An example is aptamer truncation, wherein specific regions are removed while retaining target-binding domains. In a study by Shawn et al. (2002), a truncated version of an aptamer targeting human prostate cancer cells expressing PMSA retained its binding affinity while exhibiting reduced nonspecific interactions, highlighting the potential of this approach to mitigate unwanted effects. (Lupold, Hicke, Lin, & Coffey, 2002) Switchable aptamers represent another innovative avenue. These aptamers can undergo structural changes upon binding to the target, leading to functional alterations. Ying et al. (2011) monitored the real-time conformational change of adenosine 5'-triphosphate (ATP)-binding DNA aptamer (ABA) upon binding to the target, which is essential for recognition and biological activity. (Ying, Wang, Sutherland, & Long, 2011) Spiegelmers are the sugar enantiomers of aptamers, where the RNA spiegelmers contain L-ribose in the backbone of the oligonucleotide compared with D-ribose in the wild-type oligonucleotide. The L-ribose aptamers for a desired target are much more nuclease-resistant than wild-type ones. Kerstin et al. (2007) studied the antagonist effect of the anti-amylin RNA spiegelmer on rat subfornical organs and area postrema as a biostable antagonist for high plasma amylin levels in certain pancreatic tumors. (Bilik et al., 2007) These alterations augment aptamer stability and fine-tune their interaction kinetics, potentially minimizing off-target effects and maximizing their therapeutic impact. The strategic fusion of chemical ingenuity and biological insight in aptamer modifications exemplifies the dynamic convergence of molecular engineering and medical science.

1.3.2 Aptamer-based therapeutic approach and delivery

Armed with the optimized aptamer, the subsequent stage involves designing the therapeutic approach. This design hinges on the specific interaction between the aptamer and its target, manifesting as targeted drug delivery, the inhibition of disease-associated molecules, or the modulation of cellular pathways. Additionally, aptamer-based therapies can act as therapeutic carriers and reduce unwanted interactions and side effects. As an example, a specific HER2 RNA

aptamer was conjugated to the anti-cancer drug Mertansine as a platform of a targeted high-performance anti-cancer drug in HER2-positive breast cancer. (Jeong et al., 2020)

Aptamer conjunction therapy is an innovative strategy that integrates aptamers with other therapeutic approaches to enhance treatment efficacy. Rooted in the inherent specificity of aptamers for disease-associated targets, this approach aims to leverage their precision while synergistically capitalizing on the mechanisms of complementary therapies. The rationale lies in the ability of aptamers to deliver therapeutic payloads with remarkable accuracy, minimizing unintended effects. This strategy offers several advantages, including heightened targeting precision, potential synergistic effects, treatment resistance mitigation, and adaptability to various therapeutic agents. Illustrative applications include the conjugation of aptamers with cytotoxic drugs, as Bagalkot et al. (2006) demonstrated, where aptamer-doxorubicin (Dox) conjugates exhibited selective drug delivery to prostate cancer cells, enhancing the therapeutic impact and reducing the side effects. (Bagalkot, Farokhzad, Langer, & Jon, 2006)

Additionally, coupling aptamers with nanoparticles, such as PSMA-RNA aptamer conjugated to the liposome, is called an “autosome” that can encapsulate Dox and show selective toxicity for PSMA-positive cancer cells. (Baek et al., 2014) This approach facilitates targeted delivery of therapeutic payloads. Moreover, aptamers can augment immunotherapies, as shown by Lee et al. (2008), by nuclease-resistant RNA that can protect acetylcholine receptors in human cells from the effect of the autoantibodies in myasthenia gravis. (S. W. Lee & Sullenger, 1997) While promising, the approach necessitates careful consideration of dosage, timing, and potential interactions. Preclinical validation remains crucial to ascertain safety and the potential for synergistic benefits before embarking on clinical trials. In essence, aptamer conjunction therapy underscores a strategic fusion of aptamers' precision and adaptability with other therapeutic modalities, promising a dynamic and potent approach to addressing intricate disease processes.

1.3.3 Aptamer-based therapeutic efficiency and clinical evaluation

The aptamer's efficacy is validated initially within controlled laboratory conditions (in vitro), using cell cultures or biochemical assays. This phase gauges the aptamer's functional attributes and ability to influence the target molecule or pathway. Subsequently, preclinical evaluation steps into the spotlight, involving studies in animal models (in vivo) to assess the aptamer's performance within living organisms. These preclinical investigations provide insights into efficacy, safety, and potential side effects, facilitating informed decisions for the clinical phase.

Aptamer-based therapies that demonstrate promise through preclinical evaluations advance to clinical trials, a rigorous process divided into three phases. Phase I entails safety assessments in a small group, while Phase II expands to a larger population, assessing safety and efficacy. Phase III corroborates these findings in a broader patient base. Successful outcomes from clinical trials usher the therapy into regulatory approval. This marks a pivotal juncture wherein the therapy becomes an authorized treatment, poised to make a tangible impact on patient care.

Beyond regulatory approval, vigilant post-market surveillance is indispensable in tracking the therapy's performance, safety, and any unforeseen effects emerging as it enters real-world applications. In summation, the development of aptamer-based therapies encapsulates a meticulous sequence of stages, seamlessly amalgamating scientific acumen and systematic processes to create tailored and targeted interventions for diverse medical conditions. This comprehensive overview strives to shed light on the journey aptamer-based therapies undertake, underscoring their transformative potential in the realm of biopharmaceuticals.

The landscape of aptamer-based therapies spans from clinical trials to market-approved treatments, showcasing their growing significance in diverse medical fields. Pegaptanib (Macugen) is a standout example, the first FDA-approved intervention for AMD. Pegaptanib's mechanism, targeting VEGF, curtails aberrant blood vessel growth in the retina. (Ng et al., 2006) Furthermore,

the ongoing clinical trials of NOX-A12, an L-RNA enantiomer, reveal its potential as an aptamer-based therapy to enhance immunotherapies like in diabetic glomerulosclerosis by targeting the CXCL12 chemokine. (Sayyed et al., 2009) AS1411 is another promising aptamer candidate, under phase II clinical study, which is being investigated for acute myeloid leukemia (AML) and renal cell carcinoma, harnessing its nucleolin-targeting property. (Bates, Laber, Miller, Thomas, & Trent, 2009; Rosenberg et al., 2014) In anticoagulants, ARC1779 targets the von Willebrand factor, with REG1 (Pegnivacogin) taking a dual-pronged approach targeting factors IXa and Xa. (Gilbert et al., 2007; Lincoff et al., 2016) These examples underscore aptamers' versatility, from neovascular AMD to cancer therapeutics and anticoagulation management, exemplifying their role as potent tools in advancing medical interventions. Other aptamers that have translated into clinical studies are summarized in Table 1.3

Table 1.3. FDA-approved therapeutics aptamers or under clinical studies

Aptamer	Target	Modification	Indication	Phase	Reference
Pegabtanib (Mucogen)	VEGF	PEG conjugated-*2′-O-methyl purine/2′-fluoro pyrimidine with two 2′-ribo purines, 3′inverted dT*	Age-related macular degeneration (AMD)	Approved	(Group et al., 2006), (Ng et al., 2006)
Avacincapted pegol (Izervay or Zimura) *(*ARC1905)	Complement factor C5	2′-fluoropyrimidine truncated RNA with 2′-O-Methyl ribopurines, 3′-linked deoxythymidine and 40 kDa PEG to the 5′ end	AMD	Approved	(Drolet et al., 2016)
Fovista (El0030)	PDGF	36t truncated aptamer with replacing two trinucleotide groups with pentaethylene glycol spacer. 2′-F or 2′-OMe replacement for deoxynucleotides and 40kDa PEG end.	AMD	Phase III Clinical study	(Drolet et al., 2016)
AS1411	Nucleolin	G-rich DNA	Acute myeloid leukemia Metastatic renal cell carcinoma	Phase II	(Bates et al., 2009; Rosenberg et al., 2014)
NOX-A12 NOX-E36 NOX-H94	CXCL12 (olaptesed pegol)	L-RNA with PEG at 3˜	Diabetic nephropathy, CLL, Multiple myeloma.	Phase II	(Sayyed et al., 2009; Vater & Klussmann, 2015)

Aptamer	Target	Modification	Indication	Phase	Reference
	CCL2 (emapticap pegol) Anti-Hepcidin (lexaptepid pegol)				(Ludwig et al., 2017)
ARC1779	von Willebrand factor (Archemix)	2˜-OMe DNA with one phosphorothioate linkage conjugated with 20 KDa PEG.	Thrombotic microangiopathies and carotid artery disease	Phase II	(Gilbert et al., 2007; Jilma et al., 2010) (Jilma-Stohlawetz, Knobl, Gilbert, & Jilma, 2012)
RB006 and the anti-dote RB007 (REG1) and REG2	Factor IXa	2′-ribo purine/2′-fluoro Pyrimidine, 2′-O-methyl antidote. 40KDa PEG	Coronary artery disease	Phase III, II, I	(M. Liu, Zaman, & Fortenberry, 2021)
HD1 (RRC 183) HD22 HD1-22	Thrombin	Single-strand DNA with locked nucleic acid Combination of HD1 and HD22 by poly dA linker	Anti-coagulation during Coronary bypass graft procedure	Phase I Pre-clinical Pre-clinical	(M. Liu et al., 2021; Ponce & Hong, 2019)
NU172	Thrombin	Unmodified ssDNA	Anti-coagulation during Coronary bypass graft procedure	Phase II	(M. Liu et al., 2021)

Aptamer	Target	Modification	Indication	Phase	Reference
BAX499 (ARC19499)	Tissue factor pathway inhibitor	2˜-O-methyl truncated RNA with inverted dT with 5˜hexylamine linker and 40KDa PEG	For bleeding associated with hemophilia	Phase I	(Waters et al., 2011)
Edifoligide (E2F Decoy)	E2F(cell - cycle transcription factor	Decoy oligodeoxynucleotide (DNA)	In the failure of human primary bypass vein grafting,	Phase III	(Conte et al., 2006)
RRE Decoy	Rev	RNA-RRE transcription unit in a double-copy murine retroviral vector	In HIV-1	Phase II	(Kohn et al., 1999; T. C. Lee, Sullenger, Gallardo, Ungers, & Gilboa, 1992)
TAR Decoy	tat	Chimaric small nucleolar RNA TAR-decoy	AIDS-related lymphoma	Phase II	(DiGiusto et al., 2010; Michienzi, Li, Zaia, & Rossi, 2002)
NF-kappaB Decoy	Nuclear factor kappa B (NF-kB) DNA	DNA	Atopic dermatitis Restenosis	Phase II	(Suzuki, Tezuka, Morishita, & Isobe, 2009)

1.4 Mass Spectrometry in aptasensor development

Mass Spectrometry (MS) measures the molecules based on the gas phase's mass-to-charge ratio (m/z). The target molecules become ionized either in positive or negative charge using multiple ionization techniques based on the type of samples introduced to the MS. For instance, the liquid-type samples become ionized using electron spray ionization (ESI), or Atmospheric pressure chemical ionization (APCI), while the gas-type of samples using Electron impact (EI) or chemical ionization (CI). The ideal ionization techniques for the solid-type samples are Matrix-assisted laser desorption ionization (MALDI) and Desorption electrospray ionization (DESI). These ionization techniques are the most common in analyzing biomolecules, mainly those used in clinical applications and personalized medicine. The target molecules are usually extracted from the biological matrix and introduced to the MS through several inlet devices such as liquid chromatography (LC), GC, CE, or solid platform.

The separation performance of MS is based on the resolution power of the technique, which is associated with the application of the analysis. The MS techniques are classified into low-resolution, such as quadrupole (Q) and ion trap (IT) analyzers, while the high-resolution, such as the Fourier-transform ion cyclotron resonance (FTICR), orbitrap, and Time-of-Flight (TOF). Hyphenated technologies improved the MS resolving power and analytical capabilities, such as triple quadrupoles (QQQ), quadrupoles with the time of flight (QTOF), QFTICR, or TOF/TOF. Improving the resolving power of the inlet techniques and successful hyphenation between the MS analyzers improve the overall analytical performance. Another dimension of separation to these analytical tools was revolutionized, mainly when the ion mobility (IM) technology was integrated as a post-ionization separation technology. IM is based on the movement of ions within a specific environment, usually a gas. When subjected to an electric field within the gas, the ion separation is based on their movement speed.

Two distinct acquisition methods are used mainly in global analyses to improve the number of detected molecules. These methodologies are Data-Dependent Acquisition (DDA) and Data-Independent Acquisition (DIA). DDA is a more traditional approach; for instance, an ion surpasses a predefined intensity threshold in proteomics, and the instrument isolates and fragments it. The resulting fragment spectra, known as MS/MS or tandem mass spectra, offer detailed information about the peptide's sequence and structure. DDA is particularly effective for identifying known peptides and proteins because it selectively triggers the fragmentation of the most intense peaks, increasing the chances of detecting and identifying abundant species.

On the other hand, DIA is a newer and more advanced technique designed to address some of DDA's limitations. In DIA, the MS systematically fragments all ions within a specified m/z range as they elute from the chromatographic column. This generates a continuous stream of fragment spectra for all detected ions, regardless of their abundance. DIA excels in quantifying peptides and proteins, providing consistent and comprehensive sample coverage. While DIA data can be more complex than DDA data, modern data analysis methods have evolved to handle this complexity effectively. With DIA, researchers can perform retrospective data analysis, allowing them to re-interrogate their data for specific peptides or proteins of interest, even after the initial acquisition. DDA is well-suited for peptide and protein identification, especially for less complex samples. At the same time, DIA shines in quantitative analysis and achieving thorough proteome coverage, making it particularly valuable for extensive proteomics investigations. The choice between DDA and DIA hinges on specific research objectives and the sample's complexity under examination.

MS stands as an indispensable pillar in biology, offering a versatile toolkit with applications that deeply enhance our understanding of biological systems at the molecular level. It is essential in numerous critical domains, including proteomics, metabolomics, lipidomics, and glycomics. In proteomics, MS enables identifying and quantifying proteins within biological samples, unraveling the intricacies of cellular processes, and shedding light on post-translational modifications (PTM) and protein interactions. Likewise, metabolomics couples MS to profile and quantify small

molecules, providing invaluable insights into metabolic pathways and the discovery of biomarkers crucial for disease diagnosis and monitoring. In the expanding field of lipidomics, MS offers a window into the complex world of lipids, elucidating their roles in cellular processes and disease pathogenesis.

Conversely, Glycomics relies on MS to characterize intricate carbohydrate structures and understand their significance in cellular functions. MS also plays a pivotal role in structural biology, drug discovery, and environmental and forensic biology, making it an indispensable tool across various sides of biological research. In essence, MS is not merely a tool but a cornerstone that continues to drive innovation and progress in the biological sciences, enabling researchers to explore the molecular intricacies of life itself.

As biosensors and biologics therapies target all classes of biomolecules, MS plays a significant role in their advancement at several stages detailed above. In addition, MS can be utilized as the readout tool for the sensor and identify the target molecules covered in this section.

1.4.1 MS for peptide and ssDNA Sequencing for aptasensor development

Mass spectrometry is a vital asset in aptasensor development, offering profound insights into diverse aspects, including peptide sequencing, single-stranded DNA (ssDNA) sequencing, and the intricate characterization of aptamer-target interactions. These contributions of MS to aptasensor technology have been underscored in a range of literature studies.

In peptide sequencing within aptasensors, Malkawi et al. (2023) highlighted MS’s pivotal role in identifying and validating proteins as a targeted element at digested peptides (Bottom-up approach). (Malkawi, Jafari, et al., 2023) The precision of mass measurements and the detailed fragmentation patterns provided by MS/MS are instrumental in elucidating peptide sequences, ensuring the aptasensor's specificity. Moreover, Cantor and coworkers (1996) emphasized the

relevance of MS in DNA sequencing, describing a high throughput sequencing method using the MALDI-TOF MS method. (Koster et al., 1996)

Furthermore, characterizing aptamer-target interactions has been advanced through MS-based techniques. In a study by Basri et al. (2018), MS is applied to characterize aptamer-ligand interactions with all details. (Gulbakan et al., 2018) The technique aids in unraveling the binding kinetics and thermodynamics of these interactions, providing crucial insights into aptamer-target complex formation. These empirical studies collectively affirm the significance of MS in enriching the molecular understanding and performance of aptasensors, thus furthering their potential applications in various domains of biosensing and diagnostics.

1.4.2 MS biomarker discovery for biosensor targets

Developing biosensors for target molecules requires validating these molecules as biomarkers for a particular disease. MS is essential in biomarker discovery and biosensor target identification, particularly in the intricate landscape of proteomics and metabolomics, as reviewed extensively by Nasrin et al. (2018) and Zhouet al. (2022). (Amiri-Dashatan, Koushki, Abbaszadeh, Rostami-Nejad, & Rezaei-Tavirani, 2018; Zhou & Zhong, 2022) Its diverse applications drive the quest to unearth potential biomarkers linked to specific diseases and pinpoint essential drug targets.

In biomarker discovery, MS is a powerful instrument for delving into the proteome within biological samples. This in-depth protein profiling is the initial step in identifying potential biomarkers by unveiling differential expression patterns between disease-afflicted and healthy samples. MS's remarkable ability to discern PTMs adds a layer of complexity to this pursuit, as PTMs often relate to disease states. MS provides a comprehensive view of the proteome's PTM landscape, offering the possibility of uncovering biomarkers intricately associated with specific modifications. Moreover, applying targeted proteomics through MS, exemplified by techniques like Selected Reaction Monitoring (SRM) or MRM, plays a pivotal role in validating potential

biomarkers by enabling the precise quantification of specific proteins or peptides across extensive sample cohorts. For example, our comprehensive proteomic analysis, utilizing MRM-MS, has uncovered a panel of protein biomarkers that hold promise for enhancing the diagnosis and monitoring of rheumatoid arthritis disease. In this cohort, we identified a set of proteins that exhibited significant alterations in RA patients compared to healthy controls. (Malkawi, Nimer, et al., 2023)

MS emerges as a linchpin in target identification and unveiling protein-protein interactions and potential drug targets. The amalgamation of affinity proteomics with MS techniques facilitates the elucidation of intricate protein networks entwined with a target of interest, thereby contributing substantively to the process of target validation. Additionally, MS finds extensive utility in chemical proteomics, where it aids in identifying small molecule ligands interacting with proteins. This approach enhances our comprehension of drug targets and delves into the mechanisms of action for bioactive compounds. The synergistic integration of MS data with other omics data augments its potency, offering a comprehensive perspective on cellular processes and, thus, expediting the identification of targets nestled within multifaceted biological pathways. The versatility of MS, coupled with its capability to furnish both quantitative and qualitative insights, firmly establishes it as an indispensable instrument in the tireless pursuit of diagnostic biomarkers and potential drug targets spanning diverse diseases and biological contexts.

1.4.3 MS for binding confirmation for aptamer selection on a platform

In aptamer selection, binding the target analyte to the solid platform, such as beads, is essential. Most research groups use immunological techniques to confirm the binding, which is hindered by several drawbacks, such as cross-reactivity and reproducibility in antibody production. This is a crucial step in selection to ensure the quality and coverage of binding supports the quality of the selected aptamer, mainly from an affinity and specificity standpoint. MS is an indispensable tool for validating binding interactions during the aptamer selection process, specifically when

conducted on a platform. Its role is pivotal in confirming the capacity and strength of the interactions between aptamers and the supporting material for the selection, adding a layer of rigor to the selection process. In 2023, a novel ssDNA aptamer for sCD80 protein was selected using SELEX, where the protein-beads interaction and quality and the relative quantity of the bound targets to the beads during selection were determined using the high-resolution MS method. (Malkawi, Jafari, et al., 2023)

One of the key applications lies in integrating MS within the SELEX process. Here, MS aids in the critical step of affinity selection, where aptamers demonstrating strong binding affinity to the target are isolated. Through MS, the binding of potential aptamers to the target is unequivocally confirmed. This stringent validation ensures that only aptamers exhibiting high specificity proceed to subsequent selection rounds, enhancing the overall quality of the aptamer pool.

Additionally, MS/MS, a powerful technique within the MS realm, provides insights into the intricate binding mechanisms governing aptamer-target interactions. By fragmenting the aptamer-target complex, MS/MS unveils crucial details such as binding sites and interactions, whether they involve hydrogen bonds, electrostatic forces, or other molecular forces. Such mechanistic clarity is instrumental in comprehending the aptamer's binding specificity and fine-tuning its performance. Furthermore, MS facilitates the quantification of binding affinity by precisely measuring the dissociation constant (Kd) between the aptamer and its target. This quantification is achieved using isotope-labeled aptamers or target molecules, ensuring highly accurate assessments of binding stoichiometry and affinity. Basri et al. (2018) demonstrated a native EIS-MS approach for aptamer-ligand complex characterization, including types of interactions, complex stereochemistry, and binding affinity (Kd). (Gulbakan et al., 2018) MS enriches the aptamer selection process by delivering rigorous confirmation of binding interactions and mechanistic insights, ultimately bolstering the utility of aptamers across various applications, from diagnostics to therapeutics. Moreover, aptamers can be used as affinity reagents to increase the sensitivity of

the SRM-detection method for low-abundance proteins in the blood, as Radko et al. (2020) described. (Radko et al., 2020)

1.4.4 MS for protein-aptamer interaction site identification

Mass spectrometry is an invaluable technique for studying the interaction between proteins and aptamers and identifying their binding sites, which is identical to the epitope mapping in antibody and antigen binding. This method offers a deep understanding of these interactions at the molecular level. In detail, the protein and aptamer under investigation are meticulously isolated and purified. Ensuring the purity of these samples is critical for accurate results. LC is a common and useful method for separating and purifying the aptamer-target molecule before introducing it to the MS. Although a bottom-up approach by enzymatically digesting the protein into smaller peptides before subjecting it to high-resolution MS is very useful for studying aptamer-protein interaction, top-down MS gives more comprehensive insights into the complex interaction interfaces (J. Zhang, Reza Malmirchegini, Clubb, & Loo, 2015) sites of ligand binding (Yin & Loo, 2010) and the surface topology. (Li, Wolff, Van Orden, & Loo, 2014)

A prime example of the power of MS in this context can be found in a study by Zhang et al. (2017). The researchers used native top-down MS to analyze the binding of a specific aptamer to thrombin, demonstrating the specificity of this technique in pinpointing aptamer binding sites on the protein. They successfully identified the aptamer binding site and characterized the interaction at the molecular level. MS is an indispensable tool for unraveling the intricacies of protein-aptamer interactions. (J. Zhang, Loo, & Loo, 2017) As Zhang et al. demonstrated, its ability to identify binding sites enhances our understanding of the molecular mechanisms governing these interactions, ultimately contributing to advances in drug discovery and molecular biology. Understanding the macromolecular complexes in biological systems is challenging, especially with low-abundant interacting partners. Aptamer-affinity (AptA) purification method is an alternative to the immunoprecipitation method for purifying interacting proteins and studying these

interactions, avoiding drawbacks associated with antibodies. AptA-MS is an aptamer-based affinity purification method Ray et al. (2020) demonstrated to study protein-protein interaction with MS. This study used a specific and high-affinity green fluorescent protein RNA aptamer (GFP-Apt) to identify the novel interactions of human Heat Shock Factor 1 (HSF1) tagged with GFP. (Ray et al., 2020)

1.4.5 MS as the biosensor's detection method

Mass spectrometry has emerged as a potent and adaptable method for biosensor detection, gaining recognition for its remarkable sensitivity, specificity, and flexibility. Traditionally, MS has been associated with analytical chemistry and proteomics, but its application in biosensing has broadened its horizons significantly. The MS's exceptional sensitivity allows for the detection of molecules even at trace concentrations. This heightened sensitivity is especially valuable when identifying minute amounts of biomarkers or analytes is essential, such as early disease diagnosis and monitoring. Moreover, MS offers outstanding specificity by furnishing precise m/z measurements, an indispensable feature for distinguishing closely related biomolecules and minimizing false positives. This is particularly pertinent in clinical settings, where diagnostic accuracy is paramount.

MS exhibits its competency in multiplexing in biosensing, enabling the simultaneous detection of multiple analytes within a single sample. Such multiplexed assays are promising in applications like biomarker discovery and drug development. Additionally, MS provides quantitative information about analyte concentrations, thus facilitating accurate measurements and robust statistical analyses. Ju et al. 2021 were the first to introduce the MS-biosensor concept as an approach for multiplexing analysis of clinical biomolecules. (J. Hu, Liu, Chen, Shangguan, & Ju, 2021) MS can be employed for label-free detection, streamlining assay development, and reducing associated costs. Its versatility encompasses various biomolecule types, spanning proteins, peptides, nucleic acids, lipids, and metabolites.

MS biosensors can be classified according to the device structure and the ionization mechanism into three major types: biochip and mass tag-based associated with MALDI (MALDI-MS), probe (pen) based for in situ and in vivo clinical studies, and other biosensing technology integrated with MS-biosensing, such as SPR and microfluidics. The biochip and the mass tag-based biosensor depend on the specific interaction of the self-assembled monolayer of the recognition element (oligonucleotide, enzyme, antibody, lipid) with the target biomolecule. As a detection method, the laser desorption technique transfers energy or electrons to the target molecule through a specific matrix. The development of microarray biochips enables the multiplex analysis of different biomolecules and a high throughput screening, as reviewed by Ju et al. (2021). Since integrating biochips with the laser desorption MS techniques, many research groups successfully developed MS biosensors for different applications, as extensively reviewed by Chu et al. (2023). In 2002, Proteins, peptides, and carbohydrates were self-assembled on Au-chips (SAMDI-MS) as a tool for enzyme activity studies. (Su & Mrksich, 2002) The successful characterization of the SAM in SAMDI-MS increased the potential to use different recognition elements, such as oligonucleotides, lipids, and small molecules. In 2005, Becher et al. demonstrated a DNA-protein microarray to study the Ras-protein-receptor interaction. (Christian F. W. Becker Dr., 2005)

Gunnarsson et al. in 2010 reported a sensitive MS-biosensor (TOF secondary ion mass (TOF-SIMS) for multiplex detection of target DNA sequences using a surface-immobilized DNA probe and barcoding liposomes conjugated with capture DNA strand. (Gunnarsson, Sjovall, & Hook, 2010), the microarray biochip-MS sensor can be Au-based, silicon-based, paper-based, ITO-based, and other nanomaterial. Developing nanomaterials as mass tags bound to the biological moiety allows for multiplex analysis and enhances the sensitivity of MS biosensors. The variety of microarray substrates and the mass tags nanomaterials increases the potential of using MS in biosensors. It is worth mentioning that the use of MS in biochip biosensors is limited due to the complex and time-consuming preparation of bio-array chips and the wide use of Abs as recognition elements, which is susceptible to damage during the experiment. Enhancing the stability of the

biosensing probe, such as using aptamers, has great potential to advance the integration of MS in biosensing and biomarker discovery.

Probe/pen MS sensing techniques were developed for in situ and in vivo detection and identification of specific biological information. Probe electrospray ionization technology (PESI) is widely applied for in vivo non-destructive biological analysis. PESI was used directly in different biological samples to measure other compounds, as reviewed extensively by Chu et al.2023. (Chu et al., 2023)

Pen/knife-like MS is a biosensing technique that relies on the rapid evaporative ionization MS (REIMS) for tissue samples, especially in tumor margin detection. Using probe/pen-based MS techniques has significantly improved how we analyze substances. These techniques provide several advantages beneficial to researchers in different scientific fields. They offer the ability to precisely examine specific areas, conduct real-time analyses, use minimal sample quantities, adapt to various types of samples, analyze samples in their natural settings, and reduce the risk of contamination. As technology evolves, these techniques will become even more crucial in biosensing, leading to the discovery of exciting new possibilities and applications in the years ahead.

The recent research focused on integrating MS with other biosensing techniques to advance biosensors' precision and sensitivity and to achieve complementary performance in different fields. SPR-MS is one of the most common integrated biosensors with offline or online approaches, as Chu et al. (2023) reviewed extensively. The online coupling approach gained great attention among researchers, as it can improve the detection speed and prevent the denaturation of the sample. Zhang et al. 2016, described a dielectric barrier discharge ionization-based interface for online coupling SPR with MS to study different interacting biomolecules. (Y. Zhang et al., 2016) The fusion of SPR with MS can specifically recognize protein bindings and perform highly sensitive and precise qualitative and quantitative analyses. This integration creates an excellent analytical

instrument for the examination of biomolecule interactions. Microfluidic chips and SAW devices are other techniques that can be coupled with MS for high-throughput qualitative and quantitative analysis.

Employing MS-based biosensors, the researchers accurately identified specific biomarkers indicative of cancer, thereby emphasizing the clinical relevance and potential of MS in disease diagnostics. MS is an invaluable asset in the biosensor toolkit, offering precision, versatility, and sensitivity across various applications, ranging from clinical diagnostics to pharmaceutical development, proteomics, metabolomics, environmental monitoring, and food safety.

1.4.6 MS method for biosensor validation

Mass spectrometry is a powerful tool in validating biosensors, offering a rigorous approach to understanding the interactions between biosensors and their target analytes. This validation process is critical for ensuring the reliability and accuracy of biosensor measurements, particularly in clinical and analytical applications.

Biosensor validation encompasses several critical facets, including sensitivity, specificity, accuracy, precision, and the limit of detection (LOD), as described in section 2.5. a comparative study between a developed biosensor and a golden standard method is a critical validation step in some cases to prove the method's robustness and to ensure the good performance of the biosensor under different conditions. A well-established quantitative MS method can effectively evaluate the biosensor's performance by comparing the results obtained by both methods. For example, developing accurate and comparable protein concentration assays is crucial in clinical diagnosis. Tingting et al. (2019) used the isotope dilution MS (IDMS) as a standard method to evaluate a human-immunoglobulin SPR biosensor's performance as an accurate protein concentration quantification method. (T. Hu, Wu, Sun, Su, & Yang, 2020)

Real sample testing using clinical or environmental samples further bolsters the biosensor's validation, ensuring its applicability in practical scenarios. The biosensor's reproducibility and stability are evaluated under varying conditions, and statistical analyses are employed to assess the congruence between biosensor-derived data and MS results. By integrating MS into the validation framework, researchers are equipped with a robust methodology that quantifies the biosensor's performance and enriches the validation process by providing structural insights into the captured analytes. Mirón-Mérida et al. (2021) reviewed this multidimensional approach, taking fumonisin B1 as an example, enhancing biosensors' credibility and utility across diverse scientific and clinical applications. (Miron-Merida, Gong, & Goycoolea, 2021)

1.5 Mass Spectrometry in aptamer-based Targeted therapy

Aptamer-based targeted therapy (Aptatherapy) constitutes a distinct subcategory within the broader biologics domain. Biologics encompass diverse therapeutic agents from living organisms, from monoclonal antibodies to cell-based therapies. Aptatherapy, however, represents a specialized class of biologics centered on aptamers—short, single-stranded DNA or RNA molecules engineered to exhibit high specificity and affinity for target molecules, typically proteins.

MS's role in developing and assessing aptamer-based targeted therapies focusing on their clinical efficacy is a pivotal and well-established facet of precision medicine. Aptamers engineered for highly specific target binding offer immense promise for personalized and precisely targeted therapeutic interventions. Within scientific inquiry and clinical translation, MS emerges as a cornerstone tool, contributing significantly to the realization of aptamer-based treatments.

MS's involvement commences with aptamer characterization, as demonstrated for the first time by Smith and coworkers (1993), after observing a duplex small oligonucleotide by ESI-MS, ensuring the aptamer's sequence integrity and structural fidelity. (K. J. Light-Wahl, 1993) Beyond this, MS

is pivotal in identifying and validating target molecules, which aptamers are meticulously designed to engage with. MS contributes to the foundation of Aptatherapy by confirming the specificity and affinity of these crucial interactions, a fundamental step in the development process. Moreover, MS is indispensable in studying the pharmacokinetics and pharmacodynamics of aptamer-based therapies and tracking their behavior within biological systems. This is exemplified by the work of Healy et al. (2004), which elucidated the pharmacokinetics and the in vivo biodistribution of anti-TGFβ−2 aptamer using MALDI-TOF, an insight of paramount importance in clinical translation. (Healy et al., 2004)

MS can quantitatively monitor target molecules or relevant biomarkers in patient samples, a pivotal aspect in assessing treatment outcomes. Furthermore, MS-driven structural insights into aptamer-target complexes facilitate the design of optimized aptamers with enhanced binding properties. Through MS, the quality of aptatherapy can be stringently controlled during manufacturing, ensuring their safety and efficacy. As evidenced in multiple clinical trials and studies reviewed by kellie et al. (2020), MS contributes significantly to biomarker discovery and monitoring of adverse events, adding a layer of precision to aptatherapy in clinical settings. (Kellie et al., 2021) The symbiotic relationship between aptatherapy and MS underscores their potential to revolutionize targeted and personalized medicine.

1.5.1 Study protein-aptamer binding using H/D exchange.

Employing Hydrogen/Deuterium exchange mass spectrometry (H/D exchange MS) to investigate the binding between proteins and aptamers represents a robust strategy for deciphering the intricate structural nuances of this interaction. This methodology offers profound insights into how proteins and aptamers engage at the molecular level, shedding light on binding regions, protein conformation changes, and protein dynamics alterations. In the context of a scientific manuscript, it is imperative to outline the procedural intricacies and emphasize the significance of this approach.

The process commences with the isolation and purification of both the protein and the aptamer to ensure the purity and integrity of the samples. Following this, the formation of the protein-aptamer complex is pivotal. The H/D exchange experiment is then initiated by exposing the complex to a deuterated solvent (D_2O), which leads to the exchange of hydrogen atoms in the protein with deuterium atoms from the solvent. Notably, this exchange predominantly occurs in protein regions not engaged in strong binding interactions with the aptamer. Quenching the exchange reaction is a critical step, achieved by lowering the pH and temperature, thus halting further exchange. Subsequently, enzymatic digestion of the protein into smaller peptides using a protease is performed to prepare the samples for MS analysis.

The MS analysis of the digested peptides is a pivotal aspect of the methodology. H/D exchange increases the mass of each peptide, with deuterium atoms replacing hydrogen atoms. By meticulously measuring the mass shift for each peptide, researchers can elucidate the regions of the protein that experienced hydrogen exchange upon aptamer binding. This analysis provides valuable data for mapping the aptamer binding site on the protein and understanding the structural implications of this interaction. Notably, this technique is underscored by its capability to complement structural data from other methods, such as X-ray crystallography or NMR, creating a comprehensive portrait of the protein-aptamer interaction.

Numerous studies have substantiated this approach. In 2014, Jørgensen and coworkers used H/D exchange-MS to study the regulatory effect of RNA aptamer on serpin plasminogen activator inhibitor-1 (PAI-1), which protected the conformation of the protein from the active state to the latent state. In their work, the binding of the aptamer to the target protein induced the protection of HDX at the protein-aptamer interface and other specific areas, indicating the structural instability of these regions for the transition of the protein to the latent phase, revealing the precise binding interface and structural alterations induced by the interaction. (Trelle, Dupont, Madsen, Andreasen, & Jorgensen, 2014)

A study by Tuske et al. (2020) illustrates the power of HDX-MS in studying the structural dynamics of HIV-1 reverse transcriptase (RT) alone and in the presence of ultra-high affinity DNA aptamer, offering structural insights into the aptamer-protein interaction. (Tuske et al., 2020). In conclusion, HDX-MS is an invaluable tool in unraveling the intricacies of protein-aptamer interactions, offering both mechanistic insights and structural clarity that hold profound implications for developing aptamer-based therapeutics and diagnostics.

1.5.2 MS for In vivo and In vitro studying the activity of the aptamer therapy.

Mass spectrometry is an indispensable analytical technique that holds profound promise for the comprehensive evaluation of the efficiency of aptamer therapy, both in in vitro and in vivo contexts. This versatile tool is pivotal in unraveling the molecular intricacies governing aptamer-based treatments, providing a multi-dimensional lens to assess their efficacy and therapeutic potential.

In vitro investigations constitute a foundational step in the assessment of aptamer therapy. MS can be effectively harnessed to confirm and quantify the binding interactions between aptamers and their target molecules, often proteins. Understanding the astrochemistry of ligand-target binding is crucial in determining the potency of a therapeutic agent as a part of the drug development procedure. Cassiday et al. (2002) were the first to conduct an ESI-MS in studying the stereochemistry of aptamer-ligand interaction. This study reveals that anti-human transcription factor RNA aptamer can inhibit the binding of the transcription factor with the target DNA in a 1:1 molar ratio of RNA aptamer to NF-kappaB homodimer. (Cassiday et al., 2002) Researchers can gauge the strength and specificity of aptamer engagement through precise mass spectral analysis of the protein pre- and post-aptamer binding.

Furthermore, the kinetics of aptamer-protein interactions are paramount for understanding their dynamics. MS techniques, such as SPR-MS, are exemplars in this regard, enabling the

characterization of binding kinetics. This was manifestly demonstrated in the work of Lupu et al. (2020), who employed SPR-MS to elucidate the kinetics of an aptamer binding to C-met protein, a glycosylated receptor tyrosine kinase of the hepatocyte growth factor (HGF). (Lupu et al., 2020) By dissecting the association and dissociation rates, researchers gain profound insights into the rapidity and strength of aptamer binding. Such insights are invaluable for optimizing therapeutic regimens and predicting aptamer behavior in a biological milieu. Structural changes induced by aptamer binding are another facet that can be explored through MS. This aspect was underscored in the study by Mironov et al. (2014), which utilized kinetic capillary electrophoresis with mass spectrometry (KCE-MS) to study the stability of G-quadruplex structure upon binding to the anti-cancer drug, cisplatin. (Mironov, Okhonin, Khan, Clouthier, & Berezovski, 2014) This structural information is pivotal for elucidating the mechanistic underpinnings of aptamer-mediated therapeutic activity.

Biomarker analysis, a critical facet of therapeutic assessment, can also be facilitated through MS. Researchers can gather insights into treatment efficacy by monitoring changes in biomarker levels in response to aptamer therapy. These insights have been validated in numerous clinical studies, with MS serving as an essential for biomarker discovery and validation. Subramanian et al. 2016 DESI-M to study the phosphatidylcholine level in monitoring the therapeutic response of Nucleolin-aptamer in retinoblastoma. (Subramanian et al., 2016) As aptamer therapy advances toward clinical translation, in vivo studies are imperative for assessing real-world therapeutic outcomes. MS, in conjunction with pharmacokinetics, plays a central role in this domain. MS-based techniques can track the distribution, metabolism, and elimination of aptamers within living organisms, offering invaluable insights into their behavior within the intricate physiological background. This knowledge is pivotal for optimizing dosing regimens and ensuring aptamers reach their intended targets. In 2004, Healy et al. successfully demonstrated MALDI-TOF to study the tissue distribution and the pharmacokinetics of the ani-TGFβ-2 and the modified version in rats. In this study, prolonging the PEGylated aptamer clearance facilitated tissue and organ distribution. (Healy et al., 2004) Clinical sample analysis bridges beachside research and patient

care. MS can be applied to analyze clinical samples from patients undergoing aptamer therapy, offering the unique ability to assess aptamer-target interactions and associated biomarkers quantitatively. These insights enable clinicians to tailor therapies to individual patients, optimizing treatment outcomes. Additionally, MS can serve as a guard for adverse events associated with aptamer-based therapies. By analyzing changes in patients' biomolecular profiles, potential adverse effects can be swiftly detected and monitored, enhancing patient safety. In vivo, MS techniques hold promise in directly assessing the engagement of aptamers with their targets within live organisms. This real-time monitoring of aptamer activity within the complex physiological environment is invaluable for understanding treatment dynamics and efficacy.

1.6 Conclusion

In summary, mass spectrometry (MS) is a highly versatile and influential technique that has revolutionized our comprehension of biological systems and significantly improved applications in biomedicine. Recently, scientists have embarked on a journey to integrate MS into the world of aptamers, harnessing the capabilities of this technology to propel advances in diverse fields, notably biomarker discovery and personalized medicine. However, it is worth noting that our comprehensive understanding of the interplay between MS and aptamers is still a work in progress. In this review, we probed into this synergy, elucidating how it shapes progress in life sciences and holds immense potential for future advancements. This integration commences with the pairing of MS with aptamer selection and characterization. By doing so, researchers can more effectively craft high-affinity aptamers, thereby enhancing their overall performance. In the realm of aptasensors, MS shines by offering structural insights into the interactions between aptamers and their targets, paving the way for a deeper understanding of binding mechanisms and facilitating tailored applications. The impressive specificity, sensitivity, and precision of MS make it ideal for multiplexed target detection from a single sample. Its synergy with aptamers also extends to developing and evaluating aptamer-based therapeutics. MS entails assessing aptamer-drug conjugates' binding affinity and stability and monitoring their behavior in living organisms,

including how they are distributed and metabolized. Furthermore, the amalgamation of MS and aptamers holds tremendous potential for personalized medicine. It can help pinpoint specific biomarkers and tailor treatments based on individual patient profiles, offering a more precise and effective approach to healthcare. Nonetheless, this integration faces a set of formidable challenges. These include improving sensitivity, especially for detecting low-abundance molecules, enhancing the specificity of aptamers by meticulously selecting those with minimal cross-reactivity, particularly in multiplex analyses, and addressing the issues related to the cost and stability of aptamer modifications, such as chemical conjugations and structural adjustments. Furthermore, scientists endeavoring to merge MS with aptamers need access to appropriate equipment and expertise to wield it effectively. Translating aptamer-MS technology into clinical practice presents another hurdle, entailing rigorous compliance with regulatory standards, rigorous validation studies, and the establishment of standardized protocols to guarantee the accuracy and consistency of results. Despite these challenges, the commitment of researchers and ongoing progress in both MS and aptamer technologies promise to resolve many of these issues. As these fields continue to advance, the synergistic alliance between MS and aptamers is poised to usher in innovative solutions for many scientific and clinical applications.

References

Abeer K. Malkawi, R. M. N., Maha Almogren, Afshan Masood, Abdulrahman S. Alarfaj, Hicham Benabdelkamel, Anas M. Abdel Rahman, Mohamed Siaj,. (2023). Quantitative Analysis of Soluble Costimulatory Molecules as Potential Diagnostic Biomarkers for Rheumatoid Arthritis using LC-MS/MS in MRM Mode,. *Clinica Chimica Acta,, 117501*. doi:10.1016/j.cca.2023.117501

Abnous, K., Danesh, N. M., Alibolandi, M., Ramezani, M., & Taghdisi, S. M. (2017). Amperometric aptasensor for ochratoxin A based on the use of a gold electrode modified with aptamer, complementary DNA, SWCNTs and the redox marker Methylene Blue. *Microchimica Acta, 184*(4), 1151-1159. doi:10.1007/s00604-017-2113-7

Akyilmaz, E., Yorganci, E., & Asav, E. (2010). Do copper ions activate tyrosinase enzyme? A biosensor model for the solution. *Bioelectrochemistry, 78*(2), 155-160. doi:10.1016/j.bioelechem.2009.09.007

Amiri-Dashatan, N., Koushki, M., Abbaszadeh, H. A., Rostami-Nejad, M., & Rezaei-Tavirani, M. (2018). Proteomics Applications in Health: Biomarker and Drug Discovery and Food Industry. *Iran J Pharm Res, 17*(4), 1523-1536.

Ayodele, O. O., Adesina, A. O., Pourianejad, S., Averitt, J., & Ignatova, T. (2021). Recent Advances in Nanomaterial-Based Aptasensors in Medical Diagnosis and Therapy. *Nanomaterials (Basel), 11*(4). doi:10.3390/nano11040932

Baek, S. E., Lee, K. H., Park, Y. S., Oh, D. K., Oh, S., Kim, K. S., & Kim, D. E. (2014). RNA aptamer-conjugated liposome as an efficient anticancer drug delivery vehicle targeting cancer cells in vivo. *J Control Release, 196*, 234-242. doi:10.1016/j.jconrel.2014.10.018

Bagalkot, V., Farokhzad, O. C., Langer, R., & Jon, S. (2006). An aptamer-doxorubicin physical conjugate as a novel targeted drug-delivery platform. *Angew Chem Int Ed Engl, 45*(48), 8149-8152. doi:10.1002/anie.200602251

Bagalkot, V., Zhang, L., Levy-Nissenbaum, E., Jon, S., Kantoff, P. W., Langer, R., & Farokhzad, O. C. (2007). Quantum dot-aptamer conjugates for synchronous cancer imaging, therapy, and sensing of drug delivery based on bi-fluorescence resonance energy transfer. *Nano Lett, 7*(10), 3065-3070. doi:10.1021/nl071546n

Bai, Y., Xu, T., & Zhang, X. (2020). Graphene-Based Biosensors for Detection of Biomarkers. *Micromachines (Basel), 11*(1). doi:10.3390/mi11010060

Barrera-Avalos, C., Luraschi, R., Vallejos-Vidal, E., Mella-Torres, A., Hernandez, F., Figueroa, M., . . . Sandino, A. M. (2021). The Rapid Antigen Detection Test for SARS-CoV-2 Underestimates the Identification of COVID-19 Positive Cases and Compromises the Diagnosis of the SARS-CoV-2 (K417N/T, E484K, and N501Y) Variants. *Front Public Health, 9*, 780801. doi:10.3389/fpubh.2021.780801

Bates, P. J., Laber, D. A., Miller, D. M., Thomas, S. D., & Trent, J. O. (2009). Discovery and development of the G-rich oligonucleotide AS1411 as a novel treatment for cancer. *Exp Mol Pathol, 86*(3), 151-164. doi:10.1016/j.yexmp.2009.01.004

Bilik, K. U., Erguven, E., Klussmann, S., Jarosch, F., Wielinga, P. Y., Lutz, T. A., & Riediger, T. (2007). In-vitro and in-vivo antagonistic action of an anti-amylin Spiegelmer. *Neuroreport, 18*(17), 1855-1859. doi:10.1097/WNR.0b013e3282f1ab04

Buglak, A. A., Samokhvalov, A. V., Zherdev, A. V., & Dzantiev, B. B. (2020). Methods and Applications of In Silico Aptamer Design and Modeling. *Int J Mol Sci, 21*(22). doi:10.3390/ijms21228420

Burmeister, P. E., Lewis, S. D., Silva, R. F., Preiss, J. R., Horwitz, L. R., Pendergrast, P. S., . . . Keefe, A. D. (2005). Direct in vitro selection of a 2'-O-methyl aptamer to VEGF. *Chem Biol, 12*(1), 25-33. doi:10.1016/j.chembiol.2004.10.017

Candia, J., Daya, G. N., Tanaka, T., Ferrucci, L., & Walker, K. A. (2022). Assessment of variability in the plasma 7k SomaScan proteomics assay. *Sci Rep, 12*(1), 17147. doi:10.1038/s41598-022-22116-0

Cao, J. T., Yang, J. J., Zhao, L. Z., Wang, Y. L., Wang, H., Liu, Y. M., & Ma, S. H. (2018). Graphene oxide@gold nanorods-based multiple-assisted electrochemiluminescence signal amplification strategy for sensitive detection of prostate specific antigen. *Biosens Bioelectron, 99*, 92-98. doi:10.1016/j.bios.2017.07.050

Cassiday, L. A., Lebruska, L. L., Benson, L. M., Naylor, S., Owen, W. G., & Maher, L. J., 3rd. (2002). Binding stoichiometry of an RNA aptamer and its transcription factor target. *Anal Biochem, 306*(2), 290-297. doi:10.1006/abio.2002.5710

Cennamo, N., Pasquardini, L., Arcadio, F., Vanzetti, L. E., Bossi, A. M., & Zeni, L. (2019). D-shaped plastic optical fibre aptasensor for fast thrombin detection in nanomolar range. *Sci Rep, 9*(1), 18740. doi:10.1038/s41598-019-55248-x

Chai, C., Xie, Z., & Grotewold, E. (2011). SELEX (Systematic Evolution of Ligands by EXponential Enrichment), as a powerful tool for deciphering the protein-

DNA interaction space. *Methods Mol Biol, 754*, 249-258. doi:10.1007/978-1-61779-154-3_14

Chen, C. H., Chernis, G. A., Hoang, V. Q., & Landgraf, R. (2003). Inhibition of heregulin signaling by an aptamer that preferentially binds to the oligomeric form of human epidermal growth factor receptor-3. *Proc Natl Acad Sci U S A, 100*(16), 9226-9231. doi:10.1073/pnas.1332660100

Christian F. W. Becker Dr., R. W. D., Werner Bouschen Dr., Ralf Seidel Dr., Branko Kolaric, Pascal Lang, Hendrik Schroeder Dr., Oliver Müller Priv.-Doz. Dr., Christof M. Niemeyer Prof. Dr., Bernhard Spengler Prof. Dr., Roger S. Goody Prof. Dr., Martin Engelhard Prof. Dr. (2005). Direkter Nachweis von Protein-Protein-Wechselwirkungen durch Massenspektrometrie an Protein-DNA-Mikroarrays. *Angewandte Chemie, 117*(46), 7808-7812. doi:10.1002/ange.200502908

Chu, F., Wei, W., Shuaibu, N. S., Feng, H., Wang, X., & Pan, Y. (2023). Mass Spectrometry-Based Biosensing and Biopsy Technology. *Chemosensors, 11*(8), 419.

Chushak, Y., & Stone, M. O. (2009). In silico selection of RNA aptamers. *Nucleic Acids Res, 37*(12), e87. doi:10.1093/nar/gkp408

Conte, M. S., Bandyk, D. F., Clowes, A. W., Moneta, G. L., Seely, L., Lorenz, T. J., . . . Investigators, P. I. (2006). Results of PREVENT III: a multicenter, randomized trial of edifoligide for the prevention of vein graft failure in lower extremity bypass surgery. *J Vasc Surg, 43*(4), 742-751; discussion 751. doi:10.1016/j.jvs.2005.12.058

Contreras Jimenez, G., Eissa, S., Ng, A., Alhadrami, H., Zourob, M., & Siaj, M. (2015). Aptamer-based label-free impedimetric biosensor for detection of progesterone. *Anal Chem, 87*(2), 1075-1082. doi:10.1021/ac503639s

Dausse, E., Barre, A., Aime, A., Groppi, A., Rico, A., Ainali, C., . . . Di Primo, C. (2016). Aptamer selection by direct microfluidic recovery and surface plasmon resonance evaluation. *Biosens Bioelectron, 80*, 418-425. doi:10.1016/j.bios.2016.02.003

de-los-Santos-Álvarez, N., Lobo-Castañón, M. J., Miranda-Ordieres, A. J., & Tuñón-Blanco, P. (2008). Aptamers as recognition elements for label-free analytical devices. *Trends in Analytical Chemistry, 27*, 437-446.

DiGiusto, D. L., Krishnan, A., Li, L., Li, H., Li, S., Rao, A., . . . Zaia, J. A. (2010). RNA-based gene therapy for HIV with lentiviral vector-modified CD34(+) cells in patients undergoing transplantation for AIDS-related lymphoma. *Sci Transl Med, 2*(36), 36ra43. doi:10.1126/scitranslmed.3000931

Drolet, D. W., Green, L. S., Gold, L., & Janjic, N. (2016). Fit for the Eye: Aptamers in Ocular Disorders. *Nucleic Acid Ther, 26*(3), 127-146. doi:10.1089/nat.2015.0573

Ellington, A. D., & Szostak, J. W. (1990). In vitro selection of RNA molecules that bind specific ligands. *Nature, 346*(6287), 818-822. doi:10.1038/346818a0

Ellington, A. D., & Szostak, J. W. (1992). Selection in vitro of single-stranded DNA molecules that fold into specific ligand-binding structures. *Nature, 355*(6363), 850-852. doi:10.1038/355850a0

Ferapontova, E. E., Olsen, E. M., & Gothelf, K. V. (2008). An RNA aptamer-based electrochemical biosensor for detection of theophylline in serum. *J Am Chem Soc, 130*(13), 4256-4258. doi:10.1021/ja711326b

Fitzwater, T., & Polisky, B. (1996). [17] A SELEX primer. In *Methods in Enzymology* (Vol. 267, pp. 275-301): Academic Press.

Fu, X., He, J., Zhang, C., Chen, J., Wen, Y., Li, J., . . . Yu, C. (2019). Trimetallic signal amplification aptasensor for TSP-1 detection based on Ce-MOF@Au and AuPtRu nanocomposites. *Biosens Bioelectron, 132*, 302-309. doi:10.1016/j.bios.2019.02.054

Gilbert, J. C., DeFeo-Fraulini, T., Hutabarat, R. M., Horvath, C. J., Merlino, P. G., Marsh, H. N., . . . Schaub, R. G. (2007). First-in-human evaluation of anti von Willebrand factor therapeutic aptamer ARC1779 in healthy volunteers. *Circulation, 116*(23), 2678-2686. doi:10.1161/CIRCULATIONAHA.107.724864

Giorgi-Coll, S., Marin, M. J., Sule, O., Hutchinson, P. J., & Carpenter, K. L. H. (2019). Aptamer-modified gold nanoparticles for rapid aggregation-based detection of inflammation: an optical assay for interleukin-6. *Mikrochim Acta, 187*(1), 13. doi:10.1007/s00604-019-3975-7

Gnoth, C., & Johnson, S. (2014). Strips of Hope: Accuracy of Home Pregnancy Tests and New Developments. *Geburtshilfe Frauenheilkd, 74*(7), 661-669. doi:10.1055/s-0034-1368589

Group, V. I. S. i. O. N. C. T., Chakravarthy, U., Adamis, A. P., Cunningham, E. T., Jr., Goldbaum, M., Guyer, D. R., . . . Patel, M. (2006). Year 2 efficacy results of 2 randomized controlled clinical trials of pegaptanib for neovascular age-related macular degeneration. *Ophthalmology, 113*(9), 1508 e1501-1525. doi:10.1016/j.ophtha.2006.02.064

Gulbakan, B., Barylyuk, K., Schneider, P., Pillong, M., Schneider, G., & Zenobi, R. (2018). Native Electrospray Ionization Mass Spectrometry Reveals Multiple Facets of Aptamer-Ligand Interactions: From Mechanism to Binding Constants. *J Am Chem Soc, 140*(24), 7486-7497. doi:10.1021/jacs.7b13044

Gunnarsson, A., Sjovall, P., & Hook, F. (2010). Liposome-based chemical barcodes for single molecule DNA detection using imaging mass spectrometry. *Nano Lett, 10*(2), 732-737. doi:10.1021/nl904208y

Haghighi, M., Khanahmad, H., & Palizban, A. (2018). Selection and Characterization of Single-Stranded DNA Aptamers Binding Human B-Cell Surface Protein CD20 by Cell-SELEX. *Molecules, 23*(4). doi:10.3390/molecules23040715

Healy, J. M., Lewis, S. D., Kurz, M., Boomer, R. M., Thompson, K. M., Wilson, C., & McCauley, T. G. (2004). Pharmacokinetics and biodistribution of novel aptamer compositions. *Pharm Res, 21*(12), 2234-2246. doi:10.1007/s11095-004-7676-4

Hong, P., Li, W., & Li, J. (2012). Applications of aptasensors in clinical diagnostics. *Sensors (Basel), 12*(2), 1181-1193. doi:10.3390/s120201181

Hu, D., Liang, H., Wang, X., Luo, F., Qiu, B., Lin, Z., & Wang, J. (2020). Highly Sensitive and Selective Photoelectrochemical Aptasensor for Cancer Biomarker CA125 Based on AuNPs/GaN Schottky Junction. *Anal Chem, 92*(14), 10114-10120. doi:10.1021/acs.analchem.0c02117

Hu, J., Liu, F., Chen, Y., Shangguan, G., & Ju, H. (2021). Mass Spectrometric Biosensing: A Powerful Approach for Multiplexed Analysis of Clinical Biomolecules. *ACS Sens, 6*(10), 3517-3535. doi:10.1021/acssensors.1c01394

Hu, T., Wu, L., Sun, X., Su, P., & Yang, Y. (2020). Comparative study on quantitation of human myoglobin by both isotope dilution mass spectrometry and surface plasmon resonance based on calibration-free analysis. *Anal Bioanal Chem, 412*(12), 2777-2784. doi:10.1007/s00216-020-02504-z

Huang, B. T., Lai, W. Y., Chang, Y. C., Wang, J. W., Yeh, S. D., Lin, E. P., & Yang, P. C. (2017). A CTLA-4 Antagonizing DNA Aptamer with Antitumor Effect. *Mol Ther Nucleic Acids, 8*, 520-528. doi:10.1016/j.omtn.2017.08.006

Ishikawa, F. N., Chang, H. K., Curreli, M., Liao, H. I., Olson, C. A., Chen, P. C., . . . Zhou, C. (2009). Label-free, electrical detection of the SARS virus N-protein with nanowire biosensors utilizing antibody mimics as capture probes. *ACS Nano, 3*(5), 1219-1224. doi:10.1021/nn900086c

Ishizuka, T., Yamashita, A., Asada, Y., & Xu, Y. (2017). Studying DNA G-Quadruplex Aptamer by (19)F NMR. *ACS Omega, 2*(12), 8843-8848. doi:10.1021/acsomega.7b01405

Jackson, M. A., Ahmann, A., & Shah, V. N. (2021). Type 2 Diabetes and the Use of Real-Time Continuous Glucose Monitoring. *Diabetes Technol Ther, 23*(S1), S27-S34. doi:10.1089/dia.2021.0007

Jellinek, D., Lynott, C. K., Rifkin, D. B., & Janjic, N. (1993). High-affinity RNA ligands to basic fibroblast growth factor inhibit receptor binding. *Proc Natl Acad Sci U S A, 90*(23), 11227-11231. doi:10.1073/pnas.90.23.11227

Jeong, H. Y., Kim, H., Lee, M., Hong, J., Lee, J. H., Kim, J., . . . Kim, S. C. (2020). Development of HER2-Specific Aptamer-Drug Conjugate for Breast Cancer Therapy. *Int J Mol Sci, 21*(24). doi:10.3390/ijms21249764

Ji, J., Pang, Y., Li, D., Huang, Z., Zhang, Z., Xue, N., . . . Mu, X. (2020). An aptamer-based shear horizontal surface acoustic wave biosensor with a CVD-grown single-layered graphene film for high-sensitivity detection of a label-free endotoxin. *Microsyst Nanoeng, 6*, 4. doi:10.1038/s41378-019-0118-6

Jilma, B., Paulinska, P., Jilma-Stohlawetz, P., Gilbert, J. C., Hutabarat, R., & Knobl, P. (2010). A randomised pilot trial of the anti-von Willebrand factor aptamer ARC1779 in patients with type 2b von Willebrand disease. *Thromb Haemost, 104*(3), 563-570. doi:10.1160/TH10-01-0027

Jilma-Stohlawetz, P., Knobl, P., Gilbert, J. C., & Jilma, B. (2012). The anti-von Willebrand factor aptamer ARC1779 increases von Willebrand factor levels and platelet counts in patients with type 2B von Willebrand disease. *Thromb Haemost, 108*(2), 284-290. doi:10.1160/TH11-12-0889

K. J. Light-Wahl, D. L. S., B. E. Winger, C. G. Edmonds, D. G. Camp II, B. D. Thrall, and R. D. Smith. (1993). Observation of a small oligonucleotide duplex by electrospray ionization mass spectrometry. *Journal of the American Chemical Society, 115*(2), 803–804. doi:10.1021/ja00055a070

Kellie, J. F., Tran, J. C., Jian, W., Jones, B., Mehl, J. T., Ge, Y., . . . Bateman, K. P. (2021). Intact Protein Mass Spectrometry for Therapeutic Protein Quantitation, Pharmacokinetics, and Biotransformation in Preclinical and Clinical Studies: An Industry Perspective. *J Am Soc Mass Spectrom, 32*(8), 1886-1900. doi:10.1021/jasms.0c00270

Kenan, D. J., & Keene, J. D. (1999). In vitro selection of aptamers from RNA libraries. *Methods Mol Biol, 118*, 217-231. doi:10.1385/1-59259-676-2:217

Khati, M., Schuman, M., Ibrahim, J., Sattentau, Q., Gordon, S., & James, W. (2003). Neutralization of infectivity of diverse R5 clinical isolates of human immunodeficiency virus type 1 by gp120-binding 2'F-RNA aptamers. *J Virol, 77*(23), 12692-12698. doi:10.1128/jvi.77.23.12692-12698.2003

Kim, N. H., Lee, S. J., & Moskovits, M. (2010). Aptamer-mediated surface-enhanced Raman spectroscopy intensity amplification. *Nano Lett, 10*(10), 4181-4185. doi:10.1021/nl102495j

Kim, S. H., Thoa, T. T. T., & Gu, M. B. (2019). Aptasensors for environmental monitoring of contaminants in water and soil. *Current Opinion in Environmental Science & Health, 10*, 9-21. doi:https://doi.org/10.1016/j.coesh.2019.09.003

Kohn, D. B., Bauer, G., Rice, C. R., Rothschild, J. C., Carbonaro, D. A., Valdez, P., . . . Church, J. (1999). A clinical trial of retroviral-mediated transfer of a rev-responsive element decoy gene into CD34(+) cells from the bone marrow of human immunodeficiency virus-1-infected children. *Blood, 94*(1), 368-371.

Koster, H., Tang, K., Fu, D. J., Braun, A., van den Boom, D., Smith, C. L., . . . Cantor, C. R. (1996). A strategy for rapid and efficient DNA sequencing by mass spectrometry. *Nat Biotechnol, 14*(9), 1123-1128. doi:10.1038/nbt0996-1123

Kourlas, H., & Schiller, D. S. (2006). Pegaptanib sodium for the treatment of neovascular age-related macular degeneration: a review. *Clin Ther, 28*(1), 36-44. doi:10.1016/j.clinthera.2006.01.009

Kubik, M. F., Bell, C., Fitzwater, T., Watson, S. R., & Tasset, D. M. (1997). Isolation and characterization of 2'-fluoro-, 2'-amino-, and 2'-fluoro-/amino-modified RNA ligands to human IFN-gamma that inhibit receptor binding. *J Immunol, 159*(1), 259-267.

Kwon, M., Chun, S. M., Jeong, S., & Yu, J. (2001). In vitro selection of RNA against kanamycin B. *Mol Cells, 11*(3), 303-311.

Lasserre, P., Balansethupathy, B., Vezza, V. J., Butterworth, A., Macdonald, A., Blair, E. O., . . . Corrigan, D. K. (2022). SARS-CoV-2 Aptasensors Based on Electrochemical Impedance Spectroscopy and Low-Cost Gold Electrode Substrates. *Anal Chem, 94*(4), 2126-2133. doi:10.1021/acs.analchem.1c04456

Lee, S. W., & Sullenger, B. A. (1997). Isolation of a nuclease-resistant decoy RNA that can protect human acetylcholine receptors from myasthenic antibodies. *Nat Biotechnol, 15*(1), 41-45. doi:10.1038/nbt0197-41

Lee, T. C., Sullenger, B. A., Gallardo, H. F., Ungers, G. E., & Gilboa, E. (1992). Overexpression of RRE-derived sequences inhibits HIV-1 replication in CEM cells. *New Biol, 4*(1), 66-74.

Li, H., Wolff, J. J., Van Orden, S. L., & Loo, J. A. (2014). Native top-down electrospray ionization-mass spectrometry of 158 kDa protein complex by high-resolution Fourier transform ion cyclotron resonance mass spectrometry. *Anal Chem, 86*(1), 317-320. doi:10.1021/ac4033214

Lin, P. H., Chen, R. H., Lee, C. H., Chang, Y., Chen, C. S., & Chen, W. Y. (2011). Studies of the binding mechanism between aptamers and thrombin by circular dichroism, surface plasmon resonance and isothermal titration calorimetry. *Colloids Surf B Biointerfaces, 88*(2), 552-558. doi:10.1016/j.colsurfb.2011.07.032

Lincoff, A. M., Mehran, R., Povsic, T. J., Zelenkofske, S. L., Huang, Z., Armstrong, P. W., . . . Investigators, R.-P. (2016). Effect of the REG1 anticoagulation system versus bivalirudin on outcomes after percutaneous coronary intervention (REGULATE-PCI): a randomised clinical trial. *Lancet, 387*(10016), 349-356. doi:10.1016/S0140-6736(15)00515-2

Ling, K., Jiang, H., Li, Y., Tao, X., Qiu, C., & Li, F. R. (2016). A self-assembling RNA aptamer-based graphene oxide sensor for the turn-on detection of theophylline in serum. *Biosens Bioelectron, 86*, 8-13. doi:10.1016/j.bios.2016.06.024

Liu, M., Zaman, K., & Fortenberry, Y. M. (2021). Overview of the Therapeutic Potential of Aptamers Targeting Coagulation Factors. *Int J Mol Sci, 22*(8). doi:10.3390/ijms22083897

Liu, X., Hou, Y., Qin, Y., Cheng, J., Hou, J., Wu, Q., & Liu, Z. (2023). Selection of a Novel DNA Aptamer Specific for 5-Hydroxymethylfurfural Using Capture-SELEX. *Biosensors (Basel), 13*(5). doi:10.3390/bios13050564

Liu, X., Li, H., Jia, W., Chen, Z., & Xu, D. (2017). Selection of aptamers based on a protein microarray integrated with a microfluidic chip. *Lab on a Chip, 17*(1), 178-185.

Liu, Y., Kuan, C. T., Mi, J., Zhang, X., Clary, B. M., Bigner, D. D., & Sullenger, B. A. (2009). Aptamers selected against the unglycosylated EGFRvIII ectodomain and

delivered intracellularly reduce membrane-bound EGFRvIII and induce apoptosis. *Biol Chem, 390*(2), 137-144. doi:10.1515/BC.2009.022

Lu, R. M., Hwang, Y. C., Liu, I. J., Lee, C. C., Tsai, H. Z., Li, H. J., & Wu, H. C. (2020). Development of therapeutic antibodies for the treatment of diseases. *J Biomed Sci, 27*(1), 1. doi:10.1186/s12929-019-0592-z

Ludwig, H., Weisel, K., Petrucci, M. T., Leleu, X., Cafro, A. M., Garderet, L., . . . Engelhardt, M. (2017). Olaptesed pegol, an anti-CXCL12/SDF-1 Spiegelmer, alone and with bortezomib-dexamethasone in relapsed/refractory multiple myeloma: a Phase IIa Study. *Leukemia, 31*(4), 997-1000. doi:10.1038/leu.2017.5

Lupold, S. E., Hicke, B. J., Lin, Y., & Coffey, D. S. (2002). Identification and characterization of nuclease-stabilized RNA molecules that bind human prostate cancer cells via the prostate-specific membrane antigen. *Cancer Res, 62*(14), 4029-4033.

Lupu, L., Wiegand, P., Huttmann, N., Rawer, S., Kleinekofort, W., Shugureva, I., . . . Przybylski, M. (2020). Molecular Epitope Determination of Aptamer Complexes of the Multidomain Protein C-Met by Proteolytic Affinity-Mass Spectrometry. *ChemMedChem, 15*(4), 363-369. doi:10.1002/cmdc.201900489

Malkawi, A. K., Jafari, M., Ohlund, L., Sleno, L., Abdel Rahman, A. M., & Siaj, M. (2023). A diagnostic electrochemical aptasensor development for sCD80 protein detection in human serum. *Biosens Bioelectron, 242*, 115696. doi:10.1016/j.bios.2023.115696

Malkawi, A. K., Nimer, R. M., Almogren, M., Masood, A., Alarfaj, A. S., Benabdelkamel, H., . . . Siaj, M. (2023). Quantitative analysis of soluble costimulatory molecules as potential diagnostic biomarkers for rheumatoid arthritis using LC-MS/MS in MRM mode. *Clin Chim Acta, 548*, 117501. doi:10.1016/j.cca.2023.117501

Marciniak, R. A., Garcia-Blanco, M. A., & Sharp, P. A. (1990). Identification and characterization of a HeLa nuclear protein that specifically binds to the trans-activation-response (TAR) element of human immunodeficiency virus. *Proc Natl Acad Sci U S A, 87*(9), 3624-3628. doi:10.1073/pnas.87.9.3624

Martinez-Roque, M. A., Franco-Urquijo, P. A., Garcia-Velasquez, V. M., Choukeife, M., Mayer, G., Molina-Ramirez, S. R., . . . Alvarez-Salas, L. M. (2022). DNA aptamer selection for SARS-CoV-2 spike glycoprotein detection. *Anal Biochem, 645*, 114633. doi:10.1016/j.ab.2022.114633

McKeague, M., & Derosa, M. C. (2012). Challenges and opportunities for small molecule aptamer development. *J Nucleic Acids, 2012*, 748913. doi:10.1155/2012/748913

McKeague, M., Velu, R., Hill, K., Bardoczy, V., Meszaros, T., & DeRosa, M. C. (2014). Selection and characterization of a novel DNA aptamer for label-free fluorescence biosensing of ochratoxin A. *Toxins (Basel), 6*(8), 2435-2452. doi:10.3390/toxins6082435

Michaud, M., Jourdan, E., Villet, A., Ravel, A., Grosset, C., & Peyrin, E. (2003). A DNA aptamer as a new target-specific chiral selector for HPLC. *J Am Chem Soc, 125*(28), 8672-8679. doi:10.1021/ja034483t

Michienzi, A., Li, S., Zaia, J. A., & Rossi, J. J. (2002). A nucleolar TAR decoy inhibitor of HIV-1 replication. *Proc Natl Acad Sci U S A, 99*(22), 14047-14052. doi:10.1073/pnas.212229599

Miron-Merida, V. A., Gong, Y. Y., & Goycoolea, F. M. (2021). Aptamer-based detection of fumonisin B1: A critical review. *Anal Chim Acta, 1160*, 338395. doi:10.1016/j.aca.2021.338395

Mironov, G. G., Okhonin, V., Khan, N., Clouthier, C. M., & Berezovski, M. V. (2014). Conformational Dynamics of DNA G-Quadruplex in Solution Studied by Kinetic Capillary Electrophoresis Coupled On-line with Mass Spectrometry. *ChemistryOpen, 3*(2), 58-64. doi:10.1002/open.201400002

Mo, T., Liu, X., Luo, Y., Zhong, L., Zhang, Z., Li, T., . . . Chen, X. (2022). Aptamer-based biosensors and application in tumor theranostics. *Cancer Sci, 113*(1), 7-16. doi:10.1111/cas.15194

Naresh, V., & Lee, N. (2021). A Review on Biosensors and Recent Development of Nanostructured Materials-Enabled Biosensors. *Sensors (Basel), 21*(4). doi:10.3390/s21041109

Ng, E. W., Shima, D. T., Calias, P., Cunningham, E. T., Jr., Guyer, D. R., & Adamis, A. P. (2006). Pegaptanib, a targeted anti-VEGF aptamer for ocular vascular disease. *Nat Rev Drug Discov, 5*(2), 123-132. doi:10.1038/nrd1955

Nutiu, R., & Li, Y. (2005). In vitro selection of structure-switching signaling aptamers. *Angew Chem Int Ed Engl, 44*(7), 1061-1065. doi:10.1002/anie.200461848

O'Connell, D., Koenig, A., Jennings, S., Hicke, B., Han, H. L., Fitzwater, T., . . . Varki, A. (1996). Calcium-dependent oligonucleotide antagonists specific for L-selectin. *Proc Natl Acad Sci U S A, 93*(12), 5883-5887. doi:10.1073/pnas.93.12.5883

Pagratis, N. C., Bell, C., Chang, Y. F., Jennings, S., Fitzwater, T., Jellinek, D., & Dang, C. (1997). Potent 2'-amino-, and 2'-fluoro-2'-deoxyribonucleotide RNA inhibitors of keratinocyte growth factor. *Nat Biotechnol, 15*(1), 68-73. doi:10.1038/nbt0197-68

Pfeiffer, F., & Mayer, G. (2016). Selection and Biosensor Application of Aptamers for Small Molecules. *Front Chem, 4*, 25. doi:10.3389/fchem.2016.00025

Plach, M., & Schubert, T. (2020). Biophysical Characterization of Aptamer-Target Interactions. *Adv Biochem Eng Biotechnol, 174*, 1-15. doi:10.1007/10_2019_103

Ponce, A. T., & Hong, K. L. (2019). A Mini-Review: Clinical Development and Potential of Aptamers for Thrombotic Events Treatment and Monitoring. *Biomedicines, 7*(3). doi:10.3390/biomedicines7030055

Ponikova, S., Tluckova, K., Antalik, M., Viglasky, V., & Hianik, T. (2011). The circular dichroism and differential scanning calorimetry study of the properties of DNA aptamer dimers. *Biophys Chem, 155*(1), 29-35. doi:10.1016/j.bpc.2011.02.004

Prante, M., Segal, E., Scheper, T., Bahnemann, J., & Walter, J. (2020). Aptasensors for Point-of-Care Detection of Small Molecules. *Biosensors (Basel), 10*(9). doi:10.3390/bios10090108

Radko, S., Ptitsyn, K., Novikova, S., Kiseleva, Y., Moysa, A., Kurbatov, L., . . . Archakov, A. (2020). Evaluation of Aptamers as Affinity Reagents for an Enhancement of SRM-Based Detection of Low-Abundance Proteins in Blood Plasma. *Biomedicines, 8*(5). doi:10.3390/biomedicines8050133

Ramezani, M., Abnous, K., & Taghdisi, S. M. (2017). Optical and Electrochemical Aptasensors for Sensitive Detection of Streptomycin in Blood Serum and Milk. *Methods Mol Biol, 1572*, 403-420. doi:10.1007/978-1-4939-6911-1_26

Ray, J., Kruse, A., Ozer, A., Kajitani, T., Johnson, R., MacCoss, M., . . . Lis, J. T. (2020). RNA aptamer capture of macromolecular complexes for mass spectrometry analysis. *Nucleic Acids Res, 48*(15), e90. doi:10.1093/nar/gkaa542

Rechnitz, G. (1978). Biochemical electrodes uses tissues slice. *Chem Eng News, 56*, 16-21.

Riley, K. R., Gagliano, J., Xiao, J., Libby, K., Saito, S., Yu, G., . . . Bonin, K. (2015). Combining capillary electrophoresis and next-generation sequencing for aptamer selection. *Anal Bioanal Chem, 407*(6), 1527-1532. doi:10.1007/s00216-014-8427-y

Rosenberg, J. E., Bambury, R. M., Van Allen, E. M., Drabkin, H. A., Lara, P. N., Jr., Harzstark, A. L., . . . Laber, D. A. (2014). A phase II trial of AS1411 (a novel nucleolin-targeted DNA aptamer) in metastatic renal cell carcinoma. *Invest New Drugs, 32*(1), 178-187. doi:10.1007/s10637-013-0045-6

Roulet, E., Busso, S., Camargo, A. A., Simpson, A. J., Mermod, N., & Bucher, P. (2002). High-throughput SELEX SAGE method for quantitative modeling of transcription-factor binding sites. *Nat Biotechnol, 20*(8), 831-835. doi:10.1038/nbt718

Salimi, A., Khezrian, S., Hallaj, R., & Vaziry, A. (2014). Highly sensitive electrochemical aptasensor for immunoglobulin E detection based on sandwich assay using enzyme-linked aptamer. *Anal Biochem, 466*, 89-97. doi:10.1016/j.ab.2014.08.019

Sangam, S. A. M. a. V. G. (2017). Optimized Performance Validation of Biosensors with High Fault Tolerance. *EEE 7th International Advance Computing Conference (IACC)*, 322-325. doi:10.1109/IACC.2017.0076.

Sayyed, S. G., Hagele, H., Kulkarni, O. P., Endlich, K., Segerer, S., Eulberg, D., . . . Anders, H. J. (2009). Podocytes produce homeostatic chemokine stromal cell-derived factor-1/CXCL12, which contributes to glomerulosclerosis, podocyte loss and albuminuria in a mouse model of type 2 diabetes. *Diabetologia, 52*(11), 2445-2454. doi:10.1007/s00125-009-1493-6

Schlecht, U., Malave, A., Gronewold, T., Tewes, M., & Lohndorf, M. (2006). Comparison of antibody and aptamer receptors for the specific detection of thrombin with a nanometer gap-sized impedance biosensor. *Anal Chim Acta, 573-574*, 65-68. doi:10.1016/j.aca.2006.01.016

Shen, H., Wang, J., Liu, H., Li, Z., Jiang, F., Wang, F. B., & Yuan, Q. (2016). Rapid and Selective Detection of Pathogenic Bacteria in Bloodstream Infections with Aptamer-Based Recognition. *ACS Appl Mater Interfaces, 8*(30), 19371-19378. doi:10.1021/acsami.6b06671

Shen, P., Li, M., Li, R., Han, B., Ma, H., Hou, X., . . . Wang, J.-J. (2022). Aptamer-functionalized smart photonic hydrogels: application for the detection of thrombin in human serum. *NPG Asia Materials, 14*(1), 94. doi:10.1038/s41427-022-00443-y

Song, J. H., Lee, S. M., Park, I. H., Yong, D., Lee, K. S., Shin, J. S., & Yoo, K. H. (2019). Vertical capacitance aptasensors for real-time monitoring of bacterial growth and antibiotic susceptibility in blood. *Biosens Bioelectron, 143*, 111623. doi:10.1016/j.bios.2019.111623

Strehlitz, B., Nikolaus, N., & Stoltenburg, R. (2008). Protein Detection with Aptamer Biosensors. *Sensors (Basel), 8*(7), 4296-4307. doi:10.3390/s8074296

Su, J., & Mrksich, M. (2002). Using mass spectrometry to characterize self-assembled monolayers presenting peptides, proteins, and carbohydrates. *Angew Chem Int Ed Engl, 41*(24), 4715-4718. doi:10.1002/anie.200290026

Subramanian, N., Srimany, A., Kanwar, J. R., Kanwar, R. K., Akilandeswari, B., Rishi, P., . . . Krishnakumar, S. (2016). Nucleolin-aptamer therapy in retinoblastoma: molecular changes and mass spectrometry-based imaging. *Mol Ther Nucleic Acids, 5*(8), e358. doi:10.1038/mtna.2016.70

Sullenger, B., Woodruff, R., & Monroe, D. M. (2012). Potent anticoagulant aptamer directed against factor IXa blocks macromolecular substrate interaction. *J Biol Chem, 287*(16), 12779-12786. doi:10.1074/jbc.M111.300772

Suzuki, J., Tezuka, D., Morishita, R., & Isobe, M. (2009). An initial case of suppressed restenosis with nuclear factor-kappa B decoy transfection after percutaneous coronary intervention. *J Gene Med, 11*(1), 89-91. doi:10.1002/jgm.1266

Tan, H., Ma, L., Guo, T., Zhou, H., Chen, L., Zhang, Y., . . . Yu, Y. (2019). A novel fluorescence aptasensor based on mesoporous silica nanoparticles for selective and sensitive detection of aflatoxin B(1). *Anal Chim Acta, 1068*, 87-95. doi:10.1016/j.aca.2019.04.014

Tasset, D. M., Kubik, M. F., & Steiner, W. (1997). Oligonucleotide inhibitors of human thrombin that bind distinct epitopes. *J Mol Biol, 272*(5), 688-698. doi:10.1006/jmbi.1997.1275

Tombelli, S., Minunni, M., Luzi, E., & Mascini, M. (2005). Aptamer-based biosensors for the detection of HIV-1 Tat protein. *Bioelectrochemistry, 67*(2), 135-141. doi:10.1016/j.bioelechem.2004.04.011

Trelle, M. B., Dupont, D. M., Madsen, J. B., Andreasen, P. A., & Jorgensen, T. J. (2014). Dissecting the effect of RNA aptamer binding on the dynamics of plasminogen activator inhibitor 1 using hydrogen/deuterium exchange mass spectrometry. *ACS Chem Biol, 9*(1), 174-182. doi:10.1021/cb400619v

Tuerk, C., MacDougal, S., & Gold, L. (1992). RNA pseudoknots that inhibit human immunodeficiency virus type 1 reverse transcriptase. *Proc Natl Acad Sci U S A, 89*(15), 6988-6992. doi:10.1073/pnas.89.15.6988

Tuske, S., Zheng, J., Olson, E. D., Ruiz, F. X., Pascal, B. D., Hoang, A., . . . Arnold, E. (2020). Integrative structural biology studies of HIV-1 reverse transcriptase binding to a high-affinity DNA aptamer. *Curr Res Struct Biol, 2*, 116-129. doi:10.1016/j.crstbi.2020.06.002

Vater, A., & Klussmann, S. (2015). Turning mirror-image oligonucleotides into drugs: the evolution of Spiegelmer((R)) therapeutics. *Drug Discov Today, 20*(1), 147-155. doi:10.1016/j.drudis.2014.09.004

Venugopal, V. (2002). Biosensors in fish production and quality control. *Biosens Bioelectron, 17*(3), 147-157. doi:10.1016/s0956-5663(01)00180-4

Wang, J. (2008). Electrochemical glucose biosensors. *Chem Rev, 108*(2), 814-825. doi:10.1021/cr068123a

Wang, Y., Li, D., Ren, W., Liu, Z., Dong, S., & Wang, E. (2008). Ultrasensitive colorimetric detection of protein by aptamer-Au nanoparticles conjugates based on a dot-blot assay. *Chem Commun (Camb)*(22), 2520-2522. doi:10.1039/b801055b

Waters, E. K., Genga, R. M., Schwartz, M. C., Nelson, J. A., Schaub, R. G., Olson, K. A., . . . McGinness, K. E. (2011). Aptamer ARC19499 mediates a procoagulant hemostatic effect by inhibiting tissue factor pathway inhibitor. *Blood, The Journal of the American Society of Hematology, 117*(20), 5514-5522.

White, R., Rusconi, C., Scardino, E., Wolberg, A., Lawson, J., Hoffman, M., & Sullenger, B. (2001). Generation of species cross-reactive aptamers using "toggle" SELEX. *Mol Ther, 4*(6), 567-573. doi:10.1006/mthe.2001.0495

Wiegand, T. W., Williams, P. B., Dreskin, S. C., Jouvin, M. H., Kinet, J. P., & Tasset, D. (1996). High-affinity oligonucleotide ligands to human IgE inhibit binding to Fc epsilon receptor I. *J Immunol, 157*(1), 221-230.

Wu, Y. Y., Hsieh, I. S., Tung, C. H., Weng, C. H., Wu, J. E., Yu, J. S., . . . Chen, Y. L. (2022). A novel DNA aptamer targeting lung cancer stem cells exerts a therapeutic effect by binding and neutralizing Annexin A2. *Mol Ther Nucleic Acids, 27*, 956-968. doi:10.1016/j.omtn.2022.01.012

Xiao, Y., Lubin, A. A., Heeger, A. J., & Plaxco, K. W. (2005). Label-free electronic detection of thrombin in blood serum by using an aptamer-based sensor. *Angew Chem Int Ed Engl, 44*(34), 5456-5459. doi:10.1002/anie.200500989

Yang, C. J., Jockusch, S., Vicens, M., Turro, N. J., & Tan, W. (2005). Light-switching excimer probes for rapid protein monitoring in complex biological fluids. *Proc Natl Acad Sci U S A, 102*(48), 17278-17283. doi:10.1073/pnas.0508821102

Yang, Q., Zhang, X., Kumar, S., Singh, R., Zhang, B., Bai, C., & Pu, X. (2020). Development of Glucose Sensor Using Gold Nanoparticles and Glucose-Oxidase Functionalized Tapered Fiber Structure. *Plasmonics, 15*(3), 841-848. doi:10.1007/s11468-019-01104-7

Yao, C., Qi, Y., Zhao, Y., Xiang, Y., Chen, Q., & Fu, W. (2009). Aptamer-based piezoelectric quartz crystal microbalance biosensor array for the quantification of IgE. *Biosens Bioelectron, 24*(8), 2499-2503. doi:10.1016/j.bios.2008.12.036

Yi Peng, L. L., Xiaojiao Mu, Lin Guo. (2013). Aptamer-gold nanoparticle-based colorimetric assay for the sensitive detection of thrombin. *Sensors and Actuators B: Chemical, Volume 177*, 818-825. doi:/10.1016/j.snb.2012.12.004

Yin, S., & Loo, J. A. (2010). Elucidating the site of protein-ATP binding by top-down mass spectrometry. *J Am Soc Mass Spectrom, 21*(6), 899-907. doi:10.1016/j.jasms.2010.01.002

Ying, Y. L., Wang, H. Y., Sutherland, T. C., & Long, Y. T. (2011). Monitoring of an ATP-binding aptamer and its conformational changes using an alpha-hemolysin nanopore. *Small, 7*(1), 87-94. doi:10.1002/smll.201001428

Yoo, E. H., & Lee, S. Y. (2010). Glucose biosensors: an overview of use in clinical practice. *Sensors (Basel), 10*(5), 4558-4576. doi:10.3390/s100504558

Youn, H., Lee, K., Her, J., Jeon, J., Mok, J., So, J. I., . . . Ban, C. (2019). Aptasensor for multiplex detection of antibiotics based on FRET strategy combined with aptamer/graphene oxide complex. *Sci Rep, 9*(1), 7659. doi:10.1038/s41598-019-44051-3

Yu, F., Li, H., Sun, W., Xu, D., & He, F. (2019). Rapid selection of aptamers based on protein microarray. *RSC advances, 9*(17), 9762-9768.

Zamay, G. S., Zamay, T. N., Kolovskii, V. A., Shabanov, A. V., Glazyrin, Y. E., Veprintsev, D. V., . . . Zamay, A. S. (2016). Electrochemical aptasensor for lung cancer-related protein detection in crude blood plasma samples. *Sci Rep, 6*, 34350. doi:10.1038/srep34350

Zhang, J., Loo, R. R. O., & Loo, J. A. (2017). Structural Characterization of a Thrombin-Aptamer Complex by High Resolution Native Top-Down Mass Spectrometry. *J Am Soc Mass Spectrom, 28*(9), 1815-1822. doi:10.1007/s13361-017-1751-7

Zhang, J., Reza Malmirchegini, G., Clubb, R. T., & Loo, J. A. (2015). Native top-down mass spectrometry for the structural characterization of human hemoglobin. *Eur J Mass Spectrom (Chichester), 21*(3), 221-231. doi:10.1255/ejms.1340

Zhang, Y., Xu, S., Wen, L., Bai, Y., Niu, L., Song, D., & Liu, H. (2016). A dielectric barrier discharge ionization based interface for online coupling surface plasmon resonance with mass spectrometry. *Analyst, 141*(11), 3343-3348. doi:10.1039/c6an00561f

Zhao, N., Pei, S. N., Parekh, P., Salazar, E., & Zu, Y. (2014). Blocking interaction of viral gp120 and CD4-expressing T cells by single-stranded DNA aptamers. *Int J Biochem Cell Biol, 51*, 10-18. doi:10.1016/j.biocel.2014.03.008

Zheng, X., Yang, L., Sun, Q., Zhang, L., & Le, T. (2023). Development and Validation of Aptasensor Based on MnO(2) for the Detection of Sulfadiazine Residues. *Biosensors (Basel), 13*(6). doi:10.3390/bios13060613

Zhou, J., & Zhong, L. (2022). Applications of liquid chromatography-mass spectrometry based metabolomics in predictive and personalized medicine. *Front Mol Biosci, 9*, 1049016. doi:10.3389/fmolb.2022.1049016

CHAPTER 2 (SCIENTIFIC ARTICLE)

QUANTITATIVE ANALYSIS OF SOLUBLE COSTIMULATORY MOLECULES AS POTENTIAL DIAGNOSTIC BIOMARKERS FOR RHEUMATOID ARTHRITIS USING LC-MS/MS IN MRM MODE

Abeer K. Malkawi[1], Refat M. Nimer[2], Maha Almogren[3], Afshan Masood[1], Abdulrahman S. Alarfaj[5], Hicham Benabdelkamel[4], Anas M. Abdel Rahman[3,6,7]*, Mohamed Siaj[1]*

[1]Department of Chemistry, University of Quebec at Montreal, Montreal, QC H3C3P8, Canada

[2] Department of Medical Laboratory Sciences, Jordan University of Science and Technology, Irbid 22110, Jordan

[3]Metabolomics Section, Department of Clinical Genomics, Center for Genomics Medicine, King Faisal Specialist Hospital and Research Centre (KFSHRC), Riyadh 11211, Saudi Arabia

[4]Proteomics Resource Unit, Obesity Research Center, College of Medicine, King Saud University, P.O. Box 2925 (98), Riyadh 11461, Saudi Arabia

[5] Department of Medicine, Rheumatology Unit, College of Medicine, King Saud University, Riyadh, Saudi Arabia

[6]Department of Biochemistry and Molecular Medicine, College of Medicine, Al Faisal University, Riyadh, Saudi Arabia

[7]Department of Chemistry, Memorial University of Newfoundland, St. John's, NL, A1C 5S7, Canada

Clinica Chimica Acta 548 (2023) 117501, DOI: 10.1016/j.cca.2023.117501

* Co-correspondence: Prof. Mohamed Siaj (siaj.mohamed@uqam.ca), Dr. Anas Abdel Rahman (aabdelrahman46@kfshrc.edu.sa

CONTRIBUTION OF THE MAIN AUTHOR AND CO-AUTHORS

Abeer Malkawi, Dr. Anas Abdel Rahman, and Prof. Mohamed Siaj conceived the idea of this project. Abeer Malkawi designed the experiment and developed the mass spectrometry method and run the validation and the patient samples and drafted the manuscript. Dr. Refat Nimr, Dr. Abdulrahman S. Alarfaj and Dr. Afshan designed the clinical project, recruited the study patients from their clinic. Ms. Maha Almogren and Dr. Hicham Benabdelkamel helped in the mass spectrometry setup. Dr. Abdel Rahman and Prof. Siaj have critically reviewed the manuscript. All authors approved the current version of the manuscript for publication.

Abstract

Background and aims: Rheumatoid arthritis (RA) is a chronic autoimmune disease. RA-induced immunological responses are coordinated by T-cell stimulation. The costimulatory signal CD28-B7 is essential for T-cell activation by interacting CD28 with CD80 and CD86 costimulatory proteins. CTLA4 is another costimulatory protein that binds to CD80 and CD86 to inhibit T-cell activity. The soluble costimulatory proteins: sCD80, sCD86, sCD28, and sCTLA-4 were detected and quantified in human plasma and correlated with RA development. As potential diagnostic biomarkers for RA, developing a sensitive, specific, and reproducible method for quantifying these costimulatory molecules in human plasma and establishing quantitative ranges for each protein in healthy and RA patients' plasma is essential for advancing the clinical diagnostic and health outcomes.

Materials and methods: A novel quantitative liquid chromatography-tandem spectrometry (LC-MS/MS) technique using multiple reaction monitoring (MRM) modes was developed and validated to measure soluble costimulatory molecules sCTLA4, sCD28, sCD80, and sCD86 in human plasma samples. Furthermore, the method was applied to determine sCTLA4, sCD28, sCD80, and sCD86 levels in plasma samples from RA patients (n= 23) and healthy controls (n=21).

Results: The method was successfully developed and validated according to international inter- and intra-assay precision and accuracy guidelines. The linearity of the method was achieved between 0.5 nM to 100 nM for each protein with a correlation coefficient of > 0.998. The plasma level of sCTLA4, sCD80, and sCD86 in RA patients was significantly elevated compared to controls. RA patients had 63.32 ± 17.63 nM sCTLA4 and controls 36.05 ± 18.83 nM; $p<0.0001$. The performance of the four proteins was determined using ROC curves, where sCTLA4 showed the highest diagnostic and clinical performance compared to the others.

Conclusions: This study reports the first use of LC-MS/MS in MRM mode to accurately quantify soluble costimulatory molecules in plasma samples as potential RA diagnostic biomarkers. Determination of the reference range for each protein with high selectivity and sensitivity increases the potential for utilizing this method as a clinical diagnostic.

Keywords: Rheumatoid arthritis (RA); liquid chromatography-tandem spectrometry (LC-MS/MS); multiple reaction monitoring (MRM); soluble costimulatory molecules; CTLA4; CD80; CD86; CD82

2.1 Introduction

Rheumatoid arthritis (RA) is a systemic chronic and inflammatory joint illness caused by the immune system incorrectly attacking healthy tissue, resulting in particular destruction and functional impairment (Smolen et al., 2018). Women are more prone to disease than men, with rates rising between 30 and 55 years old (Sweeney & Firestein, 2004).

Joint damage and disability can worsen without proper treatment for RA. People with the same diagnosis or at different phases of the disease experience reflecting the disease's variety of symptoms (Smolen et al., 2018). Certain patients with RA (termed seronegative RA) do not produce autoantibodies despite this being a hallmark of the disease (Sweeney & Firestein, 2004). Genetic predisposition exists for this disease, but environmental factors influence its onset (Deane et al., 2017).

Since RA is an autoimmune disease, immune cells, including B-cells, T-cells, and macrophages, play essential roles in disease development and progression (Yap et al., 2018). T-cells enter synovial joints due to inflammation, become activated, and then secrete different cytokines, such as interleukins and tumor necrosis factor (TNF) (Kapoor, Martel-Pelletier, Lajeunesse, Pelletier, & Fahmi, 2011). Due to these cytokines' differential expression, the condition is persistent and results in bone loss, cartilage degradation, and the release of proinflammatory markers. Rheumatoid factor (RF) and anti-citrullinated protein antibodies (ACPA) are examples of autoantibodies produced due to T-cell activation, which also causes B-cell differentiation. Certain proteins (fibrin, vimentin, fibronectin, collagen type II) are strongly expressed in the synovial membrane during inflammation, and ACPA recognizes them only after they have been citrullinated (Chimenti et al., 2015). RA is indicated by the existence of RF and ACPA autoantibodies, considered the main biomarkers for RA diagnosis and therapeutic monitoring. Although RF and

ACPA can be developed before the onset of symptoms of RA, using only these biomarkers for diagnosis is not enough. RF overlaps with other autoimmune diseases, such as systemic lupus erythematous, and ACPA-negative patients are also seen. Different scoring systems have been developed for monitoring disease activity, such as the American College of Rheumatology/European League Against Rheumatism (ACR/EULAR) score, the 28-joint disease activity score (DAS28), simple disease activity index (SDAI), and clinical disease activity index (CDAI). (Atzeni et al., 2017) However, these scoring systems have disadvantages in their selective criteria; a multi-biomarker disease activity test has been developed for disease monitoring. The discovery of new biomarkers for RA using large-scale genomic, transcriptomic, proteomic, and other "omic" technologies will advance the system for early diagnosis and treatment decision-making.

Normally, T-cells need two signals to become wholly activated. The initial signal is generated when a T-cell receptor (TCR) binds to a major histocompatibility complex (MHC) molecule on the surface of an antigen-presenting cell (APC) (Manikwar, Kiptoo, Badawi, Büyüktimkin, & Siahaan, 2012). The second signal is sent through the costimulatory route (CP). The Cluster of Differentiation (CD) costimulatory proteins CD80 (B7-1) and CD86 (B7-2) are involved in the traditional CP for T-cell activation known as the CD28-B7 route (Tai, Wang, Korner, Zhang, & Wei, 2018). B cells, monocytes/macrophages, and dendritic cells primarily express CD80 and CD86, also known as B7 molecules. These molecules become more abundant when these cells are activated (W. Liu et al., 2021). CD28 is a receptor on resting T-cells that provides costimulatory signals by interacting with the ligands CD80 and CD86 (Alegre, Frauwirth, & Thompson, 2001). Upon activation, another T-cell receptor, cytotoxic T-lymphocyte-associated protein 4 (CTLA4), is expressed. CTLA4 belongs to the CD28 family of receptors and has coinhibitory functions (Gotsman, Sharpe, & Lichtman, 2008). It can also bind to the CD80 and CD86 antigens. While this helps to regulate T-cell activity, it can also lead to an undesired immune response.

CD80, CD86, CD28, and CTLA4 are all costimulatory molecules that belong to the immunoglobulin superfamily because they have structural similarities with immunoglobulin (Ig) domains (Buck, 1992; Cao, Zou, Luo, Chen, & Zhang, 2012). The extracellular domains that are necessary for binding and biological activity are referred to as Ig-like domains. Ig-like domains may be variable (IgV)-like or constant (IgC)-like in their structure and function. Several isoforms of these molecules have been identified and characterized. Nevertheless, soluble forms of these molecules have been detected in the bloodstreams of healthy individuals, which are dramatically enhanced in numerous medical disorders such as hematological malignancies, asthma, and RA (Hock et al., 2004; Ip, Wong, Leung, & Lam, 2006; Wong, Lit, Tam, Li, & Lam, 2005).

The discovery of the soluble costimulatory proteins in human circulation and the correlation between their level and the development of different autoimmune diseases, such as RA, increase the attention to studying these molecules for more understanding of the pathology of these diseases and utilizing them as surrogate biomarkers. The significant correlation and association between the circulating level of these molecules and RA activity, the inter-correlation between serum sCTLA4 and sCD28, sCD28 and sCD80, or sCTLA4 and sCD80 in RA patients, and the ability for non-invasive measurement of all are advantages for using these molecules as disease biomarkers for early diagnosis and more personalized treatment.

While immunoassay-based methods, such as enzyme-linked immunosorbent assay (ELISA), are commonly used in clinical validation and diagnostic of protein biomarkers (Cabrera et al., 2012; Matsuyama et al., 2022; Shi, Xie, Deng, Chen, & Xiao, 2004; Simone et al., 2014), they are often employed to quantify specific molecules in biological fluids (Stevens & Pukala, 2020). Although immunoassay-based procedures are supposed to be sensitive, there is a possibility of cross-reactivity due to antibody specificity. In addition, cost, time, and the use of animals in antibody production are all disadvantages (Krastins et al., 2013). As a result, there is a continuing need for a quick, sensitive, specific, and low-cost approach for detecting and quantifying physiologically active proteins such as costimulatory molecules.

Multiple reaction monitoring (MRM), a targeted method based on mass spectrometry (MS), is becoming a promising tool for fast, accurate, and sensitive measurement of potential protein candidates in biological samples and biomedical contexts, mostly with triple quadrupole (QQQ) MS instruments (Doerr, 2013; Kondrat, McClusky, & Cooks, 1978). The quantities of native proteins can be determined from the proteolytic peptide concentrations, which surrogate the native proteins using the MRM method (Kondrat et al., 1978; Kuzyk, Parker, Domanski, & Borchers, 2013; Malkawi et al., 2019). The precise and sensitive quantification of proteins by MS is enabled with this method. Adding stable isotopes in proteomic workflows enables quantification by comparing the ion signals from labeled and non-labeled peptides. This significantly improves the accuracy and consistency of protein quantification based on MS (M. A. Galal, Abdel Jabar, Zhra, Abdel Rahman, & Aljada, 2021; Scott, Turko, & Phinney, 2015).

This study aimed to develop LC-MS/MS techniques for measuring a panel of four proteins: sCD80, sCD86, sCD28, and sCTLA4. We also aimed to determine the healthy and pathogenic clinical ranges for these soluble costimulatory molecules to establish a cut-off range for each protein using the developed method by evaluating the levels of their associated signature peptides in human plasma.

2.2 Materials and Methods

2.2.1 Materials and chemicals

Methanol, acetonitrile (ACN), formic acid (FA), dithiothreitol (DTT), iodoacetamide (IAA), and ammonium bicarbonate (ABC) were purchased from Sigma-Aldrich (St. Louis, MO, USA). Unlabeled and labeled (13C6, 15N2 labeled Lys and 13C6, 15N4 labeled Arg) peptides were custom synthesized by Biomatik Corporation (Kitchener, ON, Canada). RapiGest SF MS detergent was obtained from Waters Corporation (Milford, MA, USA).

2.2.2 Subjects and blood samples

2.2.2.1 Ethical Approval and Participant Recruitment

The study participants' recruitment and protocols were reviewed by the Institutional Review Board of the College of Medicine at King Saud University (IRB No. E-21-6341) and approved before commencing the study. Prior to inclusion, written informed consent was obtained, where adult patients with a known history of RA were consecutively recruited from the outpatient Rheumatology clinics at King Khaled University Hospital at King Saud University Medical City (KSUMC). The physician confirmed the RA diagnosis based on ACR/EULAR 2010 criteria (Aletaha et al., 2010; Rosenfeld et al., 1999). A total of 23 patients with RA were initially assessed for enrollment. Among them, 21 patients met the inclusion criteria and were finally selected. Control plasma samples (n=23) were obtained from the blood bank and healthy age-matched volunteers. The baseline demographic information and clinical laboratory parameters, including complete blood count with an erythrocyte sedimentation rate (ESR), lipid markers, liver function tests, fasting glucose, glycated hemoglobin, and C-reactive protein (CRP), were collected from the patient's medical records **(**Table 2.1**).** The design and procedures of the study were conducted under the Declaration of Helsinki.

2.2.2.2 Sample collection

Blood samples were collected from the patients and the controls by venipuncture into EDTA-coated vacutainer tubes (Vacutainer, BD Biosciences, San Jose, CA, USA). Plasma was obtained after centrifugation (15 min, 3000 × g) of the samples and stored at −80°C until used.

2.2.3 Selection of Signature Peptide

The protein sequences of human (*homo sapiens*) CD28, CD80, CD86, and CTLA4 were identified using The National Center for Biotechnology Information (NCBI) protein database. The accession numbers are P33681, P42081, P16410, P10747, respectively. A list of possible signature peptides

was generated by conducting *in-silico* digestion of proteins with trypsin, a commonly used protease for generating peptides in proteomics research. To perform this step, we utilized the PeptideMass tool, a bioinformatics resource portal developed by the Swiss Institute of Bioinformatics (SIB) and known for its reliability and accuracy in peptide mass calculations. Using this tool, we generated a list of possible signature peptides that we could use to identify and quantify the proteins in our samples. This step was critical in our research, allowing us to streamline the identification process and obtain accurate and reliable results (Food & Drug Administration, 2018; Mariam Ahmed Galal, Jabar, Zhra, Rahman, & Aljada, 2021; Guideline, 2005). To validate that the identified peptides were specifically linked to the target proteins, they were examined using the Basic Local Alignment Search Tool (BLAST) to search for similar protein sequences in the NCBI database (Guideline, 2005). Furthermore, signature peptides were chosen based on the peptide's length (5-25 amino acids), peptide stability using the ProtParam tool (http://web.expasy.org/protparam/ accessed 22 June 2022), and water solubility was calculated using Innovagen's peptide calculator for peptides (PepCalc.com, accessed 22 June 2022). As a result, SP was identified for each protein and checked experimentally using PeptideAtlas (http://peptideatlas.org, accessed on 23 June 2022). We synthesized these signature peptides as light and heavy versions, with the latter being stable isotope labeled (SIL). We created these customized synthetic peptides for our method to use as standards and internal standards (IS). By using these peptides as standards and IS, we were able to accurately quantify the proteins in our samples and identify any potential discrepancies in our results. This step was crucial in ensuring our findings' reliability and accuracy, allowing us to obtain precise protein abundance measurements in our samples (Nimer et al., 2022; Sumaily et al., 2022).

Table 2.1. Demographic and Clinical Characteristics of Rheumatoid Arthritis (RA) and Healthy Groups

Item	RA (*n*=21)	Controls (*n*=23)	P value
Gender(M/F)	(5/16)	(17/9)	
Age	47.8 ± 13.5	40.7 ± 10.36	0.06
BMI	29.2 ± 4.8	28.8 ± 4.0	0.80
Hb (g/L)	126.8 ± 9.0	139.2 ± 7.0	<0.01
WBC 10^9/L	6.5 ± 1.8	6.6 ± 2.4	0.88
RBC (x 10^{12}/L)	4.3 (4.2-4.5)	4.8 (4.4-5.1)	<0.01
Lymphocyte (x 10^9/L)	2.4 (1.8-2.8)	2.2 (2-3.1)	1
Neutrophil (x 10^9/L)	3.2 (2.2-4.05)	3.6 (1.6-5.2)	0.95
PLT (x 10^9/L)	307.4 ± 85.1	320.1 ± 84.5	0.62
ESR (mm/hr)	36 (28-71)	6 (5-8)	<0.01
ALT (U/L)	19 (17-24)	23 (20-27)	0.07
AST (U/L)	16 (14-20)	18.4(16.3-20.4)	0.22
Albumin (g/L)	36.6 ± 3.54	40.2 ± 3.4	<0.01
Glucose (mmol/L)	4.9 ± 0.5	4.6 ± 0.4	0.62
Total Cholesterol (mmol/L)	4.3 ± 0.69	4.5 ± 1.1	0.34
HDL Cholesterol (mmol/L)	1.4 ± 0.41	1.3 ± 0.26	0.41
LDL Cholesterol (mmol/L)	2.3 (1.9-2.8)	2.6 (2.1-3.4)	0.21
Triglycerides (mmol/L)	1.0 (0.9-1.15)	1.02 (0.7-1.2)	0.75
HbA1C %	5.4 ± 0.5	5.2 ± 0.3	0.11
CRP (mg/L)	4.3 (2.1-19.7)	2 (1-3.4)	<0.01

Values are expressed as mean ± standard deviation or median and interquartile range in the parenthesis. A significant difference between RA and control (independent t-test, P value <0.05 for parametric tests and Mann Whitney U test, P value <0.05 for non-parametric tests). BMI: body mass index, Hb: hemoglobin, WBC: white blood cells, RBC: red blood cells, PLT: platelets, ESR: erythrocyte sedimentation rate, ALT: alanine aminotransferase, AST: aspartate transaminase, HDL: high-density lipoprotein, LDL: low-density lipoprotein, HbA1C: glycated hemoglobin, CRP: C-reactive protein.

2.2.4 Development of MRM Transition for peptides

2.2.4.1 Stock and working solution preparation.

A stock solution of each labeled and unlabeled peptide (2.0 mg/mL) was prepared in H2O. For tuning the mass spectrometric conditions and chromatographic optimization, 10.0 µg/mL working solutions were prepared by dilution in mobile phase A: B (0.1% FA in H2O: 0.1% FA in 50% ACN: MeOH).

2.2.4.2 LC-MS/MS analysis

For signal optimization, 10.0 µg/mL solutions of the labeled and unlabeled peptides were injected into the LC-MS/MS system XEVO TQ-MicroS (Waters Corporation, Boston, MA, USA) in the positive-ionization electrospray (+ESI) mode with a flow rate of 300 µL/min. The desolvation and the ion source temperatures were 350 °C and 150 °C, respectively. The precursor ion of the peptides was detected in capillary and cone voltages at 3 kV and 20 V, respectively. The optimal MRM transitions for each peptide were optimized and selected for quantitative and qualitative purposes. Peptides were chromatographed using ultra-high-pressure liquid chromatography (UPLC) ACQUITY UPLC BEH C18, 1.7 µm, 2.1 x 100 mm column using a gradient profile for mobile phase B (0.1% formic acid in 50% ACN: MeOH) was 0-10 min 10% B, 10-11 min 90% B, 11-15 10% B. A mixture of peptide solution was acquired at a flow rate of 0.30 mL/min 15 minutes of running time. The injection volume of samples was 10 µl. General MS parameters were modified for LC-MS/MS. The ion source desolvation temperature was 450 C. The ion source desolvation and cone gas flows were 900 L/Hr, and 50 L/Hr, respectively. The MS capillary and cone source were 2 KV, and 40 V, respectively.

2.2.5 Plasma sample preparation

2.2.5.1 In-Solution tryptic digestion

According to the manufacturer's instructions, the samples' protein concentration was determined using the 2D Quant kit (GE Healthcare, Uppsala, Sweden). The sample volume was equivalent to 50ug of protein and was taken for tryptic digestion. Proteins were precipitated using 4x acetone and adding an initial volume of 50µl of 0.1% RapiGest in 50 mM ammonium bicarbonate until completely dissolved. Samples were next denatured by incubating them for 15 min at 80°C followed by reduction by adding DTT at a final concentration of 10 mM after the samples cooled down. A second incubation was carried out for 30 min at 60°C; the samples were alkylated using iodoacetamide at a final concentration of 10 mM for each sample. The samples were next vortexed and incubated for 40 min at drak room temperature. 2.5 µl of trypsin (1 µg/ml) were added to the samples in a ratio of 1:20 of trypsin to protein. The samples were incubated overnight at 37°C to facilitate the digestion process. 20 µl of 10% formic acid was added and incubated for 30 minutes at 80°C to remove the surfactant. We then separated the supernatant by centrifugation and subsequently lyophilized it. After 20 minutes of centrifugation at 14,000 rpm, the digested peptides' supernatant was collected for solid-phase extraction (SPE).

2.2.5.2 Solid-phase extraction (SPE)

To further purify the peptides after tryptic digestion, SPE was used. The sorbent was moistened with deionized water after conditioning the SPE cartridge (Waters Oasis PRiME, USA) with 100% methanol. The samples and labeled peptides were diluted in a loading buffer (0.1% FA in dH2O) before being run through the sorbent. Double washing with deionized water to remove undesirable substances. 0.1% FA in 50% ACN was used to elute the tryptic peptides and dry the samples to a constant volume using SavantTM DNA Concentrator SpeedVac (Thermo Scientific, USA). For LC-MSMS analysis, the sample dry extracts were reconstituted in 100 uL mobile phase (90:10) with 0.1% FA in H_2O:0.1% FA in ACN.

2.2.6 LC-MS/MS Method Validation

2.2.6.1 Curve linearity

A mixture of unlabeled peptides (20 µg/ml) was diluted to generate a calibration curve and QC samples. An internal standard (20.0 µg/ml) was added in constant amounts. Peptide calibration curves were created and run over three consecutive days for linearity assessment. The peptides signal as area ratios (standard area/internal standard area, IS) were plotted on the y-axis along with the standard solution nominal concentrations on the x-axis. The peptides' signal linearity was assessed by regression as correlation coefficient (R^2) and the precision and accuracy of the calibration levels.

2.2.6.2 Specificity and sensitivity

The calibration curves' lower limits of quantification (LOQ) and the limits of detection (LOD) for each peptide were determined over three consecutive days. The peptides LOQ, the lowest point on the calibration curve, were at least ten times the signal's standard deviation of the blank. The LOD and LOQ S/N ratios were at least 3 and 10, respectively. The accuracy of the LOQ had to be within the range of 80-120% and a daily variance of < 20%. Consequently, the LOD was adjusted using an S/N ratio of at least 3.

2.2.6.3 Inter- and intraday validation

The repeatability (intraday precision) and reproducibility (interday precision) of the three QC concentrations were evaluated to assess the precision and accuracy of the method. Six samples of low-quality control samples (LQC), medium-quality control samples (MQC), and high-quality control samples (HQC) were analyzed on the same day (intraday) and three different days (interday) for repeatability determination and evaluation.

Percent RSD was used to evaluate the signal variability in this study. The intraday precision of each quality control (QC) was calculated using the formula: (σ of measured QC concentrations on day x / mean of measured concentrations on day x) × 100%. The interday precision was calculated using the formula: (σ of measured QC concentrations over three days/mean of measured QC concentrations over three days) × 100%. It was ensured that the difference between one day and the next was kept under 20%. The intraday accuracy of each QC was determined using the formula: (mean measured concentration / nominal concentration) × 100%. The interday accuracy was also calculated using the formula: (mean measured concentration over three days / nominal QC concentration) × 100%. The accuracy of calibrators was deemed acceptable within 80–120% for LOQ and 85-115% for the other standard levels.2.6.4. Peptide stability study

The stability of the selected signature peptides was tested by preparing and analyzing three QC samples (High, medium, and low) under different storage conditions, including room temperature (RT), refrigerator (4 °C), and freezer (-20 °C), and comparing them to freshly prepared QCs. The storage stability of each QC level was assessed by calculating the molecular stability, which was determined by multiplying the average area ratio of the examined sample by the average area ratio of the fresh sample and then multiplying by 100%.

2.2.6.4 Carryover

An assay carryover was examined by injecting the highest standard six times and three blank samples.

2.2.7 Data and Statistical Analysis

Statistical data analysis for the clinical variables between cases and controls was conducted using the Statistical Package for Social Sciences (SPSS) version 26 (SPSS Inc., Armonk, NY, USA), and a p-value of <0.01 was considered statistically significant. Shapiro–Wilk test was performed to determine the normality of the distribution of the continuous variables. Continuous data are

represented as mean and standard deviation (SD) for normally distributed variables or median and interquartile range for skewed distributions. A comparison of means was made for normally distributed variables (non-significant Shapiro-Wilk test $p>0.05$) using the independent samples t-test. Comparison for non-normally distributed variables (Shapiro-Wilk test <0.05) was done using the Mann-Whitney U test.

The data was acquired, processed, and visualized using the LC-MS/MS MassLynx software, version 4.1 (Waters Corporation, Massachusetts, USA). The quantitative signal data were presented as a mean value and SD. A comparison was made between the means of sCD80, sCD86, sCD28, and sCTL4 protein levels in a healthy control group and patients with RA using LC-MS/MS. The statistical analysis was performed using GraphPad Prism 6.01(Version 6.01; Graph Pad Software, La Jolla, CA, USA) with p-values less than 0.05 considered significant (as shown in the figure legends). The graphs were created using GraphPad Prism, version 6.01

2.3 Results

2.3.1 Signature peptide selection and LC-MS/MS method development

CD80, CD86, CD28, and CTLA4 protein sequences, including soluble isoforms, were obtained in a FASTA format from UniProt. Subsequently, using PeptideMass, the peptide sequences that are expected to be produced by trypsin digestion in the theory of these proteins (UniProt ID: P33681, P42081, P16410, P10747, respectively) were obtained and confirmed using Skyline Program (version 19.1, Seatle, WA, USA). The costimulatory molecules' signature peptides were selected using the criteria mentioned in the methodology section. The signature peptides that are stable during genetic mutation were chosen.

Appendix A Table A.1 lists the signature peptides' characteristics unique to the sCD80, sCD86, sCD28, and sCTLA4 proteins. For the absolute measurement of these proteins, the chosen signature peptides were synthesized in two forms: one with a regular molecular weight (referred

to as the "light" variant) and the other with a heavier molecular weight due to the incorporation of stable isotopes (known as the "SIL" variant). These two types were used as references and the comparison in the analysis. Calibration curves were created using standard reference materials to measure the peptide linearity signals. The ionization efficiency of each peptide in the calibration curve and the unknown sample must be identical because the signature peptide and the labeled internal standard (IS) possess the same physiochemical characteristics, such as proton affinity, which impacts ionization efficiencies. Various analytical variables, including ion suppression and ionization efficiency, were compensated for in this study by utilizing isotopically labeled copies of each peptide as internal standards that co-eluted at the same retention time. The concentration of each peptide and the signals for the light (analyte) and heavy (internal standard) were determined Field (Mariam Ahmed Galal et al., 2021) accurately.

The LC-MS/MS technique was evaluated by applying a mixture of signature peptides and their labeled analogs for each target protein. The MRM transitions were tuned to produce the most abundant precursor and product ions for each peptide at the optimal cone voltage and collision energy. The ion source and triple quadrupole analyzer were adjusted accordingly. The impact energy was tuned between 48 and 80 eV, and the cone voltage was varied between 26 and 46 V. The selection of the optimal ions was based on representative extracted ion chromatograms, as illustrated in Figure.2.1. The optimum parameters for the LC-MS/MS method were summarized in appendix A Table A.1, including the retention time (RT), precursor ion (Q1), and product ion (Q2)

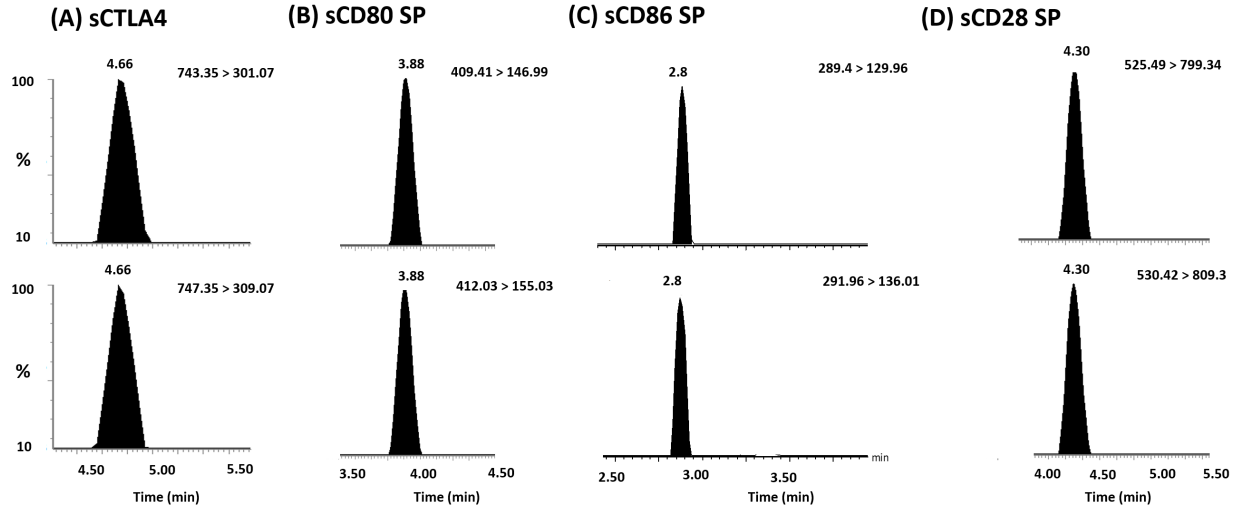

Figure 2.1. Representative extracted ion chromatogram (EIC) of each protein signature peptide (SP) and its internal standard's (IS) quantitative transitions. (A) sCTLA4 SP (top) and sCTLA4 IS (bottom), (B) sCD80 SP (top) and sCD80 IS (bottom), (C) sCD86 SP (top) and sCD86 IS (bottom), and (D) sCD28 SP (top) and sCD28 IS (bottom).

2.3.2 LC-MS/MS Method Validation Study

Validation of bioanalytical procedures was performed following FDA regulations (Food & Drug Administration, 2018).

2.3.2.1 Calibration Curve Linearity

To determine the ranges and linearities of protein measurement (sCTLA4, sCD80, sCD86, sCD28), calibration curves were created for each signature peptide of each protein. The extracted ion chromatograms of sCTLA4, sCD80, sCD86, and sCD28 SP and the correspondence internal standards are shown in Figure 2.1A, B, C, and D, respectively. The calibration curves for sCD28, sCD86, sCD80, and sCTLA4, SP **(**Figure 2.2 A, B, C, and D**)** were linear. They covered the 0.5 to 100 nM range, with correlation coefficients (R^2) of 0.9999, 0.9981, 0.9999, and 0.9998, respectively, representing great linearity. The linearity study over three consecutive days is summarized in **(**Appendix A Table A.2**).**

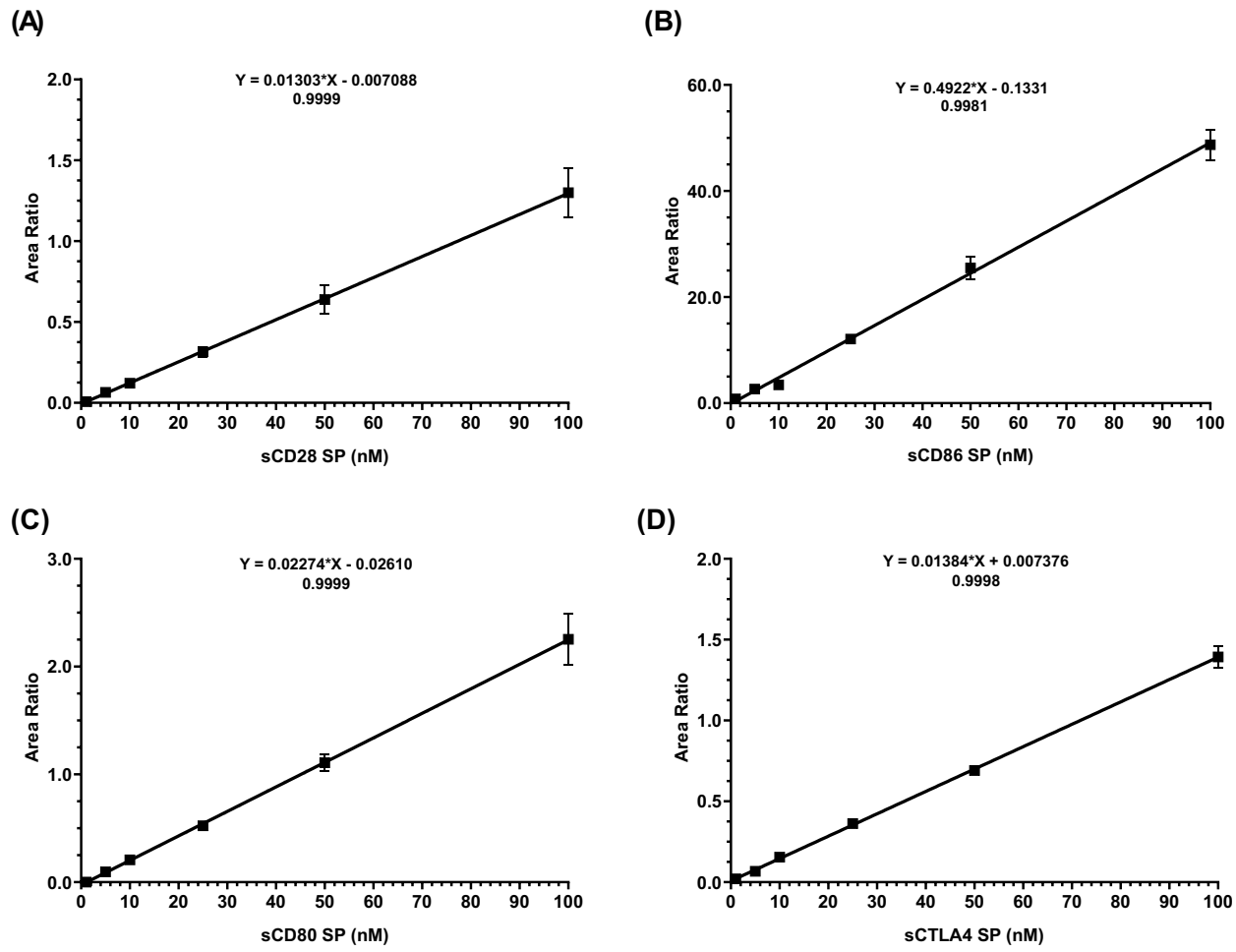

Figure 2.2. Representative calibration curves for the tryptic digested proteins using their signature peptides-based MRM method (A) sCD28 SP, (B) sCD86 SP, (C) sCD80 SP, and (D) sCTLA4 SP.

2.3.2.2 Method Specificity and Sensitivity

The method sensitivity was evaluated following the procedure described in the methods section, and the results are shown in **(**Appendix A Table A.2**)**. For each signature peptide, a LOQ of 0.5 nM was determined. The lack of interferences with identical transition and retention periods for the MRM was defined as specificity. In this method, the specificity was evaluated using LC-MS/MS. In addition, no significant carryover signal was detected in the blank sample, which was less than 20% of the LOQ, described in the methodology section.

2.3.2.3 Inter- and Intraday Validation

Replicates of LQC, MQC, and HQC samples (n=6) (with concentrations of 1.5 nM, 35.0 nM, and 75.0 nM, respectively) were analyzed on the same day (intraday) and three separate days (interday) to determine accuracy and precision. Each sample replicates per QC level was examined twice for each analyte. As shown in **(**Appendix A Table A.3**)**, the signature peptide signals exhibited intra/interday variability of less than 15% and intra/ interday accuracy ranging from 85% to 115%. These values were within the tolerance limits established by the ICH and FDA (EMEA, 2006; Guideline, 2005). Both Intra- and inter-day validations showed good levels of accuracy and precision.

2.3.2.4 Peptide Stability Study

In triplicate, the signature peptide stability was assessed using QC samples (1.5, 35.0, and 75.0 nM). Stability tests were conducted under three storage conditions (room temperature for 24 hours, 4°C for one week, and -20°C for one month). The stability of signature peptides from each protein ranged from 78.5% to 113.0%, as demonstrated in **(**Appendix A Table A.4**).**

2.3.3 sCTLA4, sCD80, sCD86, and sCD28 absolute quantification in human samples

2.3.3.1 Biomarker diagnostic evaluation

Circulating sCTLA4, sCD80, sCD86, and sCD28, absolute concentrations were determined using the selective signature peptides specific for each protein. Comparing RA patients to a control group showed no significant difference in sCD28 levels between RA patients versus healthy control **(**Figure 2.3A**) (**Table 2.2**).** However, a considerable increase in sCD80, sCD86, and sCTLA4 was found in RA patients compared to healthy control **(**Figure 2.3B, C, and D**) (**Table 2.2**).**

Sensitivity and specificity are shown on the ROC curve's y-axis and x-axis, respectively, Figure 2.4. The ideal position is shown in the upper left corner, where all true positives and no false positives were detected. A test with 1 area under the ROC curve (AUC) is considered perfect. sCD28, sCD80, sCTLA4, and sCD86 ROC's AUC values in control and RA groups were 0.5043, 0.8712, 0.8929, and 0.8636, with a 99% confidence interval and a p-value of less than 0.0001. The rest of the costimulatory molecules showed lower diagnostic and analytical performance than sCTLA4 in distinguishing between RA patients and healthy controls.

2.3.3.2 Normal reference range determination

Table 2.2 summarizes the mean, standard error of the mean, minimum/maximum values, and 95% reference intervals for the sCD28, sCD80, sCTLA4, and sCD86 proteins in plasma, based on their corresponding signature peptide concentrations.

The range of normal levels of the proteins in clinical settings was determined by measuring the concentration of analytes based on their corresponding signature peptides in RA and control samples (n=21 and n=22, respectively) according to the guidelines of the Clinical and Laboratory Standards Institute and the International Federation of Clinical Chemistry. (Sasse, 2000; Solberg, 1993). Based on the findings, a reference range for healthy people was established, with the top

and bottom 5% of measured participants excluded from the upper and lower bounds. Table 2.2 provides an overview of this information.

For controls and RA patients, the reference range for sCD28 is between 7.713 and 8.169 nM, 7.708 and 8.112 nM, respectively. sCD80 levels ranged between 61.94 and 101.9 nM for control and 131.2 to 207.3 nM for RA patients. sCD86 levels ranged between 1.712 and 2.316 nM for control and 2.92 to 3.718 nM for RA patients. Moreover, the reference range of sCTLA4 falls between 27.71 and 44.4 nM for control and between 55.29 and 71.34 nM for RA patients.

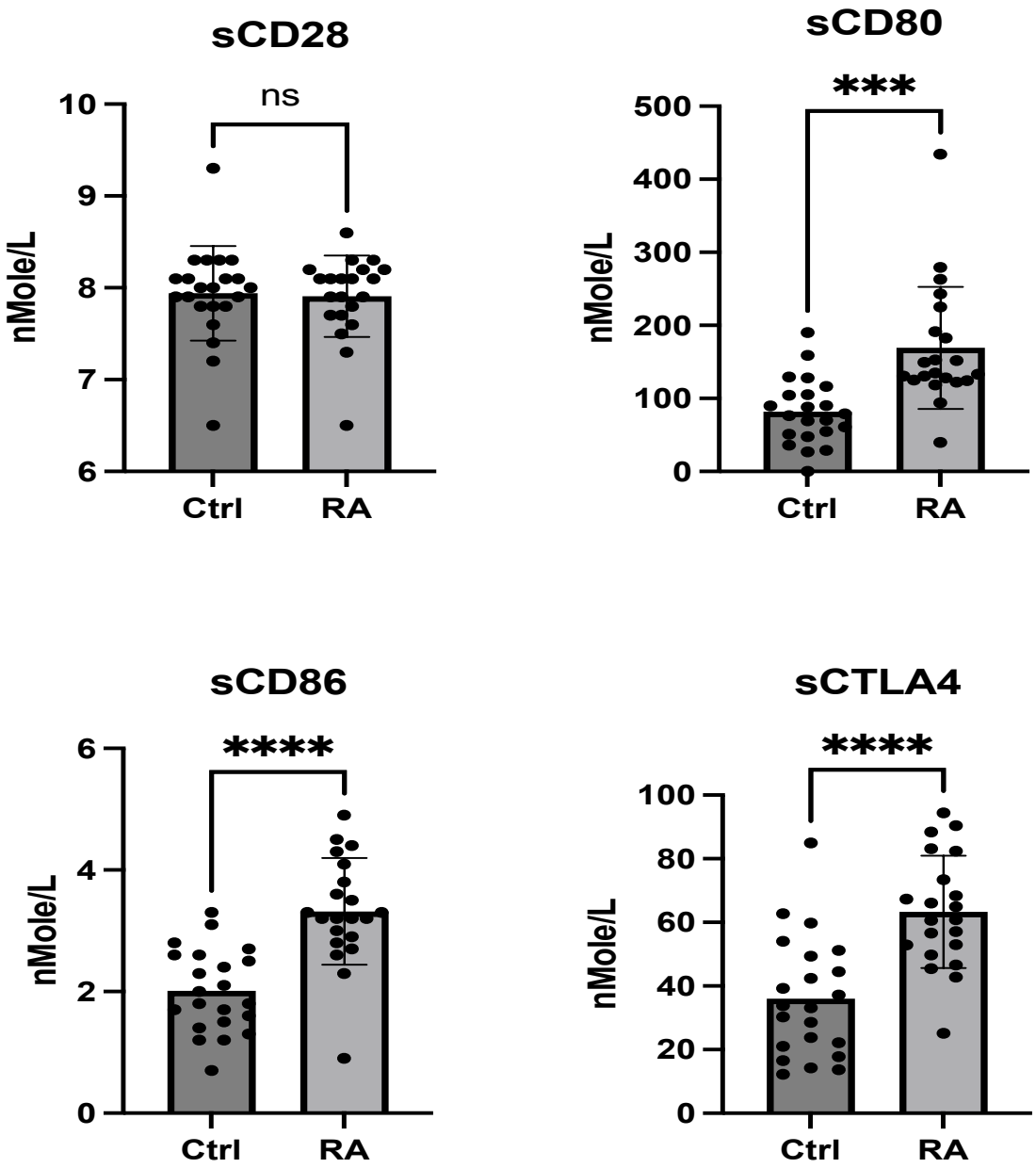

Figure 2.3. Scattered dot plot with bar plot (mean with SD) of A) sCD28, B) sCD80, C) sCD86, and D) sCTLA4. P-value are defined as ns: not significant >0.05, *** 0.0001, **** <0.0001.

Table 2.2. A summary of the clinical reference ranges for sCD28, sCD80, sCD86, and sCTLA4 proteins in nM was determined based on signature peptide concentrations in the plasma of the RA and control groups.

	sCD28		**sCD80**		**sCD86**		**sCTLA4**	
	Ctrl	RA	Ctrl	RA	Ctrl	RA	Ctrl	RA
Minimum	6.5	6.5	0.4	39.7	0.7	0.9	12.3	25.1
Maximum	9.3	8.6	190	434.3	3.3	4.9	85	94.4
Range	2.8	2.1	189.6	394.6	2.6	4	72.7	69.3
Mean	7.941	7.91	81.91	169.3	2.014	3.319	36.05	63.32
Std. Deviation	0.5152	0.4437	45.04	83.58	0.6812	0.8767	18.83	17.63
Std. Error of Mean	0.1098	0.09683	9.603	18.24	0.1452	0.1913	4.015	3.847
Lower 95% CI of mean	7.713	7.708	61.94	131.2	1.712	2.92	27.71	55.29
Upper 95% CI of mean	8.169	8.112	101.9	207.3	2.316	3.718	44.4	71.34
Coefficient of variation	6.49%	5.61%	54.99%	49.38%	33.83%	26.41%	52.23%	27.84%

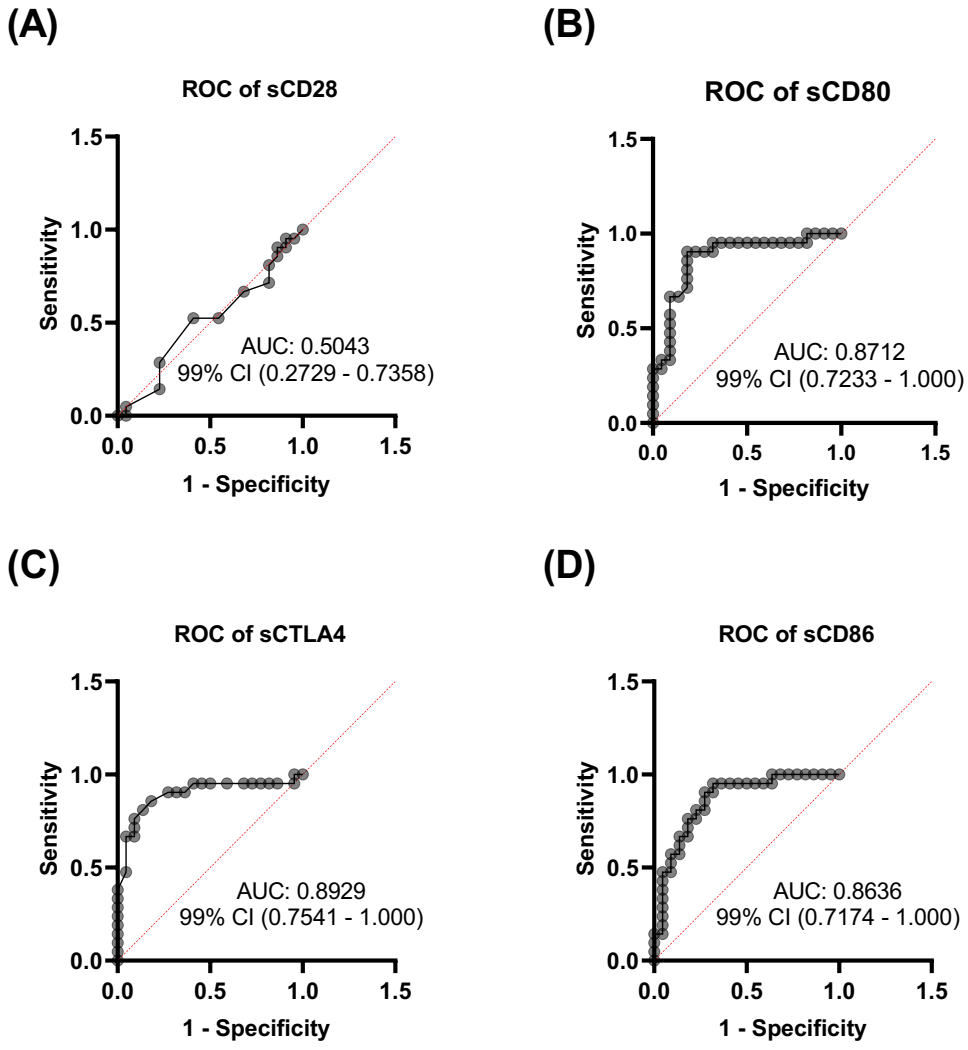

Figure 2.4. The sensitivity and selectivity of RA were evaluated based on signature peptides from sCD28, sCD80, sCTLA4, and sCD86. The performance of the four proteins was determined using ROC curves. The AUC for sCD28 SP was 0.5043 (99% CI, p-value 0.9612), sCD80 SP was 0.8712 (99% CI, p-value <0.0001), sCTLA4 SP was 0.8929 (99% CI, p-value <0.0001), and sCD86 SP was 0.8636 (99% CI, p-value <0.0001). The dashed red lines indicate the random classifiers (x = y). Instances classified above the line were positive, and those below the line were negative.

2.4 Discussion

This study aimed to develop a novel MRM LC-MS/MS method for determining the circulating levels of sCTLA4, sCD80, sCD28, and sCD86 in patients with RA, as potential diagnostic biomarkers. The results showed that sCTLA4, sCD80, and sCD86 levels were significantly higher in patients with RA than in control, consistent with previous studies and the conservation of sCD28 level.

The pathogenesis of RA is complex as it is a heterogeneous disease. The most important aspect of treatment is to reduce and prevent joint disease and inflammation, which is the reason for the pain and disability in patients with RA. Diagnosing the ongoing inflammatory process has relied on CRP and ESR as markers of inflammation, which are also included as components of the ACR/EULAR and the DAS28 scores. Although these conventional markers have been used routinely, their utility is questionable. Previous studies have shown that patients with active disease do not display elevations in their levels (Kay et al., 2014).

Moreover, CRP and ESR lack specificity and rise in the blood when inflammation is present (He et al., 2020). One of the main proponents for developing an autoimmune response in RA is through the disturbances of T-cell activation mediated by costimulatory molecules, whose dysregulation leads to chronic inflammation and joint destruction in RA. Because of their direct involvement in disease development, their levels can correlate better with disease activity than conventional biomarkers (Kotulska, Kopeć-Mędrek, Grosicka, Kubicka, & Kucharz, 2015). Moreover, since they are involved in early immune responses and T-cell activation, which occur even before the onset of clinical symptoms, they have the potential to serve as early diagnostic biomarkers (Cope, Schulze-Koops, & Aringer, 2007).

sCTLA4 has been recognized to be more important in the early stage of immune activation as it is expressed in non-stimulated T-cells compared to membranous mCTLA4, expressed only in

activated T-cells. (M. F. Liu, Wang, Chen, & Fung, 2003) In this study, sCTLA4 was significantly elevated in RA patients compared to healthy controls with higher ROC's AUC value than the other molecules indicating a significant role in RA development. This finding agrees with the previous study, where a significant correlation between the disease activity and sCTLA4 existed throughout the entire RA patient cohort (Cao et al., 2012). sCTLA4 could interfere with the interaction between mCTLA-4 and B7-costimulatory molecules expressed on the surface of APCs, affecting the inhibitory signal and enhancing the immune response. Although the exact immunopathological role sCTLA-4 in RA development is unclear, the circulating serum sCTLA-4 could act as a surrogate biomarker for RA disease activity.

CTLA-4 has a higher affinity to B7 molecules (CD80 and CD86) than CD28 has; thus, the high level of binding of sCTLA-4 to B7 molecules in RA patients could explain the upregulation of sCTLA-4, sCD80, sCD86, and conservation of sCD28 compared to control. In contrast, it has been observed that CD28 is slightly overexpressed in the synovial fluid of RA patients and that the production of its soluble form, sCD28, is increased in the serum compared to healthy individuals (Cao et al., 2012; M. F. Liu et al., 1996). Another study suggests that the accumulation of T-cells lacking CD28 characterizes the autoimmune response in RA (Bryl et al., 2005). This finding explains the non-significant change in the level of sCD28 in the sera of RA patients.

The soluble form of the co-stimulatory molecules is released due to the alternative splicing or enzymatic cleavage of the membranous structure (Hock et al., 2004). Although sCD80 and sCD86 have been approved to bind to their receptors, CD28 and CTLA-4, the biological effect of In-vivo generated soluble co-stimulatory molecules is still unclear. The recombinant sCD80 and sCD86 can inhibit or activate the T-cell response depending on the activation of the CTLA-4 signal or CD28 signal, respectively, indicating the important role of these molecules in immunoregulation (Hock et al., 2004; Rennert et al., 1997). In addition, blocking both CD80 and CD86 during the initial stage of collagen-induced arthritis (CIA) induction in animal models can stop the progression of the disease, which may imply that these costimulatory molecules have therapeutic

potential (Kremer et al., 2003; Lubberts et al., 2004; Odobasic, Leech, Xue, & Holdsworth, 2008). In this study, the increase in the serum level of these molecules in patients with RA is associated with disease development, and manipulating their level has clinical applications. Previous studies investigated the altered cell surface expression of the costimulatory molecules and the elevated level of the soluble form of these molecules in sera of RA patients; however, no clear cut-off range was determined in normal and disease serum or plasma. This study established the clinical reference range for both the controls and the RA patients as a tool for clinical diagnosis. The development of a novel, robust, absolute quantification method for the panel of four molecules (sCD80, sCD86, sCD28, and sCTLA-4) using LC-MS/MS allows for the sensitive and specific detection of these molecules in a complex matrix like a serum. The high specificity of the method overcomes some challenges associated with using the immunoassay methods in biomarkers discovery, such as cross-reactivity. The high-throughput analysis and multiplexing of the developed method, reducing time and cost compared to traditional one-at-a-time approaches with accurate and precise quantification of target analytes, advance our understanding of the disease mechanism, and add a powerful tool for identifying and validating biomarkers with diagnostic, prognostic, and therapeutic potential.

After successfully developing a precise method for quantifying the four costimulatory molecules, a comprehensive study involving a large group of individuals is required. This study examines the relationship between these molecules and their inter-correlation, shedding light on their levels' association with disease severity and stage. To achieve this, patients will be classified based on a scoring system like the DAS28 score.

Their correlation with other diagnostic and inflammatory parameters will be investigated to gain further insights into the clinical significance of these molecules. This includes exploring their relationship with factors such as RF, ACPA, serum proinflammatory cytokines, and chemokines. Additionally, the impact of immunosuppressants on the plasma levels of these molecules will be assessed better to understand their role in the context of treatment.

2.5 Conclusions

To the best of our knowledge, this is the first time the soluble costimulatory molecules sCTLA4, sCD28, sCD80, and sCD86 have been absolutely quantified using an MRM LC-MS/MS strategy. In order to quantify soluble costimulatory molecules, our study introduced a highly sensitive and accurate LC-MS/MS method that depends on signature peptides corresponding to these soluble costimulatory in plasma. This technique has been successfully validated. Our results show that costimulatory molecules sCTLA4, sCD80, and sCD86 levels elevated significantly in RA patients, making them potential diagnostic biomarkers for RA. While LC-MS/MS is susceptible to "isobaric" interferences, the "ion suppression effect" reduces the method's selectivity. It remains the gold standard for analytical methods requiring precise and sensitive protein quantification. In the future, this method can be utilized to determine the amount of soluble costimulatory molecules sCTLA4, sCD28, sCD80, and sCD86 for routine testing for RA.

References

Alegre, M.-L., Frauwirth, K. A., & Thompson, C. B. (2001). T-cell regulation by CD28 and CTLA-4. *Nature Reviews Immunology, 1*(3), 220-228.

Aletaha, D., Neogi, T., Silman, A. J., Funovits, J., Felson, D. T., Bingham III, C. O., . . . Cohen, M. D. (2010). 2010 rheumatoid arthritis classification criteria: an American College of Rheumatology/European League Against Rheumatism collaborative initiative. *Arthritis & rheumatism, 62*(9), 2569-2581.

Atzeni, F., Talotta, R., Masala, I. F., Bongiovanni, S., Boccassini, L., & Sarzi-Puttini, P. (2017). Biomarkers in Rheumatoid Arthritis. *Isr Med Assoc J, 19*(8), 512-516.

Bryl, E., Vallejo, A. N., Matteson, E. L., Witkowski, J. M., Weyand, C. M., & Goronzy, J. J. (2005). Modulation of CD28 expression with anti-tumor necrosis factor alpha therapy in rheumatoid arthritis. *Arthritis Rheum, 52*(10), 2996-3003. doi:10.1002/art.21353

Buck, C. A. (1992). *Immunoglobulin superfamily: structure, function and relationship to other receptor molecules.* Paper presented at the Seminars in cell biology.

Cabrera, R., Fitian, A. I., Ararat, M., Xu, Y., Brusko, T., Wasserfall, C., . . . Nelson, D. R. (2012). Serum levels of soluble CD25 as a marker for hepatocellular carcinoma. *Oncol Lett, 4*(4), 840-846. doi:10.3892/ol.2012.826

Cao, J., Zou, L., Luo, P., Chen, P., & Zhang, L. (2012). Increased production of circulating soluble co-stimulatory molecules CTLA-4, CD28 and CD80 in patients with rheumatoid arthritis. *Int Immunopharmacol, 14*(4), 585-592. doi:10.1016/j.intimp.2012.08.004

Chimenti, M., Triggianese, P., Conigliaro, P., Candi, E., Melino, G., & Perricone, R. (2015). The interplay between inflammation and metabolism in rheumatoid arthritis. *Cell death & disease, 6*(9), e1887-e1887.

Cope, A. P., Schulze-Koops, H., & Aringer, M. (2007). The central role of T cells in rheumatoid arthritis. *Clin Exp Rheumatol, 25*(5 Suppl 46), S4-11.

Deane, K. D., Demoruelle, M. K., Kelmenson, L. B., Kuhn, K. A., Norris, J. M., & Holers, V. M. (2017). Genetic and environmental risk factors for rheumatoid arthritis. *Best Pract Res Clin Rheumatol, 31*(1), 3-18. doi:10.1016/j.berh.2017.08.003

Doerr, A. (2013). Mass spectrometry–based targeted proteomics. *Nature Methods, 10*(1), 23-23. doi:10.1038/nmeth.2286

EMEA, I. (2006). *Topic Q 2 (R1), Validation of Analytical Procedures: Text and Methodology.* Paper presented at the International Conference on Harmonisation of Technical Requirements for Registration of Pharmaceuticals for Human Use.

Food, & Drug Administration, U. (2018). Bioanalytical method validation guidance for industry. *US Department of Health and Human Services*, 1-41.

Galal, M. A., Abdel Jabar, M., Zhra, M., Abdel Rahman, A. M., & Aljada, A. (2021). Absolute quantification of senescence mediators in cells using multiple reaction monitoring liquid chromatography-Tandem mass spectrometry. *Anal Chim Acta, 1184*, 339009. doi:10.1016/j.aca.2021.339009

Galal, M. A., Jabar, M. A., Zhra, M., Rahman, A. M. A., & Aljada, A. (2021). Absolute quantification of senescence mediators in cells using multiple reaction monitoring liquid chromatography-Tandem mass spectrometry. *Analytica chimica acta, 1184*, 339009.

Gotsman, I., Sharpe, A. H., & Lichtman, A. H. (2008). T-cell costimulation and coinhibition in atherosclerosis. *Circulation research, 103*(11), 1220-1231.

Guideline, I. H. T. (2005). *Validation of analytical procedures: text and methodology Q2 (R1).* Paper presented at the International conference on harmonization, Geneva, Switzerland.

He, Y., Tang, J., Wu, B., Yang, B., Ou, Q., & Lin, J. (2020). Correlation between albumin to fibrinogen ratio, C-reactive protein to albumin ratio and Th17 cells in patients with rheumatoid arthritis. *Clinica Chimica Acta, 500*, 149-154. doi:https://doi.org/10.1016/j.cca.2019.10.009

Hock, B. D., Starling, G. C., Patton, W. N., Salm, N., Bond, K., McArthur, L. T., & McKenzie, J. L. (2004). Identification of a circulating soluble form of CD80: levels in patients with hematological malignancies. *Leuk Lymphoma, 45*(10), 2111-2118. doi:10.1080/10428190410001712199

Ip, W. K., Wong, C. K., Leung, T. F., & Lam, C. W. (2006). Plasma concentrations of soluble CTLA-4, CD28, CD80 and CD86 costimulatory molecules reflect disease severity of acute asthma in children. *Pediatr Pulmonol, 41*(7), 674-682. doi:10.1002/ppul.20432

Kapoor, M., Martel-Pelletier, J., Lajeunesse, D., Pelletier, J.-P., & Fahmi, H. (2011). Role of proinflammatory cytokines in the pathophysiology of osteoarthritis. *Nature Reviews Rheumatology, 7*(1), 33-42.

Kay, J., Morgacheva, O., Messing, S. P., Kremer, J. M., Greenberg, J. D., Reed, G. W., . . . Furst, D. E. (2014). Clinical disease activity and acute phase reactant levels are discordant among patients with active rheumatoid arthritis: acute phase reactant levels contribute separately to predicting outcome at one year. *Arthritis Research & Therapy, 16*(1), R40. doi:10.1186/ar4469

Kondrat, R. W., McClusky, G. A., & Cooks, R. G. (1978). Multiple reaction monitoring in mass spectrometry/mass spectrometry for direct analysis of complex mixtures. *Analytical chemistry, 50*(14), 2017-2021.

Kotulska, A., Kopeć-Mędrek, M., Grosicka, A., Kubicka, M., & Kucharz, E. J. (2015). Correlation between erythrocyte sedimentation rate and C-reactive protein level in patients with rheumatic diseases. *Reumatologia, 53*(5), 243-246. doi:10.5114/reum.2015.55825

Krastins, B., Prakash, A., Sarracino, D. A., Nedelkov, D., Niederkofler, E. E., Kiernan, U. A., . . . Garces, A. (2013). Rapid development of sensitive, high-throughput, quantitative and highly selective mass spectrometric targeted immunoassays for clinically important proteins in human plasma and serum. *Clinical biochemistry, 46*(6), 399-410.

Kremer, J. M., Westhovens, R., Leon, M., Di Giorgio, E., Alten, R., Steinfeld, S., . . . Nuamah, I. F. (2003). Treatment of rheumatoid arthritis by selective inhibition of T-cell activation with fusion protein CTLA4Ig. *New England Journal of Medicine, 349*(20), 1907-1915.

Kuzyk, M. A., Parker, C. E., Domanski, D., & Borchers, C. H. (2013). Development of MRM-Based Assays for the Absolute Quantitation of Plasma Proteins. In H. Bäckvall & J. Lehtiö (Eds.), *The Low Molecular Weight Proteome: Methods and Protocols* (pp. 53-82). New York, NY: Springer New York.

Liu, M. F., Kohsaka, H., Sakurai, H., Azuma, M., Okumura, K., Saito, I., & Miyasaka, N. (1996). The presence of costimulatory molecules CD86 and CD28 in rheumatoid arthritis synovium. *Arthritis Rheum, 39*(1), 110-114. doi:10.1002/art.1780390115

Liu, M. F., Wang, C. R., Chen, P. C., & Fung, L. L. (2003). Increased expression of soluble cytotoxic T-lymphocyte-associated antigen-4 molecule in patients with

systemic lupus erythematosus. *Scand J Immunol, 57*(6), 568-572. doi:10.1046/j.1365-3083.2003.01232.x

Liu, W., Yang, Z., Chen, Y., Yang, H., Wan, X., Zhou, X., . . . Zhang, Y. (2021). The association between CTLA-4, CD80/86, and CD28 gene polymorphisms and rheumatoid arthritis: an original study and meta-analysis. *Frontiers in Medicine, 8*, 598076.

Lubberts, E., Koenders, M. I., Oppers-Walgreen, B., Van Den Bersselaar, L., Coenen-de Roo, C. J., Joosten, L. A., & Van Den Berg, W. B. (2004). Treatment with a neutralizing anti-murine interleukin-17 antibody after the onset of collagen-induced arthritis reduces joint inflammation, cartilage destruction, and bone erosion. *Arthritis & Rheumatism: Official Journal of the American College of Rheumatology, 50*(2), 650-659.

Malkawi, A. K., Masood, A., Shinwari, Z., Jacob, M., Benabdelkamel, H., Matic, G., . . . Rahman, A. M. A. (2019). Proteomic Analysis of Morphologically Changed Tissues after Prolonged Dexamethasone Treatment. *Int J Mol Sci, 20*(13). doi:10.3390/ijms20133122

Manikwar, P., Kiptoo, P., Badawi, A. H., Büyüktimkin, B., & Siahaan, T. J. (2012). Antigen-specific blocking of CD4-specific immunological synapse formation using BPI and current therapies for autoimmune diseases. *Medicinal research reviews, 32*(4), 727-764.

Matsuyama, Y., Asanuma, K., Yoshida, K., Hagi, T., Iino, T., Nakamura, T., & Sudo, A. (2022). The role of soluble CD80 in patients with soft tissue tumors. *Journal of Orthopaedic Surgery and Research, 17*(1), 404. doi:10.1186/s13018-022-03283-2

Nimer, R. M., Sumaily, K. M., Almuslat, A., Abdel Jabar, M., Sabi, E. M., Al-Muhaizea, M. A., & Abdel Rahman, A. M. (2022). Dystrophin Protein Quantification as a Duchenne Muscular Dystrophy Diagnostic Biomarker in Dried Blood Spots Using Multiple Reaction Monitoring Tandem Mass Spectrometry: A Preliminary Study. *Molecules, 27*(12). doi:10.3390/molecules27123662

Odobasic, D., Leech, M. T., Xue, J. R., & Holdsworth, S. R. (2008). Distinct in vivo roles of CD80 and CD86 in the effector T-cell responses inducing antigen-induced arthritis. *Immunology, 124*(4), 503-513. doi:10.1111/j.1365-2567.2007.02802.x

Rennert, P., Furlong, K., Jellis, C., Greenfield, E., Freeman, G. J., Ueda, Y., . . . Gray, G. S. (1997). The IgV domain of human B7-2 (CD86) is sufficient to co-stimulate T lymphocytes and induce cytokine secretion. *Int Immunol, 9*(6), 805-813. doi:10.1093/intimm/9.6.805

Rosenfeld, M., Emerson, J., Accurso, F., Armstrong, D., Castile, R., Grimwood, K., . . . Wagener, J. (1999). Diagnostic accuracy of oropharyngeal cultures in infants and young children with cystic fibrosis. *Pediatr Pulmonol, 28*(5), 321-328. doi:10.1002/(sici)1099-0496(199911)28:5<321::aid-ppul3>3.0.co;2-v

Sasse, E. A. (2000). How to define and determine reference intervals in the clinical laboratory; approved guideline. *NCCLS documents C28-A2*.

Scott, K. B., Turko, I. V., & Phinney, K. W. (2015). Quantitative performance of internal standard platforms for absolute protein quantification using multiple reaction monitoring-mass spectrometry. *Analytical chemistry, 87*(8), 4429-4435.

Shi, H. Z., Xie, Z. F., Deng, J. M., Chen, Y. Q., & Xiao, C. Q. (2004). Soluble CD86 protein in serum samples of patients with asthma. *Thorax, 59*(10), 870-875. doi:10.1136/thx.2004.021840

Simone, R., Pesce, G., Antola, P., Rumbullaku, M., Bagnasco, M., Bizzaro, N., & Saverino, D. (2014). The soluble form of CTLA-4 from serum of patients with autoimmune diseases regulates T-cell responses. *Biomed Res Int, 2014*, 215763. doi:10.1155/2014/215763

Smolen, J. S., Aletaha, D., Barton, A., Burmester, G. R., Emery, P., Firestein, G. S., . . . Yamamoto, K. (2018). Rheumatoid arthritis. *Nature Reviews Disease Primers, 4*(1), 18001. doi:10.1038/nrdp.2018.1

Solberg, H. (1993). A guide to IFCC recommendations on reference values. *Journal of the International Federation of Clinical Chemistry, 5*(4), 162-165.

Stevens, K. G., & Pukala, T. L. (2020). Conjugating immunoassays to mass spectrometry: Solutions to contemporary challenges in clinical diagnostics. *TrAC Trends in Analytical Chemistry, 132*, 116064. doi:https://doi.org/10.1016/j.trac.2020.116064

Sumaily, K. M., Nimer, R., Alzahrani, M., Abdel Jabar, M., Alodib, A., Sabi, E. M., . . . Abdel Rahman, A. M. (2022). CFTR protein quantification as a cystic fibrosis diagnostic biomarker in dried blood spots using multiple reaction monitoring tandem mass spectrometry. *J Pharm Biomed Anal, 216*, 114801. doi:10.1016/j.jpba.2022.114801

Sweeney, S. E., & Firestein, G. S. (2004). Rheumatoid arthritis: regulation of synovial inflammation. *The international journal of biochemistry & cell biology, 36*(3), 372-378.

Tai, Y., Wang, Q., Korner, H., Zhang, L., & Wei, W. (2018). Molecular mechanisms of T cells activation by dendritic cells in autoimmune diseases. *Frontiers in pharmacology, 9*, 642.

Wong, C. K., Lit, L. C., Tam, L. S., Li, E. K., & Lam, C. W. (2005). Aberrant production of soluble costimulatory molecules CTLA-4, CD28, CD80 and CD86 in patients with systemic lupus erythematosus. *Rheumatology (Oxford), 44*(8), 989-994. doi:10.1093/rheumatology/keh663

Yap, H. Y., Tee, S. Z., Wong, M. M., Chow, S. K., Peh, S. C., & Teow, S. Y. (2018). Pathogenic Role of Immune Cells in Rheumatoid Arthritis: Implications in Clinical Treatment and Biomarker Development. *Cells, 7*(10). doi:10.3390/cells7100161

CHAPTER 3
(SCIENTIFIC ARTICLE)

A DIAGNOSTIC ELECTROCHEMICAL APTASENSOR DEVELOPMENT FOR SCD80 PROTEIN DETECTION IN HUMAN SERUM

Abeer K. Malkawi[a], Maziar Jafari[a], Leanne Ohlund[a], Lekha Sleno[a], Anas M. Abdel Rahman[b,c,d], Mohamed Siaj[a*]

[a] Department of Chemistry, Université du Québec à Montréal, Montreal, QC, H3C 3P8, Canada

[b] Metabolomics Section, Department of Clinical Genomics, Center for Genome Medicine, King Faisal Specialist Hospital and Research Centre (KFSHRC), Riyadh, Saudi Arabia

[c] Department of Biochemistry and Molecular Medicine, College of Medicine, Alfaisal University, Riyadh, 11350, Saudi Arabia

[d] Department of Chemistry, Memorial University of Newfoundland, St. John's, A1C 5S7, NL, Canada

Biosens Bioelectron. 2023 Dec 15:242:115696. DOI: 10.1016/j.bios.2023.115696

.

* Correspondence:
Professor Mohamed Siaj,
Email: siaj.mohamed@uqam.ca

CONTRIBUTION OF THE MAIN AUTHOR AND CO-AUTHORS

Abeer Malkawi and Prof. Mohamed Siaj conceived the idea of this project. Abeer Malkawi designed the experiment, conducted the SELEX, and biosensor experiments, and drafted the manuscript. Maziar Jafari performed part of the characterization experiment, while Leanne Ohlund, Lekha Sleno, and Anas Abdel Rahman helped in the mass spectrometry experiment. Prof. Siaj have critically reviewed the manuscript. All authors approved the current version of the manuscript for publication.

Abstract

Elevating soluble CD80 (sCD80) in human serum is a natural response to autoimmune diseases such as rheumatoid arthritis (RA). The level of sCD80 is associated with RA development and prognosis; therefore, it is potentially used as a biomarker. sCD80 is commonly measured in human serum using immunoassays (e.g., ELISA) with multiple drawbacks, mainly cross-reactivity. Aptamer-based biosensors (aptasensors) development for quantifying and detecting different biological molecules demonstrates applicability in next-generation medicine and biomarker detection. Herein, we selected a specific aptamer for sCD80 by conventional in-vitro selection process (SELEX) with the high-affinity aptamer (Kd = 47.69 nM). A sensitive aptasensor, for the first time, was developed on a screen-printed gold electrode (AuSPE) platform compatible with easy-to-use label-free electrochemical impedance spectroscopy. The immobilization of the aptamer on the gold surface and the presence of sCD80 in a complex with the aptamer were characterized by photo-induced force microscopy, which revealed the uniform assembly of the aptamer monolayer and the distribution of sCD80 on the electrode surface. The developed aptasensor showed a linear performance (0.025-10.0 nM of protein) with a detection limit of 8.0 pM. Furthermore, the aptasensor was tested in a biological matrix, where a linear signal was observed for the increased amount of spiked sCD80 (R2 = 0.9887). The recovery of the spiked amounts ranged from 105-125% with coefficient of variation (CV%) <7%, which supported the applicability of this sensor in detecting sCD80 for diagnosis.

Keywords

Systemic evolution of ligand by exponential enrichment (SELEX); rheumatoid arthritis biomarkers; label-free electrochemical impedance spectroscopy; photo-induced force microscopy; costimulatory proteins; Aptamer.

3.1 Introduction

Rheumatoid Arthritis (RA) is a chronic inflammatory disease that causes local inflammation in synovial joints (synovitis), resulting in the erosion of bones and the destruction of joints (Chimenti et al., 2015). The autoimmunity and persistent activation of T-cells in RA are associated with the co-stimulatory CD28-B7 pathway. In this pathway, CD80 and CD86 proteins interact with CD28 to activate T-cells, while interacting these two proteins with CTLA-4 negatively impacts the T-cell activation (Hock et al., 2002; Salomon & Bluestone, 2001). CD80 is a type-1 transmembrane glycoprotein member of the Ig superfamily expressed on the surface of activated antigen-presenting cells. The extracellular domains of CD80, Ig-like, are essential for binding and triggering biological activity (Kakoulidou, Giscombe, Zhao, Lefvert, & Wang, 2007). In addition to the full length, a soluble form of CD80 (sCD80) can be generated by alternative splicing or by the enzymatic cleavage of membrane domains (Kakoulidou et al., 2007). sCD80, the extracellular domain of CD80 (1 to 256 AA), has been detected in the human circulation of healthy and autoimmune individuals, (Hock et al., 2004; Ip, Wong, Leung, & Lam, 2006; Wong et al., 2008; Wong, Lit, Tam, Li, & Lam, 2005). sCD80 can bind to both receptors, CD28 and CTLA-4, and affect the T-cell activity (Faas et al., 2000). Although the In-vivo generated sCD80's physiological role is unclear, an elevated level was reported abnormally in the serum of different autoimmune diseases patients such as hematological malignancies, systemic lupus atheromatous (SLE) and many others (Hock et al., 2004; Wong et al., 2005). The study of sCD80 in various disease contexts may help researchers understand how immune responses are regulated and identify new disease biomarkers and treatment approaches.

In RA patients, the sCD80 level was significantly elevated, positively correlated with other RA markers, and therapeutically reduced as a response to immunosuppressant treatment (Cao, Zou, Luo, Chen, & Zhang, 2012; Wan et al., 2006). Accordingly, sCD80 plays an important role in exacerbating RA and is a potential biomarker for the disease.

Immunoassay-based techniques, mainly ELISA, are available for sCD80 analysis. The clinical range or pathogenic cut-off value has been determined consistently in some studies. However, most of the studies focused on the level of comparison between healthy individuals and autoimmune disease patients. ELISA is a reliable technique for biomolecular analysis. However, the structural similarity between the sCD80 and other proteins and the potential cross-reactivity of the antibody limits the specificity of this assay. Additionally, the use of animals and the time-consuming procedure increase the need to develop alternative methods to quantify sCD80 in serum. A mass spectrometry-based approach was just reported to specifically determine the levels of four main co-stimulatory proteins, including sCD80 in RA patients for diagnostic purposes. (Abeer K. Malkawi, 2023).

Aptasensor development for bio-molecule detection and quantification is an emerging research discipline in laboratory medicine (Chinnappan et al., 2021; Eissa et al., 2018). Aptamers' cost efficiency, high stability, and better reproducibility became an alternative to the antibodies in the diagnostic assay (Ahirwar et al., 2019; L. Liu et al., 2021). Unlike antibodies, aptamers can be selected in-vitro with systematic evolution of ligands by exponential enrichment (SELEX), (Stoltenburg, Reinemann, & Strehlitz, 2007).

Combining aptamer and microchip sensing material enhances aptasensor applications in medical fields, including biomarker detection, cancer testing, drug monitoring, and detecting infectious microorganisms. Electrochemical detection methods in aptasensors offer real-time, label-free detection, improving diagnostic test speed and accuracy. Notably, diagnostic aptasensors have been developed for prostate cancer biomarker (PSA) and rapid detection of SARS-CoV-2. (Abrego-Martinez et al., 2022; Hassani et al., 2020) Nucleic acid aptamers adopt a three-dimensional structure when binding to targets, facilitating interaction with a redox system on conductive support for electron transfer probing.

In this study, a novel aptasensor for sCD80 detection in human serum was developed using a simple, one-step label-free impedance spectroscopy detection technique. ssDNA-specific aptamer was selected with remarkable affinity for the sensor development. This aptasensor is the first reported biosensor for sCD80 detection with remarkable sensitivity and selectivity. This research represents a significant step in developing biosensors for potential use in autoimmune disease diagnoses such as RA.

3.2 Methodology:

3.2.1 All reagents and chemicals are listed in supplementary material, Appendix B.1.

3.2.2 In-vitro aptamer selection for sCD80 (SELEX)

Initially, the targeted protein sCD80 was coupled with NTA-Ni agarose beads, and the coupling confirmation was performed using liquid chromatography-high resolution mass spectrometry (LC-HRMS) as detailed in Appendix B.1 and B.2. The designated ssDNA library consisted of ~10^{15} random sequences with a random region of 60 nucleotides flanked by two fixed primers of 18 nucleotides at 3′ and 5′ ends, 5′-ATATCATATGCTCCAATT-N_{60}-AGATCGCAAGTGTAAATA -3′ (96-mer). The primers were used as binding sites for polymerase chain reaction (PCR) amplification of each ssDNA sequence. 3 nmole of the initial library in 300 µL binding buffer (PBS buffer, pH 7.4, 100 mM NaCl, 2 mM $MgCl_2$, 5 mM KCl) was denatured (90ºC, 5 min), chilled (ice, 10 min), and then left at RT for 5 min. The mixture of ssDNA and immobilized target protein on beads (280 pmole) of protein on 5 µL slurry) was incubated in a binding buffer for 2 hours with end-over-end rotation. After the incubation, the solution was spun down to remove the unbound DNA and washed several times with binding buffer to remove the weakly and non-specifically bound ssDNA molecules by monitoring the fluorescent signal decaying in the wash. Afterward, the ssDNA species firmly bound to the sCD80 were eluted by preheated elution buffer (7 M urea in binding buffer). The eluted ssDNA was desalted and concentrated by ultrafiltration membrane centrifugal filters with a 3 kDa cut-off. Subsequently, the ssDNA pool was amplified

by a conventional PCR protocol (Appendix B.3). Subsequently, the PCR product was denatured and extracted using 12% polyacrylamide gel (PAGE) (Appendix B.4), where a fixed amount of ssDNA (120 pmole) was used for each following cycle. After the 12 selection cycles, the ssDNA pool was cloned, sequenced, and aligned as described in Appendic B.5.

The dissociation constant (K_d) for each selected ssDNA aptamer was determined by the fluorescent assay as described in Appendix B.6.

3.2.3 Aptasensor development for sCD80 detection

A screen-printed gold electrode (AuSPE) (BioDevice Technology, Nomi, Ishikawa, Japan) was used to develop the aptasensor. The gold surface was fabricated by 50 mM Potassium hydroxide (KOH) in 30% H_2O_2 for 10 minutes, followed by potential sweep at -200 mV to 100 mV (vs. Ag/AgCl) once at scan rate 50 mV/s as reported elsewhere (Heiskanen, Spegel, Kostesha, Ruzgas, & Emneus, 2008). Before aptamer immobilization on the gold surface, the disulfide labeled ssDNA aptamer in binding buffer at pH 7.4 was heated at 90ºC for 5 minutes and cooled at 4 ºC for 10 and then stood at RT for 5 minutes. 10 µL of 1.5 µM treated ssDNA was drop-cast at the gold surface and incubated for at least 12 hours at 4ºC; the electrode was rinsed with the binding buffer to remove the unbound aptamers. The aptamer-modified electrode was incubated with 1 µM of 6-mercapto-1-hexanol (MCH) in 10 mM PBS for 30 minutes at RT to block non-specific adsorption. The developed aptamer sensing probe was then used for sensing application or kept in the binding buffer at 4 ºC. Aptamer concentration and protein incubation time optimization was performed on AuSPE as described in the Appendix B.7.

3.2.4 Cyclic voltammetry (CV) and Electrochemical impedance spectroscopy (EIS) measurement

CV and EIS were performed after each step of electrode fabrication for aptasensor characterization, and the CV potential range was (-0.4 to 0.7 V]) at a scan rate of 50 mV/s. EIS was recorded at a

direct current potential of 0.12 V (vs. Ag/AgCl) in the frequency ranging from 100 kHz to 100 mHz with a sinusoidal voltage perturbation of 10 mV amplitude. The measurements were performed in the presence of 30 µL 5 mM $[Fe(CN)_6]^{-3/-4}$ in 10 mM PBS as a redox probe. Electrochemical measurements were performed with SP-300 potentiostat/galvanostat (Bio-Logic Science Instruments, lac-Beauport, QC, Canada) controlled by EC-Lab® software.

3.2.5 Atomic force microscopy (AFM) and photo-induced force microscopy (PiFM)

Atomic force microscopy (AFM) and photo-induced force microscopy (PiFM) characterization were done on the screen-printed electrode (SPE) samples' bare and conditioned surfaces with the VistaOne scanning probe microscope (SPM) (MolecularVista Inc., San-José, CA, USA) operating with the VistaScan v3.0 software. The microscopy setup was analogous to previously reported work (Abrego-Martinez et al., 2022). Herein, the scan frames were generated by slowly scanning the sample surface at 0.1 lines/s to avoid tip damage during the measurements. The laser power intensity was reduced to 1 % to minimize sample irradiation overexposure. SPM image data treatment and roughness analyses were done with the open-access software WSxM (Horcas et al., 2007). The details of AFM-PiFM characterization are described in Appendix B.8.

3.2.6 Electrochemical detection of sCD80

10 µL of different concentrations (0.025-10 nM) of sCD80 in binding buffer was drop-casted on the sensing probe surface and incubated at RT for 40 min. Consequently, the sensing probe was rinsed with binding buffer to remove the unbound protein. The impedimetric measurements were acquired at a potential of 0.14 V in the frequency range from 100 kHz to 100 mHz with an amplitude of 10mV in 30 µL of PBS solution containing 5 mM $[Fe(CN)6]^{3-/4-}$.

Different concentrations of sCD80 were spiked in diluted serum (1:100) and incubated with a sensing probe for 40 min at RT to evaluate the aptasensor applicability on biological material.

3.3 Results and Discussion

3.3.1 sCD80 aptamers selection:

A specific and high binding affinity aptamer to sCD80 was selected after 12 SELEX cycles involving negative (NS) and counter (CS) selections **(**Figure 3.1**).** A small amount of high-capacity Ni-NAT beads were coupled with sCD80 protein, where the coupling was confirmed by LC-HRMS. The protein was characterized by amino acid sequence coverage of about 79%, and the coupling was found to be 69% and 64% compared to equivalent protein solution using the two unique and highly abundant peptides for sCD80, ^{95}EHLAEVTLSVK^{105} (*m*/*z* 409.23, +3) and ^{106}ADFPTPSISDFEIPTSNIR^{124} (*m*/*z* 703.02, +3), respectively. The LC-HRMS results indicate the high coupling quality, as described in Appendix B Figure B.1. LC-HRMS was used for protein-bead coupling confirmation due to its ability to identify and characterize protein accurately and to avoid affinity-dependent techniques' drawbacks (van de Merbel, 2019).

After each cycle, for better enrichment, the ssDNA pool was amplified by PCR using a fluorescein-labeled forward primer, where 5′-poly dA20-HEGL-Reverse primer was used for PAGE separation. Incorporating hexaethylene glycol (HEGL) into the reverse primer acts as a terminator for DNA polymerization, resulting in partially double-strand with an unequal size of the two strands that were easily separated by PAGE. Using HEGL as a polymerization stopper minimizes the amplification of non-specific products, leading to improved specificity and efficiency of the selection process. Figure 3.1b shows the recovered ssDNA from each cycle, where the fluorescence intensity decreased from cycle 2 to cycle 5, indicating the non-specific ssDNA elimination in each cycle. The negative selection (after cycle 5) was performed on blank beads to eliminate the bead-specific ssDNA species. In the counter selection (after cycle 8), a His-tagged sCD86 (sCD80 analog) eliminates the low-specific aptamers to sCD80 and to His-tag group. The binding sites' saturation to the target protein has been reached after 12 enrichment cycles.

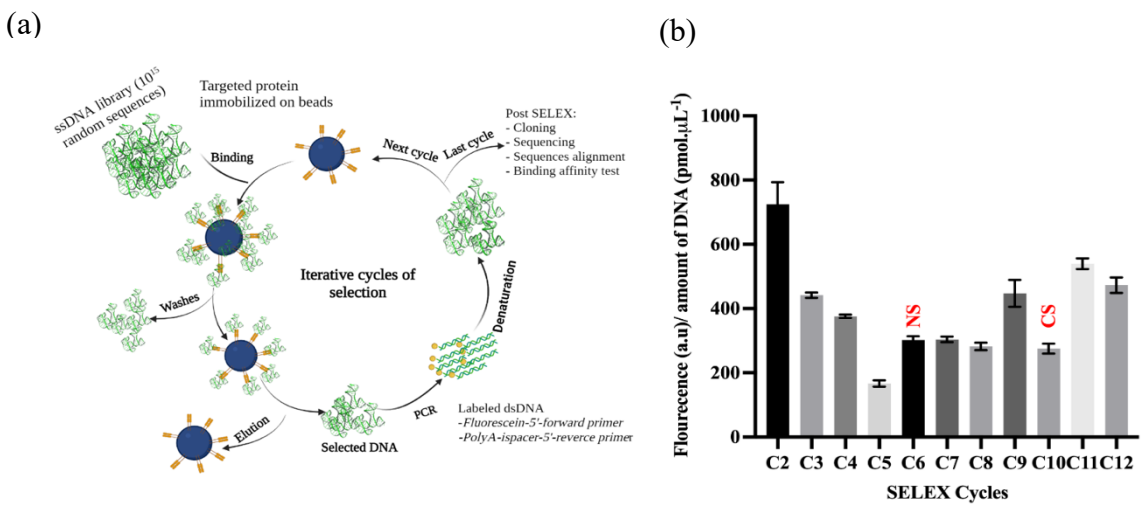

Figure 3.1. (a) Systemic Evolution of Ligands by Exponential Enrichment (SELEX) and post-SELEX workflows. (b)Enrichment of specific ssDNA aptamer for sCD80 in the successive steps of the SELEX procedure. The bar graph represents the fluorescence intensity of the eluted ssDNA from sCD80 for each round normalized to the ssDNA concentration in pmol/µL. NS represents the negative selection on blank beads, and CS represents analog selection (sCD86). The error bars represent the standard deviation of three consecutive measurements (n=3).

3.3.2 Selected aptamer identification and affinity evaluation

As shown in Appendix B Scheme B.1, in the last round of aptamer selection for sCD80, the ssDNA pool was amplified by unlabeled PCR for cloning and sequencing. The M13 amplification of ligated colonies (white colonies) was confirmed by agarose gel electrophoresis, where a band from each sequence appeared at 318 bp **(**Appendix B, Figure B.2**).** Subsequently, all selected clones were sequenced. A total of fifteen aptamers were identified and aligned into four different groups according to their common motifs. Each group was represented by one aptamer to study the binding affinity **(**Appendix B, Figure B.3**).**

The binding affinity validation of the selected aptamers against the target is crucial to reach a certain potency before utilizing it in any application. CD80-4 and CD80-16 aptamers showed the lowest K_d values of 200.5 nM and 47.69 nM, respectively, with the best fitting, as seen in Appendix B, Table B.1 and Figure B.4**.** Typically, the K_d of aptamer-target complexes ranges from low micromolar to high picomolar levels. Accordingly, these two aptamers were used for aptasensor development.

3.3.3 Aptasensor development and electrochemical characterization

The fabrication steps of the sensing probe are illustrated in Scheme 3.1. For all experiments, at least two sensors were tested independently. The condition of each step was optimized on AuSPE, as shown in Appendix B, Figure B.5 (a, b, and c)**.** Accordingly, the optimum conditions were 1.5 µM of disulfide aptamer, 1 µM MCH, and 40 minutes sCD80 incubation time. Packing density on the electrode surface significantly impacted sensor response, where denser SAM will improve the sensing result, and the thickness of the monolayer impacts the observed peak position and peak current (Brothers et al., 2020). A high concentration of thiolated aptamers, such as 1.5 µM or higher, is commonly used in aptasensor development with long incubation times (Hassani et al., 2020; Y. Liu, Zhou, & Revzin, 2013). While the high concentration employed here could

potentially lead to an increased surface thickness that might affect the sensor response, the presence of a relatively long aptamer (60 nt) containing a disulfide group appears to counterbalance this effect, leading to an appropriate packing density.

Figure B.5a showed that the highest thickness (indicated by impedance) was reached at 1.5μM aptamer; beyond, no further impedance was observed due to electrostatic repulsion between the oligonucleotide backbone. The response of the aptasensor at 1.5 μM aptamer was farther compared with the response at a lower aptamer concentration (0.5 μM), where the binding capability at this low concentration is significantly lower than the response observed at 1.5 μM (data not shown). In addition to the aptamer concentration, MCH was added to block the binding-free gold surface and to hinder the interfacial electron transfer. The MCH to the aptamer ratio was found to impact sensor response by affecting the packing of the aptamer on the electrode surface. The MCH-to-aptamer ratio was optimized based on the sensor response toward 10 nM of sCD80 protein, as seen in Appendix B, Figure B.5c. Accordingly, a 1:1.5 ratio was optimum for electrode fabrication. The low response at 1 mM MCH is due to the MCH high concentration, which may reduce the number of aptamers per area (packing density) and, accordingly, the sensing response (Brothers et al., 2020).

The electrochemical characterization of the aptasensor was achieved after each step of fabrication. Figures 3.2a-b show the cyclic voltammograms and the Nyquist plots obtained after each fabrication step. The bare gold voltammogram shows the oxidation and reduction peaks of the redox couple at 0.2 V and 0.08 V, respectively, with 120 mV peak separation (ΔE_p) and 45 μA anodic (I_A) and cathodic (I_C) current **(**Figure 3.2a**)**. The higher ΔE_p achieved and the lower I_A and I_C currents after immobilizing the disulfide-modified aptamer and MCH on the gold surface, indicating the formation of a self-assembled monolayer (SAM) **(**Figure 3.2a**)**. The incubation of the fabricated sensor with sCD80 further increased the peak-to-peak separation to 260 mV with a significant decrease in current intensity due to the blocking effect of high molecular weight protein

(25 kD) and the negative net charge of sCD80 at pH 7.4 (Z = -7), which enhanced the electrostatic repulsion with the redox probe (Abrego-Martinez et al., 2022).

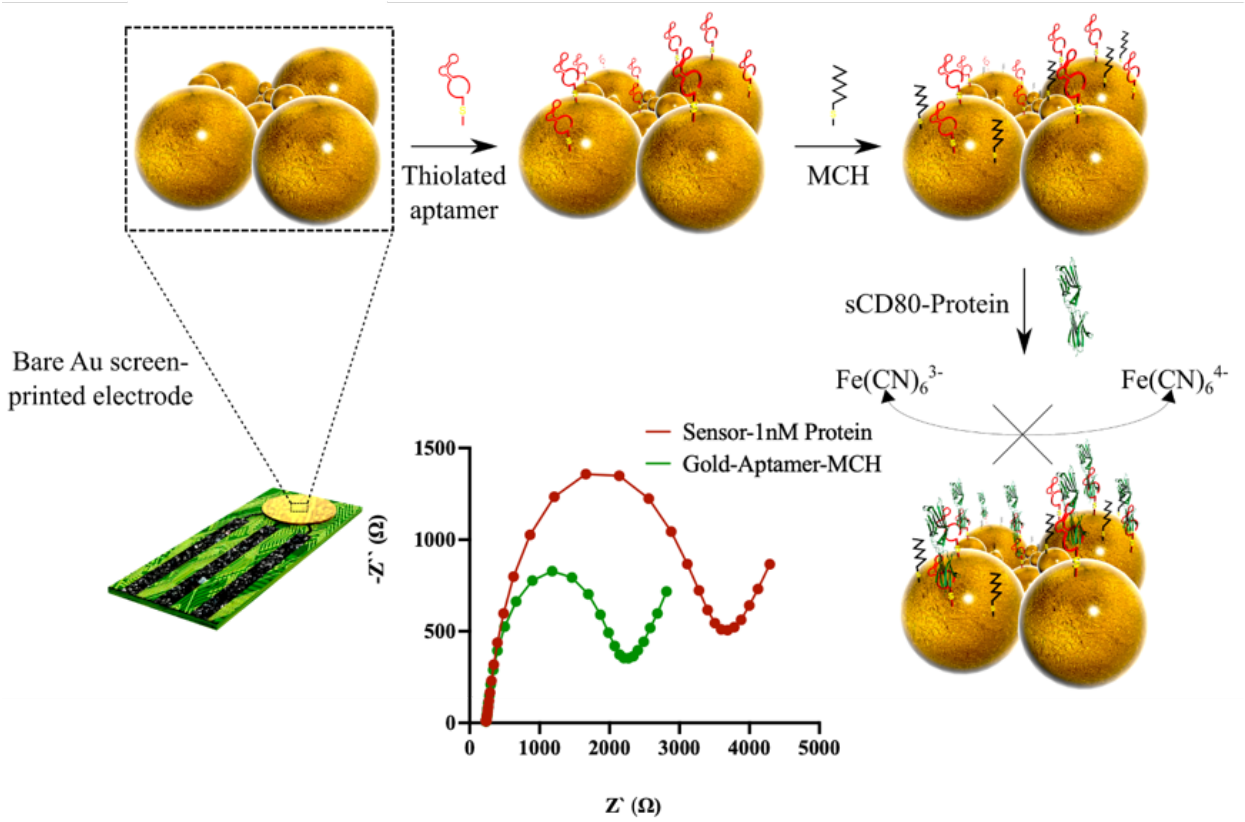

Scheme 3.1. Stepwise fabrication of sCD80 aptasensor

On the other hand, the charge transfer resistance (R_{ct}) represented by the diameter of the semicircle of the Nyquist plot **(**Figure 3.2b**)** increased from 515 ± 1 Ω to 1579 ± 0.8 Ω after aptamer immobilization, indicating the formation of SAM. Due to the surface blockage, a wider Nyquist plot was obtained after MCH addition (1826 ± 0.4 Ω). The formation of the sensor-analyte complex after incubating with protein increased the R_{ct} to 3150 ± 0.7 Ω due to mass-transfer limiting of $[Fe(CN)_6^{-3/-4}]$ to the electrode surface caused by a bulk molecule and due to the enhanced electrostatic repulsion with the redox probe. The significant change in R_{ct} after protein incubation proved the working principle of the sensor as a specific aptamer probe to be used as a recognition element in developing a biosensor for sCD80 detection.

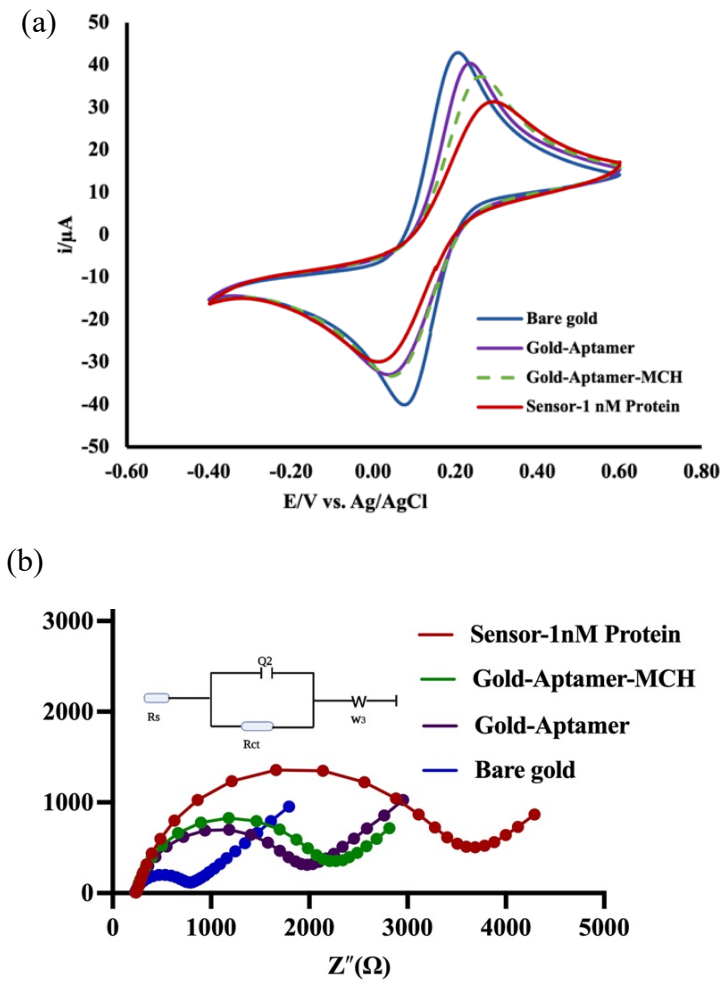

Figure 3.2. Sensor development: (a) cyclic voltammograms were obtained in the potential range of [-0.4 to 0.7 V] at 50 $mV.s^{-1}$ scan rate, and (b) EIS Nyquist plots for each aptasensor fabrication step, recorded at the direct current potential of 0.12 V in the frequency range of 100 kHz to 100 MHz with a sinusoidal voltage perturbation of 10 mV. The Randles equivalent circuit used to fit the impedance data is shown at the bottom of b. R_s is the solution resistance, R_{ct} is the charge transfer resistance, Q_2 is the constant phase element, and W_3 is the Warburg element for semi-infinite diffusion. Both graphs were measured in 30 µL 10 mM PBS containing 5 mM [$Fe(CN)_6^{3-/-4}$] as a redox probe. The fitting parameters of Nyquist plots are shown in Appendix B, Table B.4.

3.3.4 Surface microscopy characterization

Surface microscopy characterization of the biosensing platform by AFM and PiFM enabled observations of key topographical features and surface biomolecule coverage, respectively.

3.3.4.1 Topography

The commercially prepared bare AuSPE had a distinct morphology, as seen on the 10 µm × 10 µm topography **(**Figure 3.3a**)**. The roughness evaluated by the root-mean-square (RMS) of the selected area described the biosensor surface transformation events after each incubation step **(**Appendix B, Figure B.6**)**. A 1 µm × 1 µm zone from the larger 10 µm × 10 µm was magnified for each of the samples, and sections conformed to previous reports of a smoother AuSPE surface after incubation with the DNA aptamer (Bachour Junior, Batistuti, Pereira, de Sousa Russo, & Mulato, 2021; Lee et al., 2019). The roughness value decreased by 35% of the bare AuSPE. Upon incubation with the sCD80 protein, 18% more than the initial roughness was regained.

3.3.4.2 Functional group identification by PiF-IR spectroscopy

The identification of the ssDNA and of the protein–aptamer complex on the fabricated electrode was performed by recording point spectra in the mid-infrared range (770 – 1910 cm^{-1}). The bare AuSPE spectrum was the background for the AuSPE-DNA aptamer and AuSPE-DNA aptamer-sCD80 protein spectra (Appendix B, Figure B.7**)**. The strong peaks at (~875 cm^{-1}, ~1050 cm^{-1}, ~1730 cm^{-1}) and a wide band (~1100-1400 cm^{-1}) on the AuSPE-DNA aptamer **(**Figure 3.3c**)** were assigned to the phosphodiester chain, sugar-phosphate, C=X nucleotide, and base sugar entity vibrations, respectively (Parker & Quinn, 2013). In addition to the same signals marked on the AuSPE-DNA aptamer spectrum, two sharp and intense peaks at (~1125 cm^{-1}, 1180 cm^{-1}), and a broadband at (~1600-1800 cm^{-1}) on the AuSPE-DNA aptamer-sCD80 protein spectrum were observed. The DNA peaks at ~875 cm^{-1}, ~1080 cm^{-1}, and the wide band between ~1100-1400 cm^{-1} split, narrowed, and amplified, respectively. The DNA peak at ~1730 cm^{-1} broadened, intensified,

and shifted. The amide I and II vibrations explained the changes at ~1730 cm^{-1}, while the amide II vibrations caused the weak peak at ~1525 cm^{-1} (Barth, 2007; Haris, 2013; Naumann, 2013). The amide III vibrations caused the sharp, intense (~1125 cm^{-1}, 1180 cm^{-1}), weaker (~1450 cm^{-1}) peaks and the amplified wide band (~1100-1400 cm^{-1}) (Nikoo et al., 2013; Sizeland et al., 2018). The changes in the DNA environment caused by the protein made the bound and unbound aptamers chemically distinct, reflected by different phosphodiester chains (Ryu, Noda, & Jung, 2010). In addition, the surface blockage of the ssDNA aptamer by the sCD80 protein made narrower the measured band at ~1080 cm^{-1}.

3.3.4.3 Chemical mapping with PiFM

PiFM mapping at wavenumbers highlighted on the spectra depicted surficial biomolecule partitioning **(**Figure 3.3d**).** We screened all three samples at ~875 cm-1 ~1080 cm-1 ~1390 cm-1 ~1680 cm-1 and ~1730 cm-1. The bare AuSPE did not show noticeable high-intensity features, except at ~1080 cm-1, as seen on the background spectra **(**Appendix B, Figure B.7**)**. After incubation with the ssDNA aptamer, a uniform intensity signal was recorded at all scanned wavenumbers supporting uniform ssDNA-aptamer surficial coverage. After being treated with sCD80 protein, two sets of phosphodiester chains with distinct environmental characteristics were observed at all scanned wave numbers. The lower intensity color at ~875 cm-1 ~1080 cm-1 ~1390 cm-1 was associated with the vacant ssDNA-aptamer, while the bound population was shown in green, red/pale blue, and bright colonization, respectively. The topography and PiFM scan overlap at ~1400 cm-1 demonstrated the connection between morphology and biomolecule distribution **(Figure 3.3b).** The amide I scan at ~1680 cm-1 did not match the previous images of the phosphodiester chain or the base sugar, as it contained the ssDNA-aptamer nucleotide-base signal interference. The mapping at ~1680 cm-1 displayed both the ssDNA-aptamer and sCD80 protein, with more intense signal spots indicating colocalization. The mapping at ~1730 cm-1 also showed a mix of ssDNA and sCD80 coverage, with a red shift toward the amide I peak after binding with

the sCD80 protein analyte. At ~1730 cm-1, the mapping was more selective for the ssDNA-aptamer than for the sCD80 protein.

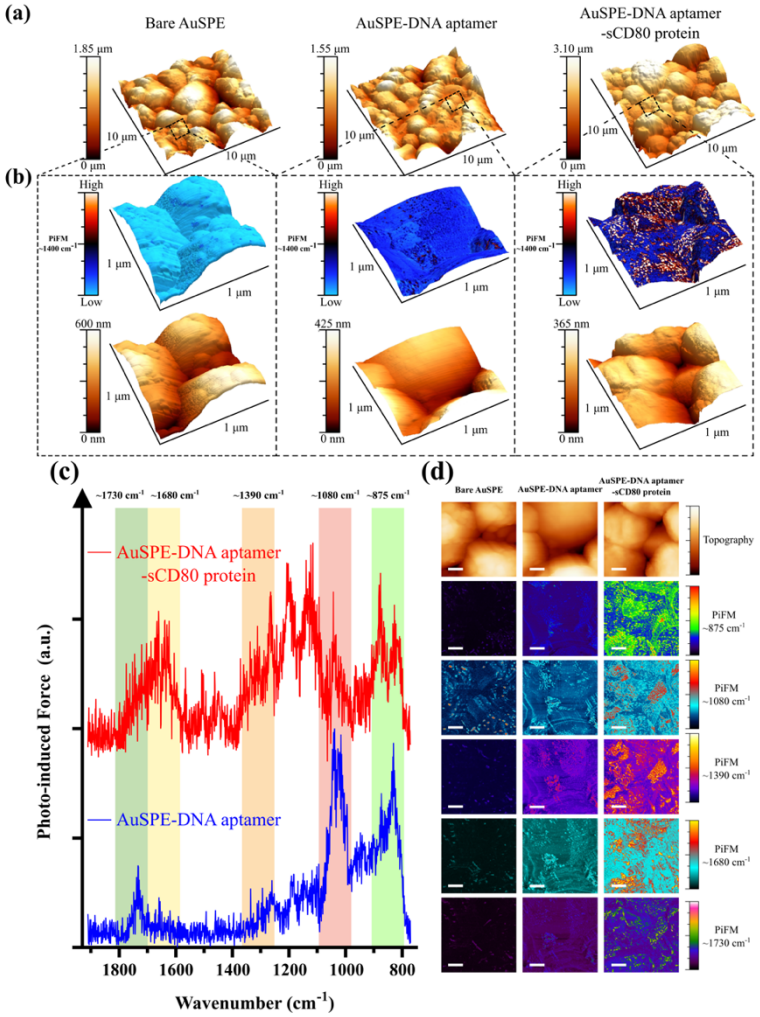

Figure 3.3. (a) Perspective view of AuSPE, AuSPE-DNA aptamer, and AuSPE-DNA aptamer-sCD80 protein 10 µm × 10 µm topography. (b) Perspective view of the samples' topography and topography overlaid with the PiFM mapping at ~1400 cm^{-1}, specific for DNA aptamer base sugar and sCD80 protein amide III moieties of a 1 µm × 1 µm magnified section. (c) Background subtracted AuSPE-DNA aptamer and AuSPE-DNA aptamer-sCD80 protein PiF-IR spectra, highlighting the wavenumbers selected for PiFM mapping in (d). (d) Topography and PiFM mapping images of the 1 µm × 1 µm magnified section in a and b, at ~875, ~1080, ~1390, ~1680, and ~1730 cm^{-1} . The lateral scale bars in all figures are 200 nm, and the vertical topography scale bar values are the same as in (b).

3.3.5 The electrochemical detection of the sCD80 protein

EIS was used as the detection method for the aptasensor response toward different concentrations of sCD80 using CD80-16 aptamer as the recognition element. The R_{ct} was measured before and after 40 minutes of incubation with (0, 0.025, 0.05, 0.1, 0.5, 1, 2,5, 5, 7.5, and 10 nM) of sCD80 in binding buffer at RT. The Nyquist plots, along with the fitting curves calculated by the Randles equivalent circuit of each concentration **(**Figure 3.4a**)**, show an increasing trend in $R_{ct,}$ which is associated with the bulkiness of the protein and electrostatic repulsion due to the negative net charge of sCD80. The response of the aptasensor was calculated as ΔR_{ct} (R-R_0), where R_0 and R are the R_{ct} before and after analyte binding, respectively. ΔR_{ct} shows a logarithmic relationship with the concentration of sCD80, as seen in Figure 3.4b. The calibration curve was constructed as the ΔR_{ct} for each concentration function of log sCD80 concentration, as seen in Figure 3.4c, which exhibits a linear relation in the range of 0.025 to 10 nM. The linear dynamic range was started from the LOQ as the lowest quantification concentration with S/N of 10:1 until it reached saturation. The linear-logarithmic regression equation is ΔR_{ct} = 1239 log [sCD80 (nM)]+2418, (R^2 = 0.9906, and the limit of detection (LOD) was 8 pM (0.2 ng/ml), the LOD is defined as the lowest detected concentration with S/N ratio of 3:1 or higher. LOD was estimated as 3*σ/S, where σ is the stander deviation of the absolute value of R_{ct} related to three independent blank measurements. S is the slope of the calibration curve. The standard deviation of the signal at 8 pM was >3 standard deviation of blank (ICH Harmonised Tripartite Guideline. *Clinical Safety Data Management: Definitions and Standards for Expedited Reporting E2A.*; 1994 [cited 2017 May).

Similarly, CD80-4 aptamer was used to build an aptasensor for sCD80 detections, as seen in Figure 3.4d. The LOD was 40 pM, and R^2 was 0.9623. According to the LOD and the K_d values, the CD80-16 aptasensor was chosen as the biosensor for sCD80 detection.

Based on these results, the sensitivity of the developed aptasensor is comparable with some commercially available ELISA kits, as summarized in Appendix B, Table B.3. They seldom

reported 0.25 to 1.4 ng/mL (8.5 to 47.5 pM) and 0.03 to 0.22 ng/mL (1-7.4 pM) in human serum. (Cao et al., 2012; Hock et al., 2006) Another study reported sCD80 normal serum levels higher than 15 ng/mL (>0.5nM) and reached 1000 ng/ml (34 nM) (Kakoulidou et al., 2007). The level is significantly higher in pathological conditions. Recently, a clinical study was conducted by our group to quantify four costimulatory proteins, including sCD80, in RA patients compared to healthy controls using a specific and accurate LC-MS/MS method in multiple reaction monitoring (MRM) mode. In this study, the reference range for sCD80 found to be (0.4-190 nM) in the control group and (39.7-434.3 nM) in RA patients (Abeer K. Malkawi, 2023) . The developed aptasensor possesses a clinical significance as the LOD 8 pM (0.2 ng/ml) is less than the lower cut-off value of the normal range in most of the previous studies, which indicates a good sensitivity, as well as the wide range of quantification with 25 pM (0.625 ng/ml) LOQ should cover the normal and pathological range in human serum by considering the dilution factor in real serum samples. Moreover, the simplicity of the procedure, the short operation time, the low cost of operation and production, the benefits of covalent binding with gold, and sensitive label-fee electrochemical detection increase the potential applicability of the developed sensor.

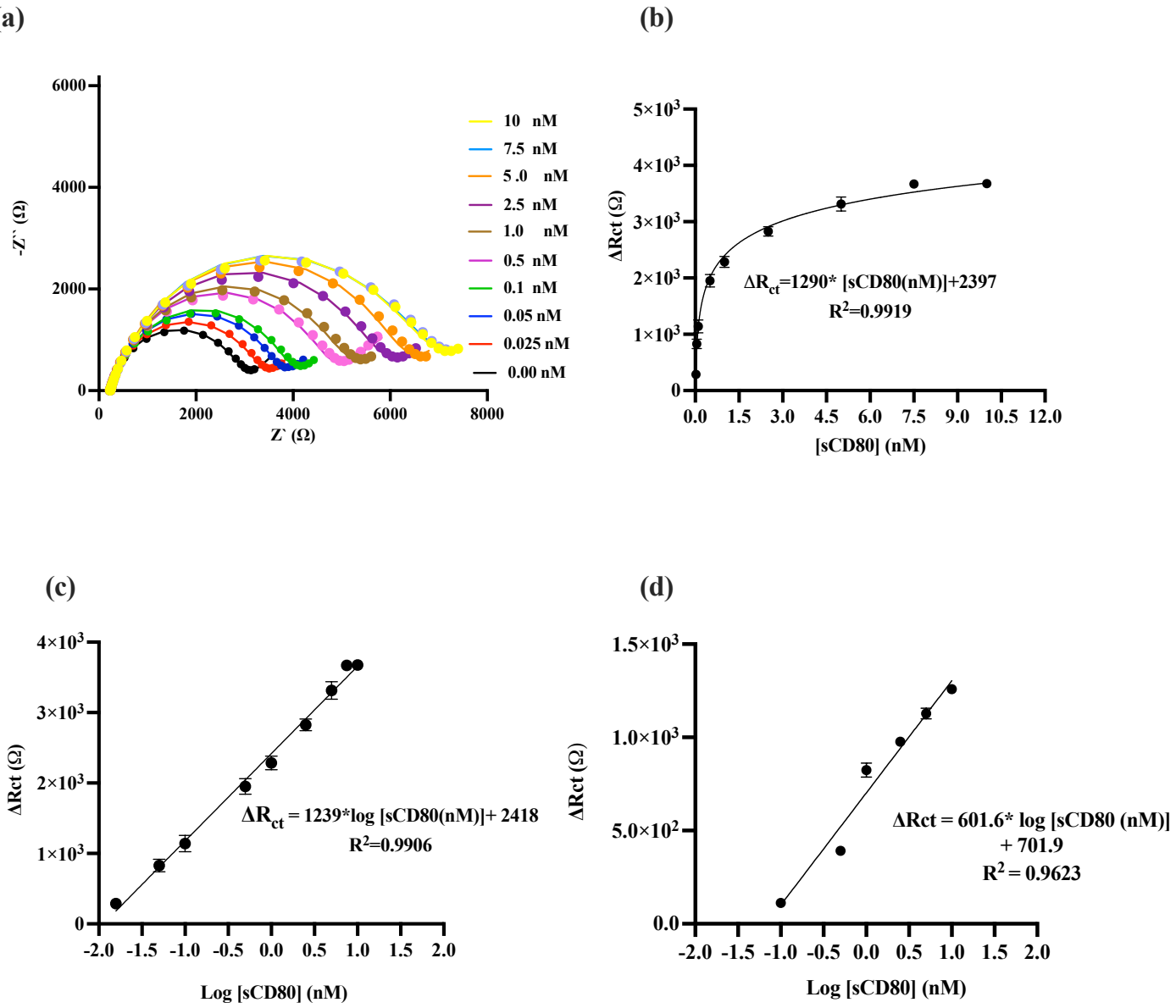

Figure 3.4. sCD80 (CD80-16) Electrochemical detection: (a) Nyquist plots of the developed aptasensor response in the optimum operating conditions toward different concentrations of sCD80 diluted in PBS. Solid lines correspond to the experimental data, while symbols correspond to the EIS data fitting. (b) The linear and (c) the semi-logarithmic calibration curve plots of the developed aptasensor. (d) Electrochemical detection of sCD80 using the lower affinity aptamer CD80-4 (Kd 200.5nM) results in a less sensitive sensor. The calibration curves were obtained from the change

of Rct ($Rct-Rct_0$) as a function of the log concentration of sCD80 diluted in PBS. The error bars represent the SD from three different replicates at each point. The fitting parameters of Nyquist plots are shown in Appendix B, Table B.5. All electrochemical measurements were recorded in PBS containing 5.0 mM of $[Fe(CN)^{-3/-4}]$.

3.3.6 Aptasensor specificity, stability, reproducibility, and application in a biological matrix

Biosensor specificity is a crucial factor to consider during development and validation. sCD80, sCD86, and sCTLA-4 belong to the immunoglobulin superfamily, which comprises the extracellular IgV-like domain (Peach et al., 1995). sCD80 and sCD86 share around 25% of sequence identity (Linsley et al., 1994) and bind to CTLA-4 through the conserved motif ^{97}MYPPPY^{102} (Xu et al., 2012). Thus, sCD86 and sCTLA-4 were chosen to test the specificity of the aptasensor toward sCD80. 5 nM of sCD80, sCD86, and sCTLA-4 was incubated with the aptasensor separately for 40 minutes at RT. The reactivity of the analogs toward the sensor was calculated as the response (ΔR_{ct}) relative to the response toward the target protein (sCD80). As shown in Figure 3.5a, $\Delta R_{ct\%}$ was 7.3% and 13% for sCD86 and sCTLA-4, respectively, which is significantly lower than the response for sCD80 (100%) with P-value <0.0001 (one-way ANOVA test with multiple comparisons). Despite the sharing sequence between sCD86 and sCD80, the aptasensor exhibited a lower reactivity toward CD86 than CTLA-4 due to the counter-selection step during SELEX using CD86-beads. To compare the specificity of the developed sensor with available immunoassays for the targeted protein sCD80, ELISA (Human CD80 ELISA Kit, Abcam, Toronto, Canada) was performed by incubating with 0.2nM of sCD80, sCD86, and sCTLA-4 as detailed in Appendix B, section B.9. The analog concentration relative to the target (sCD80) concentration shows 2.7 % for sCD86 as shown in Figure 3.5b. Accordingly, the specificity of the developed aptasensor toward sCD86 is comparable with ELISA. Interestingly, ELISA showed a high response when incubated with sCTLA-4 (36%), indicating a high cross - reactivity of the antibody with this analog. The role of MCH in blocking the non-specific binding was further evaluated by incubating two sets of sensors fabricated with only MCH in protein solution (I nM) (set 1) and serum (set 2) along with complete sensors for comparison. The response of the MCH sensor toward 1 nM protein was 2.4% of the response of a complete sensor immersed in the same solution. Similarly, in serum samples, the signal of the MCH sensor was 4.6% compared with the complete sensor. The low response in the MCH sensor indicates a good blockage of the non-specificity by the added MCH with negligible interferences.

Aptamer stability is always a concern during biosensor development, where sensor efficiency might be affected in complex biological matrices due to the nuclease activity (Ning, Hu, & Lu, 2020). In this study, the stability in serum was evaluated by incubating the aptasensor with diluted serum (1:100) for 60 min, which is a longer time needed for the application (40 min) at RT. The aptasensor had been recovered with excessive washing with binding buffer followed by water. The R_{ct} of the recovered aptasensor (in triplicates) was compared with the R_{ct} of aptasenosr incubated only with the binding buffer (control). The aptasensor conserved the resistance by 116.63% (RSD 3.4%) compared to the control, which revealed the stability of the aptasensor in serum, suggesting its applicability on serum samples for a maximum of 60 min. The long-term storage stability of aptasensor is an important factor for practical application. Different aptasensors prepared at the same time under the same conditions were evaluated on day one, after 14, 21, and 28 days of storage in a binding buffer at 4^{o}C by incubating with 1 nM of sCD80 for 40 minutes. The sensor was confirmed, based on US FDA guideline, to be stable for 14 days with 88.8% (<20% of the freshly prepared sensor). The stability was calculated as (ΔR_{ct} of the sensor after 14 days storage / ΔR_{ct} of the freshly prepared sensor) x100%.

The reproducibility of the aptasensor was investigated by testing 18 different sensors prepared on three different days under the same conditions and incubated with 1 nM of sCD80 for 40 min. The relative standard deviation of the average was calculated to be 14.14%. This variability is acceptable and can be explained by the harsh electrodeposition protocol during electrode fabrication.

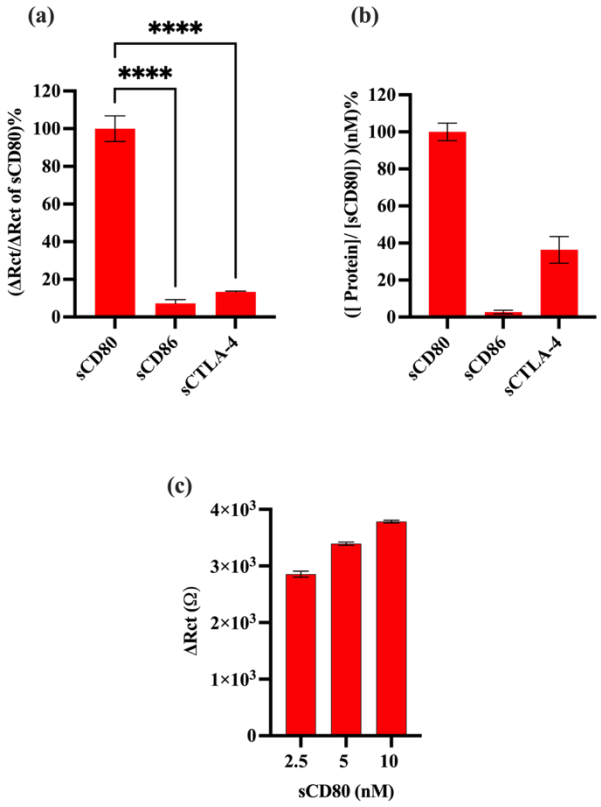

Figure 3.5. (a) The selectivity of aptasensor studied with 5 nM sCD80 analogs CD86 and CTLA-4. The response was recorded as $((\text{Rct-Rct0})_{\text{protein}}/ (\text{Rct-Rct0})_{\text{sCD80}})\%$, $Rct;\ is\ the\ charge\ transfer\ resistance\ after\ protein\ incubation,\ and\ Rct0;$ is the charge transfer resistance before binding. The error bars correspond to the SD of three replicates(n=3). **** represents the significant difference with p-value <0.0001 using one-way ANOVA test with multiple comparisons. (b) The reactivity of sCD80 human ELISA toward sCD86 and sCTLA-4, the response was recorded as (the Concentration of protein (nM)/ Concentration of sCD80 (nM))%. the error bar corresponds to the SD of three replicates (n=3). (c)The aptasensor response toward different concentrations of sCD80 spiked in serum samples. ΔRct was obtained from the response of the spiked sample after subtracting the blank response (0 spiked serum). (The error bars correspond to SD (n=3).

The applicability of the developed aptasensor on the biological matrix was investigated by adding different concentrations of sCD80 (0, 2.5, 5.0, and 10.0 nM) to human serum diluted 100-fold. As illustrated in Figure 3.5c, the sensor protein response was demonstrated after subtracting the blank serum (endogenous sCD80 level, and any potential interferences) response to be concordant with amount of spiked analyte. This finding supports the promising use of this biosensor in detecting sCD80 in the complex biological matrix for diagnostic purposes. Additionally, the recoveries of these added concentrations to serum samples were estimated using the calibration (Figure 3.4c) and found to range between 104%-125 % with RSD of less than 7% (Appendix B, Table B.2). The linear signal and the acceptable recovery from these three spiked concentrations indicate the applicability of the developed sensor in human serum; however, more data points that cover the linear range are required to test the developed sensor on human serum. As a promising tool for the practical use of the developed aptasensor in biological samples, a large cohort of patients with RA was recruited to establish clinical cut-off values toward utilizing this aptasensor for diagnosis.

3.4 Conclusion

To sum up, we have successfully created an innovative and highly specific label-free electrochemical aptasensor for detecting sCD80 in serum. This has significant potential as a diagnostic tool for autoimmune disorders, mainly RA. We constructed this biosensor by carefully selecting a high-affinity aptamer (with a Kd of 47.69 nM) through SELEX. After fine-tuning, the aptasensor reached a remarkable sensitivity, with a detection limit as low as 8 pM, and a broad measurement range (0.025-10 nM). We successfully applied the aptasensor to spiked serum samples, achieving recovery rates between 104.6-125.6%.

Yet, our approach had some limitations, including using a DNA library with 60nt random sequences. In future applications, truncating the aptamer might enhance sensitivity if required for different disease models, especially for molecular interactions. Despite the simplicity and cost-effectiveness of the label-free method, the sensor's sensitivity can be farther enhanced using a

labeled impedimetric sensing platform. Our upcoming goal involves amplifying sensitivity using various platforms, including gold nanoparticle deposition techniques.

A challenge was the variability in endogenous protein levels, which limited the establishment of precise calibrators and controls. For future steps, we plan to determine cut-off levels for sCD80 in healthy and RA serum through extensive testing on a large group. This is crucial to ultimately introducing this aptasensor for clinical use.

References

Abeer K. Malkawi, R. M. N., Maha Almogren, Afshan Masood, Abdulrahman S. Alarfaj, Hicham Benabdelkamel, Anas M. Abdel Rahman, Mohamed Siaj,. (2023). Quantitative Analysis of Soluble Costimulatory Molecules as Potential Diagnostic Biomarkers for Rheumatoid Arthritis using LC-MS/MS in MRM Mode,. Clinica Chimica Acta,, 117501. doi:10.1016/j.cca.2023.117501

Abrego-Martinez, J. C., Jafari, M., Chergui, S., Pavel, C., Che, D., & Siaj, M. (2022). Aptamer-based electrochemical biosensor for rapid detection of SARS-CoV-2: Nanoscale electrode-aptamer-SARS-CoV-2 imaging by photo-induced force microscopy. Biosens Bioelectron, 195, 113595. doi:10.1016/j.bios.2021.113595

Ahirwar, R., Dalal, A., Sharma, J. G., Yadav, B. K., Nahar, P., Kumar, A., & Kumar, S. (2019). An aptasensor for rapid and sensitive detection of estrogen receptor alpha in human breast cancer. Biotechnol Bioeng, 116(1), 227-233. doi:10.1002/bit.26819

Bachour Junior, B., Batistuti, M. R., Pereira, A. S., de Sousa Russo, E. M., & Mulato, M. (2021). Electrochemical aptasensor for NS1 detection: Towards a fast dengue biosensor. Talanta, 233, 122527. doi:https://doi.org/10.1016/j.talanta.2021.122527

Barth, A. (2007). Infrared spectroscopy of proteins. Biochimica et Biophysica Acta (BBA) - Bioenergetics, 1767(9), 1073-1101. doi:https://doi.org/10.1016/j.bbabio.2007.06.004

Brothers, M. C., Moore, D., St Lawrence, M., Harris, J., Joseph, R. M., Ratcliff, E., . . . Kim, S. S. (2020). Impact of Self-Assembled Monolayer Design and Electrochemical Factors on Impedance-Based Biosensing. Sensors (Basel), 20(8). doi:10.3390/s20082246

Cao, J., Zou, L., Luo, P., Chen, P., & Zhang, L. (2012). Increased production of circulating soluble co-stimulatory molecules CTLA-4, CD28 and CD80 in patients with rheumatoid arthritis. Int Immunopharmacol, 14(4), 585-592. doi:10.1016/j.intimp.2012.08.004

Chimenti, M. S., Triggianese, P., Conigliaro, P., Candi, E., Melino, G., & Perricone, R. (2015). The interplay between inflammation and metabolism in rheumatoid arthritis. Cell Death Dis, 6, e1887. doi:10.1038/cddis.2015.246

Chinnappan, R., Zaghloul, N. S., AlZabn, R., Malkawi, A., Abdel Rahman, A., Abu-Salah, K. M., & Zourob, M. (2021). Aptamer selection and aptasensor construction for bone density biomarkers. Talanta, 224, 121818. doi:10.1016/j.talanta.2020.121818

Eissa, S., Abdulkarim, H., Dasouki, M., Al Mousa, H., Arnout, R., Al Saud, B., . . . Zourob, M. (2018). Multiplexed detection of DOCK8, PGM3 and STAT3 proteins for the diagnosis of Hyper-Immunoglobulin E syndrome using gold nanoparticles-based immunosensor array platform. Biosens Bioelectron, 117, 613-619. doi:10.1016/j.bios.2018.06.058

Faas, S. J., Giannoni, M. A., Mickle, A. P., Kiesecker, C. L., Reed, D. J., Wu, D., . . . Rother, R. P. (2000). Primary structure and functional characterization of a soluble, alternatively spliced form of B7-1. J Immunol, 164(12), 6340-6348. doi:10.4049/jimmunol.164.12.6340

Haris, P. I. (2013). Infrared Spectroscopy of Protein Structure. In G. C. K. Roberts (Ed.), Encyclopedia of Biophysics (pp. 1095-1106). Berlin, Heidelberg: Springer Berlin Heidelberg.

Hassani, S., Salek Maghsoudi, A., Rezaei Akmal, M., Rahmani, S. R., Sarihi, P., Ganjali, M. R., . . . Abdollahi, M. (2020). A Sensitive Aptamer-Based Biosensor for Electrochemical Quantification of PSA as a Specific Diagnostic Marker of Prostate Cancer. J Pharm Pharm Sci, 23, 243-258. doi:10.18433/jpps31171

Heiskanen, A. R., Spegel, C. F., Kostesha, N., Ruzgas, T., & Emneus, J. (2008). Monitoring of Saccharomyces cerevisiae cell proliferation on thiol-modified planar gold microelectrodes using impedance spectroscopy. Langmuir, 24(16), 9066-9073. doi:10.1021/la800580f

Hock, B. D., O'Donnell, J. L., Taylor, K., Steinkasserer, A., McKenzie, J. L., Rothwell, A. G., & Summers, K. L. (2006). Levels of the soluble forms of CD80, CD86, and CD83 are elevated in the synovial fluid of rheumatoid arthritis patients. Tissue Antigens, 67(1), 57-60. doi:10.1111/j.1399-0039.2005.00524.x

Hock, B. D., Patton, W. N., Budhia, S., Mannari, D., Roberts, P., & McKenzie, J. L. (2002). Human plasma contains a soluble form of CD86 which is present at elevated levels in some leukaemia patients. Leukemia, 16(5), 865-873. doi:10.1038/sj.leu.2402466

Hock, B. D., Starling, G. C., Patton, W. N., Salm, N., Bond, K., McArthur, L. T., & McKenzie, J. L. (2004). Identification of a circulating soluble form of CD80: levels in patients with hematological malignancies. Leuk Lymphoma, 45(10), 2111-2118. doi:10.1080/10428190410001712199

Horcas, I., Fernández, R., Gómez-Rodríguez, J. M., Colchero, J., Gómez-Herrero, J., & Baro, A. M. (2007). WSXM: A software for scanning probe microscopy and a tool

for nanotechnology. Review of Scientific Instruments, 78(1), 013705. doi:10.1063/1.2432410

Ip, W. K., Wong, C. K., Leung, T. F., & Lam, C. W. (2006). Plasma concentrations of soluble CTLA-4, CD28, CD80 and CD86 costimulatory molecules reflect disease severity of acute asthma in children. Pediatr Pulmonol, 41(7), 674-682. doi:10.1002/ppul.20432

Kakoulidou, M., Giscombe, R., Zhao, X., Lefvert, A. K., & Wang, X. (2007). Human Soluble CD80 is generated by alternative splicing, and recombinant soluble CD80 binds to CD28 and CD152 influencing T-cell activation. Scand J Immunol, 66(5), 529-537. doi:10.1111/j.1365-3083.2007.02009.x

Lee, T., Park, S. Y., Jang, H., Kim, G.-H., Lee, Y., Park, C., . . . Min, J. (2019). Fabrication of electrochemical biosensor consisted of multi-functional DNA structure/porous au nanoparticle for avian influenza virus (H5N1) in chicken serum. Materials Science and Engineering: C, 99, 511-519. doi:https://doi.org/10.1016/j.msec.2019.02.001

Linsley, P. S., Greene, J. L., Brady, W., Bajorath, J., Ledbetter, J. A., & Peach, R. (1994). Human B7-1 (CD80) and B7-2 (CD86) bind with similar avidities but distinct kinetics to CD28 and CTLA-4 receptors. Immunity, 1(9), 793-801. doi:10.1016/s1074-7613(94)80021-9

Liu, L., Han, Z., An, F., Gong, X., Zhao, C., Zheng, W., . . . Zhou, Q. (2021). Aptamer-based biosensors for the diagnosis of sepsis. J Nanobiotechnology, 19(1), 216. doi:10.1186/s12951-021-00959-5

Liu, Y., Zhou, Q., & Revzin, A. (2013). An aptasensor for electrochemical detection of tumor necrosis factor in human blood. Analyst, 138(15), 4321-4326. doi:10.1039/c3an00818e

Naumann, D. (2013). Infrared Spectroscopy of Cells, Tissues, and Biofluids. In G. C. K. Roberts (Ed.), Encyclopedia of Biophysics (pp. 1057-1065). Berlin, Heidelberg: Springer Berlin Heidelberg.

Nikoo, M., Benjakul, S., Ocen, D., Yang, N., Xu, B., Zhang, L., & Xu, X. (2013). Physical and chemical properties of gelatin from the skin of cultured Amur sturgeon (Acipenser schrenckii). Journal of Applied Ichthyology, 29(5), 943-950. doi:https://doi.org/10.1111/jai.12238

Ning, Y., Hu, J., & Lu, F. (2020). Aptamers used for biosensors and targeted therapy. Biomed Pharmacother, 132, 110902. doi:10.1016/j.biopha.2020.110902

Parker, A. W., & Quinn, S. J. (2013). Infrared Spectroscopy of DNA. In G. C. K. Roberts (Ed.), Encyclopedia of Biophysics (pp. 1065-1074). Berlin, Heidelberg: Springer Berlin Heidelberg.

Peach, R. J., Bajorath, J., Naemura, J., Leytze, G., Greene, J., Aruffo, A., & Linsley, P. S. (1995). Both extracellular immunoglobin-like domains of CD80 contain residues critical for binding T cell surface receptors CTLA-4 and CD28. J Biol Chem, 270(36), 21181-21187. doi:10.1074/jbc.270.36.21181

Ryu, S. R., Noda, I., & Jung, Y. M. (2010). What is the origin of positional fluctuation of spectral features: True frequency shift or relative intensity changes of two overlapped bands? Applied Spectroscopy, 64(9), 1017-1021. doi:10.1366/000370210792434396

Salomon, B., & Bluestone, J. A. (2001). Complexities of CD28/B7: CTLA-4 costimulatory pathways in autoimmunity and transplantation. Annu Rev Immunol, 19, 225-252. doi:10.1146/annurev.immunol.19.1.225

Sizeland, K., Hofman, K., Hallett, I., Martin, D., Potgieter, J., Kirby, N., . . . Cumming, M. (2018). Nanostructure of Electrospun Collagen: Do Electrospun Collagen Fibers Form Native Structures? Materialia, 3. doi:10.1016/j.mtla.2018.10.001

Stoltenburg, R., Reinemann, C., & Strehlitz, B. (2007). SELEX--a (r)evolutionary method to generate high-affinity nucleic acid ligands. Biomol Eng, 24(4), 381-403. doi:10.1016/j.bioeng.2007.06.001

van de Merbel, N. C. (2019). Protein quantification by LC-MS: a decade of progress through the pages of Bioanalysis. Bioanalysis, 11(7), 629-644. doi:10.4155/bio-2019-0032

Wan, B., Nie, H., Liu, A., Feng, G., He, D., Xu, R., . . . Zhang, J. Z. (2006). Aberrant regulation of synovial T cell activation by soluble costimulatory molecules in rheumatoid arthritis. J Immunol, 177(12), 8844-8850. doi:10.4049/jimmunol.177.12.8844

Wong, C. K., Ho, A. W., Tong, P. C., Yeung, C. Y., Chan, J. C., Kong, A. P., & Lam, C. W. (2008). Aberrant expression of soluble co-stimulatory molecules and adhesion molecules in type 2 diabetic patients with nephropathy. J Clin Immunol, 28(1), 36-43. doi:10.1007/s10875-007-9137-4

Wong, C. K., Lit, L. C., Tam, L. S., Li, E. K., & Lam, C. W. (2005). Aberrant production of soluble costimulatory molecules CTLA-4, CD28, CD80 and CD86 in

patients with systemic lupus erythematosus. Rheumatology (Oxford), 44(8), 989-994. doi:10.1093/rheumatology/keh663

Xu, Z., Juan, V., Ivanov, A., Ma, Z., Polakoff, D., Powers, D. B., . . . Akamatsu, Y. (2012). Affinity and cross-reactivity engineering of CTLA4-Ig to modulate T cell costimulation. J Immunol, 189(9), 4470-4477. doi:10.4049/jimmunol.1201813

CHAPTER 4 (SCIENTIFIC ARTICLE)

CO-STIMULATORY PATHWAY COMPETITIVE ASSAY DEVELOPMENT USING LIQUID CHROMATOGRAPHY-TANDEM MASS SPECTROMETRY (LC-MS/MS)

Abeer K. Malkawi[a], Leanne Ohlund[a], Anas M. Abdel Rahman[b,c], Lekha Sleno[a], Mohamed Siaj[a*]

[a] Department of Chemistry, Université du Québec à Montréal, Montreal, QC, H3C 3P8, Canada

[b] Metabolomics Section, Department of Clinical Genomics, Center for Genome Medicine, King Faisal Specialist Hospital and Research Center (KFSHRC), Riyadh, Saudi Arabia.

[c] Department of Biochemistry and Molecular Medicine, College of Medicine, Alfaisal University, Riyadh, Saudi Arabia.

J Pharm Biomed Anal . 2024 May 15:242:116034. DOI: 10.1016/j.jpba.2024.116034

* Correspondence:
Professor Mohamed Siaj,
Email: siaj.mohamed@uqam.ca

CONTRIBUTION OF THE MAIN AUTHOR AND CO-AUTHORS

Abeer Malkawi and Prof. Mohamed Siaj conceived the idea of this project. Abeer Malkawi designed and conducted the experiments and drafted the manuscript. Leanne Ohlund, and Prof. Lekha Sleno provide access to the mass spectrometry facility and helped in running the samples. Dr. Anas Abdel Rahman helped in data analysis and interpretation. Prof. Sleno, Dr. Anas Abdel Rahman, and Prof. Siaj have critically reviewed the manuscript. All authors approved the current version of the manuscript for publication

Abstract:

T-cells play a significant role in the development of autoimmune diseases. The CD28-B7 costimulatory pathway is crucial for activating T-cells, and blocking this pathway is essential for treating autoimmune diseases. Therapeutic antibodies and fusion proteins that target costimulatory molecules like CD80, CD86, CTLA-4, and CD28 have been developed to explore the costimulation process and as targeted treatments. To advance our understanding of costimulation in autoimmunity and the inhibition of the costimulatory pathway, it is crucial to have an accurate, precise, and direct method for detecting and quantifying the soluble form of these molecules in body fluids and various biological systems. Herein, we developed a liquid chromatography-tandem mass spectrometry (LC-MS/MS) method for quantifying the four costimulatory proteins depending on the signature peptides derived from the soluble isoform of these proteins in multiple reaction monitoring (MRM) mode. The method was validated using the US FDA guidelines. The LOQ was determined as ~0.5 nM for the four analytes, with quantification extended to 20 nM with a correlation coefficient of R^2>0.998. The developed MRM method was used to analyze on-bead digested protein mixtures to establish a competitive assay for the CD28-B7 costimulatory pathway using CTLA4-Ig (Abatacept ™) as an FDA-approved drug for rheumatoid arthritis. The IC_{50} was determined to be 2.71 and 72.22 nM for sCD80 and sCD86, respectively. A straightforward MRM-based competitive assay will advance the knowledge about the costimulatory role in autoimmunity and the autoimmune therapeutic drug discovery, with the need for broad application on different in vitro and in vivo models to discover new targeted inhibitors.

Keywords: Costimulatory molecules; multiple reaction monitoring (MRM); Abatacept; method validation; competitive assay

4.1 Introduction:

Autoimmune diseases pose a significant challenge in clinical settings due to their chronic nature, high healthcare costs, and prevalence among young populations in their prime working and reproductive years. Autoreactive T lymphocytes are pivotal in autoimmune diseases, functioning as regulatory and effector cells. T-cell activation requires two signals; the first signal is provided by the interaction of the T-cell receptor (TCR) with its specific antigen presented on the surface of major histocompatibility complex (MHC) molecules on the surface of antigen-presenting cell (APC). The second signal comes from the co-stimulatory pathway CD28-B7 when CD28 engages with its co-stimulatory ligands, CD80 and CD86. CD28 is expressed when resting and activating T-cells. During an immune response, CD28 is sharply upregulated on the T-cell surface, which subsequently upregulates the expression of CD80 and CD86 on activated APC, such as dendritic cells, macrophages, and B-cells. (Hock et al., 2004)

Conversely, the T-cell activation upregulates the expression of cytotoxic T-lymphocyte–associated antigen 4 (CTLA-4), which has a sequence and structural homology with CD28. (Das, Ariizumi, & Cruz, 2012) CTLA-4 binds competitively with the same CD80 and CD86 ligands and suppresses the T-cell activity. (Tector, Khatri, Kozinski, Dennert, & Oaks, 2009) Therefore, CTLA-4 is a negative regulatory co-stimulatory molecule that keeps the balance between activation and inhibition of T-cells and prevents the development of autoimmunity. During autoimmunity, the balance between effector T-cells and regulatory T-cells is disturbed, leading to a loss of self-tolerance and hyperresponsiveness of T-cells. (Thompson, 1995)

The co-stimulatory molecules CD28, CD80, CD86, and CTLA-4, belong to the immunoglobulin superfamily, sharing common immunoglobulin (Ig)-like domains. (Buck, 1992) The Ig-like domains, either variant (IgV)- or constant (IgC)-like domains, are extracellular-representing domains essential for binding and biological activity. (Kakoulidou, Giscombe, Zhao, Lefvert, & Wang, 2007)

Many studies demonstrated the role of these proteins in the pathogenesis of different autoimmune diseases, such as rheumatoid arthritis (RA), hematological malignancies, and systemic lupus erythematosus (SLE). (Cao, Zou, Luo, Chen, & Zhang, 2012; Hock et al., 2002; Hock et al., 2004; Wong, Lit, Tam, Li, & Lam, 2005) In hematological malignancies, the expression of membranous B7 molecules (mCD80 and mCD86) has been associated with poor prognosis. (Maeda et al., 1998) The high cell-surface expression of CD80 and CD86 and the CTLA4 gene polymorphism are associated with SLE development (Wong et al., 2005). The increased expression of costimulatory molecules in synovial T-cells and peripheral blood B lymphocytes is associated with the development of RA, a chronic autoimmune disorder characterized by inflammation of the joints, leading to pain, stiffness, and swelling. In addition to the full-length sequences of these proteins, soluble isoforms, which result from alternatively spliced mRNA or due to enzymatic cleavage of the molecules from the cell surface, had been identified and detected in human serum. (Ip, Wong, Leung, & Lam, 2006; Kakoulidou et al., 2007) These soluble forms lack the transmembrane domain and demonstrate potent immunoregulatory activity. (Hock et al., 2006) The soluble recombinant costimulatory molecules conserve the extracellular domain and can interact to either inhibit or activate the immune response depending on the level of B7 (CD80 and CD86) binding to CD28 or CTLA-4. (Hock et al., 2004)

In different autoimmune diseases, the serum soluble costimulatory molecule levels were correlated with the disease development and their downregulation by immunosuppressants. (Cao et al., 2012; Ip et al., 2006) Conversely, these molecules are linked in their level in autoimmune patients' sera as a response to these diseases' pathogenesis. (Cao et al., 2012)

These costimulatory molecules (CD28, CD80, CD86, CTLA-4) are attractive targets for therapeutic manipulation of autoimmune diseases. For instance, interrupting the CD28-B7 pathway by a fusion protein CTLA4-Ig (Abatacept™) is an efficient biological therapy in rheumatoid arthritis. (Weisman et al., 2006) CTLA4-Ig competitively binds to CD80/CD86 and inhibits T-cells' activation, which controls autoimmunity. (Xu et al., 2012) Identifying compounds

that are specifically interpreting costimulation as targeted therapy for autoimmune diseases needs a robust and precise method. Most of the developed methods for detecting and quantifying these molecules in biological fluids to understand their biological role or for the discovery of new inhibitors rely on immunoassays such as ELISA. (Cao et al., 2012; Ip et al., 2006; Wong et al., 2005). Although these methods are widely used, they have some disadvantages, such as antibody specificity and cross-reactivity, especially for structurally similar molecules as the costimulatory proteins. The semi-quantitative fashion is associated with interferences and cannot be multiplexed. The technological improvement in mass spectrometry-based proteomics enhances the pre-clinical drug discovery approaches by overcoming the limitation associated with conventional methods. Multiple reaction monitoring (MRM) mass spectrometry is a targeted approach that provides rigorous quantification of proteins using surrogate signature peptides with stable isotope-labeled internal standard. Recently, the success of MRM in protein quantification enhances the utilization of the method for designing competitive assays as part of drug discovery and biological pathways understanding, such as the development of a direct assay to study the Coactivator-Associated Arginine Methyltransferase 1 inhibitor's potency using MRM and many others.(Zhang et al., 2022) Taking advantage of this approach, we developed and validated a targeted LC-MRM based on selected signature peptides for the absolute quantification of a panel of four co-stimulatory proteins. In addition, the developed method was used to establish a competitive assay for the CD28-B7 pathway, using Abatacept^{TM} as a platform for biologic development and biosimilar evaluation.

4.2 Experimental section:

4.2.1 Chemicals and Reagents

All peptides, labeled(The red-colored and underlined arginine and lysine are labeled with ^{13}C and ^{15}N as shown in Table 4.2) and unlabeled, were custom synthesized by Biomatik (Kitchener, ON, Canada) with purity >95% and delivered as powder. Dithiothreitol (DTT), iodoacetamide (IAM), formic acid (FA), ammonium bicarbonate (ABC), methanol, acetonitrile (ACN), acetic acid,

phosphate-buffered saline (PBS), and trypsin were purchased from Sigma-Aldrich (Oakville, ON, Canada). Human soluble B7-1/CD80 Fc chimera protein (sCD80), and human soluble B7-2/CD86 Fc chimera (sCD86) recombinant protein were purchased from R&D systems (Toronto, ON, Canada). sCTLA-4 recombinant human protein was obtained from Thermofisher Scientific (Saint-Laurent, QC, Canada). Recombinant human soluble protein sCD28 (His-tag) was purchased from Abcam (Cambridge, UK). InvivoMmAB recombinant ctla-4-IG (human) was purchased from Bio X Cell (Lebanon, NH, US).

4.2.2 Signature peptide selection by high-resolution mass spectrometry:

4.2.2.1 Protein in-solution trypsin digestion:

The human recombinant soluble co-stimulatory proteins (sCD80, sCD86, sCTLA-4, and sCD28) were digested with trypsin as follows: 10 µg of protein in 100 µL PBS was brought to 300 µL using 100 mM ABC. The protein disulfide bonds were reduced by adding 10 µL of 100 mM DTT and incubating for 20 min at 37 ºC. The reduced disulfide bonds were alkylated by adding 15 µL of 100 mM IAM and incubated for 30 min at 37 ºC in the dark. 20 µL of 0.1 mg/mL trypsin in 50 mM acetic acid was added to the sample and incubated at 37 ºC for up to 16 hours.

4.2.2.2 Solid-phase extraction (SPE)

Hydrophilic-lipophilic balance solid phase extraction with 30mg stationary phase/1cc cartridge (Oasis HLB-SPE) (Waters Corporation, Milford, MA, USA) was used to desalt the digest and concentrate the tryptic peptides. The HLB cartridge was conditioned with 1 mL of 100% methanol and 1 mL of water. The digested samples were diluted up to 1 mL total volume with water and loaded on the HLB cartridge and washed with 1 mL of water. Afterward, tryptic peptides were eluted with 100% methanol and completely dried using a Speed Vac (UVS800DDA-115, ThermoFisher, Asheville, NC, USA). The dry extracts were reconstituted in 100 µL of 10% ACN, 0.2% FA before analysis.

4.2.2.3 Liquid chromatography high-resolution mass spectrometry method (LC-HRMS):

Tryptic peptides were separated by reversed-phase chromatography on a Shimadzu Nexera HPLC (Columbia, MD, USA) using an Aeris Peptide XB-C18 (100 Å; 100 × 2.1 mm; 1.7 µm) column (Phenomenex, Torrance, CA, USA) at 40 ºC. The mobile phase A (0.1% FA in water) and B (0.1% FA in ACN) were pumped at 0.3 mL/min using a gradient of 0.0-2.5 min 5.0% B, linear increase to 30% B at 50 min, 50% B at 55 min, 90% B at 56 min hold until 60 min, equilibrate at 5% B for 8 min. The column-eluted peptides were analyzed on a TripleTOF5600 hybrid QqTOF instrument with a DuoSpray ion source in positive ion mode (Concord, ON, Canada). The ion source temperature was set to 500°C, and the ion spray voltage was at 5000 V. The product ion spectra were generated using 30 V collision energy with a 10 V spread for fragmentation. The QqTOF system was calibrated with a set of in-house standards ranging from m/z 121-922 in MS and MS/MS mode before starting the injection batch and every 4 injections after that using an automated calibration routine with a calibrant delivery system. The mass accuracy of all ions in TOF-MS mode and fragment ions in MS/MS was consistently less than 5 ppm.

The precursor ion scan range was m/z 140-1250, while the product ion scan was m/z 80-1500. The top 15 ions per cycle (1.05 s) were selected for MS/MS in data-dependent mode (DDA). Acquired data were analyzed using ProteinPilot v5 software (Sciex, Concord, ON, Canada) by searching MS/MS data against a database containing protein sequences of human CD80, CD86, CD28, and CTLA-4 downloaded from UniProt (https://www.uniprot.org/) which also included a list of 156 common contaminant proteins provided by Sciex (https://sciex.com/products/software/proteinpilot-software). Tryptic peptides identified by ProteinPilot were verified by reviewing extracted ion chromatograms (XICs) and MS and MS/MS spectra in PeakView v2.2 and MasterView v1.1 software (Sciex, Concord, ON, Canada). A short list of peptide targets for each protein was created based on peak shape, intensity, and MS/MS

spectra fragmentation quality based on signal/noise and database score. We also used the human SRMAtlas (https://srmatlas.org/) database to guide our short-list selection. Standard peptides and an isotopically labeled version were synthesized to develop the LC-MRM method. The selected signature peptides for each protein are summarized in Table 4.1.

4.2.3 Multiple reaction monitoring (MRM) method development and optimization:

4.2.3.1 Solution preparation

The synthesized unlabeled and labeled peptides were prepared at 10 mM in 50% methanol (stock solution). A mix of 25 µl of each of the 4 peptides stock (unlabeled and labeled) was prepared and 10 µL was aliquoted into protein low-bind tubes (Eppendorf, Mississauga, ON, CA) and dried by SpeedVac and stored at -30^{o}C until use. At the time of analysis, aliquots containing 25 nmole peptides (one each of labeled and unlabeled peptide mix) were reduced by adding 50 µL of 1 mM DTT in 100 mM ABC (pH 8) and incubating for 15 min at 37 °C. Peptides were alkylated by adding 20 µL of 5 mM IAA in water and incubating for 20 min at 37 °C in the dark. The mixtures were diluted to 2 µM in 10 % ACN, 0.2% FA (v/v) in $H_2O$for MRM method optimization.

4.2.3.2 LC-MRM parameter optimization

The MRM transitions for the signature peptides, and their isotopically labeled internal standards (IS), were optimized using a Sciex QTRAP 5500 hybrid quadrupole-linear-ion trap (Concord, ON, CA) operated in electrospray positive ionization mode. Ion source and MS parameters were as follows: ESI voltage, 5000 V; source temperature, 500°C; curtain gas, 35 psi; gas 1, 50 psi; gas 2, 50 psi; entrance potential, 10V; collision exit potential, 13 V; declustering potential, 80 V. Peptides were chromatographically separated on an identical Nexera HPLC using the same column and mobile phases that was used for LC-HRMS analysis, but the gradient method was shorter. The gradient started at 5% B for 0.5min and increased linearly to 50% B in 15 min, up to 85% B in

15.1 min, and held until 16 min, and the column was re-equilibrated at 5% B for 7 min. Between five and nine MRM transitions were tested for each peptide. The top 3 transitions were selected based on peak intensity, and the fragmentation collision energy (V) was tested and optimized manually for each transition. The final method used peptide retention times to run scheduled MRM (1.5 s cycle time) with automatically optimized dwell times for each transition.

4.2.4 LC-MRM MS/MS method validation

Validation was performed according to the analytical method validation guidelines of the Food and Drug Administration (FDA). (Food) and International Conference on Harmonisation of Technical Requirements for Registration of Pharmaceuticals for Humans (ICH) (Guideline IHT). All calibrators and QCs used in the validation study were prepared from the stock solution that was prepared in the same way as in section 4.2.3.1

4.2.4.1 Curve linearity

Three calibration curves were generated over three consecutive days for the linearity test. A calibration curve for each peptide was generated in duplicate per calibration point for each day and expressed as area ratios (area of standard/ area of internal standard) (y-axis) versus the nominal concentration (x-axis). The linearity of the calibration curves was evaluated by the correlation coefficient (R^2), which should be ≥ 0.98, and the correlation of variance for each level (80-120% for LOQ and 85-115% for the other levels).

4.2.4.2 Sensitivity and carryover

The lower limit of detection (LOD) and the lower limit of quantification (LOQ) were determined through the three days calibration curve. LOQ, the lowest point in the calibration curve, was determined with acceptable accuracy and precision. The LOD and LOQ signal-to-baseline noise

ratio (S/N) was considered at least 10 and 3, respectively. The accuracy of the LOQ should be between 80–120%, and the day-to-day variation should be < 20%.

The LOD is calculated as 3.3 δ/s, where δ is the standard deviation of the intercept, and s is the slope of the calibration curve. Alongside, the carryover of the method was assessed by running blank after the high-concentration QC sample (HQC). The response in the blank should be at most 20% of LOQ.

4.2.4.3 Inter- and intraday validation

The method's performance was assessed by measuring the inter- and intraday accuracy and precision. In addition to the LOQ samples, 6 replicates of three different levels of QCs; low, medium, and high levels of QC (LQC, MQC, HQC) samples were run on the same day (intraday) and three consecutive days (interday). The concentrations of these QC samples were 1.5, 7.5, and 15 nM, respectively. The intraday precision for each QC was calculated based on: (σ (standard deviation) of measured concentrations of QC on day x / mean of measured concentrations on day x) × 100%. Also, the interday precision was calculated using the formula (σ of measured concentrations of QC in 3 days/mean of measured concentrations of 3 days) × 100%. The variability between samples on the same day or between days should not exceed 15% CV except at LOQ 20%. On the other hand, the intra and interday accuracy were calculated as (mean measured concentration on day x/nominal concentration of the QC) × 100% and (mean measured concentration over three days/nominal QC concentration) 100%, respectively. The accuracy within and between runs should be ±15% of nominal concentration except ±20% for LOQ.

4.2.4.4 Peptide stability study

The stability of all peptides was evaluated over different storage conditions; benchtop (RT), refrigerator (4^{o}C), or Freezer (-20^{o}C) for a total of 4 weeks period. This study used the three

different QC levels (LQC, MQC, HQC) in triplicates. The peptide stability was calculated as the average area ratio of the examined sample/average area ratio of the fresh sample (stored at -80°C) × 100%.

4.2.4.5 Protein linearity performance

The reliability of MRM method detection and the signal linearity at protein levels were evaluated using study proteins' standards. Therefore, all four proteins (sCD80, sCD86, sCTLA-4, and sCD28) were prepared in a solution mixture at different concentrations ranging from 50 nM-1000 nM. The protein mixture was reduced, alkylated, and digested with trypsin following the same procedure in sections 4.2.2.1 and 4.2.2.2. The IS solution mixture was added to the digested peptides (10 µl of 50nM) before being subjected to SPE as described in section 4.2.2.2. Then, the samples were analyzed using the developed LC-MRM method (section 4.2.3.2) with a calibration curve set and QCs. The linearity performance between the signature peptide (y-axis) and the protein (x-axis) levels was evaluated by the correlation coefficient (R^2).

4.2.5 CD28-B7 competition assay development

The developed LC-MRM method was used to establish a competitive assay for the co-stimulatory pathway CD28-B7 using AbataceptTM (CTLA4-Ig). The His-tagged sCD28 was immobilized on Ni-NAT beads (Thermofisher Scientific Inc., Saint-Laurent, QC, Canada) (16.8 pmole/µL of beads) as described in Appendix C section C.1**.** A mixture of a fixed amount of sCD80 (50 pmole) or sCD86 (100 pmole) with increasing concentrations of Abatacept (0-1000 nM) was added to the beads in a final volume of 200 µL and then incubated for 2 hours at RT in PBS (pH 7.4) with end-over-end rotation. After incubation, beads were washed three times with 100µL PBS. After each wash, the beads were spun down by centrifugation, and the supernatant was discarded. The beads were reconstituted in 50 µL ABC to prepare for tryptic digestion in the last wash, as detailed in Section 4.2.2.1. The digested peptides solution was brought up to 500µL by water after adding IS solution mixture (10 µL from 50 nM) and then subjected to SPE as described in section 4.2.2.2. A

protein mixture with 42, 50, and 100 pmole for sCD28, sCD80, and sCD86 was used as a digestion efficiency control sample. After that, samples were run using our developed LC-MRM method described in section 4.2.3.2 with a calibration curve set and QCs. The competition was assessed as the sCD80 or sCD86 concentration normalized to the sCD28 concentration over the range of abatacept concentrations.

4.2.6 Data and statistical analysis:

LC-MS/MS data acquisition was managed by Analyst TF v1.8 for LC-HRMS/MS and Analyst v1.7 for LC-MRM (Sciex, Concord, ON, CA). LC-MRM peak integration, calibration curve construction, and sample quantitation were done by MultiQuant software v3.0.3 (Sciex, Concord, ON, CA). Graphs were plotted using GraphPad Prism software version 6.01 (City, California, USA).

4.3 Results

4.3.1 Signature peptide selection and LC-MS/MS method optimization:

One widely used method for selecting the surrogate peptide relies on experimental data, where tryptic peptides of the soluble co-stimulatory proteins (sCD80, sCD86, sCD28, and sCTLA-4) were separated and identified in LC-HRMS using bottom-up proteomics as seen in the total ion chromatograms (TIC) in Appendix C, Figure C. 1. The protein amino acid sequence coverage was determined by searching against a protein database containing the proteins of interest. Accordingly, the sequence coverage was 80, 48, 63, and 92 % for sCD80, sCD86, sCD28, and sCTLA-4, respectively. By following the selection criteria, all selected signature peptides: (i) were unique for the target proteins, (ii) had a good response in MS (highly abundant), (iii) had a clear fragmentation pattern (i.e., y and b type ions) as seen in MS/MS spectra in Appendix C, Figure C.2. (iv) all peptides length are between 7 and 15 aa, and (v) no post-translational modification (PTM) such as methionine or cysteine except for CTLA-4 which was the only available option.

(Alexandridou, Tsangaris, Vougas, Nikita, & Spyrou, 2009; Fu et al., 2016) To PTM for the CTLA-4 signature peptide, the standard solution mixture was reduced and alkylated before constructing the calibration curve, and QCs samples. The mass accuracy of the peptides is all within 5 ppm with an identification confidence of 99.0%. Table 4.1 shows the highly abundant peptides with the amino acid sequence coverage, the selected signature peptide, and their physicochemical properties. The selected signature peptides were synthesized in standard (light) and IS (heavy, stable isotope-labeled) forms to develop the targeted MRM method.

Using a mixture solution of the four selected signature peptides and their labeled analogies, the LC-MRM parameters were optimized, including collision energy. The most abundant precursors and product ions for each peptide were obtained at the optimum collision energy, as summarized in Table 4.2. Three transitions were selected for each peptide; the most sensitive was used for quantification of the protein (quantifier transition), while the other two were used to verify retention time and the absence of any interferences (qualifier transition). The LC-MRM method parameters, such as retention time (RT), precursor ion (Q1), product ion (Q2), and optimized collision energy, are summarized in Table 4.2.

The isotopically labeled IS of each peptide co-eluted almost at the same retention time and corrects some analytical variations, such as ion suppression, fragmentation efficiency, and sample preparation, as they share the same physicochemical proprieties, such as proton affinity. Therefore, the concentration of each peptide was determined based on the observed relative response at each concentration as a ratio of peak area for the light (analyte) to the heavy (IS) and the experimentally determined linear regression equation from the standard curve.

Table 4.1. List the highly abundant tryptic peptides detected in the LC-HRMS and the selected signature peptides for each costimulatory protein.

Protein ID	**Uniprot ID**	**Sequence coverage (%)**	**Protein MW (KDa)**	**Abundant detected peptides**	**Selected signature peptides**	**Signature peptide (*m/z*)**
CD80	P33681	80	25	^{95}EHLAEVTLSVK^{105} ^{106}ADFPTPSISDFEIPTSNIR^{124} ^{10}EVATLSCGHNVSVEELAQTR^{29}	^{95}EHLAEVTLSVK^{105}	1225.20
CD86	P42081	48	26	^{74}LHNLQIK^{80} ^{63}TSFDSDSWTLR^{73} ^{146}MSVLLR^{151}	^{74}LHNLQIK^{80}	864.90
CTLA-4	P16410	63	15	^{85}AMDTGLYICK^{94} ^{16}GIASFVCEYASPGK ^{29} ^{2}MHVAQPAVVLASSR^{15}	^{16}GIASFVCEYASPGK ^{29}	1114.20

Protein ID	**Uniprot ID**	**Sequence coverage (%)**	**Protein MW (KDa)**	**Abundant detected peptides**	**Selected signature peptides**	**Signature peptide (*m/z*)**
CD28	P10747	92	42	^{5}ILVK^{10} ^{26}YSYNLFSR^{34} ^{66}TGFNCDGK^{74}	^{26}YSYNLFSR^{34}	525.25

Table 4.2: The optimized MRM conditions for each signature peptide and isotopically labeled IS. The transitions and the MRM parameters are listed. The red-colored and underlined arginine and lysine were labeled with ^{13}C and ^{15}N. Q1: Precursor ion, Q3: Product ion, DP: Declustering potential, and CE: Collision Energy

Protein	**Accession**	**peptide name**	**Q1 (m/z)**	**Charge (z)**	**Q3 (m/z)**	**Product ion type**	**Function**	**DP (v)**	**CE (v)**	**Retention time (min)**
CTLA-4	P33681	^{16}GIASFVCEYASPG<u>K</u>^{29}	743.36	2	301.19	y3 (Quan)	Standard	80	33	7.5
			743.36	2	911.39	y8 (Qual)		80	31	7.5
			495.91	3	301.19	y3 (Qual)		80	29	7.5
			747.36	2	309.19	y3 (Quan)	Internal Standard	80	33	7.5
			747.36	2	919.39	y8 (Qual)		80	31	7.5

Protein	Accession	peptide name	Q1 (m/z)	Charge (z)	Q3 (m/z)	Product ion type	Function	DP (v)	CE (v)	Retention time (min)
			498.91	3	309.19	y3 (Qual)		80	29	7.5
CD80	P33681	^{95}EHLAEVTLSVK^{105}	613.34	2	267.11	b2 (Quan)	Standard	80	35	5.7
			409.23	3	446.3	y4 (Qual)		80	22	5.7
			409.23	3	547.35	y5 (Qual)		80	22	5.7
			617.34	2	267.11	b2 (Quan)	Internal Standard	80	35	5.7
			411.89	3	454.3	y4 (Qual)		80	22	5.7
			411.89	3	555.35	y5 (Qual)		80	22	5.7
CD86	P42081	^{74}LHNLQIK^{80}	433.27	2	251.15	b2 (Qual)	Standard	80	23	3.9

Protein	Accession	peptide name	Q1 (m/z)	Charge (z)	Q3 (m/z)	Product ion type	Function	DP (v)	CE (v)	Retention time (min)
			289.18	3	251.15	b2 (Quan)		80	19	3.9
			289.18	3	365.19	b3 (Qual)		80	16	3.9
			437.27	2	251.15	b2 (Qual)	Internal Standard	80	23	3.9
			291.85	3	251.15	b2 (Quan)		80	19	3.9
			291.85	3	365.19	b3 (Qual)		80	16	3.9
CD28	P10747	^{26}YSYNLFSR^{34}	525.26	2	886.45	y7 (Quan)	Standard	80	25	6.8
			525.26	2	799.41	y6 (Qual)		80	25	6.8

Protein	Accession	peptide name	Q1 (m/z)	Charge (z)	Q3 (m/z)	Product ion type	Function	DP (v)	CE (v)	Retention time (min)
			525.26	2	636.35	y5 (Qual)		80	25	6.8
			530.26	2	896.45	y7 (Quan)	Internal Standard	80	25	6.8
			530.26	2	809.41	y6 (Qual)		80	25	6.8
			530.26	2	646.35	y5 (Qual)		80	25	6.8

4.3.2 LC-MRM method validation

4.3.2.1 Curve linearity, sensitivity, and carryover:

A 1.0 μM stock solution of peptides mixture was prepared in the mobile phase and diluted into 6 different concentrations (0.5, 1.0, 2.5, 5.0, 7.5, 10.0, and 20.0 nM) in addition to the zero calibrators (blank with IS) in duplicate. Then the IS mixture was added in a final concentration of 5.0 nM to establish the calibration curve.

The calibration curve was run over three days to determine the quantification range and the linearity of the method using linear regression. The representative extracted ion chromatograms (XICs) for all peptides and their internal standard are shown in Figure 4.1a. Good linearity was achieved through a wide calibration range (0.5-20.0 nM) for all peptides, as shown in Figure 4.1b, where the correlation coefficient was ≥0.99 with the average analyte response factor (slope) ranging between 0.2027-0.3620 and the slope was associated with instrument noise (Table 4.3). The mean value for all calibrators is within ±15% of the theoretical value, as recommended by the used validation guideline. The calibration curve linear equation was used for calculating peptide concentration.

The sensitivity of the method was determined as the lowest concentration of the calibration curve that was precisely and accurately quantified with an S/N ratio of 10. (Guideline IHT) LOQ was run in duplicate over three different days (n = 6) and found on average 0.5 nM for all peptides, as seen in Table 4.3. The accuracy and precision of the signal were within 101-103% and 3-9%, respectively.

The detection limit is the lowest concentration that can be detected but is not necessarily quantified as an exact value. Accordingly, LOD was calculated as 3.3 standard deviations of the response

divided by the slope of the calibration curve, where the response is the calibration curve intercept. The LODs of the target analytes are summarized in Table 4.3.

The carryover was assessed over three different validation runs by running three blanks after a high concentration of peptides. As a result, no carryover has been reported in any of these runs. The acceptance criteria of carryover are based on the signal detected in the blank and should not exceed 20% of the LOQ signal.

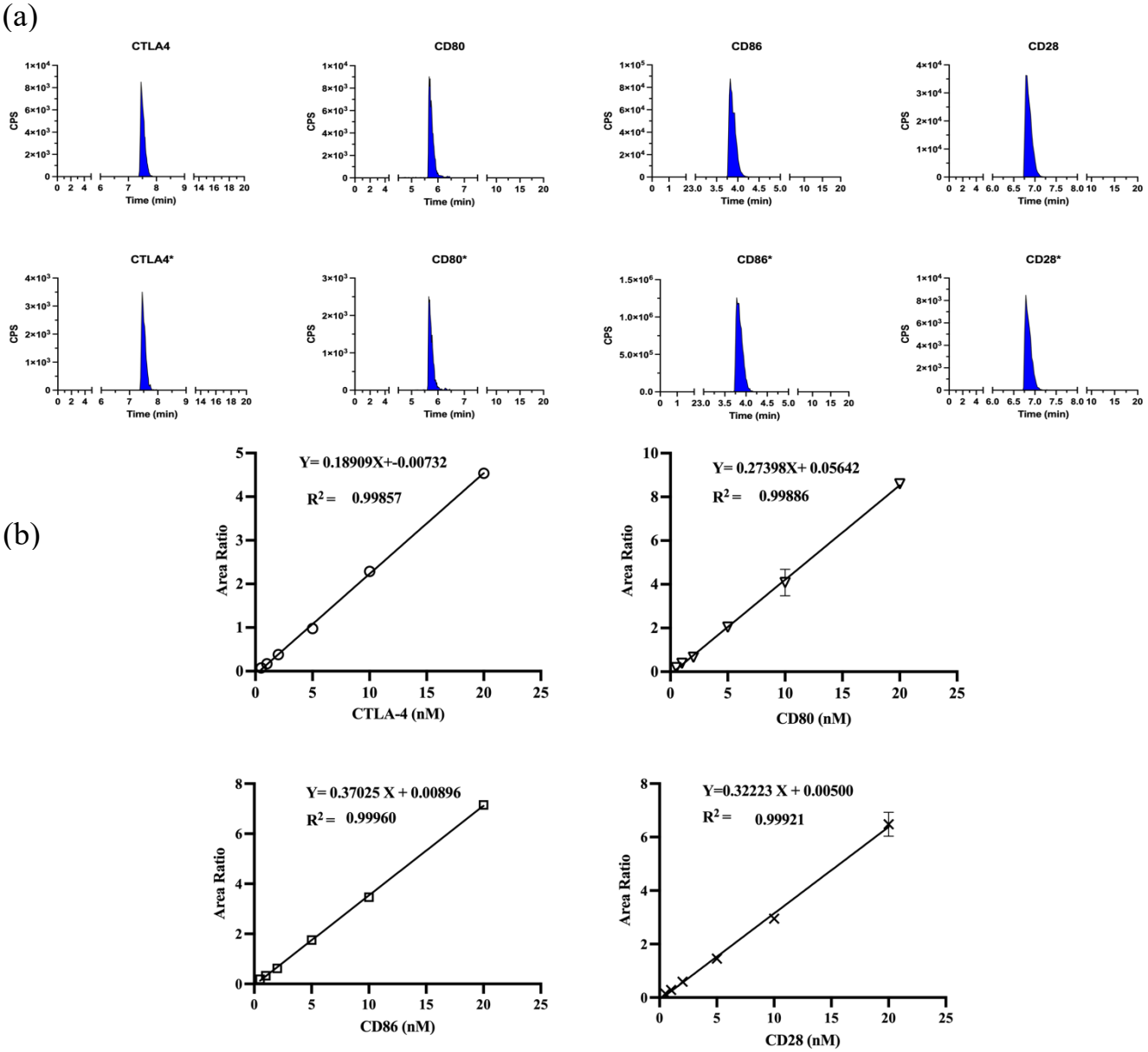

Figure 4.1. Representative extracted ion chromatograms and calibration curves. (a) Extracted ion chromatogram (XIC) for the quantitative transitions for each signature peptide and its internal standard, CPS (ions counted per second). (b) Linear calibration curves for all selected signature peptides using the quantitative transitions. Area ratio is the ratio between the standard signature peptide and its internal standard.

Table 4.3. Summary of the linearity and sensitivity (average of over three days). LOQ: lower limit of quantification, LOD: lower limit of detection

Protein	**Slope (*n*=3)**	**Intercept (*n*=3)**	**R^2 (*n*=3)**	**LOD (nM)**	**LOQ (*n*=6)**		
					LLOQ (nM)	**Interday Accuracy (%)**	**Interday precision (%)**
CTLA-4	0.202787	0.02139	0.998417	0.4250763	0.51	101.00	9.00
CD80	0.326037	0.052323	0.99835	0.07016	0.51	102.00	9.00
CD86	0.362087	0.00769667	0.999513	0.0139791	0.51	103.00	3.00
CD28	0.31774	0.01462667	0.998693	0.1020483	0.52	103.00	6.00

4.3.2.2 Inter- and intraday validation:

The method's performance was assessed by measuring the intra and interday precision and accuracy. Low, medium, and high (LQC, MQC, and HQC, respectively) concentrations within the linear range of 1.5, 7.5, and 15.0 nM in 6 replicates for each were run over three days. The signal variation was 3.61-11.0% for inter-assay and 2.6-12.14% for intra-assay, and the accuracies are within 90.6-111.34% for all QCs, as summarized in Table 4.4. Therefore, this method is satisfactory in precision and accuracy for determining and quantifying this panel of four proteins and can be used robustly to study a biological activity, such as the inhibition of the co-stimulatory pathway.

Table 4.4. Inter- and intraday validation summary. SD: standard deviation, SP: signature peptide

Protein SP (nM)	**Mean** ***(n*=18)**			**SD** **(*n*=18)**			**Intraday accuracy (%)** ***(n=6)***			**Intraday precision (%)** ***(n=6)***			**Interday precision (%)** ***(n=18)***			**Interday Accuracy (%)** ***(n=18)***		
	1.5	7.5	15.0	1.5	7.5	15.0	1.5	7.5	15.0	1.5	7.5	15.0	1.5	7.5	15.0	1.5	7.5	15.0
CTLA-4	1.43	7.24	15.15	0.11	0.87	1.66	94.40	111.34	110.76	8.42	2.80	9.11	7.63	10.96	9.55	95.51	96.60	100.97
CD80	1.56	6.98	13.59	0.09	0.74	0.86	101.45	100.48	94.91	4.80	12.14	5.64	5.03	11.00	9.67	103.90	93.11	90.60
CD86	1.56	7.46	14.65	0.08	0.36	0.55	100.51	100.93	99.17	3.85	3.63	4.84	5.53	4.25	3.68	104.12	99.41	97.70
CD28	1.50	7.48	14.73	0.10	0.46	0.62	104.04	104.98	99.99	6.76	2.60	4.40	5.08	5.06	3.61	99.78	99.74	98.21

4.3.2.3 Stability of peptides:

The stability of all 4 peptides was assessed relative to fresh samples under different conditions, including 24 hours at room temperature (~25°C), one week at 4°C, and four weeks at –20 °C. Quality control (QC) samples at three different concentrations (1.5,7.5, 15.0 nM) in triplicate were assessed, and the stability ranged between 75.0%-123.0%, as summarized in Table 4.5.

Table 4.5. Summary of signature peptide stability at different storage conditions for a determined period. SP: signature peptide, QC: quality control, RT: room temperature

Protein's SP	QC (nM)	Stability %			
		Fresh	RT	4°C	Freezer (–20 °C)
			24 h	1 Week	1 Month
CTLA-4	**1.5**	100.0	115.4	123	112.6
	7.5	100.0	88.1	75.4	78.2
	15.0	100.0	100.8	98.4	99.4
CD80	**1.5**	100.0	98.8	101	103.1
	7.5	100.0	100.2	98.7	100.3
	15.0	100.0	100.7	100.2	101.1
CD86	**1.5**	100.0	101	97.3	97.7
	7.5	100.0	100.8	97.7	99.7
	15.0	100.0	100.1	101.7	100.5
CD28	**1.5**	100.0	97.2	98.6	94.9
	7.5	100.0	94.7	99.3	96
	15.0	100.0	97.4	98.2	99.2

4.3.3 Response linearity and method performance on protein in-solution digest

The linear response of the method on actual protein digestion was evaluated, where five different protein concentrations (100-fold the peptide calibrators) were used to correlate the signature peptide signal with protein concentration. The 100-fold protein concentration was used to allow the quantification using the peptide's dynamic range. The protein digest was spiked with the heavy isotopes of the signature peptides, and then 20 µL was injected into the column. The linear correlation was achieved in the selected range with a correlation coefficient >0.99, as shown in Figure 4.2. where the calculated concentration determined by the developed MRM method corrected by a factor of 100 was correlated with the actual concentration of the proteins. It is worth mentioning that the accuracies ranged between 80-120% except for two concentrations for CTLA-4 due to the reduction/ alkylation of disulfide bond efficiency. The method's reliability for studying the targeted proteins' biological activity was achieved for further utilization.

4.3.4 CD28-B7 Competition assay development

To study the applicability of the developed method, a competition assay for CD28-B7 was established using Abatacept™ as an USFDA-approved drug that comprises the extracellular domain of CTLA-4 with high binding avidity to sCD80/sCD86. Before developing the assay, the ratio between sCD28 and sCD80 or sCD86 was evaluated through a titration experiment using four different concentrations. It was found to be 42/50 pmole and 42/100 pmole, respectively based on the first concentration at the plateau. The inhibition of binding between sCD28 and sCD80 or sCD86 by increasing Abatacept™ concentration was assessed using the developed LC-MRM method; the concentration of sCD80/sCD86 bound to sCD28 on beads was determined normalized to sCD28 concentration. After adding Abatacept™ to sCD28/sCD80 or sCD28/sCD86 mixture, the amount of sCD80 or sCD86 bound to sCD28 decreased gradually with increasing Abatacept™ concentration until it reached saturation, as shown in Figure 4.3, where the response (concentration of sCD80 or sCD86/ concentration of sCD28) was plotted with the Abatacept™ concentration and

the IC50 was calculated from the data fit using exponential decay-nonlinear regression. Figure 4.3a shows a strong inhibition of sCD80/sCD28 interaction with a fast saturation after adding abatacept due to the higher affinity toward CTLA4-Ig compared to sCD28 (10 to 100 folds).

On the other hand, CTLA4-Ig has a lower binding affinity toward sCD86 compared to sCD80, which leads to slower kinetics with lower potency than sCD80 (Figure 4.3b). The IC50 was 72.22 nM and 2.71 nM for sCD86 and sCD80, respectively. The on-beads digestion efficiency for sCD28, considering the efficiency of beads coupling and the digestion efficiency and protein interaction of sCD80/sCD86 with sCD28, were assessed and found to be 80%, 8.5%, and 26%, respectively, using a control standard sample containing sCD28, sCD80, sCD86 with the same ratio as in the competition assay samples. The successfully developed competition assay will be used to test other biological molecules as costimulatory inhibitors, such as antibodies and aptamers.

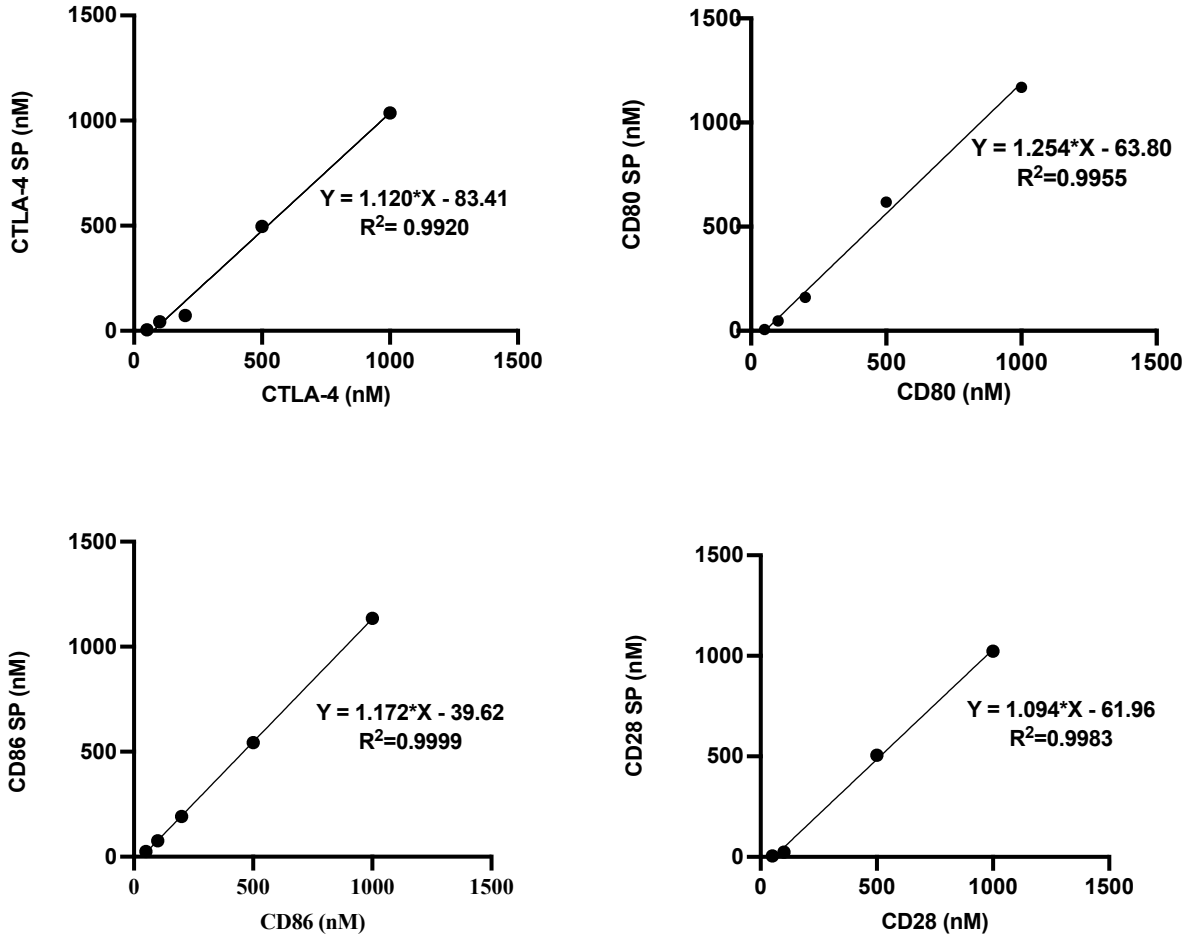

Figure 4.2. The correlation between the tryptic-digested proteins and their signature peptides using the LC-MRM MS/MS method.

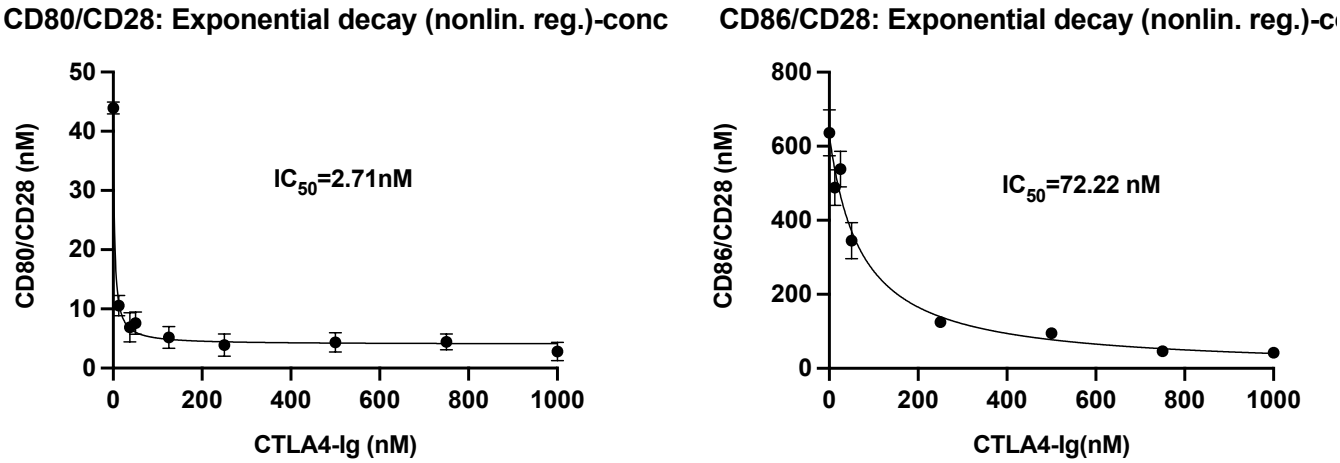

Figure 4.3. MS- based competitive assay using abatacept (CTLA4-Ig) as an inhibitor for CD28-B7 interaction. (a) The inhibition curve of CD28/CD80 and (b) is the inhibition curve of CD28/CD86, where the binding activity (concentration of the protein normalized to sCD28 concentration) plotted with the CTLA4-Ig concentration and the IC50 was calculated by fitting the curve using the exponential decay, nonlinear regression.

4.4 Discussion:

Recently, scientists have been trying to deepen their knowledge about the important role of the B7-CD28 costimulatory pathway in autoimmunity. The molecules involved in this pathway, namely CD80, CD86, CD28, and CTLA-4, contribute significantly to the functional activation of self-reactive T-cells and their differentiation, migration, and tolerance induction. The presence of these molecules in soluble forms in the body fluids, such as plasma, eases the understanding of their biological role and enables the detection and quantification of their level as potential biomarkers for different autoimmune diseases.

Some studies revealed that the level of the soluble costimulatory molecules is associated with disease development and stage in autoimmunity, and they have the same biological activity as the membranous molecules (Hock et al., 2004; Ip et al., 2006). However, the need for precise and accurate analytical methods for quantifying these molecules and studying their biological activity poses a challenge. Overcoming this obstacle is crucial for enhancing our understanding of the pathogenesis of different autoimmune diseases and developing effective drugs. In this study, an accurate and precise LC-MRM method was developed and successfully validated for quantifying these four molecules and developing a competition assay for drug discovery and biosimilar activities.

The sensitivity and specificity of the method were achieved at a wide range of quantification. In addition, the method was applied to the protein level, which enabled a successful tool to develop the competition assay for the CD28-B7 costimulatory pathway using Abatacept™ as an inhibitor model. Costimulatory protein inhibitors such as antibodies or fusion proteins like AbataceptTM, have been developed as potential therapeutic targets for autoimmune diseases, such as the antibodies or fusion proteins like Abatacept™. (Crepeau & Ford, 2017) Studying the affinity of the developed inhibitors and the inhibition potency is usually carried out using immunoassays or Biacore measurements assays. For example, the inhibition potency (IC50) of CTLA-4Fc for

CD28-CD80 as a control in studying small molecule inhibitors was 5 nM using the Homogeneous Time-Resolved Fluorescence (HTRF) assay. (Uvebrant et al., 2007) This study showed a result comparable to our finding, where distance-related energy transfer-based cell-free assay was used quantitatively. This study and our study were similar In vitro using multivalent proteins. This study showed a result comparable to our finding, where distance-related energy transfer-based cell-free assay was used quantitatively. This study and our study were similar In vitro using multivalent proteins. On the other hand, in a competition assay using AlphaLISA immunoassay, the average IC50 values of parental CTLA4-Ig were determined to be 1.2 and 17.2 nM for CD80 and CD86, respectively(Xu et al., 2012) This study determined the biological potency by evaluating the IL-2 production by inhibiting CD80 or CD86-mediated T-cell activation. In another study, the potency of Abatacept in inhibiting CD28-CD86 interaction using a T-cell stimulation assay was found to be 7.3 nM. (Oshima *et al.*, 2016) The model used can explain the higher potency for CTLA4-Ig obtained in these studies, as the cell lines used produced full-length proteins mimicking the costimulatory pathway in the body.

Although these methods efficiently study the inhibitors, either proteins or small molecules, some disadvantages, include cross-reactivity and false positive results, the suitability for high throughput analysis, and the expensive kits and reagents. (Zhang et al., 2022) Thus, the developed LC-MRM method can be used as a rapid, straightforward, and sensitive method for detecting and quantifying a panel of four proteins and as an accurate method to study the inhibitors of the CD28-B7 pathway.

In this study, the lower IC50 obtained for sCD80, and the fast saturation compared to sCD86 is due to the higher inhibition potency of CTLA4-Ig to sCD80 costimulation, as CTLA4-Ig is 100-fold less potent at inhibiting sCD86-mediated immune response compared to CD80. This fact can be explained by the faster dissociation of CD86 and the difference in avidity between sCD80 and sCD86. (Linsley et al., 1994) Recently, researchers started to use MRM MS methods as a direct way to accurately study inhibitors as potential therapeutic agents for different biological pathways and enzymatic activities involved in different diseases and clinical situations. (Zhang et al., 2022)

Our study showed a higher IC50 of CTLA4-Ig for sCD80 and sCD86 compared to the conventional methods, considering the differences in the used models and the protein length used. Most studies for determining inhibitors' potencies rely on biological assays by indirectly measuring the proliferation or biomarkers. Our study is a direct method that determines the inhibition potency by measuring the level of interacting molecules. To our knowledge, this is the first LC-MRM method developed for quantifying the four costimulatory proteins and a successful assay to study costimulatory pathway inhibitors with the need to test the developed assay on cell lines to study the costimulatory response as a future step. This method will advance the knowledge for more understanding of the CD28-B7 pathway and the costimulatory proteins. It will allow us to test different inhibitors for the pathway, including small molecules such as specific DNA aptamers developed against sCD80 by our group. (Malkawi *et al.*, 2023)

4.5 Conclusion

Herein we developed a direct, specific, accurate, and convenient LC-MRM MS method for the detection and quantification of a panel of the four costimulatory molecules: sCD80, sCD86, sCTLA-4, sCD28, depending on the selected signature peptides for each protein. The method was successfully validated with good sensitivity and a wide range of quantification. The applicability of the developed method to the mixture of the four proteins gives the ability to demonstrate the application of the LC-MRM MS method in assaying the inhibitory activity of CTLA4-Ig (Abatacept™) on CD28-B7 pathway by generating sCD80 and sCD86 inhibition curves. The IC50s for sCD80 and sCD86 have the same pattern as the published values, considering the difference in the model and the version of protein used. Furthermore, the 15 min run time allows for assessing many compounds in a high throughput manner. In addition, the described method

should be widely applicable in developing assays on cell line stimulation response and in in vivo studies.

References:

Alexandridou, A., Tsangaris, G. T., Vougas, K., Nikita, K. et Spyrou, G. (2009, Nov 15). UniMaP: finding unique mass and peptide signatures in the human proteome. *Bioinformatics*, *25*(22), 3035-3037. https://doi.org/10.1093/bioinformatics/btp516

Buck, C. A. (1992, Jun). Immunoglobulin superfamily: structure, function and relationship to other receptor molecules [Research Support, U.S. Gov't, P.H.S. Review]. *Semin Cell Biol*, *3*(3), 179-188. https://doi.org/10.1016/s1043-4682(10)80014-5

Cao, J., Zou, L., Luo, P., Chen, P. et Zhang, L. (2012, Dec). Increased production of circulating soluble co-stimulatory molecules CTLA-4, CD28 and CD80 in patients with rheumatoid arthritis [Research Support, Non-U.S. Gov't]. *Int Immunopharmacol*, *14*(4), 585-592. https://doi.org/10.1016/j.intimp.2012.08.004

Crepeau, R. L. et Ford, M. L. (2017, Aug). Challenges and opportunities in targeting the CD28/CTLA-4 pathway in transplantation and autoimmunity [Review]. *Expert Opin Biol Ther*, *17*(8), 1001-1012. https://doi.org/10.1080/14712598.2017.1333595

Das, S., Ariizumi, K. et Cruz, P. D., Jr. (2012, Sep-Oct). T-cell inhibitors: a bench-to-bedside review [Research Support, N.I.H., Extramural Research Support, U.S. Gov't, Non-P.H.S. Review]. *Dermatitis*, *23*(5), 195-202. https://doi.org/10.1097/DER.0b013e31826e43ed

Edner, N. M., Carlesso, G., Rush, J. S. et Walker, L. S. K. (2020, Dec). Targeting co-stimulatory molecules in autoimmune disease. *Nat Rev Drug Discov*, *19*(12), 860-883. https://doi.org/10.1038/s41573-020-0081-9

Food, D. A. U. B. m. v. g. f. i. U. D. o. H. a. H. S.-.).

Fu, Q., Grote, E., Zhu, J., Jelinek, C., Kottgen, A., Coresh, J. et Van Eyk, J. E. (2016, Jan). An Empirical Approach to Signature Peptide Choice for Selected Reaction Monitoring: Quantification of Uromodulin in Urine [Research Support, N.I.H., Extramural]. *Clin Chem*, *62*(1), 198-207. https://doi.org/10.1373/clinchem.2015.242495

Greaves, P. et Gribben, J. G. (2013, Jan 31). The role of B7 family molecules in hematologic malignancy. *Blood*, *121*(5), 734-744. https://doi.org/10.1182/blood-2012-10-385591

Guideline IHT, e. V. o. a. p. t. a. m. Q. R. I. c. o. h., Geneva, Switzerland; 2005.).

Hock, B. D., O'Donnell, J. L., Taylor, K., Steinkasserer, A., McKenzie, J. L., Rothwell, A. G. et Summers, K. L. (2006, Jan). Levels of the soluble forms of CD80, CD86, and CD83 are elevated in the synovial fluid of rheumatoid arthritis patients [Research Support, Non-U.S. Gov't]. *Tissue Antigens*, *67*(1), 57-60. https://doi.org/10.1111/j.1399-0039.2005.00524.x

Hock, B. D., Patton, W. N., Budhia, S., Mannari, D., Roberts, P. et McKenzie, J. L. (2002, May). Human plasma contains a soluble form of CD86 which is present at elevated levels in some leukaemia patients [Research Support, Non-U.S. Gov't]. *Leukemia*, *16*(5), 865-873. https://doi.org/10.1038/sj.leu.2402466

Hock, B. D., Starling, G. C., Patton, W. N., Salm, N., Bond, K., McArthur, L. T. et McKenzie, J. L. (2004, Oct). Identification of a circulating soluble form of CD80: levels in patients with hematological malignancies [Research Support, Non-U.S. Gov't]. *Leuk Lymphoma*, *45*(10), 2111-2118. https://doi.org/10.1080/10428190410001712199

Ip, W. K., Wong, C. K., Leung, T. F. et Lam, C. W. (2006, Jul). Plasma concentrations of soluble CTLA-4, CD28, CD80 and CD86 costimulatory molecules reflect disease severity of acute asthma in children. *Pediatr Pulmonol*, *41*(7), 674-682. https://doi.org/10.1002/ppul.20432

Janssens, I. et Cools, N. (2020, Dec). Regulating the regulators: Is introduction of an antigen-specific approach in regulatory T cells the next step to treat autoimmunity? *Cell Immunol*, *358*, 104236. https://doi.org/10.1016/j.cellimm.2020.104236

Kakoulidou, M., Giscombe, R., Zhao, X., Lefvert, A. K. et Wang, X. (2007, Nov). Human Soluble CD80 is generated by alternative splicing, and recombinant soluble CD80 binds to CD28 and CD152 influencing T-cell activation [Research Support, Non-U.S. Gov't]. *Scand J Immunol*, *66*(5), 529-537. https://doi.org/10.1111/j.1365-3083.2007.02009.x

Leng, J. H., Hu, Z. Y., Zhuo, G. C., Wang, K. Y., Wang, Z. W., Peng, L. et Zhang, Y. F. (2004, Jul). [The expression and significance of costimulatory molecule in peripheral blood B lymphocytes in rheumatoid arthritis]. *Zhonghua Nei Ke Za Zhi*, *43*(7), 519-521. https://www.ncbi.nlm.nih.gov/pubmed/15312407

Linsley, P. S., Greene, J. L., Brady, W., Bajorath, J., Ledbetter, J. A. et Peach, R. (1994, Dec). Human B7-1 (CD80) and B7-2 (CD86) bind with similar avidities but distinct kinetics to CD28 and CTLA-4 receptors [Comparative Study]. *Immunity*, *1*(9), 793-801. https://doi.org/10.1016/s1074-7613(94)80021-9

Maeda, A., Yamamoto, K., Yamashita, K., Asagoe, K., Nohgawa, M., Kita, K., Iwasaki, H., Ueda, T., Takahashi, A. et Sasada, M. (1998, Sep). The expression of co-stimulatory molecules and their relationship to the prognosis of human acute myeloid leukaemia: poor prognosis of B7-2-positive leukaemia. *Br J Haematol*, *102*(5), 1257-1262. https://doi.org/10.1046/j.1365-2141.1998.00901.x

Malkawi, A. K., Jafari, M., Ohlund, L., Sleno, L., Abdel Rahman, A. M. et Siaj, M. (2023, Dec 15). A diagnostic electrochemical aptasensor development for sCD80 protein detection in human serum. *Biosens Bioelectron*, *242*, 115696. https://doi.org/10.1016/j.bios.2023.115696

Oshima, S., Karrer, E. E., Paidhungat, M. M., Neighbors, M., Chapin, S. J., Fan, R. A., Reed, M. A., Wu, K., Wong, C., Chen, Y., Whitlow, M., Anderson, F. A., Bam, R. A., Zhang, Q., Larsen, B. R., Viswanathan, S., Devens, B. H., Bass, S. H. et Higashi, Y. (2016, May). ASP2408 and ASP2409, novel CTLA4-Ig variants with CD86-selective ligand binding activity and improved immunosuppressive potency, created by directed evolution. *Protein Eng Des Sel*, *29*(5), 159-167. https://doi.org/10.1093/protein/gzw002

Tector, M., Khatri, B. O., Kozinski, K., Dennert, K. et Oaks, M. K. (2009, Sep 22). Biochemical analysis of CTLA-4 immunoreactive material from human blood. *BMC Immunol*, *10*, 51. https://doi.org/10.1186/1471-2172-10-51

Thompson, C. B. (1995, Jun 30). Distinct roles for the costimulatory ligands B7-1 and B7-2 in T helper cell differentiation? [Review]. *Cell*, *81*(7), 979-982. https://doi.org/10.1016/s0092-8674(05)80001-7

Uvebrant, K., da Graca Thrige, D., Rosen, A., Akesson, M., Berg, H., Walse, B. et Bjork, P. (2007, Jun). Discovery of selective small-molecule CD80 inhibitors [Validation Study]. *J Biomol Screen*, *12*(4), 464-472. https://doi.org/10.1177/1087057107300464

Wan, B., Nie, H., Liu, A., Feng, G., He, D., Xu, R., Zhang, Q., Dong, C. et Zhang, J. Z. (2006, Dec 15). Aberrant regulation of synovial T cell activation by soluble costimulatory molecules in rheumatoid arthritis. *J Immunol*, *177*(12), 8844-8850. https://doi.org/10.4049/jimmunol.177.12.8844

Weisman, M. H., Durez, P., Hallegua, D., Aranda, R., Becker, J. C., Nuamah, I., Vratsanos, G., Zhou, Y. et Moreland, L. W. (2006, Nov). Reduction of inflammatory biomarker response by abatacept in treatment of rheumatoid arthritis [Clinical Trial, Phase II Multicenter Study Randomized Controlled Trial Research Support, Non-U.S. Gov't]. *J Rheumatol*, *33*(11), 2162-2166. https://www.ncbi.nlm.nih.gov/pubmed/17014006

Wong, C. K., Lit, L. C., Tam, L. S., Li, E. K. et Lam, C. W. (2005, Aug). Aberrant production of soluble costimulatory molecules CTLA-4, CD28, CD80 and CD86 in patients with systemic lupus erythematosus. *Rheumatology (Oxford)*, *44*(8), 989-994. https://doi.org/10.1093/rheumatology/keh663

Xiao, Z. X., Olsen, N. et Zheng, S. G. (2019, Apr). The essential role of costimulatory molecules in systemic lupus erythematosus. *Lupus*, *28*(5), 575-582. https://doi.org/10.1177/0961203319829818

Xu, Z., Juan, V., Ivanov, A., Ma, Z., Polakoff, D., Powers, D. B., Dubridge, R. B., Wilson, K. et Akamatsu, Y. (2012, Nov 1). Affinity and cross-reactivity engineering of CTLA4-Ig to modulate T cell costimulation. *J Immunol*, *189*(9), 4470-4477. https://doi.org/10.4049/jimmunol.1201813

Zhang, Y., van Haren, M. J., Marechal, N., Troffer-Charlier, N., Cura, V., Cavarelli, J. et Martin, N. I. (2022, May 17). A Direct Assay for Measuring the Activity and Inhibition of Coactivator-Associated Arginine Methyltransferase 1. *Biochemistry*, *61*(11), 1055-1063. https://doi.org/10.1021/acs.biochem.2c00075

CHAPTER 5

CONCLUSION AND FUTURE PERSPECTIVES

The costimulatory pathway CD28-B7 plays a crucial role in maintaining immune tolerance and preventing the development of autoimmunity. During autoimmunity, the dysregulation of this pathway can lead to a pathogenic T-cell activation against self-antigens. Given its central role in regulating the immune response, the CD28-B7 pathway has been considered a potential therapeutic target for autoimmune diseases. Additionally, the costimulatory proteins CD80, CD86, CTLA-4, and CD28 are involved in the pathogenesis of different autoimmune diseases. The tissue expression or the level of the soluble isoforms of these molecules were found to be influenced by autoimmunity and considered as potential biomarkers in different autoimmune diseases.

In this project, we hypothesize that developing an accurate, precise, and sensitive bioanalytical method using the gold-standard technique (Mass spectrometry) for the quantification of the panel of the costimulatory molecules CD80, CD86, CTLA-4, and CD28 in soluble isoform in human plasma or serum will help confirm the role of these molecules as biomarkers for autoimmune disease, Rheumatoid arthritis. Additionally, confirming the transition of this method to clinical practice using an aptasensor will facilitate its diagnostic and therapeutic application, supported by the selection of specific aptamers for the costimulatory proteins.

From this perspective, in this thesis, we targeted Rheumatoid Arthritis (RA) as an autoimmune disease model for diagnostics methods and therapeutic evaluation tool developments. Due to the lack of confirmed studies validating the co-stimulatory proteins as RA biomarkers, we conducted a well-designed study in a patient and healthy control cohort (Chapter 2). This study used a targeted proteomics approach, where an (MRM) LC-MS/MS method was developed at clinical grade for measuring these proteins in human plasma samples. One validated biomarker, sCD80, was taken forward for diagnostics aptasensor development in human serum (Chapter 3). Multiple aptamers

were selected with great affinity to sCD80 Proteins during the sensor development using SELEX. Chapter 4 introduced an (MRM) LC-MS/MS method for evaluating any inhibitor for this pathway, such as the Abatacept. This method will test all the selected aptamers in this project as potential inhibitors for the costimulatory pathway.

This research aims to advance the field by developing novel analytical methods for detecting and quantifying these costimulatory molecules, providing the scientific and medical communities with more robust, efficient, and clinically applicable methods. The overarching goal is to overcome existing limitations in current analytical techniques and contribute to refining methods used to study these critical immune system regulators. The CD28-B7 costimulatory pathway represents a promising therapeutic target due to its central role in immune regulation. Targeted interventions in this pathway can modulate immune responses precisely and tailor them, making it a focal point for therapeutic advancements in autoimmune diseases. Thus, developing a competitive assay to study potential targeted therapies is another goal of this thesis.

First, an accurate and precise (MRM) LC-MS/MS method was developed and validated for the absolute quantification of the four costimulatory molecules: sCD80, sCD86, sCTLA-4, and sCD28 based on surrogate selected signature peptides. In this cohort study on RA patients, we examined the plasma level of these molecules compared to a control group. The significant elevation of sCD80, sCD86, and sCTLA-4 in RA plasma makes them potential diagnostic biomarkers, which allows for a comprehensive understanding of the role of the costimulatory molecules and potentially influencing future diagnostic and treatment approaches for RA. This advanced analytical technique offers high sensitivity, specificity, and precision, making it suitable for accurately measuring biomarkers in various biological samples. Its ability to simultaneously monitor multiple target proteins with exceptional accuracy positions (MRM) LC-MS/MS as a promising method for routine diagnostics and biomarker quantification. (MRM) LC-MS/MS's ability to provide quantitative measurements facilitates the reliable tracking of biomarker concentrations over time. This is essential for understanding disease progression, assessing

treatment responses, and monitoring overall patient health. (MRM) LC-MS/MS bridges the gap between research and clinical applications, promoting translational research. Its adoption in routine testing could facilitate the seamless integration of cutting-edge biomarker discoveries into everyday clinical practice. As technological advancements continue and standardization efforts progress, MRM LC-MS/MS is expected to contribute significantly to advancing personalized medicine and integrating biomarker-based approaches into routine clinical diagnostics.

Second, Biosensors play a crucial role in biomarker discovery and disease diagnosis, serving as a valuable alternative or complementary method to techniques like (MRM) LC-MS/MS or ELISA. These sensors are adept at detecting specific molecules, offering several advantages in sensitivity, speed, and simplicity. Taking the advantages of aptamer, the small size, chemically synthesized, and the specific binding to the target molecule as a recognition element in the biosensor, we developed a specific and sensitive label-free electrochemical aptasensor for one of the four costimulatory molecules, sCD80. The developed aptasensor has sensitivity and specificity comparable to some commercially available ELIZA kits for sCD80 in human serum, which assures the significant potential of this aptasensor as a diagnostic tool for autoimmune disorders, especially in RA. This Aptasensor was constructed by selecting a high-affinity aptamer (Kd 47.69 nM) using SELEX. As a future step, integrating the developed aptasensor in clinical use must establish the cut-off value for the protein in patients' serum and healthy control by applying the sensor on a large cohort. Enhancing the sensitivity of the aptasensor by using different platforms, such as labeled platforms and gold nanoparticles, is another goal for the future.

The future development of aptasensors targeting the other costimulatory molecules, sCD86 and CTLA-4, represents a promising step in the evolution of diagnostic tools, particularly for autoimmune diseases. Our research group has already selected a specific ssDNA aptamer for sCD86.

The comparison with the established gold-standard method (MRM) LC-MS/MS will be crucial to assess their accuracy and reliability. If successful, aptasensors have the potential to reshape how we measure immune-related biomarkers, offering a balance between precision and accessibility in the realm of diagnostic tools.

Third, targeting the CD28-B7 costimulatory pathway is a promising autoimmune disease therapy strategy. CTLA4-Ig (Abatacept TM) is an FDA-approved drug for RA that binds to CD80/CD86 and prevents their interaction with CD28. This targeted therapy specifically targets the T-cell and modulate the immune response. For an understanding of this pathway and to design an assay that can be useful to study another potential therapeutic agent that specifically can block this costimulatory pathway mimicking Abatacept in the mechanism of action, we developed and validated an accurate (MRM) LC-MS/MS method for detection and quantification of a panel of the four costimulatory proteins, sCD80, sCD86, sCTLA-4, and sCD28. The developed method was successfully applied to assay the inhibitory effect of AbataceptTM on the CD28-B7 pathway.

This assay's high throughput will allow us to study different potential costimulatory pathway inhibitors. As a future step, our lab will evaluate the inhibitory effect of selected aptamers for sCD80 and sCD86 using the developed inhibitory assay. If successful, a cell line and in vivo study will be performed using AbataceptTM and the selected aptamers.

In summary, combining various analytical methods to investigate biomarkers is a potent and thorough approach to medical research and crafting targeted disease therapies. By merging different techniques, such as mass spectrometry, immunoassays, biosensors, and molecular imaging, scientists and healthcare professionals can gain many insights into the complex molecular terrain linked to diseases.

APPENDIX A

SUPPLEMENTARY INFORMATION FOR "QUANTITATIVE ANALYSIS OF SOLUBLE COSTIMULATORY MOLECULES AS POTENTIAL DIAGNOSTIC BIOMARKERS FOR RHEUMATOID ARTHRITIS USING LC-MS/MS IN MRM MODE"

Abeer K. Malkawi[1], Refat M. Nimer[2], Maha Almogren[3], Afshan Masood[1], Abdulrahman S. Alarfaj[5], Hicham Benabdelkamel[4], Anas M. Abdel Rahman[3,6,7*], Mohamed Siaj[1*]

[1]Department of Chemistry, University of Quebec at Montreal, Montreal, QC H3C3P8, Canada

[2] Department of Medical Laboratory Sciences, Jordan University of Science and Technology, Irbid 22110, Jordan

[3]Metabolomics Section, Department of Clinical Genomics, Center for Genomics Medicine, King Faisal Specialist Hospital and Research Centre (KFSHRC), Riyadh 11211, Saudi Arabia

[4]Proteomics Resource Unit, Obesity Research Center, College of Medicine, King Saud University, P.O. Box 2925 (98), Riyadh 11461, Saudi Arabia

[5] Department of Medicine, Rheumatology Unit, College of Medicine, King Saud University, Riyadh, Saudi Arabia

[6]Department of Biochemistry and Molecular Medicine, College of Medicine, Al Faisal University, Riyadh, Saudi Arabia

[7]Department of Chemistry, Memorial University of Newfoundland, St. John's, NL, A1C 5S7, Canada

Clinica Chimica Acta 548 (2023) 117501, DOI: 10.1016/j.cca.2023.117501

* Co-correspondence:

Prof. Mohamed Siaj (siaj.mohamed@uqam.ca)
Dr. Anas Abdel Rahman (aabdelrahman46@kfshrc.edu.sa)

Table A.1. List of the triple quadrupole method's conditions for each protein's signature peptide. The qualitative (Qual) and quantitative (Quan) transitions list each signature peptide and its labeled internal standard, including the instrumental conditions. The underlined amino acids were labeled with 13C and 15N.

Uniprot ID	Protein name (KDa)	Signature peptide	Amino acid sequence	Molecular weight (g/mol)	Precursor ion (m/z) (z)	Product ion (m/z)	Ion Type (z)	Cone voltage (V)	Collision energy (V)	Retention time (min)	Ion function
P10747	CD28 (42)	CD 28-1	K.^{26}YSYNLFSR^{34}.E	1049.13	525.49 (+2)	799.34	Y6 (+1)	32	15	4.3	Quan
						636.26	Y5 (+1)		20		Qual
		CD 28-1 (IS)	K.^{26}YSYNLFS<u>R</u>^{34}.E	1059.13	530.42 (+2)	809.30	Y6 (+1)	32	15		Quan
						646.28	Y5 (+1)		20		Qual
P33681	CD80 (25)	CD 80-2	R.^{95}EHLAEVTLSVK^{105}.A	1225.20	409.41 (+3)	267.07	B2 (+1)	30	25	3.8	Qual
									20		
						146.99	Y1 (+1)				Quan
		CD 80-2 (IS)	R.^{95}EHLAEVTLSV<u>K</u>^{105}.A	1233.39	412.03 (+3)	267.07	B2 (+1)	30	25		Quan
											Qual
						155.03	Y1 (+1)				Quan
P42081	CD86 (26)	CD 86-1	R.^{74}LHNLQIK^{80}.D	864.90	289.42 (+3)	251.13	B2 (+1)	26	15	2.88	Quan
						129.96	Y2 (+2)		20		Qual

Uniprot ID	Protein name (KDa)	Signature peptide	Amino acid sequence	Molecular weight (g/mol)	Precursor ion (m/z) (z)	Product ion (m/z)	Ion Type (z)	Cone voltage (V)	Collision energy (V)	Retention time (min)	Ion function
		CD 86-1 (IS)	R.[74]LHNLQIK[80].D	873.03	291.96 (+3)	251.11	B2 (+1)	26	15		
											Quan
						136.01	Y2 (+2)		20		Qual
P16410	CTLA4 (15)	CTLA 4-2	R.[16]GIASFVCEYASPGK[29].A	1428.40	743.35 (+2)	301.07	Y3 (+1)	27	35	5.15	Quan
						388.17	Y4 (+1)				
									20		Qual
		CTLA 4-2 (IS)	R.[16]GIASFVCEYASPGK[29].A	1436.75	747.35 (+2)	309.07	Y3 (+1)	27	20		Quan
						396.17	Y4 (+1)				
											Qual

Table A. 2. Summary of linearity and sensitivity (average of over three days). LOQ: Limit of Quantification

Protein	**Slope (*n* = 3)**	**Intercept (*n* = 3)**	**R^2 (*n* = 3)**	**LOQ (*n* = 6)**		
				nM	**Interday Accuracy (%)**	**Interday precision (%)**
sCD28	0.0130	-0.0070	0.9998	0.5	93.1	6.0
sCD80	0.0227	-0.0260	0.9998	0.5	101.2	7.3
sCD86	0.4921	0.3151	0.9989	0.5	102.3	8.2
sCTLA4	0.0139	-0.5247	0.9997	1.0	89.0	12.3

Table A.3.. Inter- and intra-day validation summary. SD: Standard Deviation, SP: Signature Peptide.

Protein	Mean (*n* =18)			SD (*n* = 18)			Accuracy (%)						Precision (%)					
							Intra-day (*n* = 6)			Inter-day (*n* = 18)			Intra-day (*n* = 6)			Inter-day (*n* = 18)		
	1.5	35.0	75.0	1.5	35.0	75.0	1.5	35.0	75.0	1.5	35.0	75.0	1.5	35.0	75.0	1.5	35.0	75.0
sCD28	1.64	35.47	71.74	0.10	2.55	5.86	111.43	97.39	95.07	109.15	101.33	95.66	11.43	3.95	8.53	10.26	5.70	7.49
sCD80	1.52	35.24	79.16	0.29	2.55	5.86	105.43	99.91	105.50	101.34	100.69	105.55	5.43	4.89	5.50	9.97	5.53	7.30
sCD86	1.48	35.24	73.67	0.16	2.90	6.33	91.57	98.49	96.25	98.36	100.69	98.22	9.43	6.90	8.26	7.67	7.15	7.10
sCTLA4	1.52	35.50	73.48	0.11	2.38	5.76	105.47	100.88	104.06	101.51	101.42	97.97	5.47	6.57	5.15	5.51	5.62	6.26

Table A.4. Summary of peptides stability at different storage conditions for a determined period. SP: Signature Peptide, QC: Quality Control, RT: Room Temperature.

Protein	QC (nM)	Stability (%)							
		Fresh (-80 °C)		RT (24 h)		4°C (1 Week)		–20 °C (1 Month)	
		Mean%	SD	Mean%	SD	Mean%	SD	Mean%	SD
sCD28	1.5	100.0	13.6	97.8	6.5	91.0	7.0	101.2	7.4
	35	100.0	4.7	102.7	1.7	81.3	13.5	100.5	3.3
	75	100.0	6.8	100.5	3.0	105.7	4.1	104.9	2.0
sCD80	1.5	100.0	2.7	89.0	6.0	92.4	8.3	96.9	15.2
	35	100.0	13.2	107.9	9.8	115.6	2.8	90.2	15.1
	75	100.0	9.6	91.6	7.6	87.0	13.8	90.2	1.1
sCD86	1.5	100.0	7.4	99.3	1.6	101.7	9.2	114.6	5.0
	35	100.0	9.4	111.2	12.2	94.5	18.9	113.0	15.9
	75	100.0	5.4	78.5	5.6	104.3	13.7	98.9	2.4
sCTLA4	1.5	100.0	10.9	99.0	0.6	105.9	6.9	105.2	4.0
	35	100.0	5.0	99.0	5.1	76.5	17.8	99.1	2.8

Protein	QC (nM)	Stability (%)							
		Fresh (-80 °C)		RT (24 h)		4°C (1 Week)		–20 °C (1 Month)	
		Mean%	SD	Mean%	SD	Mean%	SD	Mean%	SD
	75	100.0	3.1	76.7	2.2	86.3	19.9	96.5	7.0

APPENDIX B

SUPPLEMENTARY INFORMATION FOR "A DIAGNOSTIC ELECTROCHEMICAL APTASENSOR DEVELOPMENT FOR CD80 PROTEIN DETECTION IN HUMAN SERUM"

Abeer K. Malkawi[a], Maziar Jafari[a], Leanne Ohlund[a], Lekha Sleno[a], Anas M. Abdelrahman[b,c,d], Mohamed Siaj

[a] Department of Chemistry, Université du Québec à Montréal, Montreal, QC, H3C 3P8, Canada

[b] Metabolomics Section, Department of Clinical Genomics, Center for Genome Medicine, King Faisal Specialist Hospital and Research Centre (KFSHRC), Riyadh, Saudi Arabia

[c] Department of Biochemistry and Molecular Medicine, College of Medicine, Alfaisal University, Riyadh, 11350, Saudi Arabia

[d] Department of Chemistry, Memorial University of Newfoundland, St. John's, A1C 5S7, NL, Canada

Biosens Bioelectron. 2023 Dec 15:242:115696. DOI: 10.1016/j.bios.2023.115696

* Correspondence:
Professor Mohamed Siaj,
Email: siaj.mohamed@uqam.ca

B.1. Reagents and chemicals:

The ssDNA library, primers for polymerase chain reaction (PCR), the selected 4 aptamers sequences modified by FITC, 5′-Thiol C6 S–S modified CD80-4 and CD80-16 aptamer sequences were custom-synthesized by Integrated DNA Technologies Inc (Coralville, IA, USA). HisPur™ Ni-NTA Resin was obtained from Thermofisher Scientific Inc (Saint-Laurent, QC, Canada). *Taq* DNA polymerase, *Taq* PLUS DNA polymerase, and dNTPs for PCR, acrylamide/bisacrylamide (40% solution), Tetramethylethylenediamine (TEMED), and ammonium persulfate (APS) to prepare the polyacrylamide gel electrophoresis (PAGE), urea, tris-base, formamide, sodium chloride (NaCl), boric acid, EDTA disodium dihydrate, ethanol were purchased from Bishop Inc (Burlington, ON, Canada). Phosphate-buffered saline pH 7.4 (PBS), potassium ferrocyanide ($K_4Fe(CN)_6$), potassium ferricyanide ($K_3Fe(CN)_6$), magnesium chloride ($MgCl_2$), sodium azide (NaN_3), hydrochloric acid (HCl), potassium hydroxide (KOH), imidazole, agarose, Trypsin, Nuclease-free water, and hydrogen peroxide (H_2O_2) were purchased from Sigma (Oakville, ON, Canada). The extracellular part of the human B7-1/CD80 His-tag Carrier-Free Recombinant Protein (sCD80) and sCD86 were purchased from R&D systems (Toronto, ON, Canada). sCTLA-4 recombinant human protein was obtained from Thermofisher scientific (Saint-Laurent, QC, Canada). TOPO TA cloning kit with One Shot MAX Efficiency DH5α-T1 *E. coli* was purchased from Invitrogen (Burlington, ON, Canada). DNA purification kit QIA quick PCR was purchased from Qiagen (Toronto, ON, Canada). Amicon Ultra-0.5 mL centrifugal desalting filters with a 3 kDa molecular cut-off were obtained from Fischer Scientific (Ottawa, ON, Canada). Solid phase extraction cartridges (Oasis HLB-SPE) were purchased from Waters Corporation (Milford, MA, United States). Centrifuge tube filters with a cellulose acetate membrane with a pore size of 0.45 μm were purchased from Corning life sciences (Tewksbury, MA, USA).

B.2. Immobilization of sCD80 on NTA-Ni agarose beads

HisPur Ni-NTA 6% cross-linked agarose beads, with a diameter range between 45 to 165 μm, were used for sCD80 protein immobilization. In detail, 50 μL of bead resin was equilibrated with 100 μL buffer (10 mM imidazole in PBS) and incubated with 6His-tagged recombinant sCD80 protein

(8 μM) on an End-Over-End rotator for 4 hours at 4 ºC. The coupled beads were washed three times with two resin-bed volumes of washing buffer (25 mM imidazole in PBS) to remove the non-specific binding. The coupled beads were stored in a buffer (0.05% sodium azide in PBS) at 4 ºC until further use.

B.3. Bead-protein coupling confirmation using high-resolution mass spectrometry

The bound proteins (from 100 μL coupled beads) were on-bead digested using trypsin (2 μg) for four hours at 37°C, following an initial step of reduction and alkylation of disulfide bonds using dithranol and iodoacetamide (IAM) (each incubated for 30 min at 37°C, the reaction with IAM being kept in the dark). The resulting peptide digests were subsequently cleaned up using solid-phase extraction on Waters OASIS HLB cartridges (1 cc, 30 mg), with methanol elution. The tryptic peptides were separated using reversed-phase chromatography on a Shimadzu Nexera HPLC (Shimadzu Scientific Instruments, Inc., Columbia, MD, USA) equipped with a Phenomenex Aeris Peptide XB-C18 100 × 2.1 mm, 1.7 μm column at 40 ºC. The mobile phases used were A: 0.1% formic acid in water and B: 0.1% formic acid in acetonitrile, using a gradient as follows: 0-2.5 min held at 5% B, followed by a linear increase to 30% B at 50 min, up to 50% B at 55 min, and 90% B at 56 min held until 60 min. HRMS/MS analysis was performed using a Sciex TripleTOF 5600 instrument (Framingham, MA, USA), where the peptides were positively ionized using an ESI (electrospray ionization) source. The ion source temperature was at 500°C, and the ion spray voltage was 5000 V. Product ion spectra were generated at 30 V collision-offset voltage in information-dependent (IDA) mode. The precursor ion scan was ranging 140-1250 m/z, while the product ion scan was from 80-1500 m/z. Only the top 15 ions per cycle (1.05 s) were selected for MS/MS. Protein identification was achieved using Protein Pilot software (Sciex, v5.0.3), and CD80 peptides with at least 99% confidence were sequenced, within mass accuracy of precursor ions of 5 ppm. Most sensitive peptides were chosen for quantitative analysis to estimated the amount of protein-coupled on beads by comparing the standard CD80 protein at a concentration mimicking 100% coupling efficiency amount.

B.4. Polymerase chain reaction (PCR):

The forward primer used is labelled with fluorescein 5′-Flu- FWD (fluorescein-5′-ATATCATATGCTCCAATT-3′), while the reverse primer has a poly-A (20 consecutive adenine extensions) and one internal spacer of 18-carbon atoms, Hexaethylenglycol (HEGL) (5′-poly(dA_{20})-HEGL-ATATTACACTTGCGATCT-3′).

PCR amplified the extracted ssDNA pool in 19 parallel reactions with a final volume of 60 µL for each reaction. Each reaction contained a final concentration of 1× Taq buffer, 2 mM $MgCl_2$, 200 µM of dNTP mixture, 400 nM of each primer, and 4U of Taq DNA polymerase enzyme (Bioshop, Burlington, ON, Canada). Thermocycling was carried out on a T100 thermocycler (BIO-RAD, Mississauga, Ontario, Canada) using the following profiles: initial denaturing at 94°C for 3 min, then 26 cycles of (94 °C for 1 min, 47°C for 1 min, 72°C for 1 min), final extension at 72°C for 10 min, and infinite hold at 4°C.

To amplify the cultured clones, M13 primers; FWD- 5′GTAAAACGACGGCCAG3′ and REV-5′CAGGAAACAGCTATGAC3′ were used in PCR using the same concentrations that were used in the previous protocol for 50 µL final volume. The thermocycler was run as the following: initial denaturing at 94°C for 10 min, then 26 cycles of (94°C for 1 min, 55°C for 1 min, 72ºC for 1 min), final extension at 72°C for 10 min, and infinite hold at 4°C.

B.5.12% polyacrylamide gel (PAGE) and DNA extraction from the gel

8 mg of urea was dissolved in 3.5 mL water, 3.75 mL of 5× Tris/Borate/EDTA (TBE) buffer, and 6.0 mL of 40% acrylamide/bisacrylamide for 15 minutes at 45°C. 10% ammonium persulphate (113 µL) and 8.5 µL of tetramethylethylenediamine (TEMED) were added at RT to initiate polymerization. The mixture was polymerized in a 1.5 mm glass plate in the gel caster (BIO-RAD, Mississauga, Ontario, Canada).

Before the sample loading into the gel, each four PCR reactions were combined in one tube and lyophilized using speed-vac, then reconstituted in 40 µL formamide and 10 µL water and heated at 90°C for five minutes. 60 µL of the reconstituted PCR product was loaded in each well of the

gel. The gel was run in a vertical midi-format electrophoresis cell in the presence of 1× TBE buffer at 120 V for 3 hours using an electrophoresis power supply (BIO-RAD, Mississauga, Ontario, Canada).

The desired gel bands that appeared at 100 pb were excised and soaked in 3 mL of 1× Tris/ EDTA (TE) buffer to extract the DNA. Subsequently, the soaked bands were incubated at -80°C for 10 minutes, then at 50°C for 5 min, and finally at 90°C for another 5 minutes before being incubated at 37°C overnight. The extracted DNA was concentrated and desalted by ultrafiltration membrane centrifugal filters with a 3 kDa cut-off and then quantified by UV-VIS (Nanodrop ™2000/2000c, Thermo Scientific, Wilmington, DE, USA)) and the recovery from each cycle was recorded as fluorescence (Nanodrop 3300).

B.6. Cloning, sequencing, and alignment:

In the last round of SELEX, when the specific aptamers were enriched, the ssDNA pool was amplified by PCR using unlabeled primers (FWD 5′- ATATCATATGCTCCAATT-3′, and REV 5′-ATATTACACTTGCGATCT-3′). The amplified DNA was ligated in the pCR2.1-TOPO vector using the TOPO TA Cloning Kit. The ligated DNA was transformed into the E-coli component cells through the heat-shock approach and incubated (1 hr, 37ºC) in Soc media, and then the cells were grown on Lura Broth (LB) agar media. The positive colonies (white) were picked and grown in liquid LB media (overnight, 37ºC) with mild shaking. The clones were amplified by PCR (supplementary file, section 1.1) using forward and reverse M13 primers sites within the pCR2.1 TOPO TA vector of 3.9 kb in a 50 µL total PCR reaction. As described elsewhere, the DNA insertion into the plasmid was confirmed by 2% agarose gel electrophoresis. (Lee, 2012) The PCR product was sent for DNA sequencing to the Génome Québec Center of Expertise and Services (Montreal, QC, Canada). After collecting the DNA sequencing data, the aptamer-associated data were grouped according to the similarity using PRofile ALIgNEment (PRALINE) multiple sequence alignment software (Vrije University, Amsterdam). Each group's representative sequence was selected and individually evaluated for binding affinity.

B.7. Binding assays and dissociation constant (K_d) determination

Fluorescent labeling of the selected aptamers (5'-FITC-Aptamer) in binding buffer with a wide range of concentrations (0-300 nM) was heated at 90ºC for 10 minutes, 4ºC for 5 minutes and then kept at RT for another 5 minutes before incubating with 5 µL of sCD80-conjugated beads for 2 hr at RT. The beads were washed to remove the unbound aptamers. The bound aptamers were eluted by elution buffer, and the fluorescence signal was recorded (excitation (Ex) at 470 ±10 nm and emission (Em) at 515 nm) using Nanodrop 3300 (Thermo Scientific, Wilmington, DE, USA). The K_d value was depicted to construct the binding curve using non-linear regression.

B.8. Aptamer concentration and protein incubation time optimization

To optimize the aptamer concentration, cleaned AuSPEs were incubated with different concentrations (0.5, 1.5, 5, 10 µM) of disulfide-labeled aptamer for 8 h at 4°C. Before immobilization, ssDNA aptamer solution in binding buffer was heated at 90°C, then cooling on ice, followed by standing at RT for 5 min. The treated ssDNA was then drop-cast (10 µL) on the electrode surface. After the self-assembled monolayer formation, the electrode surface was rinsed with binding buffer, and the *R*ct was measured before and after modification by EIS. The impedimetric measurements were done in the presence of 5 mM $[Fe(CN)_6]^{3-/4-}$] PBS. Δ*R*ct reflected the density of the aptamer probe packed on the surface of the electrode.

Optimizing sCD80 incubation time with the probe reflects the time window required for sCD80 detection. Accordingly, 10 nM of sCD80 in binding buffer was incubated with the sensor probe at RT with different incubation times (10, 20, 30, 40, and 60 min). The response was recorded as Δ*R*ct, as the impedimetric measurements were done in the presence of 5 mM $[Fe(CN)_6]^{3-/4-}$] in PBS.

B.9. Atomic force microscopy (AFM) and photo-induced force microscopy

Atomic force microscopy (AFM) and photo-induced force microscopy (PiFM) characterization were done on the screen-printed electrode (SPE) samples' bare and conditioned surfaces with the

VistaScope scanning probe microscope (SPM) (MolecularVista Inc., San-José, CA, USA) operating with the VistaScan v3.0 software. The microscopy setup was analogous to previously reported work. (Abrego-Martinez, Jafari et al. 2022) Bare AuSPE, AuSPE-DNA aptamer, and AuSPE-DNA aptamer-sCD80 protein were held onto circular 12 mm diameter magnetic sample holders via double-sided carbon tape of the same radius. A ~20 nm lateral resolution Au-coated silicon nitride (Si3N4) probe tip (fabricated by NanosensorsTM, Neuchatel, Switzerland, cleaned and sold by MolecularVista Inc.) was utilized for producing the AFM topography and PiFM chemical mapping images. (Nowak, 2016) Scan frames of 10 μm × 10 μm and 1 μm × 1 μm were generated by slowly scanning the sample surface at 0.1 lines/s to avoid tip damage during the measurements. Scans were done in non-contact (NC) mode at 85 % setpoint with a 1 nm drive amplitude (dither). The resolution of the images was 256 × 256 pixels. Photo-induced force infrared (PiF-IR) spectra were recorded on the 10 μm × 10 μm scan frames in the mid-infrared range between 770 – 1910 cm-1 using a quantum cascade laser (QCL) (Block Engineering, Southborough, MA, USA) powered at the baseline laser power profile of 5.85 %, dissipating several 100 μW distributed in an elliptical laser spot size of ~λ × ~1.5λ. Every spectrum was recorded in 20 seconds with a resolution bandwidth (RBW) of 0.5 cm-1. The characteristic wavenumbers of the signal peaks detected on the acquired spectra of each sample were chosen for obtaining PiFM chemical mapping images on the 1 μm × 1 μm topography scan frames. The scan rate and pixel resolution of the PiFM image acquisitions were identical to those configured for the topography measurements. The laser power intensity was reduced to 1 % to minimize sample irradiation overexposure. SPM image data treatment and roughness analyses were done with the open-access software WSxM. (Horcas, Fernández et al. 2007)

B.10. Enzyme-linked immunosorbent assay

Ready-to-use plate strips pre-coated with anti-tag mAB (Abcam, Toronto, CA) was incubated with 50 μL of the prepared samples (0.2nM of CD80, CD86, and CTLA-4) in the sample diluent, followed by 50 μL of antibody cocktail (capture and detector antibody in antibody diluent) for 1h at RT on a plate shaker set to 400rpm. After discarding the content from each well, the plate was washed with 350 μL of 1X wash buffer PT three times before removing the excess liquid from

each well. The plate was then developed using TMB development solution (100 µL, at RT in the dark for 10 minutes, 400rpm). the reaction was stopped by 100 µL of prepared TMB Stop Solution, and the absorbance was recorded at 450 nm (Tecan infinite M1000 Pro Microplate reader). Each sample was prepared in triplicates, where the concentration of the samples was determined by interpolating the blank control subtracted absorbance values against the standard curve.

Peptide	*m/z* (+3)	RT (min)	Peak area (std)	Peak area (beads)	Ratio
EHLAEVTLSVK	409.2311	18.5	1.97E+06	1.36E+06	0.69
ADFPTPSISDFEIPTSNIR	703.0162	40.55	2.35E+06	1.50E+06	0.64

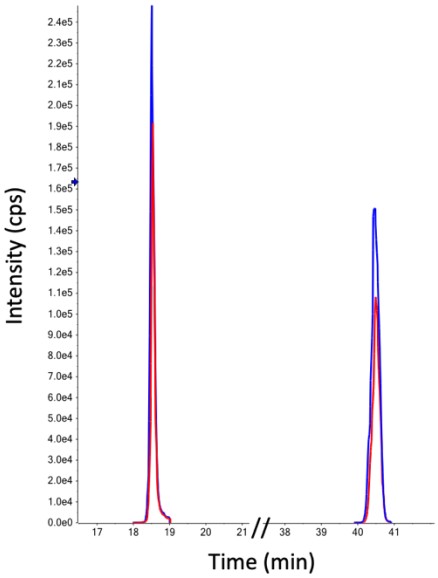

MGHTRRQGTSPSKCPYLNFFQLLVLAGLSHFCSGVIHVTKEVKEVATLS
CGHNVSVEELAQTRIYWQKEKKMVLTMMSGDMNIWPEYKNRTIFDIT
NNLSIVILALRPSDEGTYECVVLKYEKDAFKREHLAEVTLSVKADFPTPS
ISDFEIPTSNIRRIICSTSGGFPEPHLSWLENGEELNAINTTVSQDPETELYA
VSSKLDFNMTTNHSFMCLIKYGHLRVNQTFNWNTTKQEHFPDNLLPSW
AITLISVNGIFVICCLTYCFAPRCRERRRNERLRRESVRPV

Figure B.1. sCD80-beads binding confirmation using LC-HRMS. Extracted ion chromatogram (XIC) for the two highly abundant tryptic peptides, which are ^{95}EHLAEVTLSVK^{105} (left), and ^{106}ADFPTPSISDFEIPTSNIR^{124} (right). The binding efficiency was evaluated using the peak area ratio between the standard solution (blue) and coupled beads (red). The peak area and the peak area ratio for each peptide are shown in the table in the right. The sequence coverage is shown in green

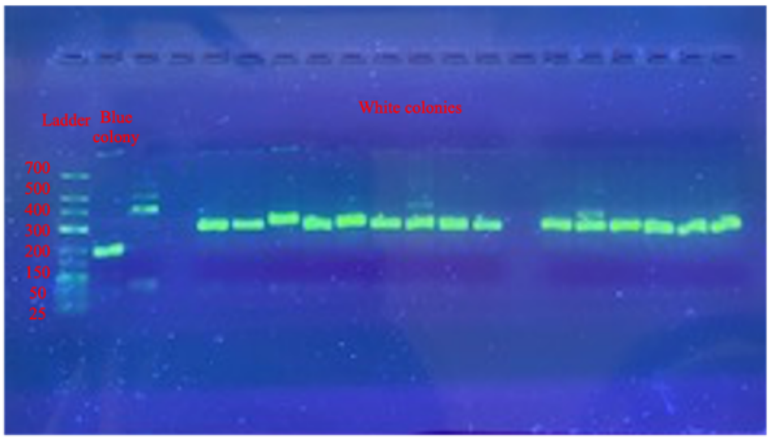

Figure B.2: Agarose gel image confirms the amplification of the ssDNA sequence in the plasmid region by M13 PCR. A band from each sequence appeared at 318 pb**.**

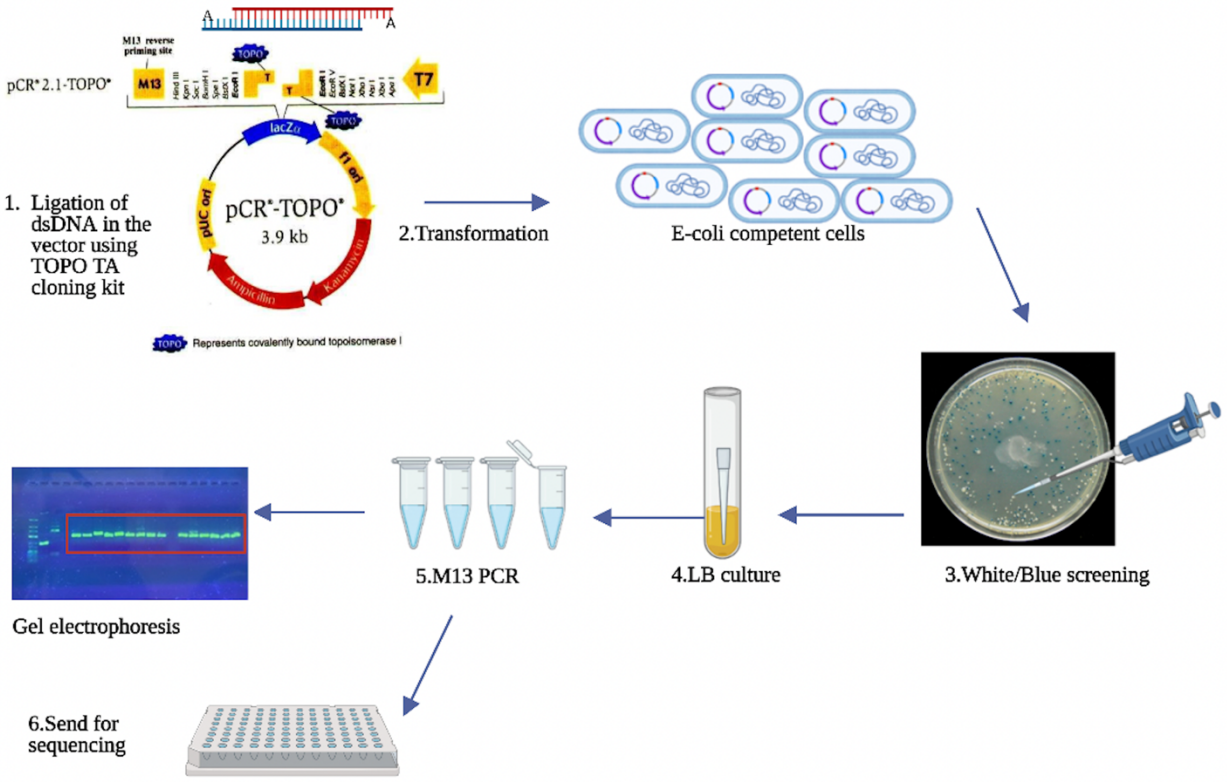

Scheme B.1*.General diagram of cloning using pCR2.1 TOPO vector*

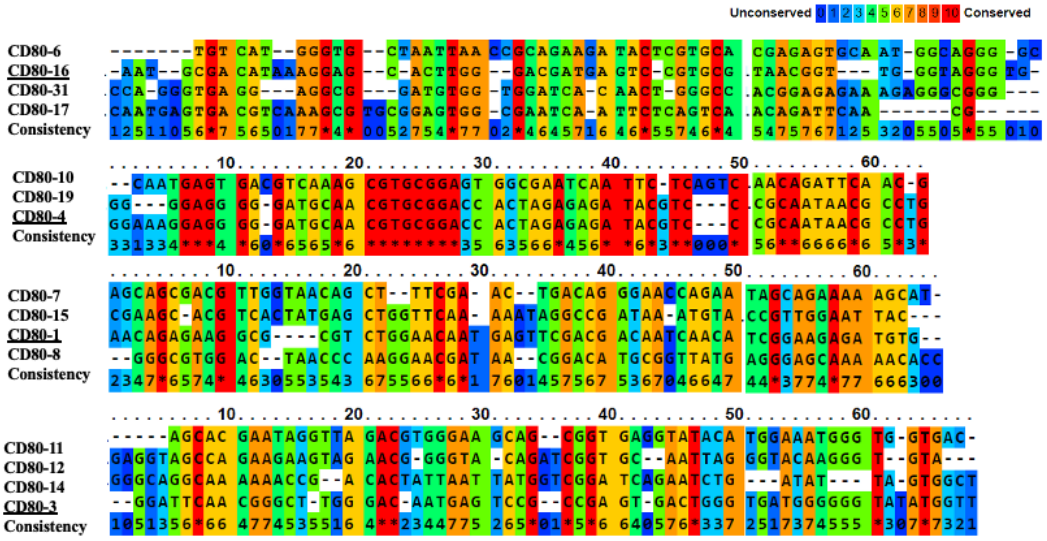

Figure B.3. sCD80 specific ssDNA aptamer sequences alignment. Fifteen sequences were aligned in four groups, and a representative aptamer from each group was chosen for the K_d study.

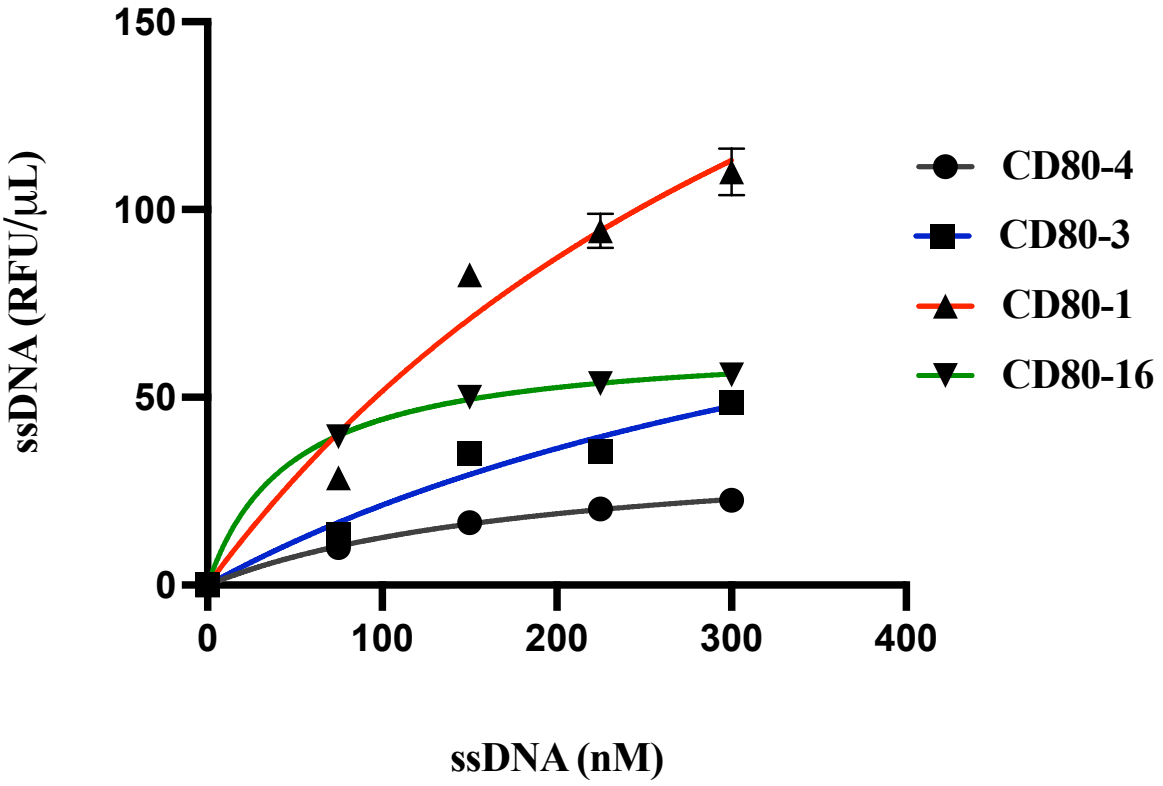

Figure B.4. Binding affinity assay between the selected ssDNA aptamers and sCD80 using fluorescence assay. The saturation curves were generated by plotting the fluorescence of ssDNA aptamers-sCD80 complex as a function of unbound ssDNA aptamers. K_d values were determined by nonlinear regression fitting. The error bars represent the SD of 3 replicates at each concentration.

Table B.1. Selected aptamer sequences and their K_d values for the target. R^2 is the binding curve regression.

Aptamer	**Sequences (5˜- 3˜)**	**Kd (nM)**	**R^2**
CD80-1	AA CAG AGA AGG CGC GTC TGG AAC AAT GAG TTC GAC GAC AAT CAA CAT CGG AAG AGA TGT G	442.3	0.9613
CD80-3	GG ATT CAA CGG GCT TGG GAC AAT GAG TCC GCC GAG TGA CTG GGT GAT GGG GGG TAT ATG GTT	487.3	0.9605
CD80-4	GG AAA GGA GGG GGA TGC AAC GTG CGG ACC ACT AGA GAG ATA CGT CCC GCA ATA ACG CCT G	200.5	0.9917
CD80-16	AA TGC GAC ATA AAG GAG CAC TTG GGA CGA TGA GTC CGT GCG TAA CGG TTG GGT AGG GTG	47.69	0.9960

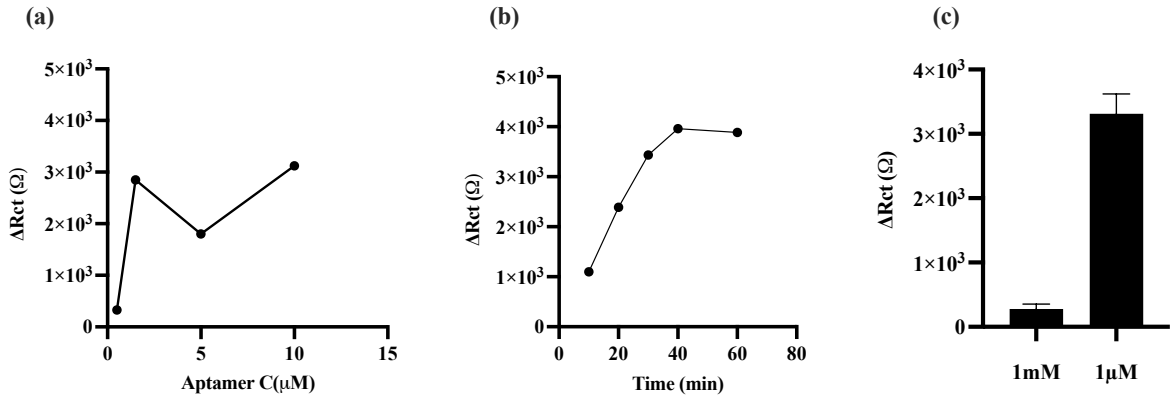

Figure B.5. Incubation time, aptamer concentration, and MCH concentration optimization: (a) Aptamer concentration optimization. The effect of the immobilized ssDNA self-assembled monolayer was evaluated by the change of charge transfer resistance ($\Delta R\mathrm{ct}$) as a function of aptamer concentration in μM. (b) The effect of sCD80 (10 nM) incubation time on the response of the aptasensor ($\Delta R\mathrm{ct}$). (c) MCH concentration optimization. The effect of MCH concentration on the sensor's response ($\Delta R\mathrm{ct}$) after incubation with 10 nM sCD80.

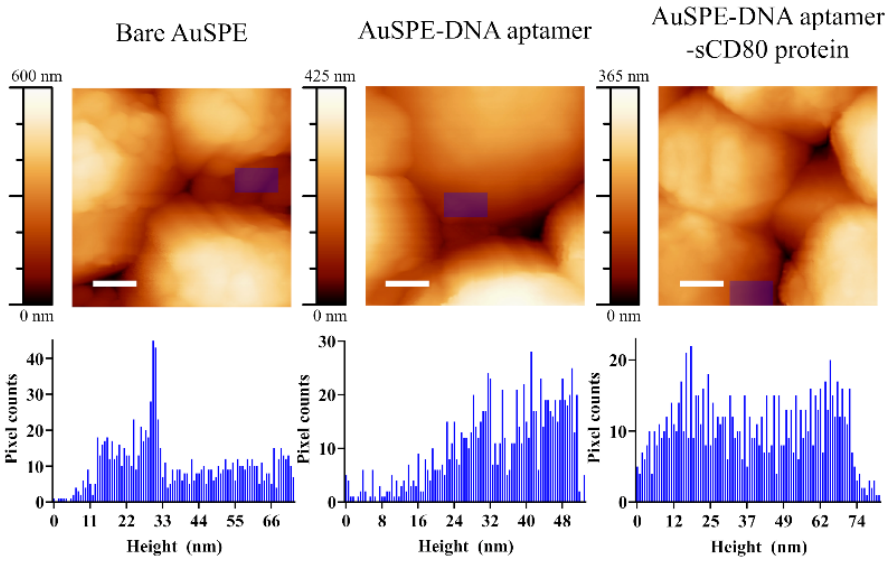

RMS roughness (nm)	18.366	12.010	21.673
Minimum value (nm)	0	0	0
Maximum value (nm)	73.277	58.119	82.495
Average height (nm)	38.037	34.690	39.397
Area selected (nm^2)	16 414	16 414	16 414

Figure B.6. Roughness evaluation of a comparable section from AuSPE, AuSPE-DNA aptamer and AuSPE-DNA aptamer-sCD80 protein sample surfaces.

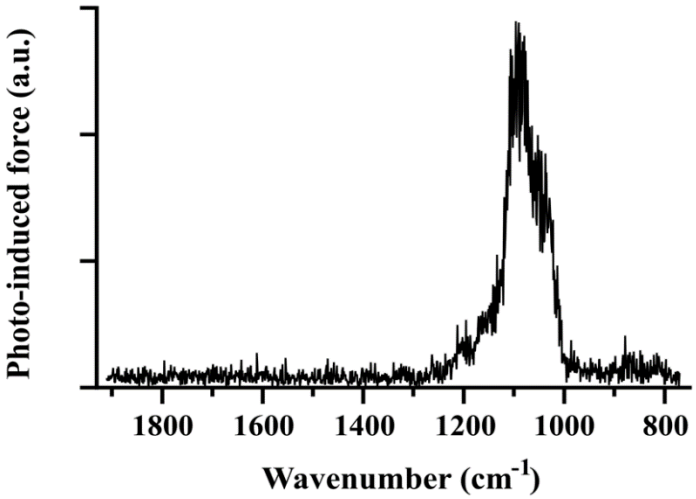

Figure B.7. PiF-IR background spectrum collected on the AuSPE sample, used for subtraction.

Table B.2. Percentage recoveries from spiked protein in human serum

sCD80 Concentration (nM)	**Recovery (%)**	**RSD (%)**
2.5	104.6	1.3
5.0	107.7	6.6
10.0	125.6	3.3

References:

Lee PY, Costumbrado J, Hsu CY, Kim YH. Agarose gel electrophoresis for the separation of DNA fragments. J Vis Exp. 2012(62). DOI: 10.3791/3923

Abrego-Martinez, J. C., Jafari, M., Chergui, S., Pavel, C., Che, D., & Siaj, M. (2022). Aptamer-based electrochemical biosensor for rapid detection of SARS-CoV-2: Nanoscale electrode-aptamer-SARS-CoV-2 imaging by photo-induced force microscopy. Biosens Bioelectron, 195, 113595. doi:10.1016/j.bios.2021.113595

Nowak D, Morrison W, Wickramasinghe HK, Jahng J, Potma E, Wan L, et al. Nanoscale chemical imaging by photoinduced force microscopy. Sci Adv. 2016;2(3):e1501571. DOI: 10.1126/sciadv.1501571

APPENDIX C

CO-STIMULATORY PATHWAY INHIBITION ASSAY DEVELOPMENT USING LIQUID CHROMATOGRAPHY-TANDEM MASS SPECTROMETRY (LC-MS/MS)

Abeer K. Malkawi[a], Leanne Ohlund[a], Lekha Sleno[a], Anas M. Abdel Rahman[b,c,d], Mohamed Siaj[a*]

[a] Department of Chemistry, Université du Québec à Montréal, Montreal, QC, H3C 3P8, Canada

[b] Metabolomics Section, Department of Clinical Genomics, Center for Genome Medicine, King Faisal Specialist Hospital and Research Centre (KFSHRC), Riyadh, Saudi Arabia

[c] Department of Biochemistry and Molecular Medicine, College of Medicine, Alfaisal University, Riyadh, 11350, Saudi Arabia

[d] Department of Chemistry, Memorial University of Newfoundland, St. John's, A1C 5S7, NL, Canada

J Pharm Biomed Anal . 2024 May 15:242:116034. DOI: 10.1016/j.jpba.2024.116034

* Correspondence: Professor Mohamed Siaj,
Email: siaj.mohamed@uqam.ca

C.1. Immobilization of sCD28 on NTA-Ni agarose beads

HisPur Ni-NTA 6% cross-linked agarose beads (45 to 165 μm diameter) were used as solid support. 25 μL of the beads resin was equilibrated with 50 μL
of buffer containing 10 mM imidazole in PBS (coupling buffer). The suspended beads were centrifuged for 2min at 0.7xG, and the supernatant was discarded. This step was repeated at least three times. Then, 35μL of 6His-tagged sCD28 (23.8μM) was incubated with the equilibrated beads in a final volume of 200 μL using the coupling buffer on an End-Over-End rotator for 4 hours at 4 ºC. The coupled beads were washed three times with 100 μL of washing buffer (PBS containing 25 mM imidazole) to block the non-specific binding. The coupled beads were stored in 0.05% sodium azide in PBS at 4 ºC until further use (final volume 1000 μL).

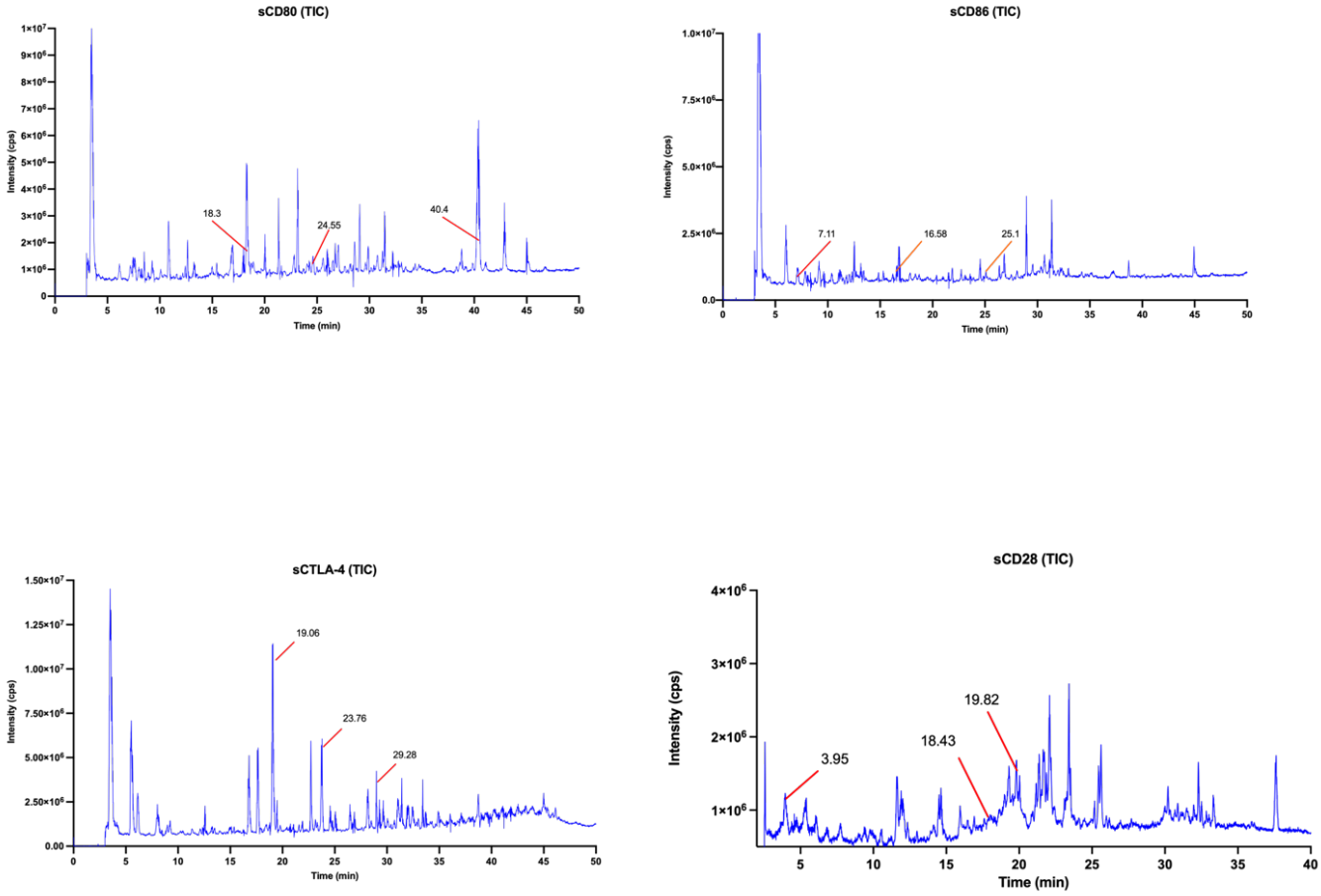

Figure C.1. The total ion chromatogram for the four proteins; sCD80, sCD86, sCTLA4, and sCD28 with the most abundant tryptic peptides

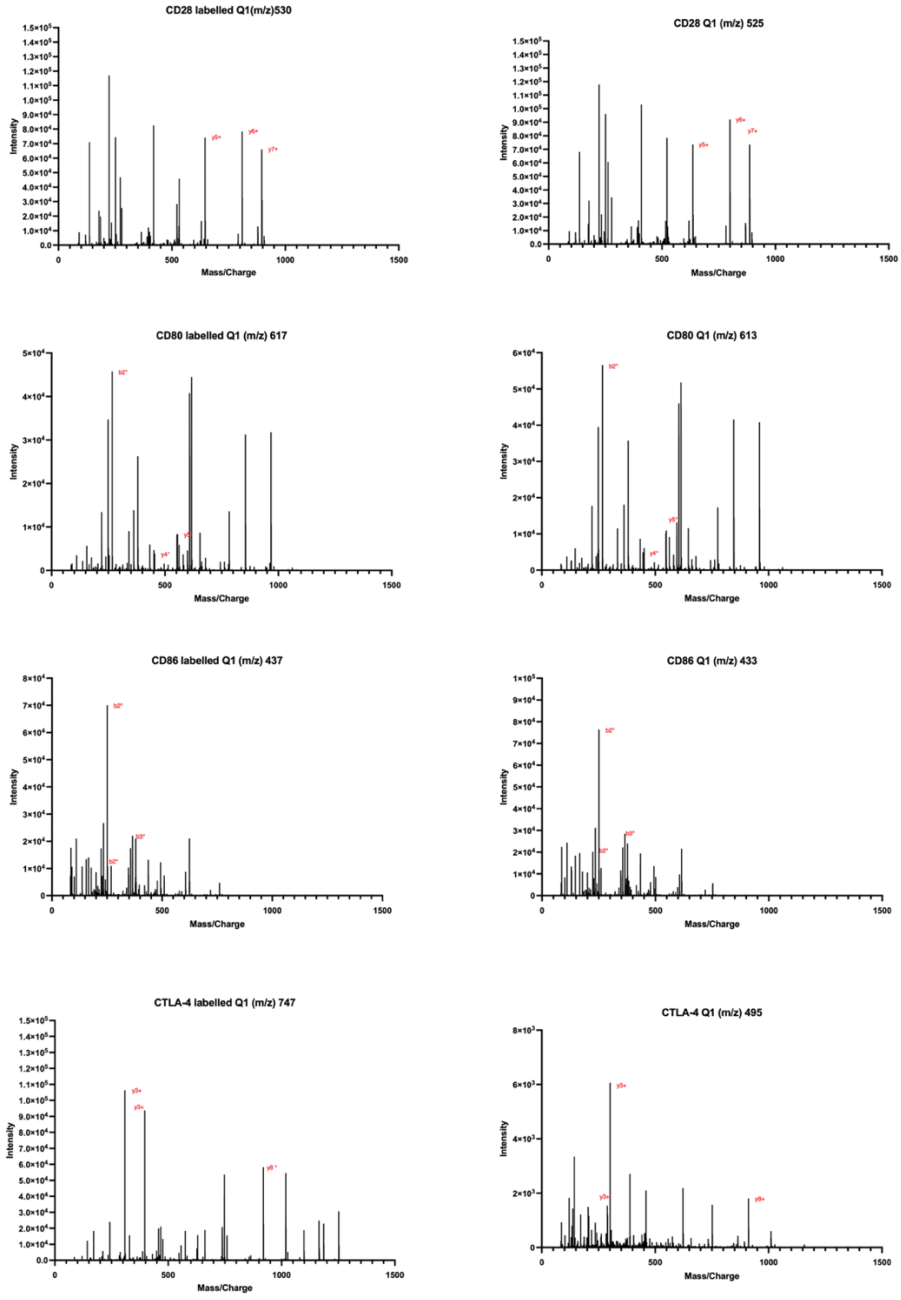

Figure C.2. Product ion spectra for the signature peptides (MS/MS) generated in the low-resolution triple quadrupole mass spectrometry.

REFERENCES

Abeer K. Malkawi, R. M. N., Maha Almogren, Afshan Masood, Abdulrahman S. Alarfaj, Hicham Benabdelkamel, Anas M. Abdel Rahman, Mohamed Siaj,. (2023). Quantitative Analysis of Soluble Costimulatory Molecules as Potential Diagnostic Biomarkers for Rheumatoid Arthritis using LC-MS/MS in MRM Mode,. Clinica Chimica Acta,, 117501. doi:10.1016/j.cca.2023.117501

Abnous, K., Danesh, N. M., Alibolandi, M., Ramezani, M., & Taghdisi, S. M. (2017). Amperometric aptasensor for ochratoxin A based on the use of a gold electrode modified with aptamer, complementary DNA, SWCNTs and the redox marker Methylene Blue. Microchimica Acta, 184(4), 1151-1159. doi:10.1007/s00604-017-2113-7

Abrego-Martinez, J. C., Jafari, M., Chergui, S., Pavel, C., Che, D., & Siaj, M. (2022). Aptamer-based electrochemical biosensor for rapid detection of SARS-CoV-2: Nanoscale electrode-aptamer-SARS-CoV-2 imaging by photo-induced force microscopy. Biosens Bioelectron, 195, 113595. doi:10.1016/j.bios.2021.113595

Ahirwar, R., Dalal, A., Sharma, J. G., Yadav, B. K., Nahar, P., Kumar, A., & Kumar, S. (2019). An aptasensor for rapid and sensitive detection of estrogen receptor alpha in human breast cancer. Biotechnol Bioeng, 116(1), 227-233. doi:10.1002/bit.26819

Akyilmaz, E., Yorganci, E., & Asav, E. (2010). Do copper ions activate tyrosinase enzyme? A biosensor model for the solution. Bioelectrochemistry, 78(2), 155-160. doi:10.1016/j.bioelechem.2009.09.007

Alegre, M.-L., Frauwirth, K. A., & Thompson, C. B. (2001). T-cell regulation by CD28 and CTLA-4. Nature Reviews Immunology, 1(3), 220-228.

Aletaha, D., Neogi, T., Silman, A. J., Funovits, J., Felson, D. T., Bingham III, C. O., . . . Cohen, M. D. (2010). 2010 rheumatoid arthritis classification criteria: an American College of Rheumatology/European League Against Rheumatism collaborative initiative. Arthritis & rheumatism, 62(9), 2569-2581.

Alexandridou, A., Tsangaris, G. T., Vougas, K., Nikita, K., & Spyrou, G. (2009). UniMaP: finding unique mass and peptide signatures in the human proteome. Bioinformatics, 25(22), 3035-3037. doi:10.1093/bioinformatics/btp516

Amiri-Dashatan, N., Koushki, M., Abbaszadeh, H. A., Rostami-Nejad, M., & Rezaei-Tavirani, M. (2018). Proteomics Applications in Health: Biomarker and Drug Discovery and Food Industry. Iran J Pharm Res, 17(4), 1523-1536. Retrieved from https://www.ncbi.nlm.nih.gov/pubmed/30568709

Atzeni, F., Talotta, R., Masala, I. F., Bongiovanni, S., Boccassini, L., & Sarzi-Puttini, P. (2017). Biomarkers in Rheumatoid Arthritis. Isr Med Assoc J, 19(8), 512-516. Retrieved from https://www.ncbi.nlm.nih.gov/pubmed/28825772

Ayodele, O. O., Adesina, A. O., Pourianejad, S., Averitt, J., & Ignatova, T. (2021). Recent Advances in Nanomaterial-Based Aptasensors in Medical Diagnosis and Therapy. Nanomaterials (Basel), 11(4). doi:10.3390/nano11040932

Bachour Junior, B., Batistuti, M. R., Pereira, A. S., de Sousa Russo, E. M., & Mulato, M. (2021). Electrochemical aptasensor for NS1 detection: Towards a fast dengue biosensor. Talanta, 233, 122527. doi:https://doi.org/10.1016/j.talanta.2021.122527

Baek, S. E., Lee, K. H., Park, Y. S., Oh, D. K., Oh, S., Kim, K. S., & Kim, D. E. (2014). RNA aptamer-conjugated liposome as an efficient anticancer drug delivery vehicle targeting cancer cells in vivo. J Control Release, 196, 234-242. doi:10.1016/j.jconrel.2014.10.018

Bagalkot, V., Farokhzad, O. C., Langer, R., & Jon, S. (2006). An aptamer-doxorubicin physical conjugate as a novel targeted drug-delivery platform. Angew Chem Int Ed Engl, 45(48), 8149-8152. doi:10.1002/anie.200602251

Bagalkot, V., Zhang, L., Levy-Nissenbaum, E., Jon, S., Kantoff, P. W., Langer, R., & Farokhzad, O. C. (2007). Quantum dot-aptamer conjugates for synchronous cancer imaging, therapy, and sensing of drug delivery based on bi-fluorescence resonance energy transfer. Nano Lett, 7(10), 3065-3070. doi:10.1021/nl071546n

Bai, Y., Xu, T., & Zhang, X. (2020). Graphene-Based Biosensors for Detection of Biomarkers. Micromachines (Basel), 11(1). doi:10.3390/mi11010060

Barrera-Avalos, C., Luraschi, R., Vallejos-Vidal, E., Mella-Torres, A., Hernandez, F., Figueroa, M., . . . Sandino, A. M. (2021). The Rapid Antigen Detection Test for SARS-CoV-2 Underestimates the Identification of COVID-19 Positive Cases and Compromises the Diagnosis of the SARS-CoV-2 (K417N/T, E484K, and N501Y) Variants. Front Public Health, 9, 780801. doi:10.3389/fpubh.2021.780801

Barth, A. (2007). Infrared spectroscopy of proteins. Biochimica et Biophysica Acta (BBA) - Bioenergetics, 1767(9), 1073-1101. doi:https://doi.org/10.1016/j.bbabio.2007.06.004

Bates, P. J., Laber, D. A., Miller, D. M., Thomas, S. D., & Trent, J. O. (2009). Discovery and development of the G-rich oligonucleotide AS1411 as a novel treatment for cancer. Exp Mol Pathol, 86(3), 151-164. doi:10.1016/j.yexmp.2009.01.004

Bilik, K. U., Erguven, E., Klussmann, S., Jarosch, F., Wielinga, P. Y., Lutz, T. A., & Riediger, T. (2007). In-vitro and in-vivo antagonistic action of an anti-amylin Spiegelmer. Neuroreport, 18(17), 1855-1859. doi:10.1097/WNR.0b013e3282f1ab04

Brothers, M. C., Moore, D., St Lawrence, M., Harris, J., Joseph, R. M., Ratcliff, E., . . . Kim, S. S. (2020). Impact of Self-Assembled Monolayer Design and Electrochemical Factors on Impedance-Based Biosensing. Sensors (Basel), 20(8). doi:10.3390/s20082246

Bryl, E., Vallejo, A. N., Matteson, E. L., Witkowski, J. M., Weyand, C. M., & Goronzy, J. J. (2005). Modulation of CD28 expression with anti-tumor necrosis factor alpha therapy in rheumatoid arthritis. Arthritis Rheum, 52(10), 2996-3003. doi:10.1002/art.21353

Buck, C. A. (1992). Immunoglobulin superfamily: structure, function and relationship to other receptor molecules. Semin Cell Biol, 3(3), 179-188. doi:10.1016/s1043-4682(10)80014-5

Buck, C. A. (1992). Immunoglobulin superfamily: structure, function and relationship to other receptor molecules. Paper presented at the Seminars in cell biology.

Buglak, A. A., Samokhvalov, A. V., Zherdev, A. V., & Dzantiev, B. B. (2020). Methods and Applications of In Silico Aptamer Design and Modeling. Int J Mol Sci, 21(22). doi:10.3390/ijms21228420

Burmeister, P. E., Lewis, S. D., Silva, R. F., Preiss, J. R., Horwitz, L. R., Pendergrast, P. S., . . . Keefe, A. D. (2005). Direct in vitro selection of a 2'-O-methyl aptamer to VEGF. Chem Biol, 12(1), 25-33. doi:10.1016/j.chembiol.2004.10.017

Cabrera, R., Fitian, A. I., Ararat, M., Xu, Y., Brusko, T., Wasserfall, C., . . . Nelson, D. R. (2012). Serum levels of soluble CD25 as a marker for hepatocellular carcinoma. Oncol Lett, 4(4), 840-846. doi:10.3892/ol.2012.826

Candia, J., Daya, G. N., Tanaka, T., Ferrucci, L., & Walker, K. A. (2022). Assessment of variability in the plasma 7k SomaScan proteomics assay. Sci Rep, 12(1), 17147. doi:10.1038/s41598-022-22116-0

Cao, J., Zou, L., Luo, P., Chen, P., & Zhang, L. (2012). Increased production of circulating soluble co-stimulatory molecules CTLA-4, CD28 and CD80 in patients with rheumatoid arthritis. Int Immunopharmacol, 14(4), 585-592. doi:10.1016/j.intimp.2012.08.004

Cao, J. T., Yang, J. J., Zhao, L. Z., Wang, Y. L., Wang, H., Liu, Y. M., & Ma, S. H. (2018). Graphene oxide@gold nanorods-based multiple-assisted electrochemiluminescence signal amplification strategy for sensitive detection of prostate specific antigen. Biosens Bioelectron, 99, 92-98. doi:10.1016/j.bios.2017.07.050

Cassiday, L. A., Lebruska, L. L., Benson, L. M., Naylor, S., Owen, W. G., & Maher, L. J., 3rd. (2002). Binding stoichiometry of an RNA aptamer and its transcription factor target. Anal Biochem, 306(2), 290-297. doi:10.1006/abio.2002.5710

Cennamo, N., Pasquardini, L., Arcadio, F., Vanzetti, L. E., Bossi, A. M., & Zeni, L. (2019). D-shaped plastic optical fibre aptasensor for fast thrombin detection in nanomolar range. Sci Rep, 9(1), 18740. doi:10.1038/s41598-019-55248-x

Chai, C., Xie, Z., & Grotewold, E. (2011). SELEX (Systematic Evolution of Ligands by EXponential Enrichment), as a powerful tool for deciphering the protein-DNA interaction space. Methods Mol Biol, 754, 249-258. doi:10.1007/978-1-61779-154-3_14

Chen, C. H., Chernis, G. A., Hoang, V. Q., & Landgraf, R. (2003). Inhibition of heregulin signaling by an aptamer that preferentially binds to the oligomeric form of human epidermal growth factor receptor-3. Proc Natl Acad Sci U S A, 100(16), 9226-9231. doi:10.1073/pnas.1332660100

Chimenti, M., Triggianese, P., Conigliaro, P., Candi, E., Melino, G., & Perricone, R. (2015). The interplay between inflammation and metabolism in rheumatoid arthritis. Cell death & disease, 6(9), e1887-e1887.

Chimenti, M. S., Triggianese, P., Conigliaro, P., Candi, E., Melino, G., & Perricone, R. (2015). The interplay between inflammation and metabolism in rheumatoid arthritis. Cell Death Dis, 6, e1887. doi:10.1038/cddis.2015.246

Chinnappan, R., Zaghloul, N. S., AlZabn, R., Malkawi, A., Abdel Rahman, A., Abu-Salah, K. M., & Zourob, M. (2021). Aptamer selection and aptasensor construction for bone density biomarkers. Talanta, 224, 121818. doi:10.1016/j.talanta.2020.121818

Christian F. W. Becker Dr., R. W. D., Werner Bouschen Dr., Ralf Seidel Dr., Branko Kolaric, Pascal Lang, Hendrik Schroeder Dr., Oliver Müller Priv.-Doz. Dr., Christof M. Niemeyer Prof. Dr., Bernhard Spengler Prof. Dr., Roger S. Goody Prof. Dr., Martin Engelhard Prof. Dr. (2005). Direkter Nachweis von Protein-Protein-Wechselwirkungen durch Massenspektrometrie an Protein-DNA-Mikroarrays. Angewandte Chemie, 117(46), 7808-7812. doi:10.1002/ange.200502908

Chu, F., Wei, W., Shuaibu, N. S., Feng, H., Wang, X., & Pan, Y. (2023). Mass Spectrometry-Based Biosensing and Biopsy Technology. Chemosensors, 11(8), 419. Retrieved from https://www.mdpi.com/2227-9040/11/8/419

Chushak, Y., & Stone, M. O. (2009). In silico selection of RNA aptamers. Nucleic Acids Res, 37(12), e87. doi:10.1093/nar/gkp408

Conte, M. S., Bandyk, D. F., Clowes, A. W., Moneta, G. L., Seely, L., Lorenz, T. J., . . . Investigators, P. I. (2006). Results of PREVENT III: a multicenter, randomized trial of edifoligide for the prevention of vein graft failure in lower extremity bypass surgery. J Vasc Surg, 43(4), 742-751; discussion 751. doi:10.1016/j.jvs.2005.12.058

Contreras Jimenez, G., Eissa, S., Ng, A., Alhadrami, H., Zourob, M., & Siaj, M. (2015). Aptamer-based label-free impedimetric biosensor for detection of progesterone. Anal Chem, 87(2), 1075-1082. doi:10.1021/ac503639s

Cope, A. P., Schulze-Koops, H., & Aringer, M. (2007). The central role of T cells in rheumatoid arthritis. Clin Exp Rheumatol, 25(5 Suppl 46), S4-11.

Crepeau, R. L., & Ford, M. L. (2017). Challenges and opportunities in targeting the CD28/CTLA-4 pathway in transplantation and autoimmunity. Expert Opin Biol Ther, 17(8), 1001-1012. doi:10.1080/14712598.2017.1333595

Das, S., Ariizumi, K., & Cruz, P. D., Jr. (2012). T-cell inhibitors: a bench-to-bedside review. Dermatitis, 23(5), 195-202. doi:10.1097/DER.0b013e31826e43ed

Dausse, E., Barre, A., Aime, A., Groppi, A., Rico, A., Ainali, C., . . . Di Primo, C. (2016). Aptamer selection by direct microfluidic recovery and surface plasmon resonance evaluation. Biosens Bioelectron, 80, 418-425. doi:10.1016/j.bios.2016.02.003

de-los-Santos-Álvarez, N., Lobo-Castañón, M. J., Miranda-Ordieres, A. J., & Tuñón-Blanco, P. (2008). Aptamers as recognition elements for label-free analytical devices. Trends in Analytical Chemistry, 27, 437-446.

Deane, K. D., Demoruelle, M. K., Kelmenson, L. B., Kuhn, K. A., Norris, J. M., & Holers, V. M. (2017). Genetic and environmental risk factors for rheumatoid arthritis. Best Pract Res Clin Rheumatol, 31(1), 3-18. doi:10.1016/j.berh.2017.08.003

DiGiusto, D. L., Krishnan, A., Li, L., Li, H., Li, S., Rao, A., . . . Zaia, J. A. (2010). RNA-based gene therapy for HIV with lentiviral vector-modified CD34(+) cells in patients undergoing transplantation for AIDS-related lymphoma. Sci Transl Med, 2(36), 36ra43. doi:10.1126/scitranslmed.3000931

Doerr, A. (2013). Mass spectrometry–based targeted proteomics. Nature Methods, 10(1), 23-23. doi:10.1038/nmeth.2286

Drolet, D. W., Green, L. S., Gold, L., & Janjic, N. (2016). Fit for the Eye: Aptamers in Ocular Disorders. Nucleic Acid Ther, 26(3), 127-146. doi:10.1089/nat.2015.0573

Eissa, S., Abdulkarim, H., Dasouki, M., Al Mousa, H., Arnout, R., Al Saud, B., . . . Zourob, M. (2018). Multiplexed detection of DOCK8, PGM3 and STAT3 proteins for the diagnosis of Hyper-Immunoglobulin E syndrome using gold nanoparticles-based immunosensor array platform. Biosens Bioelectron, 117, 613-619. doi:10.1016/j.bios.2018.06.058

Ellington, A. D., & Szostak, J. W. (1990). In vitro selection of RNA molecules that bind specific ligands. Nature, 346(6287), 818-822. doi:10.1038/346818a0

Ellington, A. D., & Szostak, J. W. (1992). Selection in vitro of single-stranded DNA molecules that fold into specific ligand-binding structures. Nature, 355(6363), 850-852. doi:10.1038/355850a0

EMEA, I. (2006). Topic Q 2 (R1), Validation of Analytical Procedures: Text and Methodology. Paper presented at the International Conference on Harmonisation of Technical Requirements for Registration of Pharmaceuticals for Human Use.

Faas, S. J., Giannoni, M. A., Mickle, A. P., Kiesecker, C. L., Reed, D. J., Wu, D., . . . Rother, R. P. (2000). Primary structure and functional characterization of a soluble, alternatively spliced form of B7-1. J Immunol, 164(12), 6340-6348. doi:10.4049/jimmunol.164.12.6340

Ferapontova, E. E., Olsen, E. M., & Gothelf, K. V. (2008). An RNA aptamer-based electrochemical biosensor for detection of theophylline in serum. J Am Chem Soc, 130(13), 4256-4258. doi:10.1021/ja711326b

Fitzwater, T., & Polisky, B. (1996). [17] A SELEX primer. In Methods in Enzymology (Vol. 267, pp. 275-301): Academic Press.

Food, & Drug Administration, U. (2018). Bioanalytical method validation guidance for industry. US Department of Health and Human Services, 1-41.

Food, D. A. U. B. m. v. g. f. i. U. D. o. H. a. H. S.-.

Fu, Q., Grote, E., Zhu, J., Jelinek, C., Kottgen, A., Coresh, J., & Van Eyk, J. E. (2016). An Empirical Approach to Signature Peptide Choice for Selected Reaction Monitoring: Quantification of Uromodulin in Urine. Clin Chem, 62(1), 198-207. doi:10.1373/clinchem.2015.242495

Fu, X., He, J., Zhang, C., Chen, J., Wen, Y., Li, J., . . . Yu, C. (2019). Trimetallic signal amplification aptasensor for TSP-1 detection based on Ce-MOF@Au and AuPtRu nanocomposites. Biosens Bioelectron, 132, 302-309. doi:10.1016/j.bios.2019.02.054

Galal, M. A., Abdel Jabar, M., Zhra, M., Abdel Rahman, A. M., & Aljada, A. (2021). Absolute quantification of senescence mediators in cells using multiple reaction monitoring liquid chromatography-Tandem mass spectrometry. Anal Chim Acta, 1184, 339009. doi:10.1016/j.aca.2021.339009

Galal, M. A., Jabar, M. A., Zhra, M., Rahman, A. M. A., & Aljada, A. (2021). Absolute quantification of senescence mediators in cells using multiple reaction monitoring liquid chromatography-Tandem mass spectrometry. Analytica chimica acta, 1184, 339009.

Gilbert, J. C., DeFeo-Fraulini, T., Hutabarat, R. M., Horvath, C. J., Merlino, P. G., Marsh, H. N., . . . Schaub, R. G. (2007). First-in-human evaluation of anti von Willebrand factor therapeutic aptamer ARC1779 in healthy volunteers. Circulation, 116(23), 2678-2686. doi:10.1161/CIRCULATIONAHA.107.724864

Giorgi-Coll, S., Marin, M. J., Sule, O., Hutchinson, P. J., & Carpenter, K. L. H. (2019). Aptamer-modified gold nanoparticles for rapid aggregation-based detection of inflammation: an optical assay for interleukin-6. Mikrochim Acta, 187(1), 13. doi:10.1007/s00604-019-3975-7

Gnoth, C., & Johnson, S. (2014). Strips of Hope: Accuracy of Home Pregnancy Tests and New Developments. Geburtshilfe Frauenheilkd, 74(7), 661-669. doi:10.1055/s-0034-1368589

Gotsman, I., Sharpe, A. H., & Lichtman, A. H. (2008). T-cell costimulation and coinhibition in atherosclerosis. Circulation research, 103(11), 1220-1231.

Group, V. I. S. i. O. N. C. T., Chakravarthy, U., Adamis, A. P., Cunningham, E. T., Jr., Goldbaum, M., Guyer, D. R., . . . Patel, M. (2006). Year 2 efficacy results of 2 randomized controlled clinical trials of pegaptanib for neovascular age-related macular degeneration. Ophthalmology, 113(9), 1508 e1501-1525. doi:10.1016/j.ophtha.2006.02.064

Guideline, I. H. T. (2005). Validation of analytical procedures: text and methodology Q2 (R1). Paper presented at the International conference on harmonization, Geneva, Switzerland.

Guideline IHT, e. V. o. a. p. t. a. m. Q. R. I. c. o. h., Geneva, Switzerland; 2005.

Gulbakan, B., Barylyuk, K., Schneider, P., Pillong, M., Schneider, G., & Zenobi, R. (2018). Native Electrospray Ionization Mass Spectrometry Reveals Multiple Facets of Aptamer-Ligand Interactions: From Mechanism to Binding Constants. J Am Chem Soc, 140(24), 7486-7497. doi:10.1021/jacs.7b13044

Gunnarsson, A., Sjovall, P., & Hook, F. (2010). Liposome-based chemical barcodes for single molecule DNA detection using imaging mass spectrometry. Nano Lett, 10(2), 732-737. doi:10.1021/nl904208y

Haghighi, M., Khanahmad, H., & Palizban, A. (2018). Selection and Characterization of Single-Stranded DNA Aptamers Binding Human B-Cell Surface Protein CD20 by Cell-SELEX. Molecules, 23(4). doi:10.3390/molecules23040715

Haris, P. I. (2013). Infrared Spectroscopy of Protein Structure. In G. C. K. Roberts (Ed.), Encyclopedia of Biophysics (pp. 1095-1106). Berlin, Heidelberg: Springer Berlin Heidelberg.

Hassani, S., Salek Maghsoudi, A., Rezaei Akmal, M., Rahmani, S. R., Sarihi, P., Ganjali, M. R., . . . Abdollahi, M. (2020). A Sensitive Aptamer-Based Biosensor for Electrochemical Quantification of PSA as a Specific Diagnostic Marker of Prostate Cancer. J Pharm Pharm Sci, 23, 243-258. doi:10.18433/jpps31171

He, Y., Tang, J., Wu, B., Yang, B., Ou, Q., & Lin, J. (2020). Correlation between albumin to fibrinogen ratio, C-reactive protein to albumin ratio and Th17 cells in patients with rheumatoid arthritis. Clinica Chimica Acta, 500, 149-154. doi:https://doi.org/10.1016/j.cca.2019.10.009

Healy, J. M., Lewis, S. D., Kurz, M., Boomer, R. M., Thompson, K. M., Wilson, C., & McCauley, T. G. (2004). Pharmacokinetics and biodistribution of novel aptamer compositions. Pharm Res, 21(12), 2234-2246. doi:10.1007/s11095-004-7676-4

Heiskanen, A. R., Spegel, C. F., Kostesha, N., Ruzgas, T., & Emneus, J. (2008). Monitoring of Saccharomyces cerevisiae cell proliferation on thiol-modified planar gold microelectrodes using impedance spectroscopy. Langmuir, 24(16), 9066-9073. doi:10.1021/la800580f

Hock, B. D., O'Donnell, J. L., Taylor, K., Steinkasserer, A., McKenzie, J. L., Rothwell, A. G., & Summers, K. L. (2006). Levels of the soluble forms of CD80, CD86, and CD83 are elevated in the synovial fluid of rheumatoid arthritis patients. Tissue Antigens, 67(1), 57-60. doi:10.1111/j.1399-0039.2005.00524.x

Hock, B. D., Patton, W. N., Budhia, S., Mannari, D., Roberts, P., & McKenzie, J. L. (2002). Human plasma contains a soluble form of CD86 which is present at elevated levels in some leukaemia patients. Leukemia, 16(5), 865-873. doi:10.1038/sj.leu.2402466

Hock, B. D., Starling, G. C., Patton, W. N., Salm, N., Bond, K., McArthur, L. T., & McKenzie, J. L. (2004). Identification of a circulating soluble form of CD80: levels in patients with hematological malignancies. Leuk Lymphoma, 45(10), 2111-2118. doi:10.1080/10428190410001712199

Hong, P., Li, W., & Li, J. (2012). Applications of aptasensors in clinical diagnostics. Sensors (Basel), 12(2), 1181-1193. doi:10.3390/s120201181

Horcas, I., Fernández, R., Gómez-Rodríguez, J. M., Colchero, J., Gómez-Herrero, J., & Baro, A. M. (2007). WSXM: A software for scanning probe microscopy and a tool for nanotechnology. Review of Scientific Instruments, 78(1), 013705. doi:10.1063/1.2432410

Hu, D., Liang, H., Wang, X., Luo, F., Qiu, B., Lin, Z., & Wang, J. (2020). Highly Sensitive and Selective Photoelectrochemical Aptasensor for Cancer Biomarker CA125 Based on AuNPs/GaN Schottky Junction. Anal Chem, 92(14), 10114-10120. doi:10.1021/acs.analchem.0c02117

Hu, J., Liu, F., Chen, Y., Shangguan, G., & Ju, H. (2021). Mass Spectrometric Biosensing: A Powerful Approach for Multiplexed Analysis of Clinical Biomolecules. ACS Sens, 6(10), 3517-3535. doi:10.1021/acssensors.1c01394

Hu, T., Wu, L., Sun, X., Su, P., & Yang, Y. (2020). Comparative study on quantitation of human myoglobin by both isotope dilution mass spectrometry and surface plasmon resonance

based on calibration-free analysis. Anal Bioanal Chem, 412(12), 2777-2784. doi:10.1007/s00216-020-02504-z

Huang, B. T., Lai, W. Y., Chang, Y. C., Wang, J. W., Yeh, S. D., Lin, E. P., & Yang, P. C. (2017). A CTLA-4 Antagonizing DNA Aptamer with Antitumor Effect. Mol Ther Nucleic Acids, 8, 520-528. doi:10.1016/j.omtn.2017.08.006

Ip, W. K., Wong, C. K., Leung, T. F., & Lam, C. W. (2006). Plasma concentrations of soluble CTLA-4, CD28, CD80 and CD86 costimulatory molecules reflect disease severity of acute asthma in children. Pediatr Pulmonol, 41(7), 674-682. doi:10.1002/ppul.20432

Ishikawa, F. N., Chang, H. K., Curreli, M., Liao, H. I., Olson, C. A., Chen, P. C., . . . Zhou, C. (2009). Label-free, electrical detection of the SARS virus N-protein with nanowire biosensors utilizing antibody mimics as capture probes. ACS Nano, 3(5), 1219-1224. doi:10.1021/nn900086c

Ishizuka, T., Yamashita, A., Asada, Y., & Xu, Y. (2017). Studying DNA G-Quadruplex Aptamer by (19)F NMR. ACS Omega, 2(12), 8843-8848. doi:10.1021/acsomega.7b01405

Jackson, M. A., Ahmann, A., & Shah, V. N. (2021). Type 2 Diabetes and the Use of Real-Time Continuous Glucose Monitoring. Diabetes Technol Ther, 23(S1), S27-S34. doi:10.1089/dia.2021.0007

Jellinek, D., Lynott, C. K., Rifkin, D. B., & Janjic, N. (1993). High-affinity RNA ligands to basic fibroblast growth factor inhibit receptor binding. Proc Natl Acad Sci U S A, 90(23), 11227-11231. doi:10.1073/pnas.90.23.11227

Jeong, H. Y., Kim, H., Lee, M., Hong, J., Lee, J. H., Kim, J., . . . Kim, S. C. (2020). Development of HER2-Specific Aptamer-Drug Conjugate for Breast Cancer Therapy. Int J Mol Sci, 21(24). doi:10.3390/ijms21249764

Ji, J., Pang, Y., Li, D., Huang, Z., Zhang, Z., Xue, N., . . . Mu, X. (2020). An aptamer-based shear horizontal surface acoustic wave biosensor with a CVD-grown single-layered graphene film for high-sensitivity detection of a label-free endotoxin. Microsyst Nanoeng, 6, 4. doi:10.1038/s41378-019-0118-6

Jilma, B., Paulinska, P., Jilma-Stohlawetz, P., Gilbert, J. C., Hutabarat, R., & Knobl, P. (2010). A randomised pilot trial of the anti-von Willebrand factor aptamer ARC1779 in patients with type 2b von Willebrand disease. Thromb Haemost, 104(3), 563-570. doi:10.1160/TH10-01-0027

Jilma-Stohlawetz, P., Knobl, P., Gilbert, J. C., & Jilma, B. (2012). The anti-von Willebrand factor aptamer ARC1779 increases von Willebrand factor levels and platelet counts in patients with type 2B von Willebrand disease. Thromb Haemost, 108(2), 284-290. doi:10.1160/TH11-12-0889

K. J. Light-Wahl, D. L. S., B. E. Winger, C. G. Edmonds, D. G. Camp II, B. D. Thrall, and R. D. Smith. (1993). Observation of a small oligonucleotide duplex by electrospray ionization mass spectrometry. Journal of the American Chemical Society, 115(2), 803–804. doi:10.1021/ja00055a070

Kakoulidou, M., Giscombe, R., Zhao, X., Lefvert, A. K., & Wang, X. (2007). Human Soluble CD80 is generated by alternative splicing, and recombinant soluble CD80 binds to CD28 and CD152 influencing T-cell activation. Scand J Immunol, 66(5), 529-537. doi:10.1111/j.1365-3083.2007.02009.x

Kapoor, M., Martel-Pelletier, J., Lajeunesse, D., Pelletier, J.-P., & Fahmi, H. (2011). Role of proinflammatory cytokines in the pathophysiology of osteoarthritis. Nature Reviews Rheumatology, 7(1), 33-42.

Kaur, H., Bruno, J. G., Kumar, A., & Sharma, T. K. (2018). Aptamers in the Therapeutics and Diagnostics Pipelines. Theranostics, 8(15), 4016-4032. doi:10.7150/thno.25958

Kay, J., Morgacheva, O., Messing, S. P., Kremer, J. M., Greenberg, J. D., Reed, G. W., . . . Furst, D. E. (2014). Clinical disease activity and acute phase reactant levels are discordant among patients with active rheumatoid arthritis: acute phase reactant levels contribute separately to predicting outcome at one year. Arthritis Research & Therapy, 16(1), R40. doi:10.1186/ar4469

Kellie, J. F., Tran, J. C., Jian, W., Jones, B., Mehl, J. T., Ge, Y., . . . Bateman, K. P. (2021). Intact Protein Mass Spectrometry for Therapeutic Protein Quantitation, Pharmacokinetics, and Biotransformation in Preclinical and Clinical Studies: An Industry Perspective. J Am Soc Mass Spectrom, 32(8), 1886-1900. doi:10.1021/jasms.0c00270

Kenan, D. J., & Keene, J. D. (1999). In vitro selection of aptamers from RNA libraries. Methods Mol Biol, 118, 217-231. doi:10.1385/1-59259-676-2:217

Khati, M., Schuman, M., Ibrahim, J., Sattentau, Q., Gordon, S., & James, W. (2003). Neutralization of infectivity of diverse R5 clinical isolates of human immunodeficiency virus type 1 by gp120-binding 2'F-RNA aptamers. J Virol, 77(23), 12692-12698. doi:10.1128/jvi.77.23.12692-12698.2003

Kim, N. H., Lee, S. J., & Moskovits, M. (2010). Aptamer-mediated surface-enhanced Raman spectroscopy intensity amplification. Nano Lett, 10(10), 4181-4185. doi:10.1021/nl102495j

Kim, S. H., Thoa, T. T. T., & Gu, M. B. (2019). Aptasensors for environmental monitoring of contaminants in water and soil. Current Opinion in Environmental Science & Health, 10, 9-21. doi:https://doi.org/10.1016/j.coesh.2019.09.003

Kohn, D. B., Bauer, G., Rice, C. R., Rothschild, J. C., Carbonaro, D. A., Valdez, P., . . . Church, J. (1999). A clinical trial of retroviral-mediated transfer of a rev-responsive element

decoy gene into CD34(+) cells from the bone marrow of human immunodeficiency virus-1-infected children. Blood, 94(1), 368-371. Retrieved from https://www.ncbi.nlm.nih.gov/pubmed/10381536

Kondrat, R. W., McClusky, G. A., & Cooks, R. G. (1978). Multiple reaction monitoring in mass spectrometry/mass spectrometry for direct analysis of complex mixtures. Analytical chemistry, 50(14), 2017-2021.

Koster, H., Tang, K., Fu, D. J., Braun, A., van den Boom, D., Smith, C. L., . . . Cantor, C. R. (1996). A strategy for rapid and efficient DNA sequencing by mass spectrometry. Nat Biotechnol, 14(9), 1123-1128. doi:10.1038/nbt0996-1123

Kotulska, A., Kopeć-Mędrek, M., Grosicka, A., Kubicka, M., & Kucharz, E. J. (2015). Correlation between erythrocyte sedimentation rate and C-reactive protein level in patients with rheumatic diseases. Reumatologia, 53(5), 243-246. doi:10.5114/reum.2015.55825

Kourlas, H., & Schiller, D. S. (2006). Pegaptanib sodium for the treatment of neovascular age-related macular degeneration: a review. Clin Ther, 28(1), 36-44. doi:10.1016/j.clinthera.2006.01.009

Krastins, B., Prakash, A., Sarracino, D. A., Nedelkov, D., Niederkofler, E. E., Kiernan, U. A., . . . Garces, A. (2013). Rapid development of sensitive, high-throughput, quantitative and highly selective mass spectrometric targeted immunoassays for clinically important proteins in human plasma and serum. Clinical biochemistry, 46(6), 399-410.

Kremer, J. M., Westhovens, R., Leon, M., Di Giorgio, E., Alten, R., Steinfeld, S., . . . Nuamah, I. F. (2003). Treatment of rheumatoid arthritis by selective inhibition of T-cell activation with fusion protein CTLA4Ig. New England Journal of Medicine, 349(20), 1907-1915.

Kubik, M. F., Bell, C., Fitzwater, T., Watson, S. R., & Tasset, D. M. (1997). Isolation and characterization of 2'-fluoro-, 2'-amino-, and 2'-fluoro-/amino-modified RNA ligands to human IFN-gamma that inhibit receptor binding. J Immunol, 159(1), 259-267. Retrieved from https://www.ncbi.nlm.nih.gov/pubmed/9200462

Kuzyk, M. A., Parker, C. E., Domanski, D., & Borchers, C. H. (2013). Development of MRM-Based Assays for the Absolute Quantitation of Plasma Proteins. In H. Bäckvall & J. Lehtiö (Eds.), The Low Molecular Weight Proteome: Methods and Protocols (pp. 53-82). New York, NY: Springer New York.

Kwon, M., Chun, S. M., Jeong, S., & Yu, J. (2001). In vitro selection of RNA against kanamycin B. Mol Cells, 11(3), 303-311. Retrieved from https://www.ncbi.nlm.nih.gov/pubmed/11459219

Lasserre, P., Balansethupathy, B., Vezza, V. J., Butterworth, A., Macdonald, A., Blair, E. O., . . . Corrigan, D. K. (2022). SARS-CoV-2 Aptasensors Based on Electrochemical Impedance Spectroscopy and Low-Cost Gold Electrode Substrates. Anal Chem, 94(4), 2126-2133. doi:10.1021/acs.analchem.1c04456

Lee, S. W., & Sullenger, B. A. (1997). Isolation of a nuclease-resistant decoy RNA that can protect human acetylcholine receptors from myasthenic antibodies. Nat Biotechnol, 15(1), 41-45. doi:10.1038/nbt0197-41

Lee, T., Park, S. Y., Jang, H., Kim, G.-H., Lee, Y., Park, C., . . . Min, J. (2019). Fabrication of electrochemical biosensor consisted of multi-functional DNA structure/porous au nanoparticle for avian influenza virus (H5N1) in chicken serum. Materials Science and Engineering: C, 99, 511-519. doi:https://doi.org/10.1016/j.msec.2019.02.001

Lee, T. C., Sullenger, B. A., Gallardo, H. F., Ungers, G. E., & Gilboa, E. (1992). Overexpression of RRE-derived sequences inhibits HIV-1 replication in CEM cells. New Biol, 4(1), 66-74. Retrieved from https://www.ncbi.nlm.nih.gov/pubmed/1536832

Li, H., Wolff, J. J., Van Orden, S. L., & Loo, J. A. (2014). Native top-down electrospray ionization-mass spectrometry of 158 kDa protein complex by high-resolution Fourier transform ion cyclotron resonance mass spectrometry. Anal Chem, 86(1), 317-320. doi:10.1021/ac4033214

Lin, P. H., Chen, R. H., Lee, C. H., Chang, Y., Chen, C. S., & Chen, W. Y. (2011). Studies of the binding mechanism between aptamers and thrombin by circular dichroism, surface plasmon resonance and isothermal titration calorimetry. Colloids Surf B Biointerfaces, 88(2), 552-558. doi:10.1016/j.colsurfb.2011.07.032

Lincoff, A. M., Mehran, R., Povsic, T. J., Zelenkofske, S. L., Huang, Z., Armstrong, P. W., . . . Investigators, R.-P. (2016). Effect of the REG1 anticoagulation system versus bivalirudin on outcomes after percutaneous coronary intervention (REGULATE-PCI): a randomised clinical trial. Lancet, 387(10016), 349-356. doi:10.1016/S0140-6736(15)00515-2

Ling, K., Jiang, H., Li, Y., Tao, X., Qiu, C., & Li, F. R. (2016). A self-assembling RNA aptamer-based graphene oxide sensor for the turn-on detection of theophylline in serum. Biosens Bioelectron, 86, 8-13. doi:10.1016/j.bios.2016.06.024

Linsley, P. S., Greene, J. L., Brady, W., Bajorath, J., Ledbetter, J. A., & Peach, R. (1994). Human B7-1 (CD80) and B7-2 (CD86) bind with similar avidities but distinct kinetics to CD28 and CTLA-4 receptors. Immunity, 1(9), 793-801. doi:10.1016/s1074-7613(94)80021-9

Liu, L., Han, Z., An, F., Gong, X., Zhao, C., Zheng, W., . . . Zhou, Q. (2021). Aptamer-based biosensors for the diagnosis of sepsis. J Nanobiotechnology, 19(1), 216. doi:10.1186/s12951-021-00959-5

Liu, M., Zaman, K., & Fortenberry, Y. M. (2021). Overview of the Therapeutic Potential of Aptamers Targeting Coagulation Factors. Int J Mol Sci, 22(8). doi:10.3390/ijms22083897

Liu, M. F., Kohsaka, H., Sakurai, H., Azuma, M., Okumura, K., Saito, I., & Miyasaka, N. (1996). The presence of costimulatory molecules CD86 and CD28 in rheumatoid arthritis synovium. Arthritis Rheum, 39(1), 110-114. doi:10.1002/art.1780390115

Liu, M. F., Wang, C. R., Chen, P. C., & Fung, L. L. (2003). Increased expression of soluble cytotoxic T-lymphocyte-associated antigen-4 molecule in patients with systemic lupus erythematosus. Scand J Immunol, 57(6), 568-572. doi:10.1046/j.1365-3083.2003.01232.x

Liu, W., Yang, Z., Chen, Y., Yang, H., Wan, X., Zhou, X., . . . Zhang, Y. (2021). The association between CTLA-4, CD80/86, and CD28 gene polymorphisms and rheumatoid arthritis: an original study and meta-analysis. Frontiers in Medicine, 8, 598076.

Liu, X., Hou, Y., Qin, Y., Cheng, J., Hou, J., Wu, Q., & Liu, Z. (2023). Selection of a Novel DNA Aptamer Specific for 5-Hydroxymethylfurfural Using Capture-SELEX. Biosensors (Basel), 13(5). doi:10.3390/bios13050564

Liu, X., Li, H., Jia, W., Chen, Z., & Xu, D. (2017). Selection of aptamers based on a protein microarray integrated with a microfluidic chip. Lab on a Chip, 17(1), 178-185.

Liu, Y., Kuan, C. T., Mi, J., Zhang, X., Clary, B. M., Bigner, D. D., & Sullenger, B. A. (2009). Aptamers selected against the unglycosylated EGFRvIII ectodomain and delivered intracellularly reduce membrane-bound EGFRvIII and induce apoptosis. Biol Chem, 390(2), 137-144. doi:10.1515/BC.2009.022

Liu, Y., Zhou, Q., & Revzin, A. (2013). An aptasensor for electrochemical detection of tumor necrosis factor in human blood. Analyst, 138(15), 4321-4326. doi:10.1039/c3an00818e

Lu, R. M., Hwang, Y. C., Liu, I. J., Lee, C. C., Tsai, H. Z., Li, H. J., & Wu, H. C. (2020). Development of therapeutic antibodies for the treatment of diseases. J Biomed Sci, 27(1), 1. doi:10.1186/s12929-019-0592-z

Lubberts, E., Koenders, M. I., Oppers-Walgreen, B., Van Den Bersselaar, L., Coenen-de Roo, C. J., Joosten, L. A., & Van Den Berg, W. B. (2004). Treatment with a neutralizing anti-murine interleukin-17 antibody after the onset of collagen-induced arthritis reduces joint inflammation, cartilage destruction, and bone erosion. Arthritis & Rheumatism: Official Journal of the American College of Rheumatology, 50(2), 650-659.

Ludwig, H., Weisel, K., Petrucci, M. T., Leleu, X., Cafro, A. M., Garderet, L., . . . Engelhardt, M. (2017). Olaptesed pegol, an anti-CXCL12/SDF-1 Spiegelmer, alone and with bortezomib-dexamethasone in relapsed/refractory multiple myeloma: a Phase IIa Study. Leukemia, 31(4), 997-1000. doi:10.1038/leu.2017.5

Lupold, S. E., Hicke, B. J., Lin, Y., & Coffey, D. S. (2002). Identification and characterization of nuclease-stabilized RNA molecules that bind human prostate cancer cells via the prostate-specific membrane antigen. Cancer Res, 62(14), 4029-4033. Retrieved from https://www.ncbi.nlm.nih.gov/pubmed/12124337

Lupu, L., Wiegand, P., Huttmann, N., Rawer, S., Kleinekofort, W., Shugureva, I., . . . Przybylski, M. (2020). Molecular Epitope Determination of Aptamer Complexes of the Multidomain Protein C-Met by Proteolytic Affinity-Mass Spectrometry. ChemMedChem, 15(4), 363-369. doi:10.1002/cmdc.201900489

Maeda, A., Yamamoto, K., Yamashita, K., Asagoe, K., Nohgawa, M., Kita, K., . . . Sasada, M. (1998). The expression of co-stimulatory molecules and their relationship to the prognosis of human acute myeloid leukaemia: poor prognosis of B7-2-positive leukaemia. Br J Haematol, 102(5), 1257-1262. doi:10.1046/j.1365-2141.1998.00901.x

Malkawi, A. K., Jafari, M., Ohlund, L., Sleno, L., Abdel Rahman, A. M., & Siaj, M. (2023). A diagnostic electrochemical aptasensor development for sCD80 protein detection in human serum. Biosens Bioelectron, 242, 115696. doi:10.1016/j.bios.2023.115696

Malkawi, A. K., Masood, A., Shinwari, Z., Jacob, M., Benabdelkamel, H., Matic, G., . . . Rahman, A. M. A. (2019). Proteomic Analysis of Morphologically Changed Tissues after Prolonged Dexamethasone Treatment. Int J Mol Sci, 20(13). doi:10.3390/ijms20133122

Malkawi, A. K., Nimer, R. M., Almogren, M., Masood, A., Alarfaj, A. S., Benabdelkamel, H., . . . Siaj, M. (2023). Quantitative analysis of soluble costimulatory molecules as potential diagnostic biomarkers for rheumatoid arthritis using LC-MS/MS in MRM mode. Clin Chim Acta, 548, 117501. doi:10.1016/j.cca.2023.117501

Manikwar, P., Kiptoo, P., Badawi, A. H., Büyüktimkin, B., & Siahaan, T. J. (2012). Antigen-specific blocking of CD4-specific immunological synapse formation using BPI and current therapies for autoimmune diseases. Medicinal research reviews, 32(4), 727-764.

Marciniak, R. A., Garcia-Blanco, M. A., & Sharp, P. A. (1990). Identification and characterization of a HeLa nuclear protein that specifically binds to the trans-activation-response (TAR) element of human immunodeficiency virus. Proc Natl Acad Sci U S A, 87(9), 3624-3628. doi:10.1073/pnas.87.9.3624

Martinez-Roque, M. A., Franco-Urquijo, P. A., Garcia-Velasquez, V. M., Choukeife, M., Mayer, G., Molina-Ramirez, S. R., . . . Alvarez-Salas, L. M. (2022). DNA aptamer selection for SARS-CoV-2 spike glycoprotein detection. Anal Biochem, 645, 114633. doi:10.1016/j.ab.2022.114633

Matsuyama, Y., Asanuma, K., Yoshida, K., Hagi, T., Iino, T., Nakamura, T., & Sudo, A. (2022). The role of soluble CD80 in patients with soft tissue tumors. Journal of Orthopaedic Surgery and Research, 17(1), 404. doi:10.1186/s13018-022-03283-2

McKeague, M., & Derosa, M. C. (2012). Challenges and opportunities for small molecule aptamer development. J Nucleic Acids, 2012, 748913. doi:10.1155/2012/748913

McKeague, M., Velu, R., Hill, K., Bardoczy, V., Meszaros, T., & DeRosa, M. C. (2014). Selection and characterization of a novel DNA aptamer for label-free fluorescence biosensing of ochratoxin A. Toxins (Basel), 6(8), 2435-2452. doi:10.3390/toxins6082435

Michaud, M., Jourdan, E., Villet, A., Ravel, A., Grosset, C., & Peyrin, E. (2003). A DNA aptamer as a new target-specific chiral selector for HPLC. J Am Chem Soc, 125(28), 8672-8679. doi:10.1021/ja034483t

Michienzi, A., Li, S., Zaia, J. A., & Rossi, J. J. (2002). A nucleolar TAR decoy inhibitor of HIV-1 replication. Proc Natl Acad Sci U S A, 99(22), 14047-14052. doi:10.1073/pnas.212229599

Miron-Merida, V. A., Gong, Y. Y., & Goycoolea, F. M. (2021). Aptamer-based detection of fumonisin B1: A critical review. Anal Chim Acta, 1160, 338395. doi:10.1016/j.aca.2021.338395

Mironov, G. G., Okhonin, V., Khan, N., Clouthier, C. M., & Berezovski, M. V. (2014). Conformational Dynamics of DNA G-Quadruplex in Solution Studied by Kinetic Capillary Electrophoresis Coupled On-line with Mass Spectrometry. ChemistryOpen, 3(2), 58-64. doi:10.1002/open.201400002

Mo, T., Liu, X., Luo, Y., Zhong, L., Zhang, Z., Li, T., . . . Chen, X. (2022). Aptamer-based biosensors and application in tumor theranostics. Cancer Sci, 113(1), 7-16. doi:10.1111/cas.15194

Naresh, V., & Lee, N. (2021). A Review on Biosensors and Recent Development of Nanostructured Materials-Enabled Biosensors. Sensors (Basel), 21(4). doi:10.3390/s21041109

Naumann, D. (2013). Infrared Spectroscopy of Cells, Tissues, and Biofluids. In G. C. K. Roberts (Ed.), Encyclopedia of Biophysics (pp. 1057-1065). Berlin, Heidelberg: Springer Berlin Heidelberg.

Ng, E. W., Shima, D. T., Calias, P., Cunningham, E. T., Jr., Guyer, D. R., & Adamis, A. P. (2006). Pegaptanib, a targeted anti-VEGF aptamer for ocular vascular disease. Nat Rev Drug Discov, 5(2), 123-132. doi:10.1038/nrd1955

Nikoo, M., Benjakul, S., Ocen, D., Yang, N., Xu, B., Zhang, L., & Xu, X. (2013). Physical and chemical properties of gelatin from the skin of cultured Amur sturgeon (Acipenser schrenckii). Journal of Applied Ichthyology, 29(5), 943-950. doi:https://doi.org/10.1111/jai.12238

Nimer, R. M., Sumaily, K. M., Almuslat, A., Abdel Jabar, M., Sabi, E. M., Al-Muhaizea, M. A., & Abdel Rahman, A. M. (2022). Dystrophin Protein Quantification as a Duchenne Muscular Dystrophy Diagnostic Biomarker in Dried Blood Spots Using Multiple Reaction Monitoring Tandem Mass Spectrometry: A Preliminary Study. Molecules, 27(12). doi:10.3390/molecules27123662

Ning, Y., Hu, J., & Lu, F. (2020). Aptamers used for biosensors and targeted therapy. Biomed Pharmacother, 132, 110902. doi:10.1016/j.biopha.2020.110902

Nutiu, R., & Li, Y. (2005). In vitro selection of structure-switching signaling aptamers. Angew Chem Int Ed Engl, 44(7), 1061-1065. doi:10.1002/anie.200461848

O'Connell, D., Koenig, A., Jennings, S., Hicke, B., Han, H. L., Fitzwater, T., . . . Varki, A. (1996). Calcium-dependent oligonucleotide antagonists specific for L-selectin. Proc Natl Acad Sci U S A, 93(12), 5883-5887. doi:10.1073/pnas.93.12.5883

Odobasic, D., Leech, M. T., Xue, J. R., & Holdsworth, S. R. (2008). Distinct in vivo roles of CD80 and CD86 in the effector T-cell responses inducing antigen-induced arthritis. Immunology, 124(4), 503-513. doi:10.1111/j.1365-2567.2007.02802.x

Oshima, S., Karrer, E. E., Paidhungat, M. M., Neighbors, M., Chapin, S. J., Fan, R. A., . . . Higashi, Y. (2016). ASP2408 and ASP2409, novel CTLA4-Ig variants with CD86-selective ligand binding activity and improved immunosuppressive potency, created by directed evolution. Protein Eng Des Sel, 29(5), 159-167. doi:10.1093/protein/gzw002

Pagratis, N. C., Bell, C., Chang, Y. F., Jennings, S., Fitzwater, T., Jellinek, D., & Dang, C. (1997). Potent 2'-amino-, and 2'-fluoro-2'-deoxyribonucleotide RNA inhibitors of keratinocyte growth factor. Nat Biotechnol, 15(1), 68-73. doi:10.1038/nbt0197-68

Parker, A. W., & Quinn, S. J. (2013). Infrared Spectroscopy of DNA. In G. C. K. Roberts (Ed.), Encyclopedia of Biophysics (pp. 1065-1074). Berlin, Heidelberg: Springer Berlin Heidelberg.

Peach, R. J., Bajorath, J., Naemura, J., Leytze, G., Greene, J., Aruffo, A., & Linsley, P. S. (1995). Both extracellular immunoglobin-like domains of CD80 contain residues critical for binding T cell surface receptors CTLA-4 and CD28. J Biol Chem, 270(36), 21181-21187. doi:10.1074/jbc.270.36.21181

Pfeiffer, F., & Mayer, G. (2016). Selection and Biosensor Application of Aptamers for Small Molecules. Front Chem, 4, 25. doi:10.3389/fchem.2016.00025

Plach, M., & Schubert, T. (2020). Biophysical Characterization of Aptamer-Target Interactions. Adv Biochem Eng Biotechnol, 174, 1-15. doi:10.1007/10_2019_103

Ponce, A. T., & Hong, K. L. (2019). A Mini-Review: Clinical Development and Potential of Aptamers for Thrombotic Events Treatment and Monitoring. Biomedicines, 7(3). doi:10.3390/biomedicines7030055

Ponikova, S., Tluckova, K., Antalik, M., Viglasky, V., & Hianik, T. (2011). The circular dichroism and differential scanning calorimetry study of the properties of DNA aptamer dimers. Biophys Chem, 155(1), 29-35. doi:10.1016/j.bpc.2011.02.004

Prante, M., Segal, E., Scheper, T., Bahnemann, J., & Walter, J. (2020). Aptasensors for Point-of-Care Detection of Small Molecules. Biosensors (Basel), 10(9). doi:10.3390/bios10090108

Puscasu, A., Zanchetta, M., Posocco, B., Bunka, D., Tartaggia, S., & Toffoli, G. (2021). Development and validation of a selective SPR aptasensor for the detection of anticancer drug irinotecan in human plasma samples. Anal Bioanal Chem, 413(4), 1225-1236. doi:10.1007/s00216-020-03087-5

Radko, S., Ptitsyn, K., Novikova, S., Kiseleva, Y., Moysa, A., Kurbatov, L., . . . Archakov, A. (2020). Evaluation of Aptamers as Affinity Reagents for an Enhancement of SRM-Based Detection of Low-Abundance Proteins in Blood Plasma. Biomedicines, 8(5). doi:10.3390/biomedicines8050133

Ramezani, M., Abnous, K., & Taghdisi, S. M. (2017). Optical and Electrochemical Aptasensors for Sensitive Detection of Streptomycin in Blood Serum and Milk. Methods Mol Biol, 1572, 403-420. doi:10.1007/978-1-4939-6911-1_26

Ray, J., Kruse, A., Ozer, A., Kajitani, T., Johnson, R., MacCoss, M., . . . Lis, J. T. (2020). RNA aptamer capture of macromolecular complexes for mass spectrometry analysis. Nucleic Acids Res, 48(15), e90. doi:10.1093/nar/gkaa542

Rechnitz, G. (1978). Biochemical electrodes uses tissues slice. Chem Eng News, 56, 16-21.

Rennert, P., Furlong, K., Jellis, C., Greenfield, E., Freeman, G. J., Ueda, Y., . . . Gray, G. S. (1997). The IgV domain of human B7-2 (CD86) is sufficient to co-stimulate T lymphocytes and induce cytokine secretion. Int Immunol, 9(6), 805-813. doi:10.1093/intimm/9.6.805

Riley, K. R., Gagliano, J., Xiao, J., Libby, K., Saito, S., Yu, G., . . . Bonin, K. (2015). Combining capillary electrophoresis and next-generation sequencing for aptamer selection. Anal Bioanal Chem, 407(6), 1527-1532. doi:10.1007/s00216-014-8427-y

Rosenberg, J. E., Bambury, R. M., Van Allen, E. M., Drabkin, H. A., Lara, P. N., Jr., Harzstark, A. L., . . . Laber, D. A. (2014). A phase II trial of AS1411 (a novel nucleolin-targeted DNA aptamer) in metastatic renal cell carcinoma. Invest New Drugs, 32(1), 178-187. doi:10.1007/s10637-013-0045-6

Rosenfeld, M., Emerson, J., Accurso, F., Armstrong, D., Castile, R., Grimwood, K., . . . Wagener, J. (1999). Diagnostic accuracy of oropharyngeal cultures in infants and young children with cystic fibrosis. Pediatr Pulmonol, 28(5), 321-328. doi:10.1002/(sici)1099-0496(199911)28:5<321::aid-ppul3>3.0.co;2-v

Roulet, E., Busso, S., Camargo, A. A., Simpson, A. J., Mermod, N., & Bucher, P. (2002). High-throughput SELEX SAGE method for quantitative modeling of transcription-factor binding sites. Nat Biotechnol, 20(8), 831-835. doi:10.1038/nbt718

Ryu, S. R., Noda, I., & Jung, Y. M. (2010). What is the origin of positional fluctuation of spectral features: True frequency shift or relative intensity changes of two overlapped bands? Applied Spectroscopy, 64(9), 1017-1021. doi:10.1366/000370210792434396

Salimi, A., Khezrian, S., Hallaj, R., & Vaziry, A. (2014). Highly sensitive electrochemical aptasensor for immunoglobulin E detection based on sandwich assay using enzyme-linked aptamer. Anal Biochem, 466, 89-97. doi:10.1016/j.ab.2014.08.019

Salomon, B., & Bluestone, J. A. (2001). Complexities of CD28/B7: CTLA-4 costimulatory pathways in autoimmunity and transplantation. Annu Rev Immunol, 19, 225-252. doi:10.1146/annurev.immunol.19.1.225

Sangam, S. A. M. a. V. G. (2017). Optimized Performance Validation of Biosensors with High Fault Tolerance. EEE 7th International Advance Computing Conference (IACC), 322-325. doi:10.1109/IACC.2017.0076.

Sasse, E. A. (2000). How to define and determine reference intervals in the clinical laboratory; approved guideline. NCCLS documents C28-A2.

Sayyed, S. G., Hagele, H., Kulkarni, O. P., Endlich, K., Segerer, S., Eulberg, D., . . . Anders, H. J. (2009). Podocytes produce homeostatic chemokine stromal cell-derived factor-1/CXCL12, which contributes to glomerulosclerosis, podocyte loss and albuminuria in a mouse model of type 2 diabetes. Diabetologia, 52(11), 2445-2454. doi:10.1007/s00125-009-1493-6

Schlecht, U., Malave, A., Gronewold, T., Tewes, M., & Lohndorf, M. (2006). Comparison of antibody and aptamer receptors for the specific detection of thrombin with a nanometer gap-sized impedance biosensor. Anal Chim Acta, 573-574, 65-68. doi:10.1016/j.aca.2006.01.016

Scott, K. B., Turko, I. V., & Phinney, K. W. (2015). Quantitative performance of internal standard platforms for absolute protein quantification using multiple reaction monitoring-mass spectrometry. Analytical chemistry, 87(8), 4429-4435.

Shen, H., Wang, J., Liu, H., Li, Z., Jiang, F., Wang, F. B., & Yuan, Q. (2016). Rapid and Selective Detection of Pathogenic Bacteria in Bloodstream Infections with Aptamer-Based Recognition. ACS Appl Mater Interfaces, 8(30), 19371-19378. doi:10.1021/acsami.6b06671

Shen, P., Li, M., Li, R., Han, B., Ma, H., Hou, X., . . . Wang, J.-J. (2022). Aptamer-functionalized smart photonic hydrogels: application for the detection of thrombin in human serum. NPG Asia Materials, 14(1), 94. doi:10.1038/s41427-022-00443-y

Shi, H. Z., Xie, Z. F., Deng, J. M., Chen, Y. Q., & Xiao, C. Q. (2004). Soluble CD86 protein in serum samples of patients with asthma. Thorax, 59(10), 870-875. doi:10.1136/thx.2004.021840

Simone, R., Pesce, G., Antola, P., Rumbullaku, M., Bagnasco, M., Bizzaro, N., & Saverino, D. (2014). The soluble form of CTLA-4 from serum of patients with autoimmune diseases regulates T-cell responses. Biomed Res Int, 2014, 215763. doi:10.1155/2014/215763

Sizeland, K., Hofman, K., Hallett, I., Martin, D., Potgieter, J., Kirby, N., . . . Cumming, M. (2018). Nanostructure of Electrospun Collagen: Do Electrospun Collagen Fibers Form Native Structures? Materialia, 3. doi:10.1016/j.mtla.2018.10.001

Smolen, J. S., Aletaha, D., Barton, A., Burmester, G. R., Emery, P., Firestein, G. S., . . . Yamamoto, K. (2018). Rheumatoid arthritis. Nature Reviews Disease Primers, 4(1), 18001. doi:10.1038/nrdp.2018.1

Solberg, H. (1993). A guide to IFCC recommendations on reference values. Journal of the International Federation of Clinical Chemistry, 5(4), 162-165.

Soldevilla, M. M., Villanueva, H., & Pastor, F. (2016). Aptamers: A Feasible Technology in Cancer Immunotherapy. J Immunol Res, 2016, 1083738. doi:10.1155/2016/1083738

Song, J. H., Lee, S. M., Park, I. H., Yong, D., Lee, K. S., Shin, J. S., & Yoo, K. H. (2019). Vertical capacitance aptasensors for real-time monitoring of bacterial growth and antibiotic susceptibility in blood. Biosens Bioelectron, 143, 111623. doi:10.1016/j.bios.2019.111623

Stevens, K. G., & Pukala, T. L. (2020). Conjugating immunoassays to mass spectrometry: Solutions to contemporary challenges in clinical diagnostics. TrAC Trends in Analytical Chemistry, 132, 116064. doi:https://doi.org/10.1016/j.trac.2020.116064

Stoltenburg, R., Reinemann, C., & Strehlitz, B. (2007). SELEX--a (r)evolutionary method to generate high-affinity nucleic acid ligands. Biomol Eng, 24(4), 381-403. doi:10.1016/j.bioeng.2007.06.001

Strehlitz, B., Nikolaus, N., & Stoltenburg, R. (2008). Protein Detection with Aptamer Biosensors. Sensors (Basel), 8(7), 4296-4307. doi:10.3390/s8074296

Su, J., & Mrksich, M. (2002). Using mass spectrometry to characterize self-assembled monolayers presenting peptides, proteins, and carbohydrates. Angew Chem Int Ed Engl, 41(24), 4715-4718. doi:10.1002/anie.200290026

Subramanian, N., Srimany, A., Kanwar, J. R., Kanwar, R. K., Akilandeswari, B., Rishi, P., . . . Krishnakumar, S. (2016). Nucleolin-aptamer therapy in retinoblastoma: molecular changes and mass spectrometry-based imaging. Mol Ther Nucleic Acids, 5(8), e358. doi:10.1038/mtna.2016.70

Sullenger, B., Woodruff, R., & Monroe, D. M. (2012). Potent anticoagulant aptamer directed against factor IXa blocks macromolecular substrate interaction. J Biol Chem, 287(16), 12779-12786. doi:10.1074/jbc.M111.300772

Sumaily, K. M., Nimer, R., Alzahrani, M., Abdel Jabar, M., Alodib, A., Sabi, E. M., . . . Abdel Rahman, A. M. (2022). CFTR protein quantification as a cystic fibrosis diagnostic biomarker in dried blood spots using multiple reaction monitoring tandem mass spectrometry. J Pharm Biomed Anal, 216, 114801. doi:10.1016/j.jpba.2022.114801

Suzuki, J., Tezuka, D., Morishita, R., & Isobe, M. (2009). An initial case of suppressed restenosis with nuclear factor-kappa B decoy transfection after percutaneous coronary intervention. J Gene Med, 11(1), 89-91. doi:10.1002/jgm.1266

Sweeney, S. E., & Firestein, G. S. (2004). Rheumatoid arthritis: regulation of synovial inflammation. The international journal of biochemistry & cell biology, 36(3), 372-378.

Tai, Y., Wang, Q., Korner, H., Zhang, L., & Wei, W. (2018). Molecular mechanisms of T cells activation by dendritic cells in autoimmune diseases. Frontiers in pharmacology, 9, 642.

Tan, H., Ma, L., Guo, T., Zhou, H., Chen, L., Zhang, Y., . . . Yu, Y. (2019). A novel fluorescence aptasensor based on mesoporous silica nanoparticles for selective and sensitive detection of aflatoxin B(1). Anal Chim Acta, 1068, 87-95. doi:10.1016/j.aca.2019.04.014

Tasset, D. M., Kubik, M. F., & Steiner, W. (1997). Oligonucleotide inhibitors of human thrombin that bind distinct epitopes. J Mol Biol, 272(5), 688-698. doi:10.1006/jmbi.1997.1275

Tector, M., Khatri, B. O., Kozinski, K., Dennert, K., & Oaks, M. K. (2009). Biochemical analysis of CTLA-4 immunoreactive material from human blood. BMC Immunol, 10, 51. doi:10.1186/1471-2172-10-51

Thompson, C. B. (1995). Distinct roles for the costimulatory ligands B7-1 and B7-2 in T helper cell differentiation? Cell, 81(7), 979-982. doi:10.1016/s0092-8674(05)80001-7

Tombelli, S., Minunni, M., Luzi, E., & Mascini, M. (2005). Aptamer-based biosensors for the detection of HIV-1 Tat protein. Bioelectrochemistry, 67(2), 135-141. doi:10.1016/j.bioelechem.2004.04.011

Trelle, M. B., Dupont, D. M., Madsen, J. B., Andreasen, P. A., & Jorgensen, T. J. (2014). Dissecting the effect of RNA aptamer binding on the dynamics of plasminogen activator

inhibitor 1 using hydrogen/deuterium exchange mass spectrometry. ACS Chem Biol, 9(1), 174-182. doi:10.1021/cb400619v

Tuerk, C., MacDougal, S., & Gold, L. (1992). RNA pseudoknots that inhibit human immunodeficiency virus type 1 reverse transcriptase. Proc Natl Acad Sci U S A, 89(15), 6988-6992. doi:10.1073/pnas.89.15.6988

Tuske, S., Zheng, J., Olson, E. D., Ruiz, F. X., Pascal, B. D., Hoang, A., . . . Arnold, E. (2020). Integrative structural biology studies of HIV-1 reverse transcriptase binding to a high-affinity DNA aptamer. Curr Res Struct Biol, 2, 116-129. doi:10.1016/j.crstbi.2020.06.002

Uehara, M., & McGrath, M. M. (2019). The Role of Costimulatory Pathways in Transplant Tolerance. Clin Lab Med, 39(1), 87-106. doi:10.1016/j.cll.2018.10.009

Uvebrant, K., da Graca Thrige, D., Rosen, A., Akesson, M., Berg, H., Walse, B., & Bjork, P. (2007). Discovery of selective small-molecule CD80 inhibitors. J Biomol Screen, 12(4), 464-472. doi:10.1177/1087057107300464

van de Merbel, N. C. (2019). Protein quantification by LC-MS: a decade of progress through the pages of Bioanalysis. Bioanalysis, 11(7), 629-644. doi:10.4155/bio-2019-0032

Vater, A., & Klussmann, S. (2015). Turning mirror-image oligonucleotides into drugs: the evolution of Spiegelmer((R)) therapeutics. Drug Discov Today, 20(1), 147-155. doi:10.1016/j.drudis.2014.09.004

Venugopal, V. (2002). Biosensors in fish production and quality control. Biosens Bioelectron, 17(3), 147-157. doi:10.1016/s0956-5663(01)00180-4

Walunas, T. L., Bakker, C. Y., & Bluestone, J. A. (1996). CTLA-4 ligation blocks CD28-dependent T cell activation. J Exp Med, 183(6), 2541-2550. doi:10.1084/jem.183.6.2541

Wan, B., Nie, H., Liu, A., Feng, G., He, D., Xu, R., . . . Zhang, J. Z. (2006). Aberrant regulation of synovial T cell activation by soluble costimulatory molecules in rheumatoid arthritis. J Immunol, 177(12), 8844-8850. doi:10.4049/jimmunol.177.12.8844

Wang, J. (2008). Electrochemical glucose biosensors. Chem Rev, 108(2), 814-825. doi:10.1021/cr068123a

Wang, Y., Li, D., Ren, W., Liu, Z., Dong, S., & Wang, E. (2008). Ultrasensitive colorimetric detection of protein by aptamer-Au nanoparticles conjugates based on a dot-blot assay. Chem Commun (Camb)(22), 2520-2522. doi:10.1039/b801055b

Waters, E. K., Genga, R. M., Schwartz, M. C., Nelson, J. A., Schaub, R. G., Olson, K. A., . . . McGinness, K. E. (2011). Aptamer ARC19499 mediates a procoagulant hemostatic effect by

inhibiting tissue factor pathway inhibitor. Blood, The Journal of the American Society of Hematology, 117(20), 5514-5522.

Weisman, M. H., Durez, P., Hallegua, D., Aranda, R., Becker, J. C., Nuamah, I., . . . Moreland, L. W. (2006). Reduction of inflammatory biomarker response by abatacept in treatment of rheumatoid arthritis. J Rheumatol, 33(11), 2162-2166. Retrieved from https://www.ncbi.nlm.nih.gov/pubmed/17014006

White, R., Rusconi, C., Scardino, E., Wolberg, A., Lawson, J., Hoffman, M., & Sullenger, B. (2001). Generation of species cross-reactive aptamers using "toggle" SELEX. Mol Ther, 4(6), 567-573. doi:10.1006/mthe.2001.0495

Wiegand, T. W., Williams, P. B., Dreskin, S. C., Jouvin, M. H., Kinet, J. P., & Tasset, D. (1996). High-affinity oligonucleotide ligands to human IgE inhibit binding to Fc epsilon receptor I. J Immunol, 157(1), 221-230. Retrieved from https://www.ncbi.nlm.nih.gov/pubmed/8683119

Wong, C. K., Ho, A. W., Tong, P. C., Yeung, C. Y., Chan, J. C., Kong, A. P., & Lam, C. W. (2008). Aberrant expression of soluble co-stimulatory molecules and adhesion molecules in type 2 diabetic patients with nephropathy. J Clin Immunol, 28(1), 36-43. doi:10.1007/s10875-007-9137-4

Wong, C. K., Lit, L. C., Tam, L. S., Li, E. K., & Lam, C. W. (2005). Aberrant production of soluble costimulatory molecules CTLA-4, CD28, CD80 and CD86 in patients with systemic lupus erythematosus. Rheumatology (Oxford), 44(8), 989-994. doi:10.1093/rheumatology/keh663

Wu, Y. Y., Hsieh, I. S., Tung, C. H., Weng, C. H., Wu, J. E., Yu, J. S., . . . Chen, Y. L. (2022). A novel DNA aptamer targeting lung cancer stem cells exerts a therapeutic effect by binding and neutralizing Annexin A2. Mol Ther Nucleic Acids, 27, 956-968. doi:10.1016/j.omtn.2022.01.012

Xiao, Y., Lubin, A. A., Heeger, A. J., & Plaxco, K. W. (2005). Label-free electronic detection of thrombin in blood serum by using an aptamer-based sensor. Angew Chem Int Ed Engl, 44(34), 5456-5459. doi:10.1002/anie.200500989

Xu, Z., Juan, V., Ivanov, A., Ma, Z., Polakoff, D., Powers, D. B., . . . Akamatsu, Y. (2012). Affinity and cross-reactivity engineering of CTLA4-Ig to modulate T cell costimulation. J Immunol, 189(9), 4470-4477. doi:10.4049/jimmunol.1201813

Yamada, A., Salama, A. D., & Sayegh, M. H. (2002). The role of novel T cell costimulatory pathways in autoimmunity and transplantation. J Am Soc Nephrol, 13(2), 559-575. Retrieved from https://www.ncbi.nlm.nih.gov/pubmed/11805188

Yang, C. J., Jockusch, S., Vicens, M., Turro, N. J., & Tan, W. (2005). Light-switching excimer probes for rapid protein monitoring in complex biological fluids. Proc Natl Acad Sci U S A, 102(48), 17278-17283. doi:10.1073/pnas.0508821102

Yang, Q., Zhang, X., Kumar, S., Singh, R., Zhang, B., Bai, C., & Pu, X. (2020). Development of Glucose Sensor Using Gold Nanoparticles and Glucose-Oxidase Functionalized Tapered Fiber Structure. Plasmonics, 15(3), 841-848. doi:10.1007/s11468-019-01104-7

Yao, C., Qi, Y., Zhao, Y., Xiang, Y., Chen, Q., & Fu, W. (2009). Aptamer-based piezoelectric quartz crystal microbalance biosensor array for the quantification of IgE. Biosens Bioelectron, 24(8), 2499-2503. doi:10.1016/j.bios.2008.12.036

Yap, H. Y., Tee, S. Z., Wong, M. M., Chow, S. K., Peh, S. C., & Teow, S. Y. (2018). Pathogenic Role of Immune Cells in Rheumatoid Arthritis: Implications in Clinical Treatment and Biomarker Development. Cells, 7(10). doi:10.3390/cells7100161

Yi Peng, L. L., Xiaojiao Mu, Lin Guo. (2013). Aptamer-gold nanoparticle-based colorimetric assay for the sensitive detection of thrombin. Sensors and Actuators B: Chemical, Volume 177, 818-825. doi:/10.1016/j.snb.2012.12.004

Yin, S., & Loo, J. A. (2010). Elucidating the site of protein-ATP binding by top-down mass spectrometry. J Am Soc Mass Spectrom, 21(6), 899-907. doi:10.1016/j.jasms.2010.01.002

Ying, Y. L., Wang, H. Y., Sutherland, T. C., & Long, Y. T. (2011). Monitoring of an ATP-binding aptamer and its conformational changes using an alpha-hemolysin nanopore. Small, 7(1), 87-94. doi:10.1002/smll.201001428

Yoo, E. H., & Lee, S. Y. (2010). Glucose biosensors: an overview of use in clinical practice. Sensors (Basel), 10(5), 4558-4576. doi:10.3390/s100504558

Youn, H., Lee, K., Her, J., Jeon, J., Mok, J., So, J. I., . . . Ban, C. (2019). Aptasensor for multiplex detection of antibiotics based on FRET strategy combined with aptamer/graphene oxide complex. Sci Rep, 9(1), 7659. doi:10.1038/s41598-019-44051-3

Yu, F., Li, H., Sun, W., Xu, D., & He, F. (2019). Rapid selection of aptamers based on protein microarray. RSC advances, 9(17), 9762-9768.

Zamay, G. S., Zamay, T. N., Kolovskii, V. A., Shabanov, A. V., Glazyrin, Y. E., Veprintsev, D. V., . . . Zamay, A. S. (2016). Electrochemical aptasensor for lung cancer-related protein detection in crude blood plasma samples. Sci Rep, 6, 34350. doi:10.1038/srep34350

Zhang, J., Loo, R. R. O., & Loo, J. A. (2017). Structural Characterization of a Thrombin-Aptamer Complex by High Resolution Native Top-Down Mass Spectrometry. J Am Soc Mass Spectrom, 28(9), 1815-1822. doi:10.1007/s13361-017-1751-7

Zhang, J., Reza Malmirchegini, G., Clubb, R. T., & Loo, J. A. (2015). Native top-down mass spectrometry for the structural characterization of human hemoglobin. Eur J Mass Spectrom (Chichester), 21(3), 221-231. doi:10.1255/ejms.1340

Zhang, Y., van Haren, M. J., Marechal, N., Troffer-Charlier, N., Cura, V., Cavarelli, J., & Martin, N. I. (2022). A Direct Assay for Measuring the Activity and Inhibition of Coactivator-Associated Arginine Methyltransferase 1. Biochemistry, 61(11), 1055-1063. doi:10.1021/acs.biochem.2c00075

Zhang, Y., Xu, S., Wen, L., Bai, Y., Niu, L., Song, D., & Liu, H. (2016). A dielectric barrier discharge ionization based interface for online coupling surface plasmon resonance with mass spectrometry. Analyst, 141(11), 3343-3348. doi:10.1039/c6an00561f

Zhao, N., Pei, S. N., Parekh, P., Salazar, E., & Zu, Y. (2014). Blocking interaction of viral gp120 and CD4-expressing T cells by single-stranded DNA aptamers. Int J Biochem Cell Biol, 51, 10-18. doi:10.1016/j.biocel.2014.03.008

Zheng, X., Yang, L., Sun, Q., Zhang, L., & Le, T. (2023). Development and Validation of Aptasensor Based on MnO(2) for the Detection of Sulfadiazine Residues. Biosensors (Basel), 13(6). doi:10.3390/bios13060613

Zhou, J., & Zhong, L. (2022). Applications of liquid chromatography-mass spectrometry based metabolomics in predictive and personalized medicine. Front Mol Biosci, 9, 1049016. doi:10.3389/fmolb.2022.1049016